DOCTORAL THESIS

Investigation of EDFA power transients in circuit-switched and packet-switched optical networks

Siham Muhyaldin

Investigation of EDFA Power Transients in Circuit-Switched and Packet-Switched Optical Networks

SIHAM MUHYALDIN

Doctor of Philosophy

ASTON UNIVERSITY

January 2009

ASTON UNIVERSITY

Investigation of EDFA Power Transients in Circuit-Switched and Packet-Switched Optical Networks

SIHAM MUHYALDIN

Doctor of Philosophy, 2009

Thesis Summary

Erbium-doped fibre amplifiers (EDFA's) are a key technology for the design of all optical communication systems and networks. The superiority of EDFAs lies in their negligible intermodulation distortion across high speed multichannel signals, low intrinsic losses, slow gain dynamics, and gain in a wide range of optical wavelengths. Due to long lifetime in excited states, EDFAs do not oppose the effect of cross-gain saturation. The time characteristics of the gain saturation and recovery effects are between a few hundred microseconds and 10 milliseconds. However, in wavelength division multiplexed (WDM) optical networks with EDFAs, the number of channels traversing an EDFA can change due to the faulty link of the network or the system reconfiguration. It has been found that, due to the variation in channel number in the EDFAs chain, the output system powers of surviving channels can change in a very short time. Thus, the power transient is one of the problems deteriorating system performance.

In this thesis, the transient phenomenon in wavelength routed WDM optical networks with EDFA chains was investigated. The task was performed using different input signal powers for circuit switched networks. A simulator for the EDFA gain dynamic model was developed to compute the magnitude and speed of the power transients in the non-self-saturated EDFA both single and chained. The dynamic model of the self-saturated EDFAs chain and its simulator were also developed to compute the magnitude and speed of the power transients and the Optical signal-to-noise ratio (OSNR). We found that the OSNR transient magnitude and speed are a function of both the output power transient and the number of EDFAs in the chain. The OSNR value predicts the level of the quality of service in the related network. It was found that the power transients for both self-saturated and non-self-saturated EDFAs are close in magnitude in the case of gain saturated EDFAs networks.

Moreover, the cross-gain saturation also degrades the performance of the packet switching networks due to varying traffic characteristics. The magnitude and the speed of output power transients increase along the EDFAs chain. An investigation was done on the asynchronous transfer mode (ATM) or the WDM Internet protocol (WDM-IP) traffic networks using different traffic patterns based on the Pareto and Poisson distribution. The simulator is used to examine the amount and speed of the power transients in Pareto and Poisson distributed traffic at different bit rates, with specific focus on 2.5 Gb/s. It was found from numerical and statistical analysis that the power swing increases if the time interval of the burst-ON/burst-OFF is long in the packet bursts. This is because the gain dynamics is fast during strong signal pulse or with long duration pulses, which is due to the stimulated-emission avalanche depletion of the excited ions. Thus, an increase in output power level could lead to error burst which affects the system performance.

Keywords: EDFA, power transients, circuit-switched and packet-switched, OSNR, ATM-IP traffic, Pareto distribution, Poisson distribution.

To my parents

Acknowledgements

First and foremost I am grateful to my supervisors Professor Keith Blow and Dr. Marc Eberhard for their patience, understanding, encouragement and guidance offered to me during my studies at Aston.

I also wish to thank Professor I. Bennion for his help during my study in Aston. I deeply appreciate his kind character and willingness to help.

My special acknowledgments also go to my fellow colleagues Dr Etallah Tahier, Terence Broderick, Jovana Petrovic, Zahariah Zakaria, Christos Braimiotis, Irina Nasieva, Dr. Juan Diego Ania-Castannon, Dr. Stanislav A. Derevyanko, and Dr. Sonia Boscolo, Musaab Nahas, Qasim Iqbal, Ahammed Shiakh . I would like to thank all of my colleagues in the Electronic Engineering department, with whom I closely collaborated during my stay in Aston.

I would also like to thank my cousins in Birmingham for their kindness, understanding and supports. My deepest gratitude also goes to all friends and families in Birmingham who made my life here so enjoyable.

For the indispensable spiritual support, I feel so much grateful to my mother and my brother (Khlid) who gave me finance support, kindness, understanding and he did everything to help me follow through tough period of my study.

Contents

List of Figures

List of Tables

Chapter 1

Introduction to optical networks

In this century, there have been impressive changes in telecommunications technology that have rapidly enhanced the users' lifestyles. The most important factor which has driven these changes is the continuous demand for an increase in the capacity of the network. A major cause of this increasing demand is the massive growth in the number of users as well as the increase in the amount of time spent by individual users on the Internet. Consequently, the bandwidth required by each user is high. Internet voice calls generate large amounts of traffic in the network in comparison to traditional voice calls. With the rapid growth in Internet traffic, broadband technology such as Digital Subscriber Line (DSL) and cable access technologies (modems) have come into the picture and provide reasonably adequate bandwidth to each user [1].

High-speed networks are now being used by businesses, for example interconnection between multiple sites of a company or between companies for business transactions. There is a strong relation between bandwidth growth and the cost of the bandwidth. For instance, telecommunication technology advances have achieved cost reduction which in turn lowers the cost of bandwidth. In contrast to previously, the client can use both phone and Internet services for a longer duration at lower cost. One of the major factors which pushes for development in the telecommunication industry, is a significant change in the type of traffic that is progressively dominating the network. Traditionally, the dominating traffic was voice, however today more demand on the network is being stimulated by data. Yet most networks are designed to support voice traffic and not data traffic. This change in the type of traffic is now causing service providers to review and reconsider their network architectures, and has

stimulated the deployment of high capacity optical networks.

Let us briefly discuss a telecommunication network architecture. A Local Exchange (LE) provides local services in metropolitan areas, and an Inter-Exchange (IX) provides long-distance services. Eventually, LE and IX overlap in their service areas. Metro networks cover the area between the client locations and interoffice networks. The latter is known as a metropolitan network and connects groups of central offices within a city or region. This network between offices within a city tends to be from a few kilometers to several tens of kilometers.

In contrast to metro networks, long-haul networks have links from several hundred to a few thousand kilometers. The services provided by metro and long-haul networks are different because the networks are different. Private networks which are owned, operated and networked by the same company and cover only a few kilometers are called Local Area Networks (LANs). Networks which are spread over a metropolitan area covering tens to a few hundred kilometers, are known as Metropolitan-Area Networks(MANs). Networks that cover even longer distances, spanning hundreds to thousands of kilometers, are known as Wide Area Networks(WANs).

Figure 1.1 [1] illustrates a typical terrestrial public fibre network architecture. The nodes in the network are central offices, sometimes called Points of Presence (POPs). In some cases, the small nodes are denoted by POPs, and the larger nodes are denoted by hubs. The links between the nodes consist of fibre pairs, or multiple fibre pairs. A ring topology is widely used to provide two links per node and this in turn provides an alternative path to reroute traffic in the case where some links fail. Mesh networks are implemented in the form of interconnected ring networks in order to provide an alternative path for traffic in case of link failures. Optical fibres are also used in undersea networks. These networks span hundreds to thousands of kilometers for paths across the beds of such wide oceans as the Atlantic and Pacific [19].

At a higher level, the networks can be divided into a metropolitan network and a long-haul network. As mentioned earlier, the former links within a region or large city, while long-haul networks link to different regions far away.

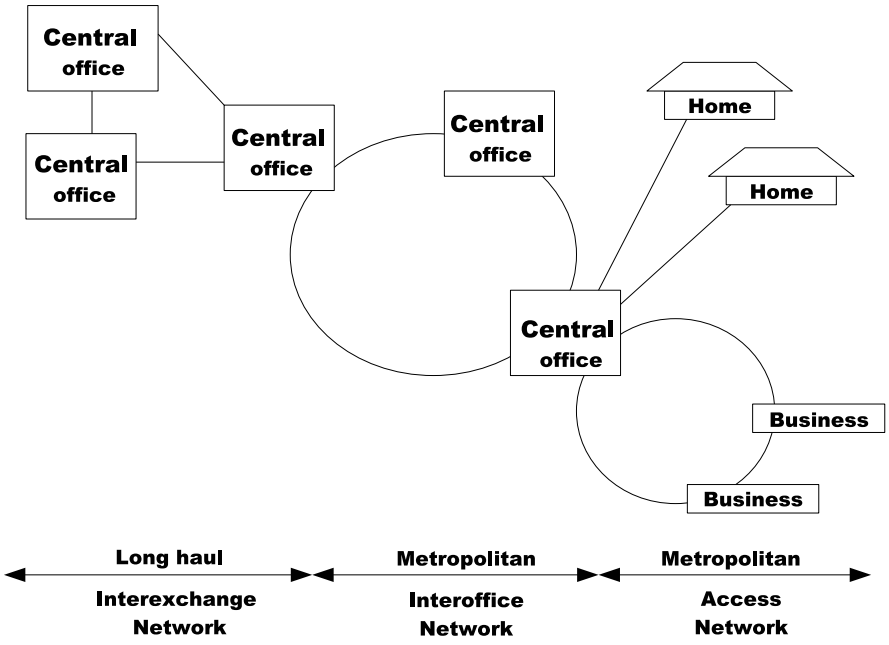

Figure 1.1: Different parts of a typical terrestrial public fibre network architecture.

1.1 Circuit switching, and packet switching services

Network services can be classified into connection-oriented services and connectionless services. In the former there is the concept of a connection between two or more parties across an underlying network. The differences in the connection-oriented services depend on the bandwidth of the connection and the type of underlying network which provides the connection. This has a strong effect on the Quality-of-Service (QoS) guarantee supplied by the network administrators to their customers [1, 20, 21].

Circuit-switched and packet-switched networks are the two fundamental types of network infrastructures. These infrastructures are based on both how traffic is multiplexed and switched within the underlying network. Figure 1.2 shows different types of Time Division Multiplexing (TDM) techniques. In a circuit switched network, the circuit-switched connection is provided to its customers, and a secure amount of bandwidth is assigned to each connection, and is available at all times from the time that the connection is set up. The total bandwidth of the connections must be less than the serving link bandwidth. The Public-Switched Telephone Network (PSTN) is the most common example of the circuit-switched network. The PSTN allocates connections to the customers with fixed amounts of bandwidth

(around 4 kHz) as soon as the connection is set up. This connection or circuit is converted to a digital 64 kb/s circuit at the central office. This type of network was originally developed to provide efficient voice streams.

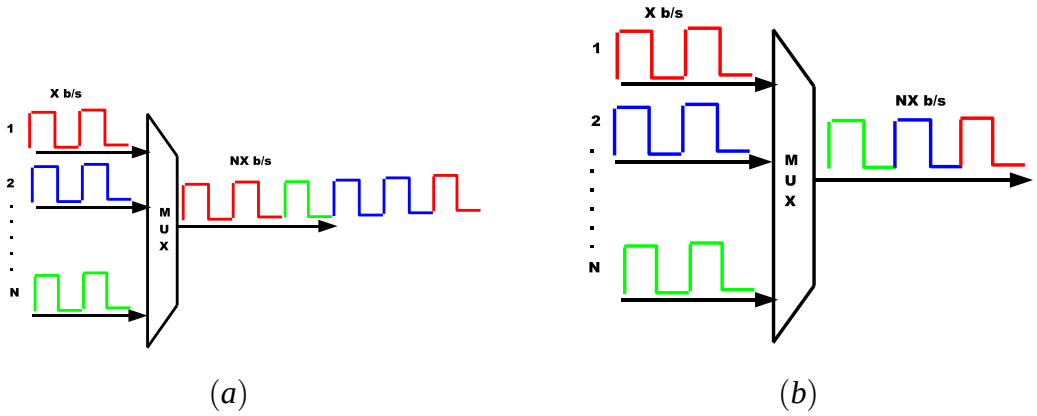

Figure 1.2: Two types of TDM, (a) statistical TDM, (b) fixed TDM.

Recently, the circuit-switched services provided by the administrator or vendor include circuits at different bit rates, starting from 64 kb/s voice circuits up to several Gb/s. These connections are leased and stay connected for long periods of time. They are known as private line services. In contrast to PSTN, the private line users do not dial up to set up the connections, the network administrator normally establishes connections using a management system.

A disadvantage of circuit-switched networks is that it is inefficient when dealing with bursty data traffic. An example of a bursty data traffic stream is web browsing. When the user is looking at recently downloaded pages, the data transmission is almost zero. However, when the user clicks on a hyperlink, a new set of data packets will be downloaded from the network. This type of data traffic requires large bandwidth from the network while it is active and very small bandwidth while the data traffic is not active. The network is designated by an average bandwidth and a peak bandwidth which is related to the long-term average burst rate and short-term burst rates, respectively. In case of the circuit-switched network, the connection and bandwidth which are reserved for long-term-average bursty data traffic will not be used efficiently for the short-term burst-data traffic.

For efficient transmission of the bursty data traffic, the packet-switched network was invented [1]. In a packet-switched network, the data stream is divided into small packets

and the packets from different sources of the same network are multiplexed. Then these packets are switched according to their destination. The destination address or the next node's address in the path is added to the payload in each packet as a header. Intermediate nodes in the path read the address and the routing information from the header of the packet which has arrived at that node, then decide where to route the packet based on the information provided in the header. The data stream will be separated back (demultiplexed) when it reaches the destination. The most well-known example of a packet-switched network is the Internet, which uses the Internet Protocol (IP) to route packets from their source to their destination. The multiplexing technique which is used by packet switching for multiplexing multiple bursty data stream together in a link is called *statistical multiplexing* see Figure 1.2 (a) [1, 3, 20].

Each bursty data stream could be either in a state of ON period or OFF period. Thus, the bandwidth required on the link is smaller than the bandwidth used in the case while all sources are simultaneously active. The advantage of *statistical multiplexing* is that it enhances the utilization of the bandwidth. However, there are also some disadvantages. In the case where a large number of bursty data stream sources are simultaneously active, the available bandwidth on the link will be not sufficient. The consequence of this is that some packets will have to be queued or buffered until the link becomes available. Therefore, the number of packets delayed and the amount of delay depends on how many packets there are in the queue ahead. The delay is a random parameter. Moreover, if the number of packets in the queue are higher than the queue size, this drives the buffer into an overflow state and, some of these packets could be lost. In such circumstances the *transport layer* (higher layer of the network) which uses Transmission Control Protocol (TCP) in the Internet, will detect this problem and ensure retransmission of all lost packets. The transport layer is explained in Section 1.3.

The packet-switched network is based on a connection independent concept. The packets belonging to a certain connection are dealt with as independent units from a related group of packets, and each may take a different route to reach their destination through the network. This is the condition with the networks using IP. This type of connectionless service is called a *datagram service*. This datagram service produces varying delays with different packets which requires the transport layer to re-sequence the arrived packets at each destination.

Best-effort service is a type of service in which the network tries to get data from source to destination with a minimum delay but without providing any guarantees. This already exists now with Internet services. The best-effort service is efficient for applications whose performances are not highly affected by random packet delays, such as web browsing and file transfers. However, this service cannot be applied to real-time video or voice calls, because these applications are highly sensitive to delay.

Another example for a packet-switched network service is *frame relay*. This service is provided by the network administration to interconnect the data networks. The user who has applied for a frame relay service will be guaranteed average bandwidth. Thus, the user can use some higher than average bandwidth for a certain time and lower than average bandwidth at other times. However, the user cannot exceed the average over a long period of time. This service can provide the user with a burst rate above the average rate but without offering any guarantees, but it is not efficient for real-time video and voice calls. Thus, there must be a packet-switched network that is capable to guarantee the QoS that has been offered by the system administrator. The QoS of the network might include average bandwidth guarantee for each connection, packet delay and the delay variation.

The Asynchronous Transfer Mode (ATM) is the outcome of these QoS guarantees [22–24]. The Internet Protocol has been developed to provide the above services. The QoS depends on having a connection-oriented layer. For instance, Multi-Protocol Label Switching (MPLS) in an IP network provides virtual circuits to assist end-to-end traffic streams [21]. The virtual circuits support certain types of QoS guarantees, by enabling better resource allocation inside the network. The enhanced resource allocation is done by forcing all packets to follow the same path inside the network. The virtual circuit does not provide a guaranteed bandwidth inside the network because the statistical multiplexing is applied to multiplex the virtual circuits within the network.

Advances in network technology and increased competition among service providers as well as increased customer demands for bandwidth have caused rapid change in the service models that are used by network management. The increased customer demand for bandwidth is making it popular to lease the lines ranging in capacity from 155 Mb/s to 10 Gb/s. Another reason for alteration is related to the availability of these circuits. The availability is defined as the percentage of time the service is available to the user. Normally, the adminis-

trators offer high percentage of availability which indicates that the network down-time does not exceed a few minutes per year. This requires the network to consider speedy restoration of service in the case of failures such as fibre cuts. There are some complicated methods which enhance the bandwidth efficiency but normally at the cost of slower restoration times.

As mentioned earlier, the circuit-switched services are different from packet-switched services, so the network providers need to operate both networks to get the necessary mixture of services. This is in fact costly because there are costs associated with each network while operating, such as maintenance, the provision of new connections and upgrading the infrastructure. Optical networks offer high capacity bandwidth to fulfill the bandwidth requirements where and when needed and provides a common infrastructure that enables the network providers to offer a range of services [1–3].

1.2 Optical networks

With the advance of optical technology, optical networks are capable of fulfilling the bandwidth requirements where and when needed. Optical fibres offer high bandwidth and are immunes to electromagnetic interference compared to copper cable. For instance, optical networks with 40 Gb/s are commercially available and are dominating the market, however twisted pair copper cables, as mentioned in category 5, which offer only 100 Mb/s at a distance of 100 m, are still widely used [25, 26]. Fibre transmission technology has evolved over the last decades to offer high bit rates over long distance, and a 3 Tbit/s (160 Gbit/s19 channels) optical signal has been successfully transmitted over 40 km of dispersion-shifted fibre [27]. Although the bandwidth into the user's home is limited with the telephone's twisted-pair copper cable bandwidth, this remains a popular method for data transmission using Digital Subscriber Loop (DSL) technology.

Another method of data transmission at a few megabits per second to each subscriber is the cable network, which offers the above rate on a shared basis using cable modem technology. In the first generation of optical networks, optical fibre was used for transmission only. Good examples are Synchronous Optical Network (SONET) and Synchronous Digital Hierarchy (SDH). In the second generation, optical fibre was used for transmission, switching and all other network intelligent functions. Before explaining the infrastructure of recent optical

networks, a brief overview of multiplexing techniques (which are an effective component in providing the capacity required by these types of networks [1–3, 20, 21]) is given.

Multiplexing techniques provide economical data transmission at higher bit rates over single fibre than data transmission at lower bit rates over multiple fibres. There are two fundamental techniques to increase the transmission capacity of a fibre, see Figure 1.3. One of these techniques is TDM which uses electronic means for interleaving the lower-speed streams to obtain a higher-speed stream. When a higher bit rate is required, Optical Time Division Multiplexing (OTDM) is used.

Another multiplexing technique to increase the transmission capacity of a fibre is Wavelength Division Multiplexing (WDM). WDM is basically the same as Frequency Division Multiplexing (FDM), which has been used in radio systems. but applied to optical communication. The basic idea of WDM is to transmit data simultaneously at multiple wavelengths over fibre. The band guard or space between these wavelengths is sufficient that the wavelengths do not interfere with each other. In recent networks, both WDM and TDM are used to increase the transmission capacity as shown in Figure 1.3. Systems with transmission capacities of many Tb/s are available over a single fibre experimentally [27], while systems with transmission capacities of 10 Gb/s to 40 Gb/s have been available commercially since the beginning of this decade, and these systems use a combination of TDM and WDM techniques [1, 2, 28].

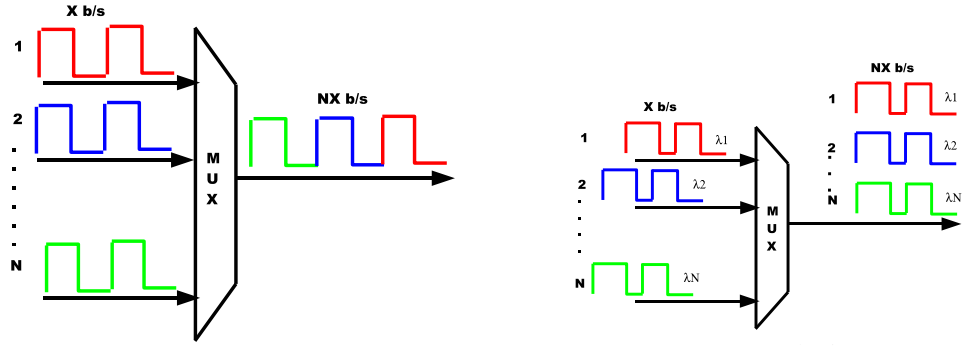

(a) (b)

Figure 1.3: Different types of multiplexing techniques used with an optical fibre network to increase the transmission capacity, (a) TDM or OTDM, and (b) WDM.

In second generation optical networks, WDM is extensively used. In this generation,

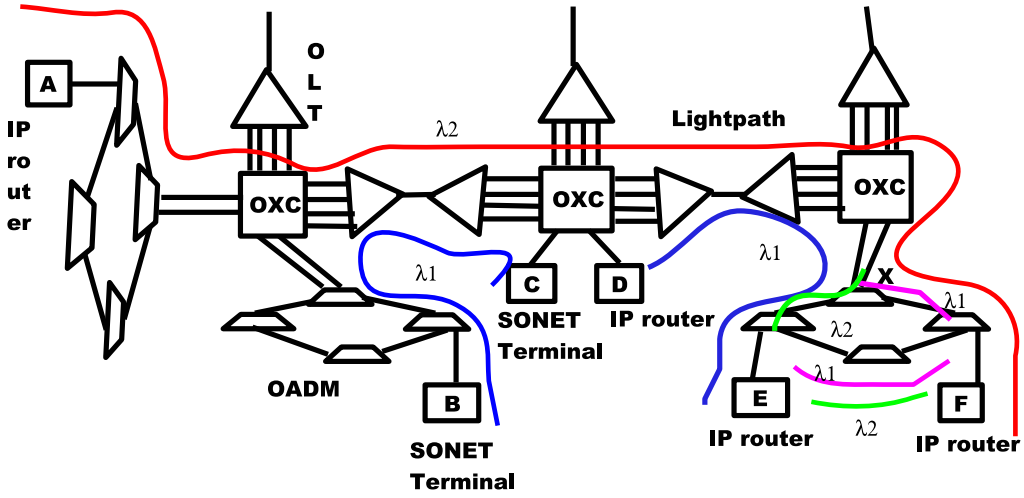

Figure 1.4: WDM Wavelength-routing network, the main network units are: Optical Line Terminals (OLTs), Optical Add/Drop Multiplexers (OADMs), and Optical Cross Connects (OXCs), the light-paths of different wavelengths (λ_1 or λ_2)are provided by the network to the users, which are IP routers or SONET terminals.

switching and routing functions, which were provided by electronic devices in the first generation, are integrated into the optical part of the network. For example, if the data is in blocks of 53 bytes or 424 bits (the cell size in ATM networks), we need 4.24 μs to process the block in a 100 Mb/s data stream, and need 42.4 ns to process the block at 10 Gb/s. The electronic devices at the node in first-generation networks perform this function, and any other data processing for the data belongs to other nodes in the network and traverses through this node. However, by assigning the latter task to the optical part of the network, the burden on the electronic devices at the node is greatly reduced.

Figure 1.4 shows a wavelength-routing network and its architecture is of a type that has been used recently. The SONET terminal and IP routers are examples of such wavelength routing networks and provide light-paths to users. Light-paths are optical paths that connect a source node to a destination node, over a wavelength on each intermediate link. The switching and routing are performed at each intermediate node and wavelength conversion may be performed along the route. In the wavelength-routing network the same wavelengths are used in the different light-paths as long as those light-paths do not share any links. This creates a re-use of the wavelength in the network [1, 2].

In Figure 1.4, six light-paths are shown. The light-path between B and C, the light-path between D and E, and the light-path between E and F are not shared in any other

links in the network so they can use the same wavelength λ_1. The light-path between A and F uses wavelength λ_2 because it is sharing a link with the light-path between B and C. The same condition exists with the light-path between D and E and therefore, it uses wavelength λ_1 while light-path between E and X uses wavelength λ_2 and the light-path between X and F uses wavelength λ_1. Wavelength conversion is performed by node X. Therefore, the light-path can be set up using wavelength λ_2 on link EX and wavelength λ_1 on link XF. The wavelength conversion capabilities within the network are essential in the absence of a sufficient number of wavelengths in the network for all shared links.

The main network units in the wavelength-routing optical network are Optical Line Terminals (OLTs), Optical Add/Drop Multiplexers (OADMs), and Optical Cross Connects (OXCs) as shown in Figure 1.4. The OLTs perform the multiplexing and demultiplexing function at source and destination of the WDM link respectively. An OADM has two line ports, where each port is carrying the composite WDM signal, and a number of local ports, where individual wavelengths are added or dropped. An OXC has a large number of ports ranging from a few tens to thousands. This OXC performs the same function of OADM but with more ports and OXCs are able to switch wavelengths from one port to another. OXCs and OADMs are capable of performing wavelength conversion efficiently. OLTs have been widely used for point to point applications. OXCs and OADMs are used in long-haul and metro networks because of the huge capacities of those networks [1, 29].

1.3 Optical layer

Before illustrating the details of the optical layer, we will briefly explain the architecture of a layered network. The network consists of different units with a variety of tasks. The network tasks are assigned into different layers as shown in Figure 1.5 and this layered model was defined by the International Standard Organization (ISO) in the early 1980s [1–3]. Each layer performs a set of functions and provides services to the layer above. At the same time each layer expects services to be provided by the layer below it. The service interface between two adjacent layers is called a Service Access Point (SAP). Since there are many sets of services between layers, there are also multiple SAPs between layers. A control and management system controls each layer in the network. The network provides connection-oriented and

connectionless services to the user. The management unit performs the setting up, taking down and managing of the state of connection between source and destination nodes.

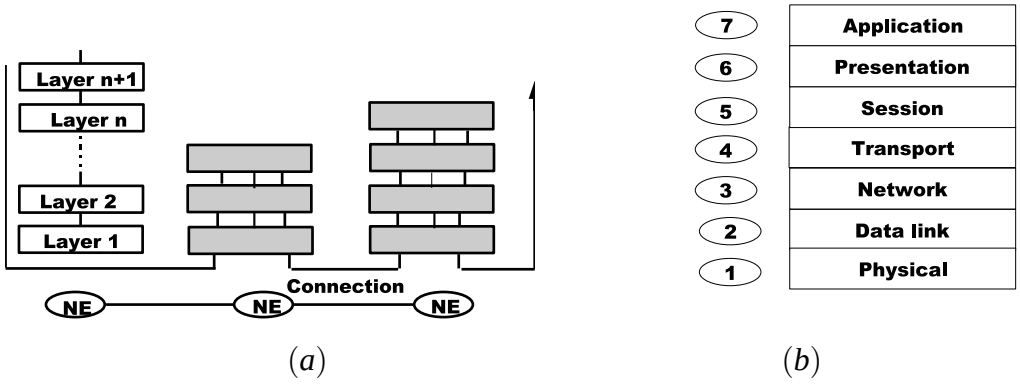

(a) (b)

Figure 1.5: Different layers of a network suggested by ISO (International Standards Organization) [1–3]; (a) Layered hierarchy of a network at each network element (NE) and (b) The classical layered hierarchy.

The following section concentrates on the connection oriented model. Each element of the network along the connection path has a set of layers starting from the lowest layer up to a certain layer in the OSI (Open Systems Interconnection) hierarchy [1–3]. The data related to different connections is multiplexed and the destination information is added to it and transmitted to the next higher layer. It is essential to specify the functions of each layer, and the interfaces between layers in the OSI model. This specification is standardized and supports the development of each layer by different developers. Optical networks consist of different layers. Each layer constitutes sub-layers as well. The classical layered hierarchy of a network which is suggested by ISO is shown in Figure 1.5(b). The *physical layer* is the lowest layer in the hierarchy which offers a specific amount of bandwidth to the next higher layers. The physical media can be optical fibre, coaxial cable, twisted-pair cable or a wireless link.

The *data link layer* is the next layer above the physical layer. The data link layer performs framing, multiplexing and demultiplexing of the data sent through the physical layer. For reliable transmission of data across the link, data is divided into frames, and framing protocols specify how data is transmitted over a physical link. This framing protocol contains overhead information for detecting and recovering link errors. Some examples of the data link protocols which operate efficiently over point to point links, are the point-to-point

protocol (PPP) and the High-level Data Link Control (HDLC) protocol. In many LANs, such as an Ethernet and token rings, the Media Access Control layer (MAC) which is included in the data link layer, manages and controls the transmissions of different nodes which share the same bandwidth.

The layer which is above the data link layer is called the *network layer*, and above the latter is the *transport layer*. The network layer provides virtual circuits (VC) or datagrams to the transport layer. This VC defines a source to destination connection with a certain set of parameters related to QoS, such as bandwidth and error rate. The data is transmitted in sequence by the source and received in the same sequence at its destination. Datagrams are small messages transmitted from source to destination with an unreliable connection. The network layer provides the routing function, passing messages from its source and delivering it to its destination. The IP layer and IP router are the main IP network elements, IP performs the routing function of packets (datagrams) in a packet-switched network. In addition, the IP provides statistical multiplexing of a number of packets and simple service restoration techniques. The IP layer has been modified to work with a different physical media, such as serial telephone lines, Ethernet, optical fibre, and coaxial cable lines. The transport layer's task is to ensure the arrival of packets in sequence and error free. An example of such layer protocol is the transmission control protocol (TCP) used in the Internet. In addition to the layers mentioned, there are layers above the transport layer, the session, presentation, and application layers. These layers are beyond the scope of this thesis.

The ATM is a networking standard that was developed to achieve many objectives, one of which was the integration of voice and data networks. An ATM network uses packets or 'cells' with a fixed size of 53 bytes = 424 bits; ATM provides a connection-oriented service (virtual circuits) and can provide different QoS guarantees. ATM is being used by system administrators as a means to provide reliable packet-switched services. Recently, more practical layered model networks use multiple protocol stacks positioned one on top of the other. Each stack includes several sublayers which may provide functions similar to physical, data link, and network layers. An example of such a system, is IP over SONET. In this case, the SONET routes and switches the connections. In other words, SONET performs the tasks of physical, data-link and network layers each of which requires at its own link. In such a scenario, the IP network treats the SONET network as supplying it with point-to-point

links between IP routers.

Another example of such a layered hierarchy network is an IP over ATM over SONET network. In some cases, an ATM use network which operates over a SONET infrastructure, to provide services for IP users, and then the converts the IP packets to ATM cells at the periphery of the network. The ATM switches are connected through a SONET infrastructure. In such a layered hierarchical network, the IP network uses the ATM network as its link layer, and the ATM network treats the SONET as its link layer.

Another layer added to the protocol hierarchy is called an optical layer. This was introduced in the second-generation of optical networks. The optical layer provides services to different user layers. Examples of user layers that reside above the optical layer are ATM, IP, SONET/SDH, Gigabit Ethernet protocol, Enterprise Serial Connection (ESCON) or Fibre channels (which provides the same function as ESCON but at a higher speeds). There are also other user layer combinations, such as ATM over optical layer or IP over ATM over optical layer. User layers use the light-paths provided by the optical layer. For example SONET networks which operate over optical layers replace connection media between two nodes with optical fibres in the physical layer. The light-path is a connection between two nodes, and a wavelength is assigned to each link on the path. Each wavelength carries data at the rate of a few gigabits per second. This is provided to the higher layer in the network based on bandwidth. The setting up or taking down of any connection path in an optical layer is performed according to inquiries from the higher layer or user. An example of this service is where the network in the circuit-switched service sets up or takes down calls in response to an inquiry from the subscriber. The network may provide permanent light-paths which were set up at the time when the network was started. This light-path service can allow high-speed connections for a variety of overlying networks.

The optical network consists of several sublayers and it provides functions which correspond to the data link and network layers in addition to the functions of the physical layer. Before the advent of the optical layer, SONET/SDH was the most widely known and was used as a transmission layer in the telecommunication network, and until now this layer has remained much the same.

The SONET layer has several features: (a) end-to-end management, (b) circuit-switched connections, (c) efficient multiplexing techniques from lower bit-rate stream to higher bit-

rate stream, (d) efficient demultiplexing techniques from high-bit rate to low-bit rate at the intermediate node, (e) high degree of network reliability and availability, and (f) comprehensive overheads that support operators to manage and observe the network. The components of the SONET network are line terminals, add/drop multiplexers (ADMs), regenerators and digital cross-connects (DCSs). The functions of the line terminals are to multiplex and demultiplex the traffic stream. Linear and ring networks use the ADMs which provide an efficient technique for dropping some of the traffic at a node and passing the rest of the traffic through the network. The regenerators regenerate the SONET signal whenever required. The function of DCSs is to switch a large number of traffic streams.

The tasks performed by the optical layer are equivalent to the tasks performed by the SONET layer. IP and SONET components use the light-paths provided by the optical layer. The low bit-rate circuit-switched traffic is multiplexed by the SONET layer and then modulated on the individual wavelength. The packet-switched high bit-rate traffic is statistically multiplexed and then modulated onto an individual wavelength. The optical layer has multiple multiplexing of the wavelengths. These wavelengths are combined into wavelength bands and they are further processed in order to produce a number of different wavelengths on a fibre. These multiple layers in the network that perform the same functions are significantly reducing network equipment costs. The SONET layer provides an efficient technique for multiplexing lower-speed connections into higher-speed connections. The SONET layer also provides an efficient mechanism for extraction of each low-speed stream from a high-speed stream. At present, it is costly to have this layer process a 10 Gb/s stream coming in on a WDM link. However the optical layer can efficiently process traffic at a bit rate 10 Gb/s on a wavelength basis, but it is not good at lower bit-rates such as 155 Mb/s. In summary the optical layer must be used for large bandwidth traffic while the SONET layer can be employed for smaller bandwidth traffic. The same idea is used in the service restoration function of these networks. The optical layer efficiently handles certain failures while the SONET layer or IP layer deals with other failures.

1.4 All-optical networks

An all-optical network belongs to the second-generation of networks. Transparency is the major feature of the light-path service provided by second-generation networks. Transparency in the network provides many useful facilities. For instance, service transparency can provide a variety of different services using the same infrastructure. In the networks where the protocols or data bit-rate have to be changed to meet future requirements, equipment compatible with the previous services may not need remodelling and the same equipment could be deployed for new requirements. The telephone network is an example of a transparent network. After a call set-up is finalized, the system provides the subscriber with a bandwidth of 4 kHz which can transmit different types of traffic on it, such as voice, data, or fax. This transparency in the telephone network has a powerful impact on our everyday facilities, and has become an important feature in the second-generation optical network.

An all-optical network is another term related to transparent networks. In other words, the data is sent from source to destination in the form of a light signal without any conversion from optical-to-electrical during its transmission. The physical layer does impose some limits on all-optical networks, due to the nature of the signals. Efficient handling of analog signals in the network requires different specification terms compared to that of digital signals and it is very difficult to operate a network that is compatible with analog and digital signals at different bit-rates.

The network is considered as a non-transparent network whenever it handles a single bit rate and protocol. The most commonly used networks today are the networks which handle digital signals with a certain range of bit rates. In-spite of the discussion on all-optical networks, electronics still plays a very important role in the management and control functions of the networks. For instance, if a signal is required to be converted from one wavelength to another, the signal is usually converted from an optical form to the electronic form and back to the optical form. The process of electronic regeneration with re-timing and reshaping, also known as 3R, is used in the paths of signals and this reduces the transparency of that path. In other words, it eliminates transparency to bit rates and framing protocols. Electronic regeneration without re-timing is called 2R if it provides transparency of bit rate without handling analog data or different modulation formats. This type of regeneration limits the number of regenerators especially at high bit rates due to the jitter which accumulates at each regenera-

tion step. The third type of electronic regeneration is called 1R, where the signal is received and retransmitted without re-timing or reshaping. The 1R regeneration can process analog data but with a lower performance compared to 2R and 3R regeneration. Optical amplifiers are extensively used for optical signal amplification without converting the optical signal to electrical form.

1.5 Optical packet switching

The most recent optical networks that provide light-paths are generally circuit-switched, although there is ongoing research in the field of optical networks to seek the possibility of providing packet-switching in the optical form. The optical packet-switched network can provide services which are provided by ATM and IP networks, such as virtual circuit services or datagram services. Each individual connection may have a bit-rate less than the total bit-rate on a wavelength or a link. In this case the network must have some time-division multiplexing facility to gather all individual connections and transmit them on one wavelength. At a high bit-rate it may be more efficient to use the OTDM [1].

The idea behind the development of optical packet switching nodes is to provide optical packet-switched technology with much higher switching capacities than conventional electronic packet switching. The node reads the header and switches the packet into the appropriate output port. In addition, the node controls the contention for output ports. All functions inside the node are performed within the optical domain. There are many limitations to signal processing in the optical domain, and one of the important factors is the lack of random access memory for buffering although these memories are available experimentally [30]. Another limitation in optical packet switching, the same as in electrical switching, is that it requires a massive amount of real-time software to control the optical network and provide a high QoS, the optical switching software is available experimentally [1, 31].

1.6 Optical communication systems

In this section the transmission basics are discussed. WDM signals are defined by the wavelength or frequency of the signals. The wavelength λ, frequency f, and the speed of light in

free space c are related by the equation: $c = \lambda f$ [1, 5]. The speed of light in free space is 2.998 x 10^8 m/s. All parameters in our simulation in this thesis will be based on the speed of light in the free space. The speed of light in a glass fibre is $(2.998 \text{ x } 10^8)/n$ m/s, where n is the refractive index of the glass, so the wavelengths varies with refractive index [7]. In free space a wavelength of 1.55 μm would correspond to a frequency of approximately 193 THz = 193 x 10^{12} Hz. Channel spacing is another critical transmission parameter. Channel spacing is defined as the spacing between two wavelengths in a WDM system. The channel spacing can also be measured in units of wavelength or frequency. The relationship between wavelength spacing and frequency spacing can be obtained by differentiating the equation $c = \lambda f$ and that gives:

$$\Delta f = -\frac{c}{\lambda_0^2}\Delta\lambda$$

This equation is accurate for optical communication systems because the wavelength spacing is small compared to the actual channel wavelength. For example, a typical spacing in WDM systems is 0.8 nm, equivalent to a frequency spacing of 100 GHz, at a wavelength λ_0 = 1550 nm. The above equation is used for calculating the channel spacing in our simulations described in Chapter 3 of this thesis.

The digital information signals in the time domain can be described as a sequence of periodic pulses. The bandwidth of a digital signal is actually decided by the signal pulse it uses (pulse width and shape). Since one pulse is employed for one bit, the pulse width is proportional to the bit period and inversely proportional to the bit rate. These digital signals have an equivalent representation in the frequency domain called the power spectrum. The energy of the signal is spread across the frequencies of the power spectrum [32]. The width of the power spectrum is the bandwidth of the signal. The bandwidth and bit rate of a digital signal are related, but the two are not exactly the same. The type of data encoding method in the communication system defines the relationship between bit rate and bandwidth. For example, the telephone line of bandwidth 4 kHz allows a bit rate of 56 kb/s allowing some sophisticated modulation techniques. Spectral efficiency defines the ratio of bit rate to bandwidth. An important issue is related to the enhancement of spectral efficiency of dense WDM systems as much as possible. The spectral efficiency is defined as η_s = b/Δv, where b is the single-channel bit rate and Δv is the channel spacing. Most commercial WDM systems in 2004 were operating with η_s less than or equal to 0.2 (b/s)/Hz, as they

were designed to transmit 10 Gb/s channels with a spacing of 50 GHz. Many laboratory experiments have illustrated that WDM systems whose channels operate at 40 Gb/s with a spacing of 100 GHz can be designed to realize system capacities of more than 2 Tb/s with a spectral efficiency of 0.4 (b/s)/Hz. Such a 50-channel system occupies a bandwidth of 5 THz that requires the whole conventional band (C-band) (approximately 1530-1565 nm). Any increase in the capacity requires either the use of both the conventional and long wavelengths band (L-band) (approximately 1565-1625 nm) or a decrease in channel spacing. For this reason, many experiments transmitted 40 Gb/s channels with a spacing of 50 GHz, provide a spectral efficiency of 0.8 (b/s)/Hz. These WDM systems either use modulation formats that are different from the standard RZ and NRZ formats or pre-filter the optical signal at the transmitter using an optical filter [33]. It is very important to note that the signal bandwidth in each channel must be smaller than the channel spacing. This will prevent interference and distortion between adjacent channels in the optical communication system. Practically, a spectral efficiency of less than 1 (b/s)/Hz can be realized when a binary modulation scheme is applied. The use of polarization multiplexing can increase above 1 (b/s)/Hz, but the improvement is limited due to the difficulty in reproducing a polarization-coded bit sequence at the receiver. Despite that, a value of 1.28 (b/s)/Hz has been achieved with polarization multiplexing. Larger values of η_s (defined as the maximum capacity of a linear channel per unit bandwidth) are possible if multilevel signalling is used. A spectral efficiency of 1.6 (b/s)/Hz was clearly achieved in an experiment in 2003 in which a format known as differential quadrature phase shift keying (DQPSK) was used in combination with polarization multiplexing [33].

WDM systems use the 1.55 μm wavelength window for two reasons, firstly the loss occurring in the optical fibre is the lowest in this window and secondly the best performance of the optical amplifiers is possible in this window. However, early WDM systems used C-band. At present, L-band and C+L-band are being used due to the development of optical amplifiers in this window.

1.7 Components of optical communication systems

The block diagram in Figure 1.6 is a general diagram of a fibre optic communication system. An optical fibre cable is used as the communication medium. The optical transmitter and receiver are designed in such a way so as to meet the requirements of the optical fibre communication channel [5, 7, 34]. In this section, an introductory overview of transmitter, 1.7.1, fibre, 1.7.2, and receiver, 1.7.3 is given.

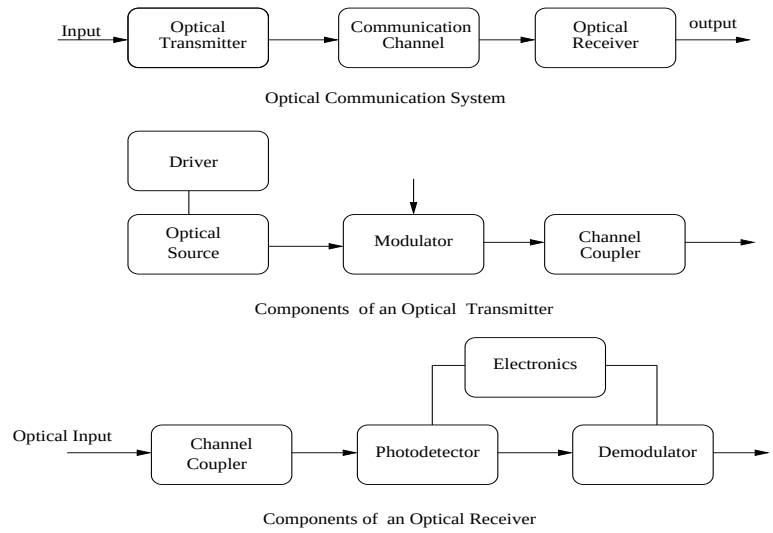

Figure 1.6: Block diagram of a fibre-optic communication system, transmitter components, and receiver components.

1.7.1 Optical transmitters

The main function of an optical transmitter is to convert the electrical signal into an optical form and then send the generated optical signal into the optical fibre which is used as a communication channel. Figure 1.6 shows the schematic diagram of an optical transmitter.

The optical source and modulator are the basic blocks of the optical transmitter [5, 34]. A coupler is normally a micro-lens that is used to focus the optical signal on the input plane of an optical fibre with maximum possible efficiency. The optical power which is generated by the transmitter is an important design parameter in optical communication systems [35]. When the transmitter power is high the spacing between amplifiers in the transmission link increases, but the maximum value of the power is limited by nonlinearity effects which will be discussed in Section 1.7.7.

Most communication systems use semiconductor lasers as optical sources, because of their narrow optical bandwidth that allows operation at high bit-rates with less dispersion, enhancing spectral efficiency. For instance, the lowest cost laser available is the Fabry-Perot, but this type of laser has the worst dispersion because of its wide optical line-width, typically of 125-500 GHz [36]. Standard Distributed Feedback (DFB)lasers typically have optical line widths on order of 12 GHz. It operates on gigabit data rates which can be a serious limitation for distances over 50 km. Screened DFB is basically the same laser design as the standard DFB, however it has been selected for its very narrow line-width, typically 1-5 GHz. This specification allows the link to reach much longer distances at gigabit data rates when data rates are in the low gigabit range and transmission distances are less than 100 km, most fibre optic transmitters use directly modulated lasers [37]. However, as the data rates and span lengths grow, wavelength chirp caused by turning a laser ON or OFF, limits the data rates. The wavelength chirp widens the effective spectral width of the laser which causes dispersion problems which will be discussed in Section 1.7.6. A laser source with no wavelength chirp and a narrow line-width provides one solution to the problem. This solution takes the form of external modulation which allows the laser to be on continuously. The modulation is accomplished by an external modulator placed outside of the laser cavity, which converts the continuous wave light into a data-coded pulse stream with the proper modulation format. Two main categories of optical modulators developed for lightwave system applications are: the electro-absorption and electro-optic materials modulators.

The performance of an external modulator is specified by the modulation bandwidth and the ON-OFF ratio, which is also known as extinction ratio [19, 38, 39].

1.7.2 The optical fibre

Optical fibres possess many characteristics that make it an excellent physical medium for high-speed transmission. By using a low-attenuation window, which is shown in Figure 1.7, the signal loss for a set of wavelengths can be made very small, thus, reducing the number of amplifiers and repeaters needed.

Figure 1.7: The attenuation regions of an optical fibre [4, 5].

Fibre is flexible, reliable in corrosive environments and is made from one of the mostly readily available substances on earth, sand (silica). Fibre transmission is immune to electromagnetic interference. This makes fibre ideal as a transmission medium unlike copper [1, 4, 5, 34]. An optical fibre operates on the principle of total internal reflection. Total internal reflection occurs when light travels at different speeds in different materials. A dimensionless number called the refractive index, relates to the different mediums through which the light is travelling. The refractive index, n, is the ratio of the velocity of light in vacuum c to velocity of light in a specific medium v [5, 7].

$$n = \frac{c}{v} \tag{1.1}$$

As light passes from one medium to another with a different index of refraction, the light is refracted. Thus, if the light passes from a lower refractive index to one with a higher

refractive index, the light is bent toward the normal axis. However, if the light passes from a higher to a lower refractive index the light is refracted away from the normal axis. *Snell's Law* calculates the amount the light is bent and is given by [5, 7]:

$$n_1 \sin\theta_1 = n_2 \sin\theta_2 \tag{1.2}$$

The angle of refraction approaches 90^0, as the angle of incidence increases. The angle of incidence is called the critical angle when the refraction angle is of value 90^0. Increasing the angle of incidence above the value of the critical angle results in total internal reflection. This is a basic principle for the operation of the optical fibre. The critical angle is calculated as follows:

$$\theta_c = sin^{-1}\frac{n_2}{n_1} \tag{1.3}$$

Where, n_1, and n_2 are the refractive indices of the core and cladding. The core of an optical fibre has a higher refractive index than the cladding $n_1 > n_2$, allowing total internal reflection. In optical fibre, propagation delays are related to the refractive index of the material. Propagation time through a fibre is calculated as follows:

$$t = \frac{L * n_{eff}}{c} \tag{1.4}$$

$$n_{eff} = \frac{\beta\lambda}{2\pi} \tag{1.5}$$

Where, t is the propagation time in seconds, L is the fibre length in meters and n_{eff} is the effective refractive index of the propagation mode, and n_{eff} is a number quantifying the phase delay per unit length in a waveguide, relative to the phase delay in vacuum, the symbol β is the propagation constant and defines phase change per unit length for light propagating in a medium or waveguide, λ is the wavelength of the propagating optical signal [40]. There are two basic types of optical fibre: multimode fibre and Single Mode Fibre (SMF). These propagation modes are determined by a parameter called the *Normalized Frequency (V)* and defined by the equation:

$$V = \frac{2\pi}{\lambda} a \sqrt{n_1^2 - n_2^2} \tag{1.6}$$

Where a is the core radius, n_1 and n_2 are the refractive indices of the core and cladding respectively, and λ is the wavelength of the optical signal. When the value of V is less than 2.405, the fibre transmits the optical signal in a single propagation mode. This happens in a SMF. The SMF, as shown in Figure 1.8, is designed by choosing a very small core

diameter ranging 5 to 10 μm. This will support the elimination of all higher order modes at the operating wavelength.

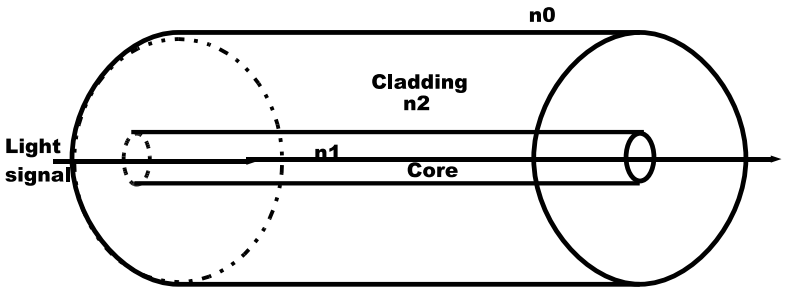

Figure 1.8: Single mode fibre.

A SMF allows the transmission of information at a higher capacity because it is able to retain the quality of each light pulse over longer distances and does not exhibit dispersion caused by multiple modes [1, 4, 5, 7, 34]. SMFs also have lower fibre attenuation than multi-mode fibre, which is typically 0.2 dB/km at wavelengths around 1550 nm. Attenuation and dispersion will be discussed in detail in Sections 1.7.5 and 1.7.6. The SMF has a few disadvantages which include: coupling of light into the core becomes more difficult due to the small core diameter, and the tolerances for single mode connectors and splices are much more demanding.

1.7.3 Optical receivers

The function of an optical receiver at the end of the optical fibre is to convert the optical signal into an electrical signal. As shown in the schematic diagram in Figure 1.6, the light detector is the basic block of the receiver [1, 5, 7, 34]. A light detector performs the conversion from the optical signal into electrical impulses, such as data, video, or audio signals that are used by the receiving end of the system. The most common detector is the semiconductor photo-diode, which produces current in response to incident light. Light striking the photo-diode creates a current in the external circuit. Both Positive-Intrinsic-Negative (PIN) photodiodes and Avalanche-Photo-Diodes (APD's) are designed to be used as detectors for fibre optic systems. Responsivity is one of the most important detector specifications because it defines the relationship between optical input and electrical output. The responsivity of a photodetector is the ratio of the current output to the light input. The higher the responsivity

of photodetectors, the better the sensitivity of the receiver. Since responsivity varies with wavelength it is specified either at the wavelength of peak responsivity or at a wavelength of interest [1, 5, 34]. Quantum efficiency is an important specification of a photodetector, and is the ratio of primary electron-hole pairs created by incident photons to the photons incident on the diode material. A few factors that prevent the quantum efficiency from being 100% are coupling losses from the fibre to the detector, absorption of light in the P or N region of the photo-diode, and leakage current in the detector.

The capacitance of a photodetector may also be specified and this will depend on the active area of the device, and the reverse voltage across the device. The response time, which is another important specification, represents the time needed for the photodiode to respond to optical inputs and produce an external current. The photodiode capacitance, the load resistance, and the design of photodiode are three parameters which determine the response time. Dark current is a small current which flows through the detector in the absence of light. This is because of the intrinsic resistance of the detector and the applied reverse voltage. The dark current contributes to the detector noise.

Noise is a phenomenon that limits detectors and is any electrical or optical energy other than the signal itself. Noise appears in all elements of a communication system. However, it is usually most critical in the receiver because the receiver is trying to interpret an already weak signal. The same noise in a transmitter is usually insignificant since the signal at the transmitter is much stronger than the attenuated signal that the receiver picks up.

There are two main categories of noise in the receiver. Shot noise occurs because the process of creating the current is a set of discrete occurrences rather than a continuous flow. As more or fewer electron-hole pairs are created, the current fluctuates, creating shot noise. Shot noise occurs when no light falls on the detector. Even without light, a small current, dark current, is thermally generated. Noise increases with the current and bandwidth. When only dark current is present, noise is at a minimum, but it increases with any current resulting from optical input. Thermal Noise is the second type of noise, it arises from fluctuations in the load resistance of the detector. The electrons in the resistor are not stationary, and their thermal energy allows them to move about. At any given moment, the net movement toward one electrode or the other generates random currents that add to and distort the signal current from the photodiode. Shot noise and thermal noise exist in the receiver independent of the

arriving optical power. The signal quality at the photodetector can be expressed as the Signal-to-Noise Ratio (SNR) [1, 5, 34]. The SNR is a ratio of average signal power and total noise power, and can be written as

$$SNR = \frac{S}{N} \tag{1.7}$$

$$SNR(dB) = 10\ \log_{10}(\frac{S}{N}) \tag{1.8}$$

In equation (1.7), the information to be transmitted is denoted by signal (S), while the integration of all noise factors over the full system bandwidth is denoted by noise (N). In equation (1.8) this ratio is expressed in decibels.

The demodulator is another important block in the receiver diagram. The type of demodulator depends on the modulation format used by the optical communication system. Intensity Modulation with Direct Detection (IM/DD) is used by most optical communication systems. A decision circuit performs the demodulation function through the identification of the bits as 1s or 0s. This decision depends on the amplitude of the received electrical signal. The efficient performance of the decision circuit depends on the SNR of the electrical signal at the photo-detector.

Figure 1.9: Relationship between BER and Q-factor for Gaussian noise statistics [5, 6].

The Bit-Error Rate (BER) or Q-value (Q-factor) can be used as the measure of the quality of the performance of the digital optical communication system [5, 41, 42]. The BER can be

specified as the average probability of incorrect bits recognized at the receiver. The receiver sensitivity can be defined as the minimum optical power that must be present at the receiver in order to achieve the performance level required for a given system. The receiver sensitivity analysis will be affected by several factors such as the source intensity noise, noise generated in amplifier and the noise in the receiver. The shot noise, as defined earlier, is the dominant form of receiver noise. Receiver noise is directly proportional to the square root of the receiver's bandwidth. The receiver sensitivity also depends on the bit-rate as some noises (such as shot noise) increase in relation to the signal bandwidth; time jitter is instability in the pulse arrival time and inter-symbol interference is the outcome of other bits interfering with the required bit. Any factors mentioned in the sensitivity analysis may affect bit error. The BER of a system can be estimated as follows [5, 7, 19, 38]:

$$BER = Q \cdot \left[\sqrt{\frac{I^2}{4\,N\,B}} \right] \tag{1.9}$$

Where N is noise power spectral density (A^2/Hz), I is the effective signal amplitude (Amperes), B is bandwidth (Hz), and Q(x) is cumulative distribution function (Gaussian distribution).

The relationship between the Q-factor and the Bit Error Rate can be written as follow:

$$\text{BER} \approx \frac{\exp(-Q^2/2)}{Q \cdot \sqrt{2\pi}}, \tag{1.10}$$

$$Q = \frac{|\mu_1 - \mu_0|}{\sigma_1 + \sigma_0} \tag{1.11}$$

where μ_1 and μ_0 are the mean of bits 1 and 0 respectively, σ_1 and σ_0 are the standard deviation of bits 1 and 0 respectively. These values can be measured from the eye-diagram of the received signal [19]. The approximate form of BER in equation (1.10) is accurate for Q $>$ 3. The BER improves as Q increases, and BER becomes less than 10^{-12} for Q > 7. The receiver sensitivity corresponds to the average optical power for which Q ≈ 6. Figure 1.9 shows the variation of the BER with the Q factor and when Q = 6, the BER$\approx 10^{-9}$ [5].

As shown in Figure 1.10 optical SNR is also a measure for the quality of the performance of the digital optical communication system [5]. The Optical signal-to-noise ratio (OSNR) is the ratio of the received optical signal power to the noise signal power. The OSNR is measured before a demodulator and its value is important because it provides information

about the received noises which are dominated by the cascaded optical amplifiers in the communication link. The OSNR gives information about the performance of the optical networks [35]. The OSNR is used in this thesis (in Chapter 6) for analysis of the quality of the received signal during power transient phenomenon of the EDFAs.

The BER and OSNR are interrelated as shown in Figure 1.10 [7]. The variation depends on the data encoding method, Figure 1.10 is for Non-Return to Zero (NRZ) data. A higher OSNR yields a lower BER. Receiver sensitivity is obtained by the optical power necessary to achieve a required OSNR, and hence a given BER. For instance, an OSNR of 10 dB would yield a BER of about 10^{-6}. Improving the OSNR by only 0.9 dB to 10.9 dB enhances the BER by a factor of 1000 times to 10^{-9} [5, 7, 19, 38].

Figure 1.10: Relationship between BER and OSNR, this curve is typical for NRZ data [7].

1.7.4 Characteristics of optical fibre

In this section, we introduce and define the characteristics of optical fibre that are related to optical communication system impairment [43].

1.7.5 Attenuation

As the light signal propagates through the fibre, it is attenuated. In other words, the power of the signal is decreased. Attenuation (loss) is a logarithmic relationship between the optical output power and the optical input power and is a measure of the loss of light power, that occurs as light pulses transmit through the length of the fibre [1, 4, 5, 7, 34]. Figure 1.7 shows the two low-attenuation regions of optical fibre [1, 4, 5]. The first is a small trough centered at about 1300 nm, has a range of about 100 nm and the attenuation is less than 0.5 dB/km. The total bandwidth in this region is about 25 THz. A second, much wider trough, is centered at about 1550 nm, has a range of about 200 nm, with attenuation as low as 0.2 dB/km. Combined, these two regions occupy a bandwidth of 50 THz. The three peaks in the loss are shown in Figure 1.7 as occurring at about 950 nm, 1240 nm, and 1390 nm. These peaks are due to the presence of residual water vapor in silica and correspond to a hydroxyl ion (OH^{-}) impurities in the fibre.

Attenuation in optical fibre is caused by several intrinsic and extrinsic factors. Two intrinsic factors are scattering and absorption. The most common form of scattering is Rayleigh Scattering, and it is caused by microscopic non-uniformities in the optical fibre. It becomes important when the size of the structures in the glass itself are comparable in size to the wavelengths of the light travelling through the glass. Thus, long wavelengths are less affected than short wavelengths. The fibre attenuation (α) decreases as the wavelength (λ) increases and is proportional to λ^{-4}. Extrinsic causes of attenuation include cable manufacturing stresses, environmental effects, and physical bending of the fibre. The decay in the power transmitted along the fibre is exponential and can be expressed as [1, 7]:

$$P_l = P_0 \, e^{(-\alpha L)} \tag{1.12}$$

Where, P_l is the optical power at distance L from the input, P_0 is the optical power at fibre input, α is the fibre attenuation coefficient. In terms of decibels, the equation may be rewritten as [5]:

$$\alpha(dB/km) = -\frac{10}{L}\log_{10}\left(\frac{P_l}{P_0}\right) \approx 4.343\alpha \tag{1.13}$$

Most of the optical communication systems use the low-loss band centered at 1550 nm. The fibre losses are compensated by using optical amplifiers in the communication link. The

in-line optical amplifiers are either semiconductor optical amplifiers or Erbium-doped fibre amplifiers (EDFA) which are discussed in Section 1.8.1. Recently, the usable bandwidth of fibres in most long-distance networks is limited by the bandwidth of the EDFAs. The low-loss band at 1550 nm is divided into three regions. The middle band from 1530 to 1565 nm is C-band where WDM communication systems run using C-band EDFAs. The band from 1565 to 1625 nm, is called L-band is used in high capacity WDM systems. The gain-shifted C-band EDFA includes the wavelength range of C-band but the peak of the spectrum is shifted from around 1550 nm to around 1560 nm (to the last region of C-band), and developed in this thesis and used for investigation of the power transients in the circuit-switched and packet-switched traffic in Chapter 4. The band below 1530 nm consists of wavelengths shorter than those in the standard C-band, is called the S-band.

1.7.6 Dispersion

The light signals travelling at different speeds through a fibre causes temporal spreading of the signal. This is either due to modal or chromatic effects [1, 4, 5, 7, 34]. The modal dispersion is also called multimode dispersion because it is a characteristic of multimode fibre only. Chromatic dispersion occurs due to material dispersion, waveguide dispersion or profile dispersion. At a wavelength near 1550 nm the chromatic dispersion goes to zero in dispersion-shifted fibre (DSF). Standard fibre, multimode or single mode, has zero dispersion at a wavelength of 1310 nm. The main advantage of single-mode fibre is that intermodal dispersion is absent because the energy of the injected pulses is transported by a single mode. However, pulse broadening does not disappear altogether. The group velocity associated with the fundamental mode is frequency dependent because of chromatic dispersion. As a result different spectral components of the pulse travel at slightly different group velocities, a phenomenon referred to as *group-velocity dispersion (GVD)*, or *fibre dispersion*.

In optical communication systems, the shape of pulses propagating is not preserved. The important parameter controlling the evolution of pulse shape is the second derivative, $\beta_2 = d^2\beta/dw^2$ of the propagation constant β. β_2 can be explained as follows, if $\beta_1 = d\beta/dw$, $1/\beta_1$ is the velocity with which the pulse propagates in optical fibre and is known as the group velocity. β_2 is related to the rate of change of group velocity with frequency. For most optical fibres, there is wavelength at which the GVD parameter $\beta_2 = 0$, and this is called

the zero dispersion wavelength. If $\beta_2 > 0$, the chromatic dispersion is defined to be normal. When $\beta_2 < 0$, the chromatic dispersion is defined to be anomalous [5]. D is called dispersion parameter and can be computed from equation (1.14) in units of ps/nm/km.

$$D = -\frac{2\pi c}{\lambda^2}\beta_2 \tag{1.14}$$

The dispersion effects cause the broadening of the lightwave pulses when the lightwave communication system is dispersion limited. The factor of pulse broadening was given by Agrawal [5]:

$$\frac{T_z}{T_0} = \sqrt{\left[1 + \left(\frac{\beta_2 \times z}{T_0^2}\right)^2\right]} \tag{1.15}$$

Where, the parameter T_0 represents the half-width at an intensity 1/e, at distance z = 0. It is related to the full-width at half-maximum (FWHM) of the pulse by the relation,

$T_{FWHM} = 2\ (ln2)^{1/2}\ T_0 \approx 1.6665\ T_0$

Where T_z is the half-width, defined similar to T_0, at distance z along the fibre. In the equation (1.16), L_D represents the dispersion length.

$$L_D = \frac{{T_0}^2}{|\beta_2|} \tag{1.16}$$

The oldest and most widely used single-mode fibre is non-dispersion-shifted fibre (NDSF). This type of SMFs were initially designed for use near 1310 nm. The NDSF has very high dispersion at 1550 nm. Thus, another SMF has been developed, the dispersion-shifted fibre(DSF), that shifted the zero-dispersion point to the 1550 nm region. It was found that while DSF performed well at the single 1550 nm wavelength, it contained serious nonlinearities when many, closely-spaced wavelengths near 1550 nm were transmitted in DWDM systems. Due to these nonlinearities other fibres were developed. These are grouped as non-zero-dispersion-shifted fibres (NZ-DSF). The fibre is available in both positive and negative dispersion varieties and is quickly becoming a widely used fibre in modern telecommunications systems [44, 45].

1.7.7 Nonlinear optical effects

Nonlinear effects in fibre have become very important as transmission lengths, optical power levels, number of wavelengths and optical fibre data rates have increased. Intense electromagnetic fields (light) produce nonlinear effects in any dielectric material. The waveguide

geometry that confines light to a small cross section over long fibre lengths makes nonlinear effects quite important in the design of modern communication systems which must be considered in designing optical systems. Such effects include Stimulated Brillouin Scattering (SBS), Stimulated Raman Scattering (SRS), Four-Wave Mixing (FWM), Self-Phase Modulation (SPM), Cross-Phase Modulation (XPM) and Inter-Modulation mixing. All these nonlinearities are important as they represent fundamental limiting mechanisms to the amount of data that can be transmitted on a single optical fibre.

The two most important parameters leading to fibre nonlinearities are the refractive index of glass which is a function of the optical power passing through the material, and the effective area of the fibre core. The equation for the refractive index of the core in an optical fibre is [5, 7]:

$$n = n_0 + n_2 \left(\frac{P}{A_{eff}} \right) \tag{1.17}$$

Where, n_0 is the refractive index of the fibre core at low optical power levels, n_2 is the nonlinear refractive index coefficient $(2.6 \times 10^{-20} m^2/\text{W}$ for silica fibre), P is the optical power, A_{eff} is the effective area of the fibre core. The intensity dependence of the refractive index is referred to as the *Kerr-nonlinearity* or *Kerr-effect*, which results in induced-phase shifts in the propagated signal, and hence spectral broadening.

The equation shows that by minimising the power, P, and maximising the effective area of the fibre, A_{eff}, the nonlinearities introduced by the power dependence of the refractive index are reduced.

- SBS occurs when a powerful light wave travels through a fibre and interacts with phonons of the acoustic vibration modes in the glass. This causes a scattering mechanism that reflects much of the light back to the source. SBS imposes an upper limit on the amount of optical power that can be usefully launched into an optical fibre. The SBS effect has a threshold optical power. When the SBS threshold is exceeded, a significant fraction of the transmitted light is redirected back toward the transmitter. This results in extra attenuation of the optical power reaching the receiver, as well as problems associated with the back reflection of the optical signal. The SBS process also introduces significant noise into the system, resulting in degraded bit error rate (BER) performance. Controlling SBS is particularly important in high-speed trans-

mission systems that employ external modulators and continuous wave (CW) laser sources. The precise threshold for the onset of the SBS effect depends on a number of system parameters including wavelength (the threshold is lower at 1550 nm than 1310 nm) and line-width of the transmitter. The SBS threshold increases proportionally as the optical sources or laser line-width increases. SBS is minimised by broadening the effective spectral width of the optical source [5, 7].

- SRS is a fibre nonlinearity similar to SBS while for SRS photons are scattered by interaction with optical phonons, and SRS has a much higher threshold [5, 7]. This mechanism causes the transfer of power from shorter wavelength signals to longer wavelength signals. SRS is much less of a problem than SBS. Its threshold is nearly a thousand times higher than SBS. SRS is a third-order nonlinear effective susceptibility.

- FWM usually appears in fibre optic transmission systems that simultaneously carry many wavelengths, such as DWDM systems [5, 7]. FWM is a third-order nonlinear effective susceptibility , as is described with a $X^{(3)}$ coefficient. It can occur if at least two different frequency components propagate together in a nonlinear fibre. A refractive index modulation at the difference frequency occurs, which creates two additional frequency components. These cross products cause problems because they often fall near or on top of the desired signals. The magnitude of the FWM products is determined by the FWM mixing efficiency [46, 47] . Two factors strongly influence the FWM mixing efficiency. The first is the channel spacing. The mixing efficiency increases greatly as the channel spacing becomes smaller. The second factor is fibre dispersion, because the mixing efficiency is inversely proportional to the fibre dispersion, being strongest at the zero-dispersion point. In all cases, the FWM mixing efficiency is expressed in dB, and more negative values are better since they indicate a lower mixing efficiency [1, 5, 34].

- SPM, like FWM, is due to the power dependency of the refractive index of the fibre core. It interacts with the chromatic dispersion in the fibre to change the rate at which the pulse broadens as it travels down the fibre. SPM causes a frequency chirp on the rising and falling edges of an optical pulse. Increasing the fibre dispersion will increase the impact of SPM but will reduce the impact of FWM. XPM is very similar

to SPM, except that it involves two pulses of light, whereas SPM needs only one pulse. XPM causes multiple pulses travelling down the fibre to interact through their mutual effect on the refractive index of the fibre. XPM causes pulses to become distorted as they interact. Fibre designs with larger effective areas reduce XPM and all other fibre nonlinearities. Inter-modulation mixing is similar to XPM and SPM except that it causes new frequency components to appear that are cross-products of the original frequencies.

1.8 Optical amplifier

Any communication medium attenuates the signal that passes through it. This is also the case with fibre optic transmission media [5]. In the silica fibres, the attenuation coefficient α varies with wavelength as mentioned in Section 1.7.5 and as shown in Figure 1.7. Thus, the transmission distance is limited for fibre optic communication systems by fibre loss. In the early stage of long-haul fibre optic communication systems development, this limitation was resolved by using optoelectronic repeaters, as discussed in Section 1.4. These regenerators have become sophisticated and costly in WDM optical networks compared to the alternative techniques available. Optical communication systems loss is self-compensated by using optical amplifiers. These amplifiers directly amplify the light signal and there is no need for signal conversion. An optical amplifier may be defined as a laser without feedback from the optical cavity. In the amplifier's gain medium, stimulated emission causes the amplification of the incoming light signal.

During the 1980s, different types of optical amplifier were developed. During the 1990s these amplifiers were applied to long-haul light-wave communication systems. First semiconductor amplifiers were used, but then fibre-based amplifiers became more interesting owing to their low coupling losses, polarization insensitivity, inter-channel crosstalk and noise figure [48]. Raman amplifiers require high pump powers (from 0.5 to 1 W), whereas semiconductor lasers do not readily provide such high power [49], thus, at present Raman amplifiers are not used as much as EDFAs. Fibre-Brillouin amplifiers have small bandwidth and it is not feasible to use them as in-line amplifiers in light-wave communication systems although they require low pump powers for operation. Silica fibres doped with rare-earth

ions were later developed as a new kind of fibre amplifier. The EDFA was found to be the most suitable for light-wave communication systems. The EDFA has been an important technology in the evolution of optical communication systems. EDFAs were first developed in 1987 and the first commercial EDFAs in 1990 [34]. EDFAs were used in 1992 for video distribution in the cable TV industries and in 1995 they were used as in-line amplifiers for the undersea trans-Pacific fibre cable system. In addition, EDFAs are used for soliton communication systems [6, 8, 50, 51]. Recently, with the development of high pump power laser diodes, the application of Raman amplifiers as a complement to EDFA amplification is being widely encouraged [52, 53].

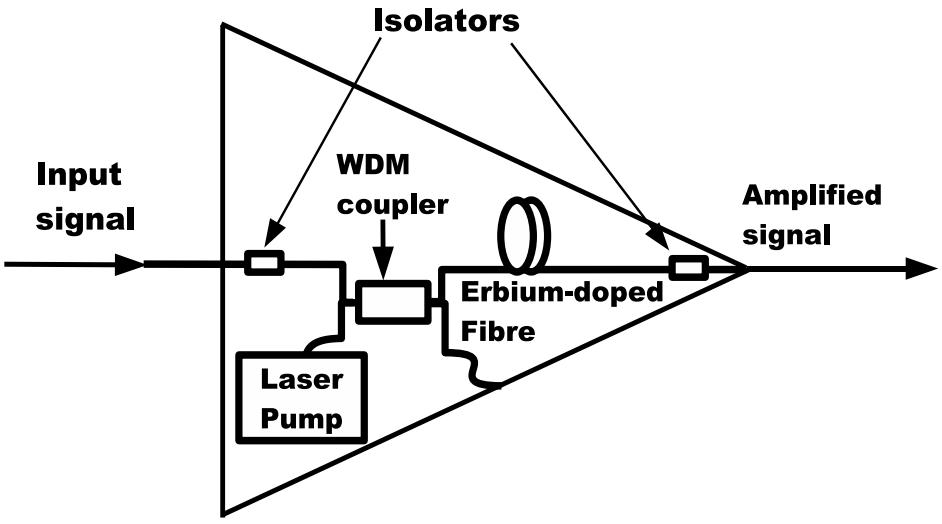

Figure 1.11: Internal structure of a simple erbium-doped fibre amplifier.

1.8.1 Erbium doped-fibre amplifier

The research on active-fibre technology in the 1550 nm wavelength region has been motivated by the development of erbium-doped glass fibres. As the result of which, research concentrated on the applications of the rare-earth doped fibre resulting in high-gain erbium-doped fibre amplifiers, the applications of these active fibres are now widespread and include optical amplifiers, lasers, switches, and a variety of nonlinear devices. The good performance of optical amplifiers and other devices enhance optical communication systems and support designers in achieving transmission requirements. The EDFA is most commonly used be-

cause of its excellent amplification properties near 1550 nm, the wavelength region in which the fibre loss is minimal [54]. As shown in Figure 1.11, the main part of the EDFA amplifier is fibre doped with erbium, a rare earth element that has suitable energy levels in its atomic structure for amplifying light signals in a band of 1530 nm to 1625 nm. The EDFA 'pump' laser injects energy into the Erbium-Doped Fibre (EDF) at a wavelength of 1480 nm or 980 nm. When the input light signal enters the EDF, this light signal stimulates the erbium ions to radiate their stored energy. This energy is added to the input light signals. This process continues along the erbium-doped fibre, growing stronger as it travels through. At the end, the light signal between wavelength of 1530 nm and 1565 nm is amplified. However, noise is generated through Amplified Spontaneous Emission (ASE) [1, 5, 34], when erbium ions are not stimulated by the input signal. These erbium ions emit light through spontaneous transition and that adds noise to the original amplified signal. The ASE noise is accumulated during the cascaded EDFAs in the network link and can degrade the network performance. However, filters can remove some of the unwanted noise. The EDFA can amplify the light signals in the C and L bands, and the hybrid EDFA can amplify the light in the wideband 1530-1625 nm (C + L band) [7, 55].

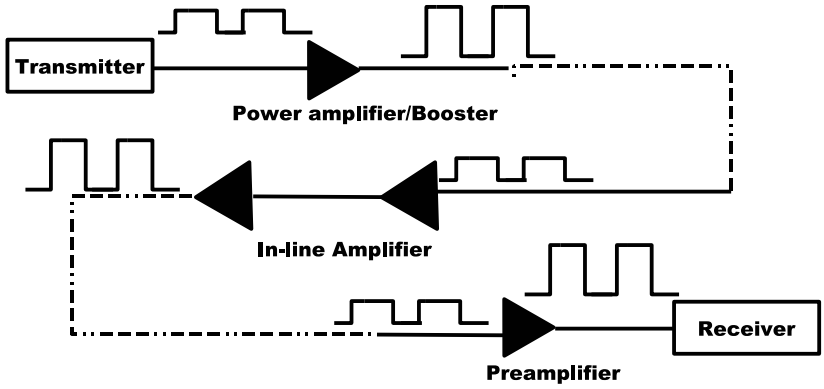

Figure 1.12: Different applications for the EDFA in optical communication networks.

The EDFA can serve many purposes in the communication network systems, as shown in Figure 1.12. There are three major functional categories of EDFAs: The power amplifier/booster is placed directly after the optical transmitter, the in-line EDFA amplifies the small signals along the network link, and the preamplifier provides loss compensation for the optical network at the receiver.

This thesis is concerned with the investigation of power transient phenomena of in-line EDFAs in WDM networks. This phenomenon affects the performance quality of the networks. The power transients which are studied in this thesis occur through system reconfiguration, as in circuit-switched networks, or the nature of the network traffic as in packet-switched networks. The EDFA's basic properties, and the modelling, and analysis of its power transients are presented in detail in the following chapters.

To mitigate the effects of EDFA optical power transients on optical networks, different protection schemes have been reported and implemented either numerically or experimentally. These approaches have been proposed to mitigate the EDFA power transients in specific conditions or for a particular application. The survey below shows some recent approaches developed to mitigate EDFA power transients.

1.9 Approaches to channel protection

In optical networks, channels will suffer from output power transients caused by a link failure, a network reconfiguration or from the nature of the traffic of the network. These power transients (which will be modelled and analysed in the following chapters), affect the performance of the networks. The QoS provided will be unacceptable to the users. The speed of the power transients is proportional to the switching time of the optical power which is input into the EDFAs in the networks. Therefore, the recovery technique which is required to protect against such power transients must be extremely fast for large networks. Several schemes to protect the cascaded EDFA network links against the fast power transients have been developed in recent years [52].

1.9.1 Pump control

The gain of an EDFA can be adjusted by the control of its pump current. One approach controls the pump current in the time scales of the spontaneous lifetime of EDFAs [8]. Another has used low-frequency feed forward compensation with a low frequency control loop [56]. Further approaches have been proposed after the discovery of fast power transients, e.g. pump control on short time-scales has been demonstrated to limit the power transients of the surviving channels [57]. The automatic pump control in a two-stage EDFA operating on a

time scale of microseconds has been implemented experimentally, 7 channels were added or dropped in an 8-channel WDM system. The power transients exceeded 6 dB without the application of a gain control technique. When the pump control technique was added to the experimental set-up, the power transients reduced to less than 0.5 dB both for power dropped and power added conditions. The speed of the control circuit was within 7-8 μs, and in this way, the power transient effects on the surviving channels decreased [58, 59].

Several other approaches have also been implemented to mitigate the effect of the EDFA optical power transients on optical networks, and have been demonstrated by both Mehta and Karkasek, including the gain control technique, to enhance the performance of all-optical EDFAs networks during power transients [60–62].

1.9.2 Link control

The disadvantage of the pump control technique mentioned above, is that it requires protection at every EDFA in the network. The word "link" here refers to a segment between two network elements or nodes, where channels can be added or dropped. Another technique to control the gain of amplifiers employs a control channel in the transmission band. An approach compensating the power transients in an EDFA at low frequencies ($<$ 1 kHz) by use of an idle compensation signal has been reported [63]. Another link control technique demonstrated by Srivastava and Zyskind uses the fast link control protection of surviving channels in the multi-wavelength optical networks. In this approach, a control channel is added before the first optical amplifier in a link (the output amplifier of a network element). The control channel is removed at the next network element. This technique protects the surviving channels on a link-by-link basis. The power of the control channel is such that total power of the signal channels and control channel is kept constant at the input of the first amplifier. This will maintain constant loading at the input of all EDFAs in the link.

Desurvire and Zirngibl have demonstrates a link control scheme [63]. The experiment used 8 channels including the control channel. The fast feedback circuit was used to align the line control channel power to maintain constant total power. The fast feedback circuit with a response time of 4 μs was used to adjust the power of the line control channel to keep the total power of the communication system constant. The signal and control channels are transmitted through seven cascaded EDFAs. The BER was measured on one of the

signal channels. It was found that, in the absence of a control channel, and when 5 out of 7 channels were added or dropped at a rate of 1 kHz, the surviving channels suffer power transients exceeding 2 dB and deterioration in BER. This power penalty is decreased to a few tenths of a dB, and BER adjusted to within the acceptable limit of network performance when the fast link control circuit was switched on [52]. Another approach, such as that used by Dimopoulos added an additional channel with the input signal channels to compensate for the increase or decrease of the input power during the single channel failures to maintain an acceptable level of survivability at low cost [64].

1.9.3 Laser control

A new scheme for link control based on laser gain control has been developed. A compensating signal in the first amplifier is generated using an optical feedback laser loop and then propagates down the link [65]. This forces the EDFA to go into lasing oscillation at an out of the band frequency, limiting the gain of the amplifier independent of the total input power. Once the power transients start to occur, the lasing signal is treated as an additional signal in the link. The laser gain control scheme has been demonstrated by Zirngibl [66]. Another approach using this technique was developed by Jackel and Richards [65]. In their approach, they succeed in combining laser control with the link control scheme mentioned above. The system stabilized within a few microseconds and the power penalty decreased to a few tenths of a dB after 6 EDFAs in the link. The draw-back of this scheme is that the speed of the response time is directly related to the laser relaxation oscillations which are generally on the order of tens of microseconds or slower [67, 68]. Homogeneous broadening of EDFAs, with the resulting spectral hole burning, can create gain variations at the signal wavelength, which will limit the range of control from this technique. This problem also applies to the link control scheme.

Much research, based on the above three basic schemes, have been implemented to mitigate the effect of the EDFA power transients in optical networks, e.g. Pavel has developed an approach both for transient power control across optical communication links, and for spectral power control at EDFA sites [69]. It is obvious that the two parameters of optical power control are: transient power control at optical line amplifier sites, and spectral power control (equalizing the optical powers of each channel in the spectrum at dynamic EDFA

sites). A transient control strategy was proposed based on a combination of feed-back and feed-forward control. A spectral control approach based on decoupling the control loops by using time-constant layering [69].

Many comparative investigations of techniques to control power transients in wavelength routed optical networks have been carried out. One of these was by Olivers [70], who analysed extreme conditions for the addition or dropping of channels. His results showed these techniques performed satisfactorily. However, differences were noticed regarding the efficiency, complexity, and implementation cost of each technique.

In addition to channel addition or removal in optical networks, there are two other types of signal disturbances that affect the performance of the optical networks: pilot tones and bursty traffic. Pilot tones are used to track and monitor the performance of each channel. Binary data can be frequency modulated upon the pilot tone, and this is important for signal routing. Tone frequencies are typically set above EDFAs natural gain dynamics, and below the links payload, i.e., between 10 and 100 kHz. Tone amplitude is below 10% of average power to avoid large penalties [71, 72]. However, due to cross-gain modulation these pilot tones induce ghost tones on surviving channels which may be mistaken as pilot tones at the receiver. Optical Burst Switching (OBS) allows for efficient resource sharing amongst numerous users which have burst-mode traffic. In bursty traffic input channel powers are turned ON and OFF for random lengths of time. As input traffic approaches self-similarity, burst lengths become comparable to EDFAs natural response time, leading to large output power swings.

The methods used to control EDFA power transients involve maintaining a constant average input power to each amplifier in the network. This can be obtained in optical networks such as SONET or SDH, that use electrical multiplexing where a continuous bit stream is transmitted along the optical link. When the traffic in the network is in burst-OFF periods, idle codes are transmitted that maintain the average power of the optical channel almost constant. Hence, EDFA power transients are not a problem for this type of network. However, the current trend is to develop and evolve these networks with all optical systems that support optical burst switching (OBS), optical packet switching (OPS), and optical circuit switching (OCS). In these type of networks, there can be large time intervals where the average power in a specific channel is zero during the network operation. The dynamic channel power and

cascades of EDFAs can produce significant transients.

A method has been developed for resolving the effects of optical power transients generated by rapid changes in the input power of EDFAs [73]. Because the amplitude and duration of the optical power transient provided by the EDFA is affected by how rapidly the input optical power to the EDFA varies, if the switching time for the input power is increased, the amplitude and duration of the power transient generated by a chain of EDFAs is decreased, see Section 6.2.3.

1.10 Thesis overview

In this chapter, a general introduction and the basics of the optical networks have been covered. The components of optical communication systems and their specifications have also been discussed. The approaches which mitigate the effect of EDFA power transients in optical networks have also been reviewed. The following chapters will describe the work of this research project in detail.

Since this research predominantly focuses on modelling and simulating the dynamic behaviour of the EDFA, and the numerical and statistical analysis of the simulation results, it is necessary to introduce the basic model of the EDFA, its fundamental properties and parameters, which are used in the simulation work. These are reviewed in Chapter 2 which also includes an explanation of techniques for simulating the differential and transcendental equations representing the EDFA dynamic and steady-state behaviour. The numerical simulation results, and their critical analysis are discussed in Chapters 3, 4, 5, 6 and 7.

Chapter 3 illustrates the gain dynamic behaviour of the EDFA in circuit-switched networks. The network configuration for providing better QoS, may require dropping or adding channels to the network, and this management process produces fluctuations in the input signal of the EDFA. This in turn produces variation in the output power of the EDFA. The chapter also presents the output power transient during the network configuration process in cascaded EDFAs. A dynamic model of the EDFA developed by Sun et al [74] has been used to build our power transient simulator. The power transients output of the simulator was validated by comparison with original model results. There was good agreement. This model is not self-saturated by its own ASE. The gain spectrum is homogeneously broadened and there

is no absorption loss of the excited-state. These conditions are fulfilled when the input signal power is high enough or when the gain, in our simulations, is less than 20 dB [75] and this is the common situation with WDM systems. These conditions are defined as gain non-self-saturated-conditions for our implementation. This definition will be used for gain saturation in the whole thesis. Also in Chapter 3 the numerical output data of this model was used to analyse the power transients in single and a chain of C-band EDFAs in circuit-switched WDM optical networks. Gain-shifted C-band EDFA was also developed from the C-band by increasing the geometry parameters, however, the ion populations and length of EDF were kept the same as in the C-band. The developed simulator was also used for testing the power transients of the gain-shifted C-band EDFA. The behaviour of the power transients of the gain-shifted C-band was analysed numerically and statistically. To the best of our knowledge this is first time this gain-shifted C-band configuration has been used for testing the power transients in WDM optical networks. If the C-band and gain-shifted C-band were connected in parallel in the WDM optical networks the optical transmission band increased.

A self-saturated model was developed as an extension of the existing model in Chapter 3. The self-saturated model is developed by adding ASE and captured-photon models to Sun's model for testing and analysing the power transients in circuit-switched WDM optical networks. This self-saturated model including ASE and captured photon noises has not been previously reported for investigations of the behaviour of the power transients in EDFAs. Chapters 4 and 5 investigate the effects of different distributions of ATM and IP traffic in the packed-switched networks on the optical power transients of a chain of EDFAs. The distribution of the ATM and IP traffic affects the performance of the network. This is because of the fluctuation in the input power which then produces a swing in the output power and degrades the OSNR of the cascaded EDFAs in the network link. These studies can also be useful in enhancing the QoS of the network. In Chapter 4, the same simulator which was developed for the EDFA model of the gain dynamic of non-self-saturated-conditions was used for examining the behaviour of power transients. In this case-study, the input source to the simulator was an ATM-IP traffic source instead of the CW signal of the circuit switched networks. In this chapter, ATM-IP traffic sources of different distributions is developed in order to analyse their effects on system performance through the power transients phenomena. Chapter 4 presents the impact of the ATM and IP traffic of Pareto distribution on the

power transients of a chain of EDFAs. The simulation uses a bit-rate of 2.5 Gb/s. In this chapter, we first investigate the ATM and IP traffic in which a Pareto distribution is only applied to the burst OFF period of the traffic (referred to as periodic traffic in the thesis). In short, the PDFs of the output power transients are plotted with associated Gaussian distribution for analysis. In the same chapter ATM and IP traffic is investigated while both burst-ON and burst-OFF periods follow the Pareto distribution and this is the case for video, web and Ethernet traffic. This study is applied both to the C-band and gain-shifted C-band cascaded EDFAs in the network link during ATM and IP traffic of truncated Pareto distribution with degree of variability of 1.2 for the burst-OFF and burst-ON periods. Analysis shows that the power transients generated by gain-shifted C-band EDFAs are worse than those generated by C-band EDFAs.

Chapter 5 presents the effect of ATM and IP traffic of Poisson distribution on power transients of a chain of EDFAs. The PDFs of the output power transients and their Gaussian fits were studied and analysed for the EDFAs model for non-self-saturated-conditions. Then, the simulation was repeated for the same traffic with the EDFA in an unsaturated condition. The numerical simulation and statistical analysis were applied to the C-band cascaded EDFA. ATM and IP traffic of Poisson distribution was used in this work for examining the behaviour of power transients singly and in a chain of EDFAs in the packet switched WDM optical networks.

Chapter 6 demonstrates the evolution of output power and OSNR transients in EDFA chains. A set of numerical simulations have been performed to investigate the permissible OSNR limits using a self-saturated EDFA dynamic model developed in Chapter 3. We are interested in OSNR limits when channels are added to the link, because this decreases the OSNR magnitude. The lower limit of OSNR, min(OSNR(t)), is calculated from simulations and then related to the network performance through the term for Bit-Error rate, using the curve that expresses the BER as a function of optical SNR. A set of numerical simulations were performed to investigate the effects of the abrupt input signal variation in chains of EDFAs on the performance of WDM optical networks. The gradual loss/addition of EDFA input power or input power shaping is reported as an approach to mitigate the effect of the power transients in the cascaded EDFA networks [64, 73].

Chapter 7 demonstrates the gain locking system for EDFA in WDM optical networks us-

ing a PID controller. The controller consisted of proportional, integral, and derivative (PID) controllers, with pump updating interval of 5 μs. The main idea presented in this chapter for mitigating the power transient phenomena, is to restore the gain to the level prior to the occurrence of the perturbation, as well as requiring the transient rise and relaxation times to be minimised, which are the main requirements from the automatic gain controller. A pump controller was used to clamp the cross-gain saturation of the EDFA when four out of eight channels in the system were dropped or added. From above it was concluded that it is possible to use the P-controller or I-controller or D-controller alone to mitigate the power transient phenomenon in a saturated EDFA. However, the performance of I- and D-controllers are better than that of the P-controller since the power transient overshoot and the total transient time is less than for the P-controller. We report the optimised controller parameters under different operating conditions and show for the first time, to our knowledge, the effect of modulation frequency, speed of dropping or adding different numbers of channels and their affect on the value of the controller gain parameters for a single EDFA.

Finally, the thesis conclusions and future work are given in Chapter 8. In the appendices, the properties of optical fibres are briefly reviewed, the basics of the EDFA rate and propagation equations are illustrated and the detail of dynamic model given. Finally, we discuss issues related to computer implementation of the simulators which have been developed.

Chapter 2

Gain dynamic model of the erbium-doped fibre amplifier

2.1 Introduction

Research into active-fibre technology within the $1.5\mu m$ wavelength region was motivated by the development of erbium-doped glass fibres. Research continued on rare-earth doped fibre until the development of high-gain erbium doped fibre amplifiers. Now active fibres are used widely in optical amplifiers, lasers, switches, and a variety of nonlinear devices [1, 5, 34]. High performance optical amplifiers and other devices enhance lightwave communication systems. EDFA technology was first announced in 1987 [76, 77]. The EDFA is the most commonly used optical amplifier due to its excellent amplification properties near 1.55μm, which is the wavelength region where the fibre losses are at a minimum [54]. EDFAs are a key technological support for driving the development of Dense Wavelength Division Multiplexing (DWDM) networks. This is due to many factors: (1) their gain spectrum covering a wide range of wavelengths, in which the fibre loss is minimal, (2) readily obtainable high-quality high-power semiconductor pump lasers, (3) being an all-fibre device makes it polarization independent, and (4) immunity to cross talk when amplifying WDM signals. EDFAs are used in WDM optical networks to compensate for the losses within fibre spans and other network elements.

Research has also demonstrated the potential of rare-earth doped fibre in photonic sys-

tems and instrumentation [6, 8, 78–80]. Models for amplifiers and lasers based on rate and propagation equations have also been presented by various researchers [6, 8, 9, 34]. These models are necessary for predicting the amplifier performance and investigating the amplifier's behaviour within different network conditions. In order to explain the model used to demonstrate the gain dynamic characteristic of the EDFA, it is essential to briefly illustrate the related EDFA basics.

2.2 Erbium-doped fibre amplifier basics

In this section, the fundamentals required to model gain in erbium-doped fibre (EDF) amplifiers are reviewed. The dynamics of the gain and amplification process are modelled by a system of coupled atomic populations and light flux propagation equations. The simplest EDFA configuration, shown in Figure 1.11 in chapter 1, consists of an erbium-doped fibre spliced into the signal transmission link of an optical network and a source of pumped light. Different pump configurations provide EDFAs with different specifications as shown in Figure 2.10, explained in the following sections in this chapter.

Figure 2.1: The three-level system used for the amplifier model. The transition rates between levels 1 and 3 are proportional to the populations in those levels and to the product of the pump flux ϕ_p and pump cross-section σ_p. The transition rates between levels 1 and 2 are proportional to the populations in those levels and to the product of the signal flux ϕ_s and signal cross-section σ_s. The spontaneous transition rates of the ion (including radiative and non-radiative contributions) are given by Γ_{32} and Γ_{21} [6, 8, 9].

The amplification mechanism in EDFAs is stimulated emission, but in this case the population inversion is achieved by optical pumping. During this process, pump photons raise electrons to excited states which exist at higher energy levels. This configuration is known

as the three-level atomic system [6, 8, 9, 34, 78] as shown in Figure 2.1 that provides the EDFA with the ideal characteristics for optical networks. This scheme consists of a ground state denoted by 1, an intermediate state labeled 3 and state 2. Since state 2 often has a long lifetime in the case of a good amplifier, it is sometimes referred to as the metastable level. As shown in Figure 2.1, the pump supplies energy to the erbium ions in the ground state, and then the ions are excited either to metastable level 2 if the pump wavelength is 1480 nm or to intermediate level 3 if the pump wavelength is 980 nm. The erbium ions in the latter case decay non-radiatively and quickly to the metastable level in time of the order of 1μs.

Apart from the wavelength of 980 nm, other wavelengths do not have adequate energy to pump ions to intermediate level 3 [77]. The erbium ions in the metastable level decay to the ground level either spontaneously within a time of the order of 10 ms, or through stimulated emission by an incoming signal. The radiated energy due to the ion decay between the metastable level and ground level corresponds to the photons of wavelengths between 1520 nm - 1570 nm. Light signals with wavelengths in this spectral region that traverse through the EDFA induce stimulated emission from the excited ions and then light signal amplification occurs due to this process. The rate equations for the population variation are written as [6,8]:

$$\frac{dN_3}{dt} = -\Gamma_{32}N_3 + (N_1 - N_3)\phi_p\,\sigma_p \tag{2.1}$$

$$\frac{dN_2}{dt} = -\Gamma_{21}N_2 + \Gamma_{32}N_3 - (N_2 - N_1)\phi_s\,\sigma_s \tag{2.2}$$

$$\frac{dN_1}{dt} = \Gamma_{21}N_2 - (N_1 - N_3)\phi_p\,\sigma_p + (N_2 - N_1)\phi_s\,\sigma_s \tag{2.3}$$

Where N_1, N_2, N_3 are the population of ions, number of ions/volume, at energy levels E_1, E_2, E_3 respectively. We denote the emission cross-sections for level 2 to 1 transition by σ_s in units of area. We denote the absorption cross-sections for level 1 to 3 transition by σ_p in units of area. Transition rate from level 2 to level 1 is denoted by Γ_{21} and is mostly due to radiative transitions. Transition rate from level 3 to level 2 is denoted by Γ_{32} and it is mostly due to non-radiative transitions. The incident pump light intensity flux at the frequency corresponding to the level 1 to level 3 transition is denoted by ϕ_p corresponds to the pump. The ϕ_p is in number of photons/time/area. The incident light intensity flux at the frequency corresponding to the level 1 to level 2 transition is denoted by ϕ_s and corresponds to the signal field. ϕ_s is the number of photons/time/area. In a steady-state situation, the time

derivatives of the ion population in each level will be zero as shown below [6]:

$$\frac{dN_3}{dt} = \frac{dN_2}{dt} = \frac{dN_1}{dt} = 0 \tag{2.4}$$

The total population of erbium ions in the fibre core is denoted by N and given by:

$$N = N_1 + N_2 + N_3 \tag{2.5}$$

From Equation (2.1), the population of level 3 can be written as:

$$N_3 = \frac{1}{1 + \Gamma_{32}/\phi_p\, \sigma_p} N_1 \tag{2.6}$$

When Γ_{32} is large (corresponding to a speedy transition from level 3 to level 2) compared to the effective pump rate into level 3, then the value of $\phi_p \sigma_p$ and N_3 is very close to zero. Thus, the population of erbium ions is mostly in levels 1 and 2. From Equation (2.6), the population of level 2 can be written as:

$$N_2 = \frac{(\phi_p \sigma_p/\Gamma_{32}) + \phi_s \sigma_s}{\Gamma_{21} + 2\phi_s \sigma_s} N_1 \tag{2.7}$$

Then, from Equation (2.5), the populations N_1, N_2 and population inversion $(N_2 - N_1)$ can be derived as:

$$N_2 - N_1 = \frac{\phi_p \sigma_p - \Gamma_{21}}{\Gamma_{21} + 2\phi_s \sigma_s + \phi_p \sigma_p} N \tag{2.8}$$

The principle of operation of an EDFA is summarized in these paragraphs. The three energy levels of erbium ions in silica are shown in Figure 2.2, and are labeled E_1, E_2, and E_3 in order of increasing energy. Each energy level in the figure is shown as a single line in an isolated ion of erbium, but each energy level is spread over a continuous energy band when these ions are doped or inserted into silica glass. The process of splitting is known as Stark splitting. The difference between the energy levels is denoted by the wavelength in nm of the photon corresponding to it. The process of spreading of energy levels is a useful characteristic of optical amplifiers because it increases the frequency or wavelength range of the signals that can be amplified. Moreover, an amplifier is capable of amplifying several wavelengths simultaneously. The erbium ions are distributed in the various levels within

each energy band in a non-uniform manner according to the Boltzmann distribution by a process known as thermalisation.

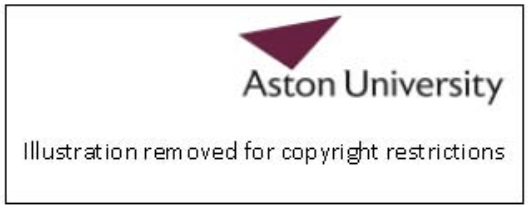

Figure 2.2: Three energy levels E_1, E_2, and E_3 of erbium ions in silica glass used in the amplification process. The fourth energy level, E_4, is present in fluoride glass not in silica glass. The difference between the energy levels is denoted by the wavelength in nm of the photon corresponding to it. The upward arrows indicate wavelengths at which the amplifier can be pumped to excite the ions into the higher energy level. The 980 nm transition corresponds to the band gap between the E_1 and E_3 levels. The 1480 nm transition corresponds to the band gap between the bottom of the E_1 to the top of the E_2 levels. The downward arrows indicate the wavelength of the photons emitted owing to stimulated and spontaneous emission [1, 6, 8].

We explained that the three energy level atomic system can be reduced into a two energy level atomic system. In the two energy level system, an optical signal at frequency f_m could be amplified only if hf_m is equal to the energy difference $(E_2 - E_1)$. Here, h is Planck's constant (6.63 x 10^{-34} J s). As we noted, these energy levels are spread into bands, thus all frequencies that correspond to the energy difference between level E_2 and level E_1 can be amplified. As a result, in the case of erbium ions in silica glass, all wavelengths in the range 1525 nm to 1570 nm can be amplified by stimulated emission from the E_2 band to the E_1. The band of wavelengths is 50 nm wide with a peak around 1532 nm. This is in the low attenuation region of SMF that is applied in optical WDM networks.

In thermal equilibrium condition, $N_1 > N_2 > N_3$. The condition for stimulated emission from E_2 to E_1 is that the $N_2 > N_1$, this can be achieved both by absorption and spontaneous emission. When the amplifier is pumped by an optical signal at wavelength 980 nm, it will cause transitions of ions from E_1 to E_3, because $N_1 > N_3$. The ions that have been moved to level E_3 by the pumping process will rapidly transit to level E_2 by the spontaneous emission. As we mentioned earlier, the lifetime for this process, τ_{32}, is about 1 μs. The ions that have

moved to level E_2 by spontaneous emission will transit to level E_1 by spontaneous process. The lifetime for this process, τ_{21}, is about 10 ms.

The erbium has pump bands at 514.5, 532, 670, 800, 980, and 1480 nm. These wavelengths correspond to the energy differences between E_1 $(^4I_{15/2})$ and the first six excited states of the erbium ion. When an amplifier is injected at any of these wavelengths, absorption of pump photon raises erbium ions to an excited state at the corresponding energy. The erbium ion decays non-radiatively to the energy level E_2 $(^4I_{13/2})$, metastable state. However, the pump efficiency is one of the factors that decides which of these wavelengths of the pump band could be used for pumping an EDFA. Pump efficiency is degraded by Excited State Absorption (ESA) transitions, the erbium ions in level E_2 can be raised to a higher excited state by absorbing pump light photons. It has been demonstrated that the ESA at E_2 does not take place at the wavelengths 980 and 1480 nm. Thus, the pumping process is more efficient, and the EDFA uses less pump power for a given gain at 980 nm than other wavelengths. However, higher power pump lasers exist at 1480 nm, in comparison to 980 nm, and so 1480 nm pumps are applied in amplifiers developed to provide high output powers.

Chemical compound, length and ion populations are the properties which affect the EDFA gain at each wavelength. These also form the basis of the design of the different types of EDFA, such as L-band or L+C band EDFAs [55, 81].

To develop a model for the EDFA, it is necessary to realize that even in a simple one-dimensional model of the fibre amplifier, the transverse shape of the optical mode and its overlap with the transverse erbium ion distribution profile are important, this is parameterized by a term denoted by the overlap factor [82]. Only that part of the optical mode that overlaps with the erbium ion distribution will stimulate absorption or emission from the Er^{3+} transitions. The whole mode, however, will experience gain or attenuation as an outcome of this interaction. For instance, for a step index fibre, if the erbium is doped only in the fibre core, since a portion of the optical mode extends into the cladding, only that portion of the optical mode that is in the core will experience the effects of the Er^{3+} present. This can be used advantageously. By doping the erbium only in the very centre of the fibre core, the erbium ions will only face the very high intensity part of the optical mode and the pump will more easily invert the maximum number of Er^{3+} ions [83]. In general, the erbium density is not necessarily constant and can vary significantly across the fibre core and cladding regions.

By considering the light fields in EDFAs to be confined in a core of very small dimensions, it is assumed the pump and the signal intensities as well as the erbium ion distribution are constant in transverse dimension and the situation simplifies to a one dimensional problem which is easier to solve.

The energy levels of rare earth ions consist of relatively well separated groups of closely spaced energy levels. The pumping wavelength required for transition to energy level 3 is different than that of energy level 2, and the assumption is made that rapid relaxation occurs from level 3 to level 2. For all practical purposes, the population in level 3 is then effectively zero, and the three level system reduces to a two level system. The whole behaviour of the EDFA can be predicted from the absorption and emission cross-sections which are shown in Figure 2.3. The thermal distribution of energy within the closely spaced energy levels causes the difference in spectral shape between the emission and absorption spectra [6, 84, 85].

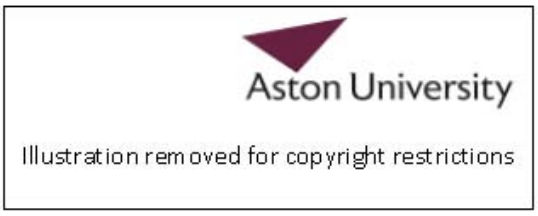

Figure 2.3: Experimentally obtained emission and absorption cross-sections of an erbium doped Ge/Al/P silica fibre [10–12].

Due to the reduction of the three-level system to a two-level system, the rate equation can be written in terms of the total population densities of level 1 and 2 as shown in more detail in Appendix B.2. The two level rate equation illustrated in Appendix B.2 was analytically investigated by Saleh et al [75]. The ASE power effect on the EDFA saturation was ignored, this was an essential assumption for the derivation of the model. Then, another

model was developed including the ASE power effect on saturation by the same research group as illustrated in [86].

2.3 Gain dynamics model of single EDFA

In this thesis, the gain dynamics behaviour of EDFAs are determined using a model, which is a single Ordinary Differential Equation (ODE), developed by Sun and Zyskind [74] incorporating time variation effects in the EDFA. The extension of Sun's model to include the ASE power is also used to investigate the OSNR performance in both the circuit-switched and ATM-IP networks. A different method was used to include ASE and other losses in the extension model and this was compared with those developed in the literature [87, 88].

The rate equation for the proportion of atoms in the first excited state $N_2(z,t)$, is shown in Equation (2.9), and the photon equation for the k^{th} channel is shown in Equation 2.10. Both these equations are used to derive the gain dynamics model in [74, 75, 86]. In the developed model, it is assumed that there is no excited-state absorption; the gain spectrum is homogeneously broadened, and the amplifier is not self-saturated by its own amplified ASE. These conditions are satisfied when the gain is less than 20 dB [75] or when the input powers are sufficiently high as is commonly the case in WDM systems. Note that with these values of gain and input signal power, the EDFA entered what is known as the saturation regime (the phenomenon that the gain of an amplifier is reduced for high input signal powers is called gain saturation, an amplifier device such as EDFA cannot maintain a fixed gain for arbitrarily high input powers, because this would require adding arbitrary amounts of power to the amplified signal [6]). This is the definition of EDFA gain saturation throughout this thesis. Under these conditions the rate equation for the fraction of atoms in the first excited state $N_2(z,t)$ is shown in Equation (2.9):

$$\frac{\partial N_2(z,t)}{\partial t} = -\frac{N_2(z,t)}{\tau} - \frac{1}{N\,A}\sum_{k=1}^{M} u_k \frac{\partial P_k(z,t)}{\partial z} \tag{2.9}$$

$$\frac{\partial P_k(z,t)}{\partial z} = N\,u_k\,\Gamma_k\left[(\sigma_k^e + \sigma_k^a)N_2(z,t) - \sigma_k^a\right]P_k(z,t) \tag{2.10}$$

Where N is the density of the active erbium ions in the fibre core of cross-section A, and τ is the spontaneous lifetime of the upper level. There are M optical channels, λ_k is wavelength of the k^{th} channel, and $P_k(z,t)$ is the optical power at location z and time t of the k^{th} channel, with overlap factor of Γ_k and σ_k^e, σ_k^a are emission and absorption cross-sections of the k^{th} channel respectively. The powers of both pump and signals are expressed in units of photons per time. Light beams propagating in the EDF from 0 to L are indicated by unit vector u_k = +1, and light beams moving from L to 0 are indicated by u_k = -1. L is the length of the EDF. The fractional populations of the upper state $N_2(z,t)$ and of the lower state $N_1(z,t)$ sum to unity, $N_2(z,t) + N_1(z,t) = 1$.

The time dependent model of an EDFA based on Equations (2.9) and (2.10) requires complicated numerical computation. However, this set of partial differential equations can be reduced to a single ODE which fulfills the conditions of most practical EDFAs. With this model, which is shown in Equation (2.11), the numerical computation is significantly simplified. A detailed derivation is shown in Appendix B.2.

$$\tau\frac{d}{dt}P_k^{IS}G_k(t) + P_k^{IS}G_k(t) + P_k^{IS}A_k =$$

$$-\sum_{j=1}^{M} P_j^{in}(t)\left\{\exp\left[\frac{P_k^{IS}G_k(t) - \left[G_{kj}^0 + A_{kj}\right]\exp\left(\frac{-t}{\tau}\right) + A_{kj}}{P_j^{IS}}\right] - 1\right\} \tag{2.11}$$

$$P_j^{IS}G_j(t) = P_k^{IS}G_k(t) - \left[G_{kj}^0 + A_{kj}\right]\exp\left(\frac{-t}{\tau}\right) + A_{kj} \tag{2.12}$$

$$P_k^{IS} = \frac{A}{\Gamma_k\left(\sigma_k^e + \sigma_k^a\right)\tau} \tag{2.13}$$

$$G_k(t) = ln\left[\frac{P_k^{out}(t)}{P_k^{in}(t)}\right] \tag{2.14}$$

$$A_k = \alpha_k L \tag{2.15}$$

$$\alpha_k = N\Gamma_k\sigma_k^a \tag{2.16}$$

$$G_{kj}(t) = P_k^{IS}G_k(t) - P_j^{IS}G_j(t) \tag{2.17}$$

$$A_{kj} = P_k^{IS}A_k - P_j^{IS}A_j \tag{2.18}$$

$$G_{kj}(t) = \left[G_{kj}^0 + A_{kj}\right]\exp\left(\frac{-t}{\tau}\right) - A_{kj} \tag{2.19}$$

Where,

$$G_{kj}^{0} = P_{k}^{IS}\, G_{k}^{0} - P_{j}^{IS} G_{j}^{0} \tag{2.20}$$

Equation (2.20) is determined by the initial conditions. Where the term P_k^{IS} is intrinsic saturation power of the k^{th} channel, $G_k(t)$ is the overall gain parameter at time t, $P_k^{out}(t)$ is the output power of the k^{th} channel at time t, $P_k^{in}(t)$ is the input power of the k^{th} channel at time t, A_k is the absorption coefficient for whole length of doped-fibre L, N is the density of the active erbium ions in the fibre core, α_k is the absorption coefficient of the k^{th} channel, $P_j^{in}(t)$ is the input power for each channel, and $G_k(0) = G_k^0$ is initial conditions for all channels from (k =1, 2,..., M). The gain in the j^{th} channel can be expressed in terms of the gain in the k^{th} channel using Equation (2.12). In other words, once the gain is calculated for the k^{th} channel (probe channel) by solving Equation (2.11), the gain of other channels can be obtained from Equation (2.12). If the EDFA is in a steady state at t = 0 (before any transition occurs) the term $(G_{kj}^0 + A_{kj})$ is substituted by zero in both Equations (2.11) and (2.12).

Initially, Equation (2.11), which represents the gain dynamics behaviour of the EDFA, is numerically implemented for the critical power transient analysis. The numerical implementation techniques are discussed in Section 2.9.

2.4 EDFA dynamics model for OSNR investigation

The dynamic model of the EDFA shown in Section 2.3 and the models introduced in [87–89] are used in this section for developing a model which includes ASE-power. This gain dynamics model is developed for analysis of OSNR both in circuit-switched and packet-switched networks.

$$\tau \frac{d}{dt} P_k^{IS} G_k(t) + P_k^{IS} G_k(t) + P_k^{IS} A_k =$$

$$-\sum_{j=1}^{M} P_j^{in}(t) \left\{ \exp\left[\frac{P_k^{IS} G_k(t) - \left[G_{kj}^0 + A_{kj} \right] \exp\left(\frac{-t}{\tau}\right) + A_{kj}}{P_j^{IS}} \right] - 1 \right\}$$

$$-P_{ASE}(t) \tag{2.21}$$

$$P_{ASE}(t) = 4 \int (exp^{G(\nu,t)} - 1)\, n_{sp}\, d\nu \tag{2.22}$$

$$\sigma^T(\nu) = \sigma^e(\nu) + \sigma^a(\nu) \tag{2.23}$$

$$n_{sp} = \left[\frac{\sigma^e(\nu)}{\sigma^T(\nu)} \frac{G(\nu,t) + A(\nu))}{G(\nu,t)} \right] \tag{2.24}$$

In Equation (2.21), all terms which were described in Section 2.3, have a similar definition. P_{ASE} is the statistical average spontaneous emission flux of an EDFA in photons/s. ASE power is computed assuming a constant inversion as stated in [86, 88]. The terms $\sigma^e(\nu)$, $\sigma^a(\nu)$ are emission and absorption cross-sections respectively, $\sigma^T(\nu)$ is the total cross-sections, $G(\nu)$ is the logarithmic gain and $A(\nu)$ is the loss, all these terms are calculated at frequency ν. The spontaneous emission factor is denoted by n_{sp}, and the factor *4* in Equation (2.22) indicates that the two different polarizations and two different directions of propagation of the ASE are considered. In case of SNR calculation, this factor is halved because the forward ASE only is used for computation.

To understand each terms in the gain dynamic Equations (2.11) and (2.21) it is essential to review briefly the main properties of EDFAs.

2.5 Properties of EDFAs

From the discussion on principles of operation of EDFAs, **gain** is the main characteristic of an amplifier. The EDFA gain is defined as the ratio of the output signal power to the input signal power as shown in Equation (2.25). It is calculated by integrating the gain coefficient $g(\lambda)$ over the length L of the erbium-doped fibre. The gain coefficient $g(\lambda)$ is calculated by summation of both the emission coefficient, $g^*(\lambda) = \Gamma_s\, N\, \sigma_e(\lambda)$, multiplied by the fractional populations of the ions in the excited state, N_2, and the absorption coefficient, $\alpha(\lambda) = \Gamma_s\, N\, \sigma_a(\lambda) > 0$, multiplied by the fractional populations of the ions of the first excited and ground states of erbium, N_1, the terms $g^*(\lambda)$ and $\alpha(\lambda)$ are shown in Equation (2.26) [77].

$$G(\lambda) = \frac{P_{out}}{P_{in}} = \int_0^L g(\lambda, z)\, dz \tag{2.25}$$

$$G(\lambda) = \int_0^L (g^*(\lambda)\, N_2(z) - \alpha(\lambda)\, N_1(z))\, dz \tag{2.26}$$

Where Γ_s is the confinement or over-lap factor of the signal mode in the EDF core, and σ_e and σ_a are emission and absorption cross-sections as a function of the wavelength. The

term $g^*(\lambda)$ is inverted gain coefficient and $\alpha(\lambda)$ is the small signal absorption coefficient. The spectra of the emission and absorption coefficients of an erbium doped Ge/Al/P silica fibre are shown in Figure 2.3. The gain coefficient can be expressed in units of dB/m. The terms mentioned are used in the numerical simulations, which focused on the analysis of the dynamic behaviour of cascaded EDFAs in WDM optical networks. These values are provided by Highwave-Technologies of France [10].

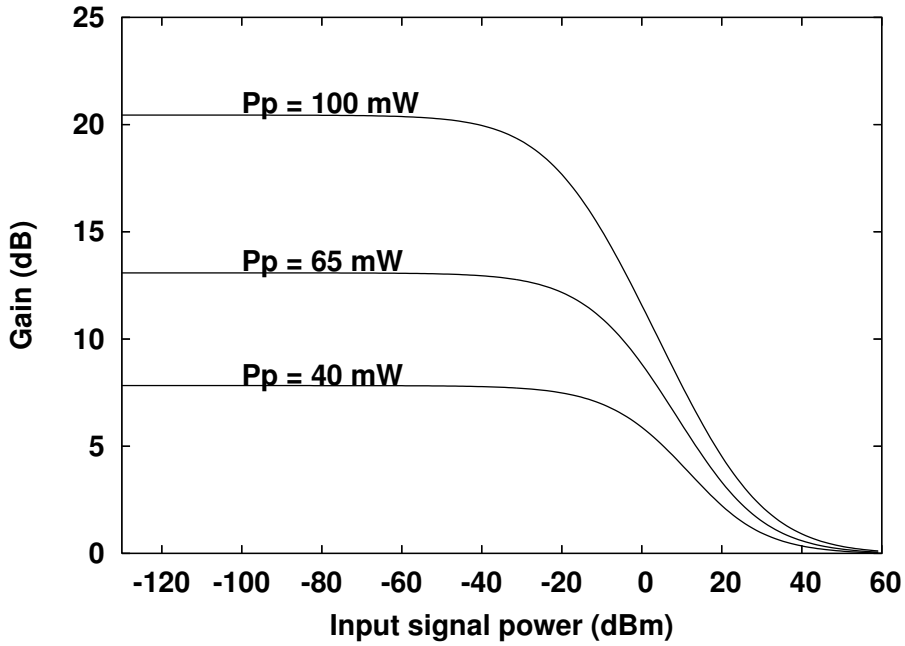

Figure 2.4: EDFA gain performance as a function of the input signal powers in dBm, at wavelength 1549.2 nm, at saturation for pump powers of 40, 65, 100 mW. (Numerical simulation results of the non-self-saturated EDFA gain dynamic Equation (2.11)).

Some other important specifications of EDFAs are the **output power and saturation power**. The output power is nearly proportional to the pump power when signal levels are high and the amplifier is saturated, as shown in Figure 2.4. This is a characteristic feature of the three-level erbium laser system, illustrated in Figure 2.1. When the amplifier is saturated, stimulated emission from an excited state induced by the signal, is balanced by pump absorption from the ground state. As the pump power increases, the signal power at which this balance occurs also increases [77]. The signal power at which the gain coefficient is decreased to half its small signal value is;

$$P_{sat} = \frac{h\nu_s A_c}{(\sigma_{es}+\sigma_{as})\Gamma_s \tau_{sp}} \left(1+\frac{\sigma_{as}P_p}{\sigma_{es}P_p^{th}}\right) \tag{2.27}$$

$$P_p^{th} = \frac{\sigma_{as}}{\sigma_{es}} \frac{h\nu_p A_c}{(\sigma_{ap} + \sigma_{as})\Gamma_p \tau_{sp}} \tag{2.28}$$

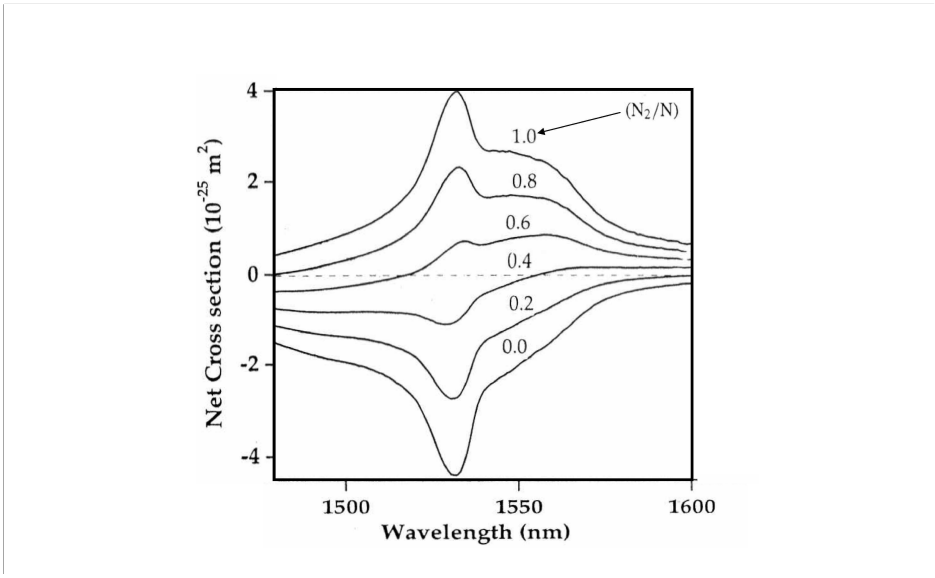

Figure 2.5: Net cross-section ($\sigma_e(N_2/N) - \sigma_a(N_1/N)$) of Er^{3+} near wavelength 1500 nm for different values of the fractional metastable-state population (N_2/N), (indicated adjacent to each curve) for cross-sections given in [6], where N_2 is metastable-state ion population, and N is the total ion population [6].

Where σ_{as} and σ_{es} are absorption and emission cross-sections at the signal wavelength respectively. A_c is the core effective area, τ_{sp} is the excited state (E_2) lifetime, P_p is the pump power. P_p^{th} is known as the pump threshold power and shown in Equation (2.28). Pump power below P_p^{th} results in a negative small signal gain coefficient, and this is associated with absorption, pump power above P_p^{th} results in a positive small signal gain coefficient, and this is associated with gain. $h\nu_p$ is the pump photon energy, Γ_p is the pump overlap factor, and σ_{ap} is the pump absorption cross-section. Equation (2.27) shows that if P_p is much higher than P_p^{th} then P_{sat} is proportional to $\frac{P_p}{P_p^{th}}$ [77].

Figure 2.5 shows the net cross-section, on a per-ion basis as a function of wavelength, for different values of inversion. We noted that the peak at 1530 nm suffers relatively more than 1550 nm as the inversion is decreased. In a range of inversions, we have observed that longer wavelengths will still be amplified while shorter wavelengths are attenuated [6].

Equations (2.27) and (2.28) describe the saturation characteristics of the EDFA. The gain characteristics of the complete amplifier are found by solving the rate equation at each point along the length of the EDF length and integrating the gain coefficient as shown in

Equation (2.25). The saturation is typically obtained primarily near the output end of the amplifier where the signal power is at its highest value, this local description provides a good qualitative understanding of the saturation behaviour of a complete amplifier [77].

The **transmission impairments** caused by the EDFAs in wavelength routed optical networks result from background noise. The amplification of the EDFA is associated with a background of ASE (defined in Appendix B.1.2), which arises when light emitted by spontaneous decay of excited erbium ions is captured by the optical fibre waveguide and then amplified in the amplifier. This ASE background adds noise that degrades amplified signals [77]. The noise figure (NF) is given by the SNR at the output divided by that corresponding to the shot noise of the signal at the input. The NF is a measure of the degradation of the signal by noise added by the EDFA. The important factors for the NF of a well-designed, high-gain EDFA are signal-spontaneous beat noise and signal shot noise, and are obtained from [8]

$$NF \cong 2\, n_{sp}\, \frac{(G-1)}{G} + \frac{1}{G} \approx\ 2\, n_{sp} \tag{2.29}$$

Where n_{sp}, is the spontaneous emission factor, shows the corresponding strengths of the stimulated emission and spontaneous emission processes. For an EDFA with uniform inversion (denoted by $N_2 - N_1$) along its length, n_{sp} is given by Equation (2.30 [77]:

$$n_{sp} = \frac{\sigma_{es} N_2}{\sigma_{es} N_2 - \sigma_{as} N_1} \tag{2.30}$$

As mentioned earlier N_1 and N_2 are the fractional ion populations of the ground and metastable states, respectively. As n_{sp} approaches unity, the better the inversion and the lower the NF. Because EDFAs can be efficiently inverted (i.e. $\frac{N_2-N_1}{N_2} \cong 1$), the NF can approach 3 dB, which is the quantum limit for optical amplifiers [77]. P_{ASE} is the ASE power of one polarization in bandwidth ($\Delta\nu$), this is one-half the total power in the bandwidth ($\Delta\nu$) of the ASE, when there is no polarization hole burning (PHB), the ASE is unpolarised. The spontaneous emission factor can be calculated from:

$$n_{sp} = \frac{P_{ASE}}{h\nu_s \Delta\nu (G-1)} \tag{2.31}$$

Where $h\nu_s$ is the photon energy, substituting n_{sp} of Equation (2.31) in Equation (2.29), we notice that the signal-spontaneous beat noise in the NF is proportional to P_{ASE} and can be shown as resulting from the addition of ASE by the EDFA. Due to that the spontaneous emission produced at the EDFA input gets maximum gain of EDFA. When the inversion is

not uniform along the length of the EDFA, the inversion near the input of EDFA has greatest impact on the noise figure [77].

$$NF \cong 2\, n_{sp}\, \frac{(G-1)}{G} + \frac{1}{G} \approx 2\, \frac{P_{ASE}}{h\nu_s \Delta\nu (G-1)} \tag{2.32}$$

In the large gain limit the NF is approximately $2n_{sp}$ $(0 \leq n_{sp} \leq 1)$. Also note that the ASE power increases with gain.

We now consider the role of the most important component - the **EDF**. A single-mode fibre is doped with erbium ions. Different techniques, such as Modified Chemical Vapor Deposition (MCVD), can be used for processing silica-based EDFs as mentioned in [90, 91]. The EDF with different properties obtained from different doping techniques, can be used for specific applications. In most applications, pump power is restricted by pump laser specification. In a number of applications, such as remotely pumped preamplifiers and the in-line amplifiers used in submarine systems, where pump power is restricted by reliability constraints, it is necessary to design EDF to produce the highest gain with the lowest possible pump power. The pump intensity experienced by all erbium ions, should be maximized through appropriate design of the EDF. The effective core area should be minimized by increasing the difference between core and cladding refractive indices, and the pump overlap factor should be maximized as shown in Equation (2.28).

In some research, pump thresholds of less than 1 mW have been obtained [92, 93]. The reduction in the pump power causes a decrease of the cost of amplifiers and an increase of their reliability. The ability of the amplifier to achieve maximum gain with minimum pump power is described as gain efficiency. One important point for comparing different EDF designs is the maximum gain efficiency which is calculated as the maximum quotient of the small-signal gain divided by the pump power. It has been shown by Kashiwada and Shigmatsu that the maximum gain efficiencies with the signal wavelength of 1533 nm are 11 dB/mW and 6.3 dB/mW for pump wavelength of 980 nm and 1480 nm respectively. The gain can be increased or decreased by the pump power, this shows that the gain efficiency at wavelength 980 nm is higher than at wavelength 1480 nm [92, 93].

Figures 2.6, 2.7, and 2.8 demonstrate the effects of the pump wavelength and power on the EDFA gain performance. These curves result from numerical simulations of the gain model described in Appendix B.2, they show good agreement with the curves obtained by Becker [6]. For example, in Figure 2.6, at signal wavelength 1530 nm, it is demonstrated

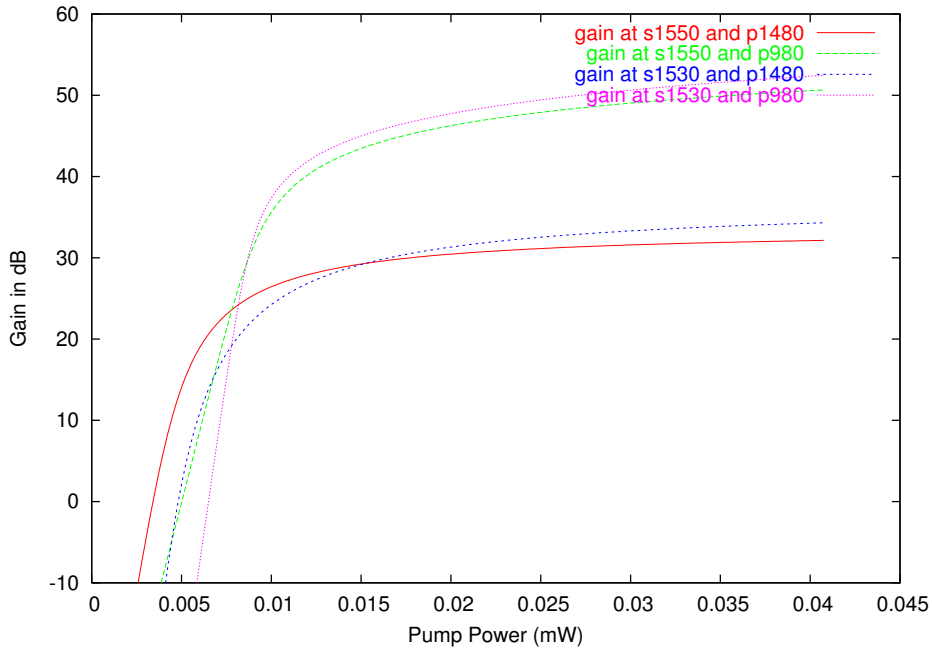

Figure 2.6: Gain as a function of pump power for fibre length of 18.8m, for two signal wavelengths 1550 nm and 1530 nm, using the pump wavelengths of 980 nm and 1480 nm. This gain excludes ASE and background loss (or absorption coefficient)(Numerical simulation results of the EDFA gain model described in Appendix B.2 [6]).

that the maximum gain efficiency is 4 dB/mW and 2 dB/mW with 980 and 1480 nm pump wavelengths respectively, we concluded that the maximum gain efficiency at wavelength 980 nm is better than at wavelength 1480 nm. However, ASE and Rayleigh scattering will limit the maximum gain obtainable in a single-stage amplifier, but multistage designs can be used to increase the maximum gain [77].

In some terrestrial applications high output power is required, thus the pump conversion efficiency should be at its maximum value; defined as $(P_{out} - P_{in})/P_p \approx (P_{out})/(P_p)$. For three level laser systems, if the pump power (P_p) is much higher than the pump threshold (P_p^{th}), the saturated output power is nearly proportional to the pump power as shown in Equation (2.27) [77]. The pump conversion efficiency is relatively independent of the waveguide geometry when the pump and signal powers are high and much higher than their intrinsic saturation power which is defined as:

$$P_{sat}^{IS} = \frac{h\nu_s A_c}{\tau_{sp}(\sigma_e(\lambda) + \sigma_a(\lambda))\Gamma_\lambda} \tag{2.33}$$

The conversion efficiency is relatively insensitive to the waveguide geometry because

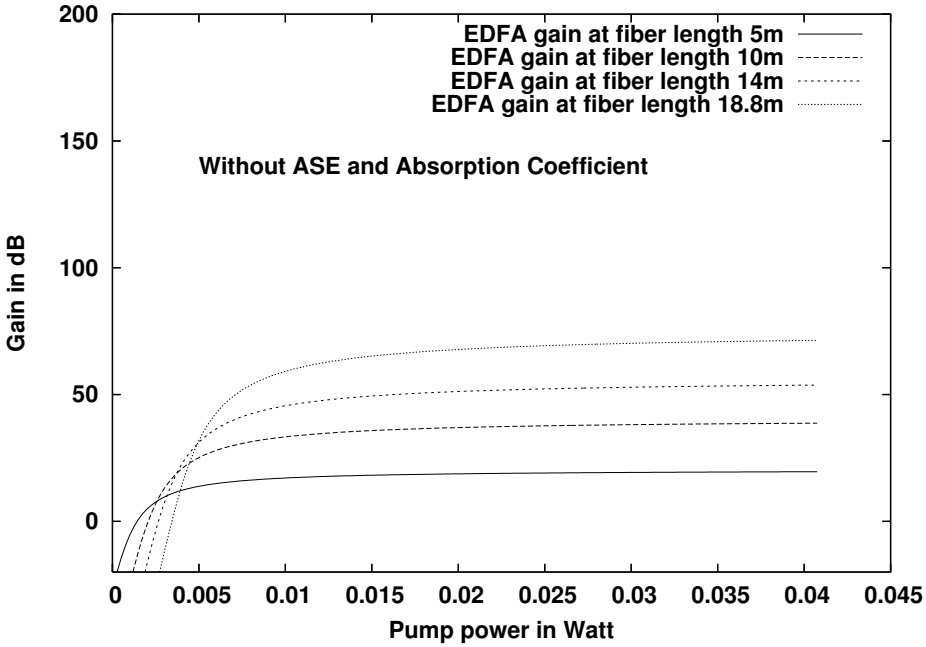

Figure 2.7: Gain as a function of pump power at signal wavelength 1550 nm and pump wavelength 1480 nm for different fibre lengths (5m, 10m, 14m, and 18.8m). This gain excludes ASE and background loss (or absorption coefficient). (Numerical simulation results of the EDFA gain model described in Appendix B.2 [6]).

of the cancellation of terms, such as effective area, over-lap factor of signal and pump, as shown in Equation (2.27). Core co-dopants and erbium concentration are useful determinants of the amplifier's saturation specification, if the erbium concentration in silica is too high, the result is an increase in cooperative up-conversion and related non-radiative dissipation of pump power. In some applications, e.g. terrestrial, high output power is more important than high gain with minimum pump power. In these applications, EDFs with larger cores and small core-cladding refractive index differences are used. This arrangement permits lower erbium concentration and thus avoids absorption of the pump photons without production of an additional signal photon. However, there is a proportional relation between the core size of the EDF and the pump threshold. For example, increasing the core size of the EDF also increases the pump threshold as shown in Equation (2.28). For power amplifiers the same specification is used in the design of its EDF, a smaller effective core area and a higher difference between the core and cladding than for standard transmission fibres [77].

Coupling loss is due to the mismatch between the EDF (with small core diameter typically 2-4 μm) and the transmission link fibre (with large core diameter typically 8-10 μm).

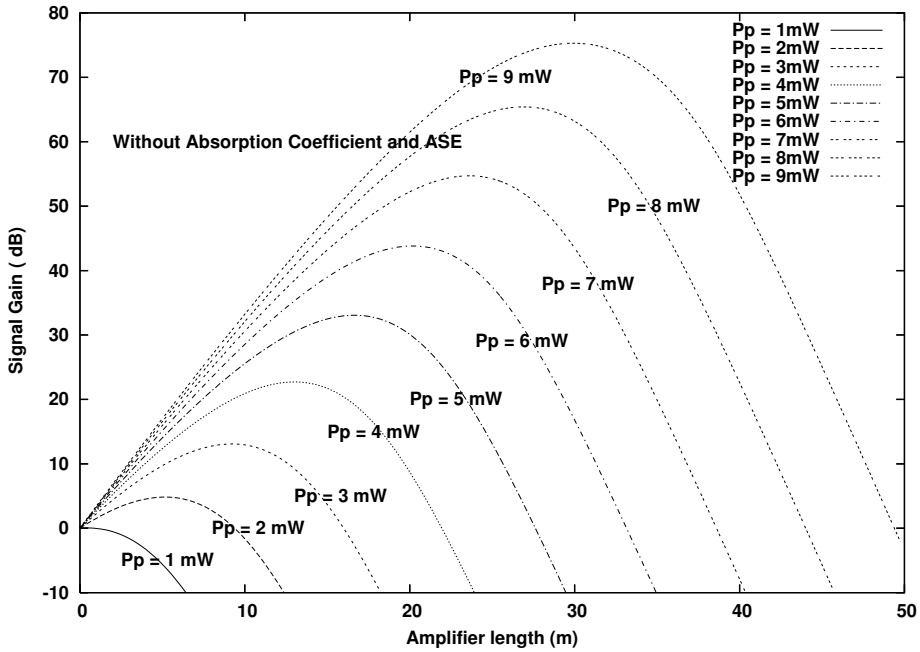

Figure 2.8: Gain as a function of EDF length (m), the curves show the optimum length yielding the maximum gain, which increases with the pump power, and simulated with the input signal power of -40 dBm. (Numerical simulation results of the EDFA gain model described in Appendix B.2 [6]).

To achieve an acceptable amount of coupling loss requires extensive efforts to resolve the mismatch problem. The coupling loss can be minimized by using a fusion splice between the EDF and the transmission link fibre. Consequently, a great deal of work was done to minimise coupling loss and typical results of a few tenths of a decibel are achieved. The total losses of the input and output in the EDFA are each less than 1.5 dB. These losses include the loss of isolators and pump-signal combiners [77].

Polarisation independence is one of the useful properties of EDFAs. The gain of EDFAs is polarization independent because of the circular symmetry of the EDF core, and the erbium ions in the glass matrix of the core are randomly oriented [94, 95]. EDFAs show PHB due to the locations of erbium ions in the glass matrix, which is internally anisotropic. PHB happens when a strong polarized signal saturates those ions arranged in a straight line with its polarization. Thus, the light (including the saturating signal and ASE) whose polarization is arranged in a straight line parallel with the polarization of the saturating signal receives an amplification slightly less than the light whose polarization is arranged orthogonally to that of the saturating signal. The effects of PHB are very small in the first amplifier of long haul

transmission systems, however, the effects get stronger with cascaded EDFAs or where the EDFAs are strongly saturated [77].

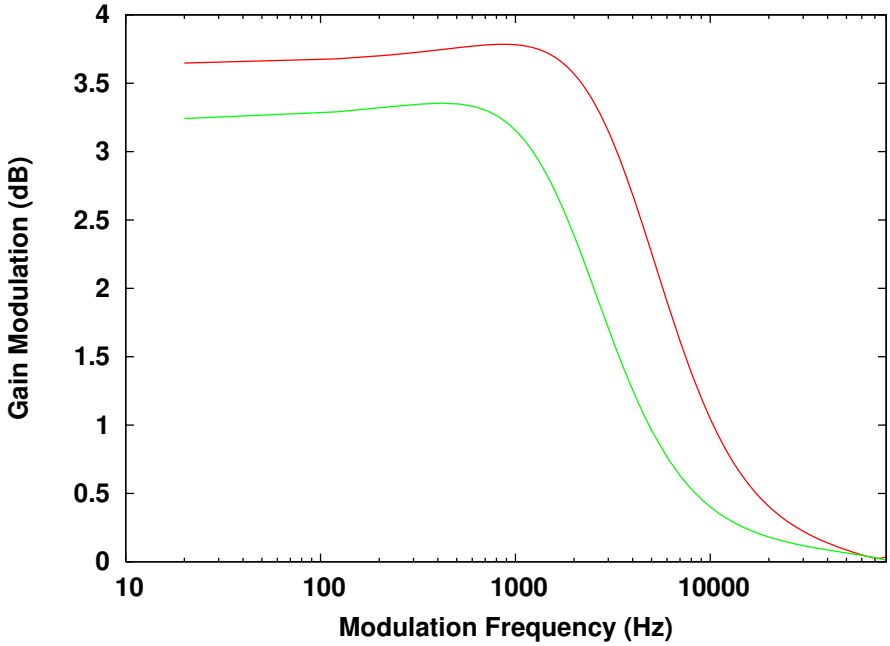

Figure 2.9: Gain modulation or gain cross talk in probe channel during sinusoidal signal amplification in another channel using the EDFA non-self-saturated gain dynamic models of the gain-shifted C-band (red) and C-band (green) (implementing Equation 2.11).

Slow **gain dynamics** of EDFAs is due to the extremely long lifetime of the first excited state ($\approx$ 10 ms), it is one of the desirable specifications of EDFAs. If the amplifier is in the saturated regime and the data rate is high enough, the modulation of the signals does not produce considerable gain modulation of the EDFAs [77,96], although the EDFA is strongly saturated. The corner frequency for the EDFA is inversely proportional to the metastable state lifetime (τ = 10 ms) and can be as low as 100 Hz. The corner frequency increases with signal and pump powers [97]. The value of the corner frequency typically stays less than 10 kHz and is given by:

$$f_c = \frac{w_c}{2\pi} = \frac{1+P_B}{2\pi\,\tau} \tag{2.34}$$

$$P_B = \sum_{k=1}^{M} \frac{P_k^{out}}{P_k^{IS}} \tag{2.35}$$

Where τ is the metastable state lifetime, f_c is the corner frequency, P_k^{out} is the EDFA output power at k^{th} channel, P_k^{IS} is the intrinsic saturation power computed from geometrical

parameters of EDFA as shown in Equation (2.33). Figure 2.9, shows the characteristic of EDFA with the cross talk phenomenon, a sinusoidally modulated input signal is used in one of WDM system channels which traverses the EDFA and the cross talk is measured through a probe channel. The cross talk values are between 0 and 3.5 dB for frequencies less than 10 kHz, and it approaches zero for frequencies higher than 10 kHz. This result shows good agreement with the result obtained by Giles [56]. In the long haul system the corner frequency increases with the length of the cascaded EDFAs, and with strongly saturated EDFA with high pump power [77].

The **gain spectrum** region of the EDFA is in the wavelength range of 1525 nm to 1565 nm, The gain spectrum is the result of both the distribution of the Stark split energy bands and the thermal distribution of their ions (as explained in Section 2.2). The gain spectrum is not flat. The shape of the gain spectrum varies with the inversion level. It can be shown from Equation (2.25) that the total gain spectrum for an EDFA or system of cascaded EDFAs is obtained by the gain coefficient averaged over the length of EDF in the EDFA or system.

$$g(\lambda,z) = g^*(\lambda)\, N_2(z) - \alpha(\lambda)\, N_1(z) \tag{2.36}$$

$$\overline{g(\lambda)} = g^*(\lambda)\, \overline{N_2} - \alpha(\lambda)\, \overline{N_1} \tag{2.37}$$

$$\overline{g(\lambda)} = [g^*(\lambda) + \alpha(\lambda)]\overline{N_2} - \alpha(\lambda) \tag{2.38}$$

Where $g^*(\lambda)$ is inverted gain coefficient and the over-bars show the calculation of the average over the length of all the EDFs in the EDFA or communication link with cascaded EDFAs. The fact that N_1 + N_2 = 1 has been used in Equation (2.38). The inversion changes with pump power and the gain spectrum for different values of the pump power is shown in Figure 2.5. In case the necessary inversion level and the probe wavelength are not selected properly, the gain spectrum can be highly non-uniform. When the average inversion level is properly selected, the gain at the wavelength near 1550 nm is significantly flat. The choice of co-dopants (the composition of the erbium-doped core) also strongly affects the flatness of the gain and the width of the gain spectra [77].

In WDM networks, flat gain amplifiers are required over the wavelengths range used in that application. The flatness of the gain can also be enhanced by including a gain-flattening

filter into the EDFA. For the best performance of the EDFA, it is essential to supply the light at the wavelengths which are specified in the erbium pump bands with adequate power to pump the EDFA. The EDFA pump should be efficient, reliable, and compact in size.

2.6 Pump configuration

For the best conversion efficiency, it is essential to supply the light at the correct wavelength (the wavelengths which are specified in the erbium pump bands) with adequate power to pump the EDFA. The EDFA pump should be efficient, reliable, inexpensive, and compact in size. Availability of suitable diode laser sources with all the above mentioned specifications at wavelengths 980 and 1480 nm make the use of EDFA in optical communications attractive. There are several advantages in pumping at a wavelength of 980 nm rather than 1480 nm, as discussed in Section 2.2.

We have already seen an EDFA with one type of pump configuration in Figure 1.11. Three different pump configurations are used in EDFA designs, a co-propagating pump and signal, a counter-propagating pump and signal, and bidirectional pumping, as shown in Figure 2.10 (a), (b), and (c) respectively. The pump configuration is chosen in accordance with the amplifier applications as discussed briefly in Section 1.8.1.

The power amplifier (booster amplifier) is positioned after the transmitter to boost the transmitter signal. The most important parameter for power amplifiers is maximum saturated output power. The output power of an EDFA can reach saturation conditions while experiencing strong input signal power. The output power for saturated amplifiers is directly proportional to the pump power. Thus, the power amplifier is designed for the most efficient conversion of pump energy into signal energy. In a single stage amplifier, the length of the EDF is made sufficient long in order the pump light can be convert completely to signal energy. Bidirectional pumping is the most suitable configuration for a power amplifier.

As far as small signal gain is concerned co-propagating and counter-propagating pumps produce the same gain but the total amount of pump power is different. The same gain level in both in the co-propagating and counter-propagating configurations is due to the similarity of the ASE profile in both cases. The bidirectional pumping produces high gain at small signal due to a different ASE profile. The preamplifier is used to improve the sensitivity of a direct

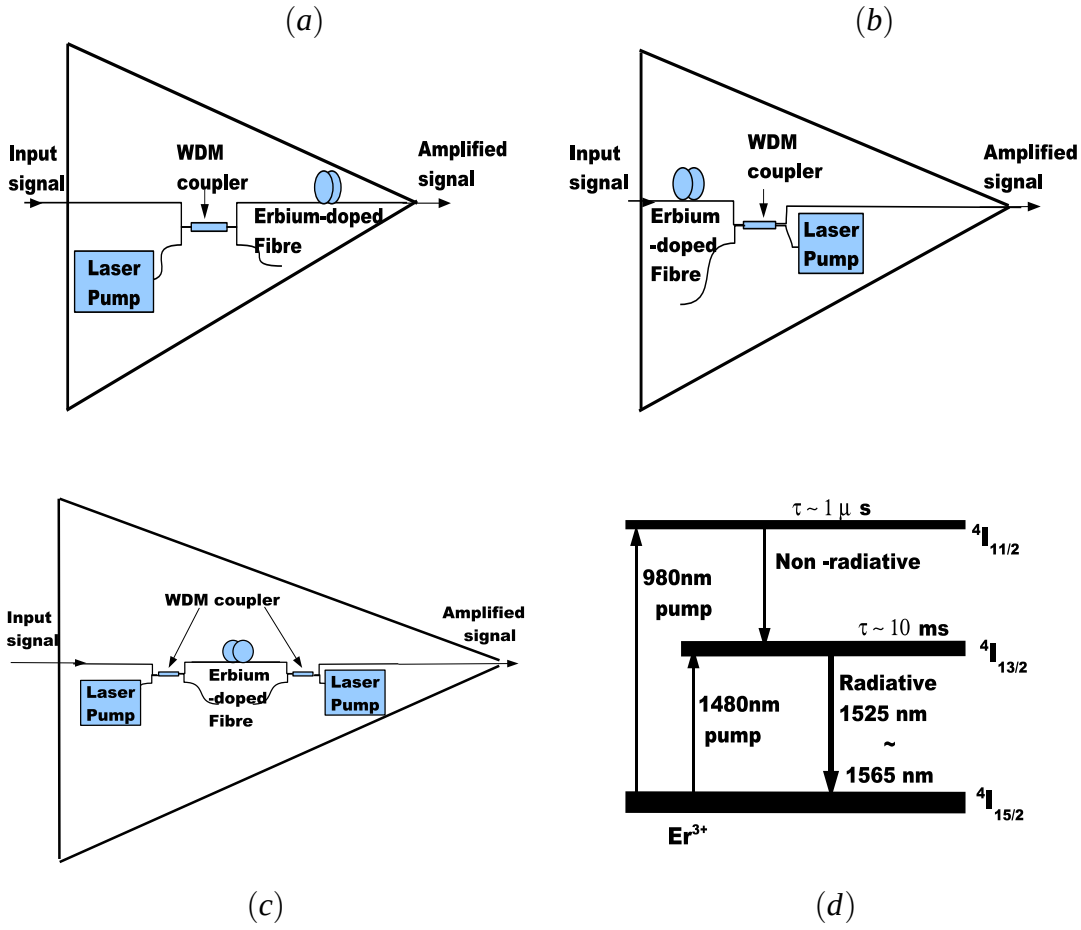

Figure 2.10: Different pump configurations for a single-stage EDFA, (a) co-propagating pump and signal, (b) counter-propagating pump and signal, (c) bidirectional pump. (d) Three energy level system used in the EDFAs amplification process.

detection receiver. The preamplifier is designed to give a low NF with high small-signal gain, as shown in Table 2.1 [15–17]. The low NF and small-signal gain can be achieved in a single stage amplifier by using a short length of EDF and counter-propagating pumping to decrease input coupling losses. In-line amplifiers must be designed with moderate gain, high output power, and NF in the range of 5-7 [17]. These parameters can be achieved using a single stage amplifier design. However, a long EDF is required to obtain high gain. In contrast, a low NF is obtained by keeping a high inversion at the input. The low NF is normally achieved using a short fibre segment [6, 77].

The two stage amplifier is the solution to achieve an efficient in-line amplifier. The specification of the preamplifier is used in the design of the first stage amplifier and booster

TYPES of EDFAs	Gain (dB)	NF
preamplifiers	20-30	3.5-4.5
booster amplifiers	5-15	5-7
In-line amplifiers	15-25	5-6.5

Table 2.1: Comparison of preamplifiers, booster amplifiers and in-line amplifiers; C-band EDFAs produced by RED-C Optical Networking Ltd [15–17].

amplifier in the second stage. Thus, with in-line amplifiers and an input signal at a low level, bidirectional and counter-propagating pumps are preferred because the effects of ASE become significant for long fibres. The in-line amplifiers for long haul systems are often of short fibre length to achieve a low noise system as mentioned above, and it requires the saturated condition for power self-regulation [6, 8]. When the signal is strong enough compared to the ASE, the pump configuration is not really an issue for the in-line amplifier. In this thesis the single stage in-line amplifier is used for investigation of the power transient phenomenon. The lengths of doped-fibre and their geometries also influence design considerations for low noise, high output in-line power amplifiers [6, 77].

2.7 Fibre lengths and geometries

In the case of in-line amplifiers, which have been used in this thesis for wavelength routed WDM optical networks, the required performance characteristics are moderate gain in the range of 15-25 dB, high output powers (typically 20 dBm for 40 channel WDM system) and operating in saturation condition (saturation power available 22 dBm [15]), and the NF in the range of 5-7 dB [16]. It is mentioned in the literature that it is difficult to optimise all three parameters (gain, output power and NF) simultaneously using a single stage design. For instance, high gain is obtained by using a long segment of erbium-doped fibre. In comparison, the best NF is achieved by maintaining a high inversion at the input and is usually best achieved with a short segment of EDF [77]. A moderate Numerical Aperture (NA) and short fibre lengths are suitable for a typical long haul in-line amplifier application as demonstrated in [18]. Thus, high NA in-line amplifiers suffer from higher background losses that affect conversion efficiency. The NF will increase as the background losses increase. The optical signal-to-noise ratio must be in an acceptable level (15.6 -13.6 dB) during transmission [6, 98].

The numerical aperture, is defined as: NA = $\frac{1}{n_0}\sqrt{n_{core}^2 - n_{cladding}^2}$ which is the sine of the maximum acceptable angle of an incident beam with respect to the fibre axis (considering the launch from air into the core), n_0 is refractive index of air. The NA also quantifies the strength of guidance, typical values are of the order of 0.1 for single-mode fibres, even though actual values vary over a relatively large range. For example, large mode area single mode fibres can have low values of NA, below 0.05, whereas some rare-earth-doped fibres have values of 0.3 and higher to get high gain efficiency. NA values around 0.3 are typical for multimode fibres. The sensitivity of a fibre to bend losses strongly diminishes with increasing NA, which causes strong confinement of the mode field in the core [40, 99].

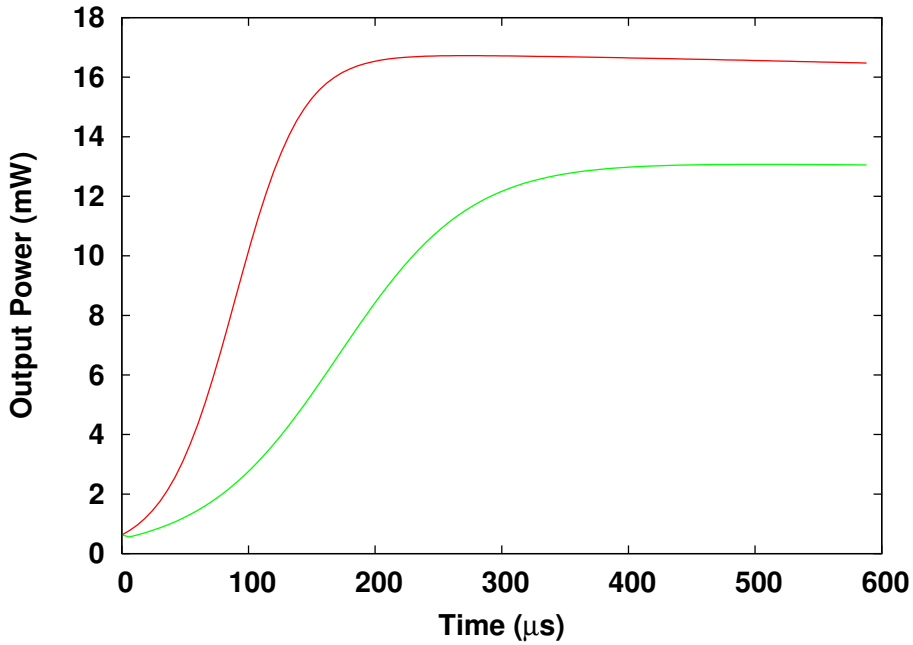

Figure 2.11: The output power of C-band (green) and gain-shifted C-band (red) EDFAs as a function of time, the output power differences are significant due to the differences in the core radius and overlap factors, the gain-shifted C-band EDFA was modelled by the variation in geometry parameters of the C-band EDFA.

The transient phenomena in multi-wavelength routed WDM networks become more obvious and increase the degradation of the signal-to-noise ratio at the receiver, especially as the number of cascaded EDFAs increase, as discussed in next chapter. Figures 2.7 and 2.8 show the effect of fibre length on the EDFA gain performance. An EDF length of 20 meters and ion population of 0.7x10^{25} ions/m^3 are used in this research for investigating EDFA performance. In the C-band amplifier, the EDF cross-section area and overlap factors of both signal and pump are 3.46 $\times 10^{-12}$ m^2, 0.0926, 0.1204 respectively and in gain-shifted C-

band amplifiers, the EDF cross-section area and overlap factors both of signal and pump are $1.574 \times 10^{-12}\ m^2$, 0.40, 0.64 respectively. The radii of the cores for C-band and gain-shifted C-band are, respectively, 0.708×10^{-6} m, and 3.461×10^{-6} m. The geometry parameters used as the basis for modelling an EDFA were mentioned when referring to the gain-shifted C-band EDFA.

Figure 2.11 shows the output power variations in the saturation regime versus time. The differences in the output power is due to differences in the geometry parameters of the fibre which is used for the modelling of C-band and gain-shifted C-band EDFAs.

2.8 EDFA effects on the dynamic phenomena in optical networks

The dynamic aspects of wavelength routed WDM optical networks are related to variations of the power at each wavelength or in the number of wavelengths of the network. The investigation of the dynamic phenomena is related to the network performance analysis. In optical networks, the EDFAs are operating in gain saturation. The gain saturation can be obtained, for constant pump power, by changing the total input power. Thus, when the input power varies, either by changes in the number of channels or by variations in channel input power, variation of the output power of all amplified channels occurs until re-balance can be reached between the absorption and emission processes. The time between the previous balance and new balance is specified by a transient period and dynamic variation in optical power, and is referred to as an optical power transient. The rate at which the EDFA gain changes during the transient period is determined by both the spontaneous lifetime of the metastable state and the total amount of saturated output power. The transient periods of gain saturation and recovery were found to be, in the early period of EDFA development, a few hundred μs [56, 100]. The effective transient period of multichannel WDM optical networks, which are characterised by high output powers, are specified by tens of μs [101]. One of the major advantages of an EDFA is the absence of inter-channel crosstalk among WDM channels by the signal modulation. Thus, the gain of the EDFA is not affected by the signal modulation in high speed data transmission rates over a few Mbit/s. This is the reason for using steady state EDFA models to describe high speed data transmission systems [102].

Research and development has been concerned with the optical power transient effects since the early stages of EDFA applications in optical networks [103]. In point-to-point links of the network, the power transient can be as high as a hundred milliwatts. When the system has been switched-on (including a pump source) for a while, if the input signal is instantaneously applied to the link, then a high transient power occurs which may damage electrical components in the receiver or optical components on the link. Transient power also occurs at system restart after a failure of the link cable.

The power transient phenomena have been characterised in the International Telecommunication Union (ITU) Recommendation G.663. This document specifies the minimization methods of the optical power transient or surge phenomena in the network link using EDFAs, such as the pump power must be reduced or switched-off when any signal failure is observed, and that after the signal channel become available, the restart of the pump laser must be performed gradually [104]. Transient phenomena can be very significant in wide-area optical networks such as long-haul submarine systems. Therefore, a lot of research has been done to mitigate the effect of the transient phenomena in wavelength routed WDM networks using EDFAs, a brief review of protection schemes of WDM networks is presented in Section 1.9.

Regarding the dynamic behaviour of the EDFA in an optical wavelength routed network, the optical power traversing the cascaded EDFAs in the link will vary according to system management requirements. For example, in channel reconfiguration, adding a new wavelength during network expansion or dropping of wavelengths during link failure. These events affect the total power input to the link because, in wavelength routed WDM networks, the wavelengths from each input link are distributed by OXC and OADM (as discussed in Chapter 1) to different output links according to the routing information. Power transients in a network link with cascaded EDFAs will induce transients in the remaining channels in the link [105]. Analysis shows that the speed of evolution of the power transients at the output of cascaded EDFAs is a multiple of the output of the single EDFA. Computations for an optical link with cascaded EDFAs showed that for the loss of a large number of channels, the power of surviving channels can alter by 1 dB within a time duration of 100 ns [106].

Moreover, in packet-switched optical networks, if the packet traffic is directly fed into the specified wavelengths, then this can result in variation in the total power applied to each

fibre link. Thus, cross-gain saturation can induce effects in channels similar to the transient phenomena of circuit switched networks resulted from channel addition or dropping [107–109]. The numerical and statistical analysis of bursty traffic is the main research topic of this thesis. Services of the optical network, such as gigabit Ethernet local area networks, multimedia, applications of variable bit rate video have been found to be associated with variable traffic behaviour [110]. The investigation has indicated that the variation increases substantially with packet interval times [111, 112], and that the traffic characteristic is self-similar in these networks [112]. Increased variability produces self-similarity, thus longer intervals of higher or lower input power are more likely to happen, this gives time for an EDFA to achieve very different gain values or cause output power swings [113, 114]. The power swing at the output of each surviving channel, due to cross-saturation effects in the amplifiers, deteriorates the quality performance of the channels through four conditions or mechanisms when channel loading varies in the network links.

First, dropping of wavelengths during link failure, increases the power in the optical link. This power increase in the link, introduces problems of optical nonlinearity. There are five main optical nonlinear effects that can deteriorate the propagating signals in the optical networks: SBS, SRS, SPM, XPM and FWM. These five non-linear effects are discussed in more detail in Section 1.7.7. The impact of these five nonlinear effects on the WDM optical network performance manifest themselves in four different ways.

Second, network reconfigurations when system expansion is demanded may require the addition of some channels, the optical power at the receiver can be reduced during the transient period which results from channel addition, which would increase the noise level. If the signal power at the receiver is lower than the receiver sensitivity, bit-error rate would strongly deteriorate [52].

Third, the power swings during the transient period may cause deterioration of optical SNR due to the change of inversion level, and also the change in gain spectrum during transient phenomena [52].

Fourth, the power swings during the transient period at the receiver may require fast optimization techniques for the receiver threshold power, this might be problematic for particular receivers [52].

For the analysis of the effects of the EDFA power transients on WDM network perfor-

mance, it is essential to implement the dynamic models (2.11), and (2.21) mentioned in Sections 2.3, and 2.4. The numerical simulation techniques used for accurate implementation of the gain dynamic models are discussed in Section 2.9.

2.9 Numerical simulation techniques

We mentioned that the gain dynamics behaviour of an EDFA is modelled by a single ODE which was derived by Sun [74, 75, 86]. There are many numerical methods for solving ODEs, such as Euler and 4^{th} order Runge-Kutta schemes [115–117]. The latter is applied in this thesis. An ODE with a specified initial value is represented in the form,

$$\frac{dG}{dt} = f(t,G), \tag{2.39}$$

$$t_0 < t < T,$$

$$G(t_0) = G_0 \tag{2.40}$$

Where G(t) is a function of time and f(t,G) is a function depending on time and gain. The independent variable t varies from t_0 to T_{end} and the initial value for G at $t = t_0$ is denoted by G_0. Thus, we are trying to find the approximate solution for G(t) at certain values of times $t_0 < t_1 <,...,< t_N = T_{end}$ for positive integer N. If we denote by G_k, the approximate solution to G(t), k = 0, 1, 2,..., N, at $t = t_k$, while the G_0 is the initial value obtained by Bisection or Newtonian methods applied to the transcendental nonlinear equations obtained at steady state conditions of the model [118]. The main aim of numerical methods is to obtain the values G_1, G_2,...,G_N, which approximate the exact values $G(t_1)$, $G(t_2)$,..., and $G(t_N)$ respectively. One method to approximate the derivative dG/dt at t = t_K is by a finite difference (G_{k+1} - G_k)/h_k, where h_k = t_{k+1} - t_k is called the grid size, this is because the derivative is specified as the limit of difference quotients:

$$\left(\frac{dG}{dt}\right)_{t=t_k} = lim_{h_K \to 0} \frac{G(t_{k+1}) - G(t_k)}{h_k} \tag{2.41}$$

Where, h_k is the grid size, and the smaller the value of h_k the more accurate the expected results, providing there is no numerical instability. Equation (2.39) can be written as:

$$\frac{G_{k+1} - G_k}{h_k} \approx \left(\frac{dG}{dt}\right)_{t=t_k} = f(t_k, G(t_k)) \approx f(t_k, G_k) \tag{2.42}$$

Equation (2.42) leads to solution by what is called the **Explicit Euler method**:

$$G_{k+1} = G_k + h_k f(t_k, G_k) \tag{2.43}$$

The initial value of G is given as G_0 at t = t_0, then G_1 can be obtained from the formula with k = 0. Then we obtain G_2 using G_1 with k = 1. This procedure can be applied iteratively until G_N is obtained. The equally spaced points are mostly used for simplicity, that is, t_k = t_0 + k*h, k= 0,1,...,N, with grid size h = (T_{end} - t_0)/N. The error is obtained by subtraction of the accurate result which is produced by solving the function analytically, and the approximate result which is obtained by solving function numerically [116].

There are some other methods that can provide greater stability, such as second-order or fourth-order Runge-Kutta methods as shown in Equations 2.44, and 2.45 respectively;

$$\begin{aligned} G_{k+1} &= G_k + (F1 + F2)/2, \\ F1 &= h_k f(t_k, G_k), \\ F2 &= h_k f(t_{k+1}, G_k + F1). \end{aligned} \tag{2.44}$$

$$\begin{aligned} G_{k+1} &= G_k + (F1 + 2F2 + 2F3 + F4)/6, \\ F1 &= h_k f(t_k, G_k), \\ F2 &= h_k f(t_k + h_k/2, G_k + F1/2), \\ F3 &= h_k f(t_k + h_k/2, G_k + F2/2), \\ F4 &= h_k f(t_{k+1}, G_k + F3). \end{aligned} \tag{2.45}$$

It is shown that the error factor between the analytical solution and the numerical solution from second-order Runge-Kutta (2.44) is proportional to h^2, second-order accuracy, while the error from Equation (2.45) is proportional to h^4, fourth-order accuracy with the proportionality value depending on higher order derivatives of the analytical solution. In comparison Euler's method has an accuracy proportional to h, first-order accuracy [116]. The fourth-order Runge-Kutta is preferred for its accuracy and is used in the numerical simulation of the ODE used to model the dynamic behaviour of the EDFA. An example of this fourth-order Runge-Kutta scheme is shown in Appendix B.6.

There are many iterative methods for the implementation of transcendental nonlinear equations such as Newtonian or Bisection algorithms for providing steady-state values for the model. This is performed by assigning dG(t)/dt = 0. The Bisection iteratively obtains a value of t for nonlinear equation f(t) = 0 in a given interval [t_0, t_{end}]. If f is a continuous function on [t_0, t_{end}], and f(t_0) and f(t_{end}) have values of opposite sign, then the Intermediate Value Theorem promises that there is at least one root r in [t_0, t_{end}] such that f(r) = 0. The aim from this iterative method is to find a sequence of numbers [r_n] such that r_n becomes very close to a root r when $n \longrightarrow \infty$.

The Bisection method assumes that a function f is continuous on [t_0, t_{end}] and f(t_0)f(t_{end}) < 0. First, in this method, the value of middle point t_{mid} = (t_0 + t_{end})/2 is computed, then verify that f(t_0)f(t_{mid}) < 0. If it is true, then f must have root in the interval [t_0, t_{mid}]. If it is false then f must have root in the interval [t_{mid}, t_{end}]. Wherever the root is, that interval must be renamed [t_0, t_{end}] but the size is reduced by half. Then this procedure is repeated until [t_{end}, t_0] or f(t_{mid}) is small, the value of t_{mid} is chosen as the approximate root solution of f. The Bisection method is chosen for implementation in this thesis as demonstrated by the example in Appendix B.7.

2.10 Summary

In this chapter, the amplification process in EDFAs is explained. The amplification mechanism is stimulated emission, but in this case the population inversion is achieved by optical pumping. During this process, pump photons raise electrons to excited states which exist at higher energy levels. This configuration is known as the three-level atomic system. It is the atomic energy level structure that provides the EDFA with the ideal characteristics for optical networks.

The gain dynamics behaviour of EDFAs are determined using a model which is a single ODE, developed by Sun and Zyskind [74]. The extension of this model to include the ASE power is also developed and implemented to investigate the OSNR performance in both circuit-switched and ATM-IP networks. It is essential for understanding of each term in the gain dynamic models, to review briefly properties such as gain, gain spectrum, transmission impairments, etc. For the best conversion efficiency, it is essential to supply the light

at the wavelengths which are specified in the erbium pump bands with adequate power to pump the EDFA. The EDFA pump should be reliable, inexpensive, and compact in size. Pumping specifications at wavelengths 980 and 1480 nm make the use of EDFAs in optical communications attractive. Three different pump configurations are used in EDFA designs, a co-propagating pump, a counter-propagating pump, and bidirectional pumping. The pump configuration is chosen in accordance with the amplifier applications.

The effects of geometric parameters in developing different EDFAs by choosing different EDF lengths, numerical apertures, ion populations and overlap factors for pump or signal wavelengths have been explained. The geometric parameters were used as the basis for modelling the gain-shifted EDFA which is referred to as gain-shifted C-band EDFA. This gain-shifted C-band EDFA is used in this thesis for studying the power transients phenomena in circuit and packet switched networks.

The EDFA effects on the dynamic phenomena in optical networks are discussed. Regarding the dynamic behaviour of the EDFA in an optical wavelength routed network, the optical power traversing the cascaded EDFA in the link may vary according to the system management requirements. For example, in channel reconfiguration, adding a new wavelength during network expansion or dropping of wavelengths during link failure. These events affect the total power input to the link. In a network link with cascaded EDFAs, increase or decrease in input power induces power transients in the remaining channels in the link.

Finally, in this thesis, a 4th order Runge-Kutta numerical method is applied for solving the single ODE for gain dynamics. This numerical technique is used for developing the simulators of the self-saturated and non-self-saturated EDFAs.

Chapter 3

EDFA power transient phenomena in circuit-switched networks

3.1 Introduction

EDFAs have appeared as a key enabling component in optical networks because they possess features (illustrated in Chapters 1 and 2) of high gain over a large range of wavelengths, low intrinsic losses, and long fluorescence time. Due to this long fluorescence time high-speed WDM point to point links do not experience the cross-gain saturation typical of networks employing semiconductor optical amplifiers. Recently, however, there has been substantial research effort into the investigation of the EDFA's transient response when reconfiguration adds or drops one or several wavelength channels in WDM circuit-switched and packet-switched networks [56, 74, 97, 100, 101, 105, 107, 119].

This chapter reviews the characteristics of EDFAs in the time domain. Firstly, the behaviour of the power transient, corresponds to the gain dynamics of the EDFA, and has consequences for performance of wavelength routed WDM networks. Secondly, issues related to the amplification of bursty traffic in a form of short pulses when the EDFA is in the saturated gain regime are discussed in Chapters 4 and 5. The discussion of other time domain effects, which are relevant to different regimes of picoseconds, femtoseconds, and soliton pulse amplification, which involve fibre dispersion and nonlinearity, are beyond the scope of this thesis. The most important characteristic of EDFAs, as mentioned earlier, in

WDM networks, is slow gain dynamics, i.e. the saturation characteristic and recovery times are typically in the range between 100 μs to 1 ms. As a result, EDFAs possess intrinsic immunity to the effects of cross talk at high data rates, as shown in this chapter and as shown in [6, 78, 79, 96]. In this chapter, numerical simulation is presented with critical analysis of the gain dynamics of EDFAs in circuit switched WDM networks.

3.2 Verification of the model

The following section involves the verification of the dynamic model on which this thesis focuses. The verification of the model has been done through a set of numerical simulations of the model; firstly, the numerical simulation of the surviving channels power transient for either the loss or addition of 1 to 7 channels out of 8 WDM channels in a single EDFA and cascaded EDFAs, secondly computing the time delay and magnitude of the rate of power transients for surviving channels to reach 1 dB after dropping or adding 4 channels out of 8 WDM channels in a single EDFA and a chain of EDFAs.

3.2.1 Numerical simulation parameters

Research by Sun et al [74] produced a dynamic model of the EDFA. As mentioned earlier, the single ordinary differential equation of the EDFA dynamic model shown in Chapter 2 is used to simulate the time-dependent EDFA gain and optical output power. Validation of the model used in this thesis was performed using extensive numerical simulations. There exists good agreement between the results of these numerical simulations and the original model [74], through the implementation of the single stage EDFA, as shown in Figure 3.1 with eight WDM channels, the same configuration as used in the original model. The eight wavelengths of the channels were chosen based on the specifications of the Multi-wavelength Optical Networking (MONET) project [120], which was applied in the original model as well. The wavelengths are shown in Table 3.1. Increasing (or decreasing) the number of channels requires only the addition (or subtraction) of a term on the right hand side (RHS) of the model. The pump channel is labelled as the first channel in Sun's model. The input signal power to each channel is -2 dBm (0.63 mW), the EDF length is 20 m. The EDF has a spontaneous lifetime of 10.5 ms, input signal power to the pump channel is 18.13dBm (65mW),

the remaining simulation parameters are shown in Table 3.1. The geometrical parameters are as shown in Table 3.2. The so-called "Giles" parameters, consist of absorption and emission cross-sections. These parameters are used for the simulation of C-band and gain-shifted C-band EDFAs, and are also shown in the curves of absorption and emission coefficient versus wavelength in Figure 2.3. The "Giles" parameters are provided by Highwave Optical Technologies [10].

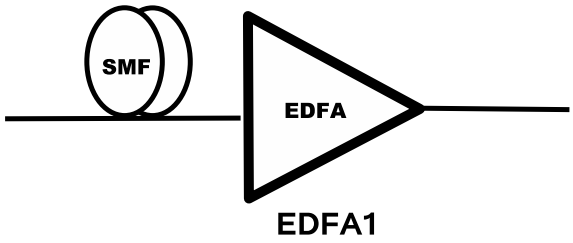

Figure 3.1: The EDFA simulation circuit layout.

Parameters	Ch0	Ch1	Ch2	Ch3	Ch4	Ch5	Ch6	Ch7	Ch8
λ_k(nm)	980	1549.2	1550.8	1552.4	1554.0	1555.6	1557.2	1558.8	1560.4
$\alpha_k(m^{-1})$	0.26	0.1582	0.1510	0.1445	0.1394	0.1335	0.1277	0.1212	0.1134
$h\upsilon P_k^{IS}$(mW)	0.83	0.3394	0.3482	0.3562	0.3621	0.3694	0.3778	0.3903	0.4068

Table 3.1: C-band EDFA simulation parameters.

TYPES	D (m)	A (m^2)	Γ_p	Γ_s	τ (ms.)	N (ions/ m^3)	NA
C-band	$1.42\text{x}10^{-6}$	$1.5742\text{x}10^{-12}$	0.1204	0.0926	10.5	$0.7\text{x}10^{25}$	0.21
g-s C-band	$2.1\text{x}10^{-6}$	$3.461\text{x}10^{-12}$	0.64	0.4	10.0	$0.7\text{x}10^{25}$	0.15

Table 3.2: C-band and gain-shifted (g-s) C-band EDFA simulation parameters, core diameter (D), cross-sectional area (A), pump-overlap factor (Γ_p), signal-overlap factor (Γ_s), spontaneous-lifetime (τ) of the upper or metastable level, total erbium ion populations (N) in fibre, and numerical aperture (NA) [6, 18].

3.2.2 Numerical simulation results

Firstly, at the steady state (i.e. prior to power transient phenomena), the output powers for all 8 wavelengths of the C-band EDFA were simulated and plotted as shown in Figure 3.2. The saturated gains of all 8 channels as shown in the figure are between 10.5dB and 11dB.

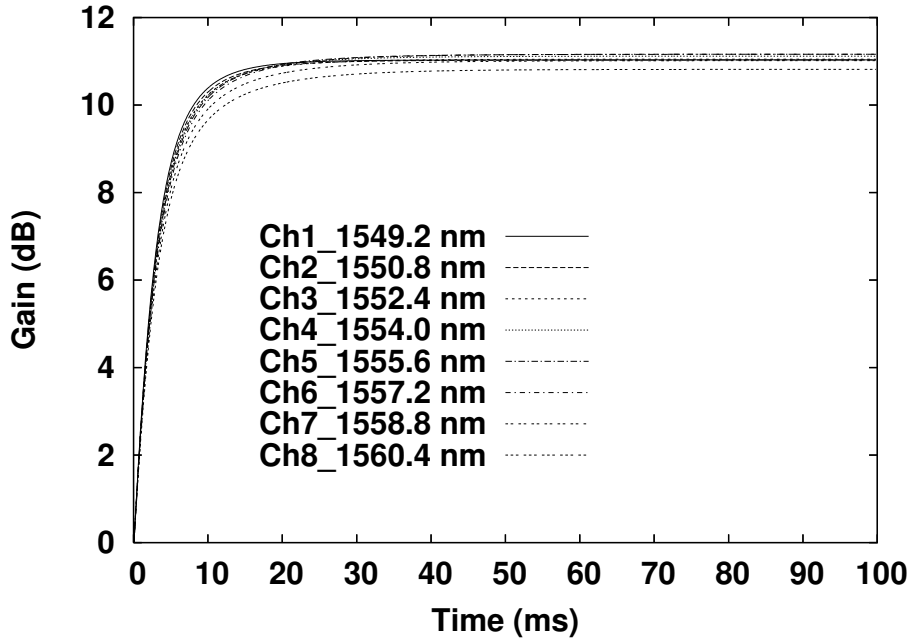

Figure 3.2: The gain of the eight channels in the network link prior to any perturbation occuring in the WDM network.

Secondly, the saturation power, P_{sat}, performance was plotted for the EDFA dynamic model. This is an important performance parameter for multichannel systems to identify both the input signal and the pump power which are required for operation in the saturation regime, see Figure 2.4. This figure illustrates saturation performance for the probe channel (1549.2 nm) at three different values of the pump power 40 mW, 65 mW, and 100 mW. The gain saturation performance was determined as the input signal power was varied from -120 dBm to 60 dBm. The input signal power which is required for each channel to operate the EDFA at saturation regime at the specified pump power was computed. The output power per channel for M identical input channels is limited to P_{sat}/M [121, 122].

The pump power was set to 65 mW at a wavelength of 980 nm. Then the amplifier gain was 13 dB for all small signal input power where the curve is a straight line, see Figure 3.3, in this region which indicates an initial linear relation between input signal power and output signal power, then the curve starts to decline and the saturation point is at -3 dB which occurs at a gain of 10 dB which results from the input power signal of -2 dBm (0.63 mW). The simulation steps mentioned above were repeated for pump power of 40 mW and 100 mW. The gain and the saturation points vary for each case as shown in Figure 2.4. A fourth order Runge-Kutta technique was used for numerical simulation of the gain dynamic model of the

EDFA, as described in Section 2.3. The simulation run-time was 100 ms with a time-step of 10 μs.

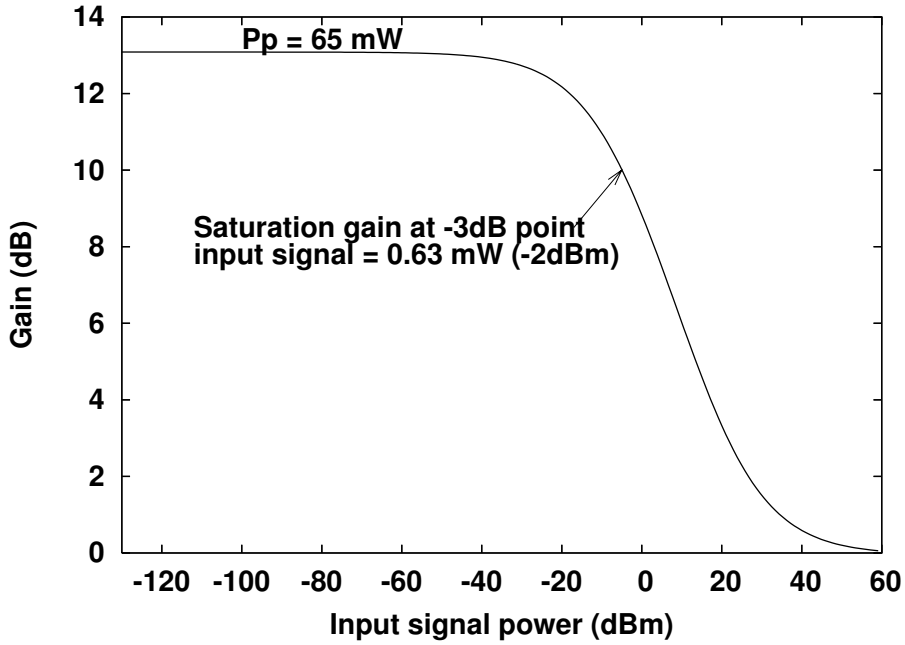

Figure 3.3: The EDFA saturated gain performance of the probe channel of wavelength 1549.2 nm, (numerical simulation result of the non-self-saturated gain dynamics model of the EDFA, described in Section 2.3).

Thirdly, simulations were performed for square-wave pulses and sinusoidal input signals to demonstrate the frequency response of the saturation induced cross talk. Square-wave pulse input signals were initially used to demonstrate the induced cross talk in the Continuous Wave (CW) simulation. Here the same simulation technique and resolution as mentioned earlier was used. The system for computing saturation induced cross talk consists of two signal channels which are multiplexed in the system. The saturated induced cross talk was deduced during the amplification of the two signal channels. First, simulation was performed using one channel at a wavelength of 1549.2 nm operating with a CW signal and the other channel at a wavelength of 1550.8 nm also operating with a square-wave signal. When the square-wave pulses at channel 2 were amplified, the leading edge of the output square pulses will experience overshoot due to gain saturation behaviour of the EDFA as shown in Figure 3.4 (a).

The pulse decay power depends on the input pulse peak power as shown in Figure 3.4 (b) [56]. The population inversion of ions related to the probe channel decreased at time 40

ms to 40.1 ms due to the amplification of square-wave signal at channel 2. This is illustrated as the exponential decay of the probe channel output power to the level lower than steady state level.

Figure 3.4 (a) shows the output power of the probe channel is reduced by 21 mW (due to existence of the square-wave pulse), this was defined as the ratio of the leading edge to the trailing edge of the square-wave pulse output power. For the probe channel, the decay (transient) time is 100 μs, then recovery time is 480 μs, the output power exponentially increases in this interval by 21 mW. This gain recovery time is of the order of the reciprocal of the pumping rate as shown in Equation (3.1). The recovery times are the same even though the peak input power or the pulse duration are varied because the parameters in the Equation (3.1) are the same [56, 122, 123], this will be discussed in more detail in Chapter 5.

$$R^{-1} = \pi r^2 h\nu_p / P_p \sigma_p \Gamma_p \tag{3.1}$$

Where r is the fibre core radius, P_p is pump power, σ_p is the absorption cross-section of the pump, Γ_p is the pump overlap factor, $h\nu_p$ is the photon energy of the pump [56].

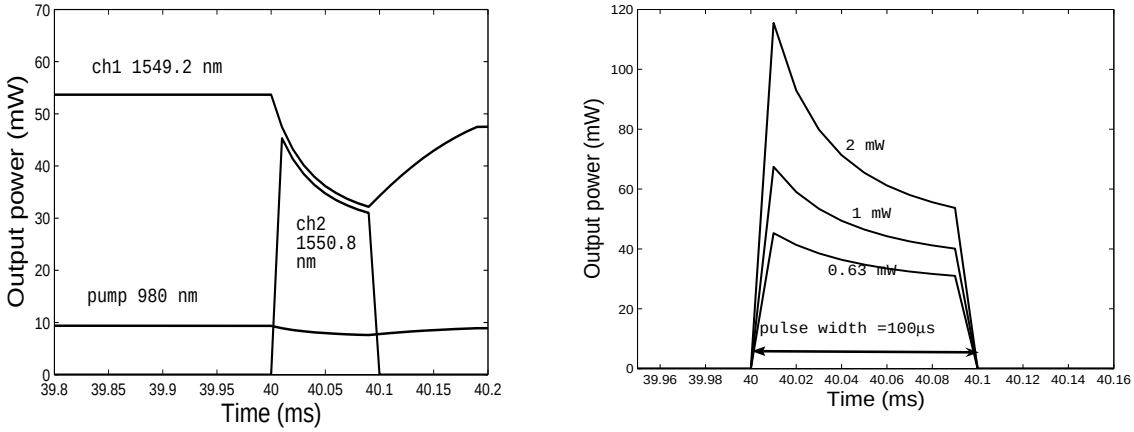

Figure 3.4: EDFA behaviour during amplification of the packetized traffic which induces cross-gain saturation in the adjacent system channels, (a) the output power transients of channel 1, CW, while the packetized traffic is amplified in channel 2, (b) the output power transients of channel 2 using the packetized traffic of different input peak powers, 0.63, 1, and 2 mW.

The second simulation was performed using identical parameters and the procedure described above while the saturating square-wave signal input is substituted by a sinusoidal

signal. Amplification of the sinusoidal signal causes decay in the output power of the probe channel. The dynamics of the population inversion and evaluation of the cross talk can be deduced from the transient response of the EDFA. The sinusoidal signal was used to compute the frequency response of the saturated induced cross talk in the amplified probe signal. Figure 3.5 shows the peak-to-peak modulation of the probe signal, normalised to the probe's average power. The corner frequency at which the response begins to decrease is 1500 Hz (gain-shifted C-band (red line)). At frequencies greater than 10 kHz, steady-state gain compression occurred, as the slow response of the EDFA's population inversion removed any high-frequency modulation of the EDFA's gain.

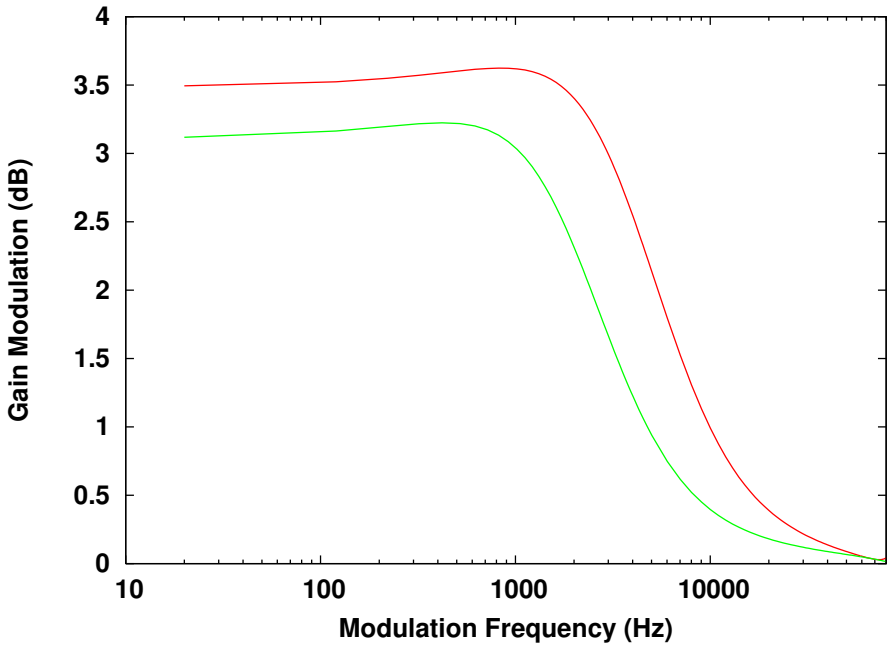

Figure 3.5: The EDFA gain modulation response during sinusoidal signal amplification as a function of the modulation frequency, numerical simulation result of the EDFA self-saturated gain dynamic model of the gain-shifted C-band (red) and C-band (green) (described in Section 2.4).

We simulated the transient response of the C-band EDFA caused by variation of the input power of the EDFA due to dropping or adding of input channels of different wavelength. The transient response refers to power transient magnitude and the duration of the power transient and its recovery time. If the output power at the steady state is denoted by p(0) and the transient output power is denoted by p(t), then p(t) - p(0) is the transient power and the time required for variation from p(0) to p(t) is the power transient time, while the time required for the output power to restore its original value or return to steady state level (i.e.

from p(t) to p(0)) is denoted by the power transient recovery time. The output power, p(t), varies from max(p(t)) to min(p(t)) depending on the loss or addition of input power to the EDFA. Figure 3.6 shows the power transient in the probe channel of wavelength 1549.2 nm after 1 to 7 channels are dropped at 60 ms and then 1 to 7 channels are added at 80 ms. The terms which are used to study and compare the power transient time response of the EDFA, firstly, the 1 dB rise- or increase-time in the power transient response refers to the time it takes for the power transient of the surviving channels to be increased by 1 dB after at least one channel has been dropped. Similarly, the term 1 dB fall- or decrease-time refers to the time it takes for the power transient of the surviving channels to be reduced by 1 dB from the peak value after at least one channel has been added to the existing channels. Secondly, the rate of the transient power or gain refers to the ratio between the transient power or gain magnitude of 1 dB and the 1 dB increase- or decrease-time.

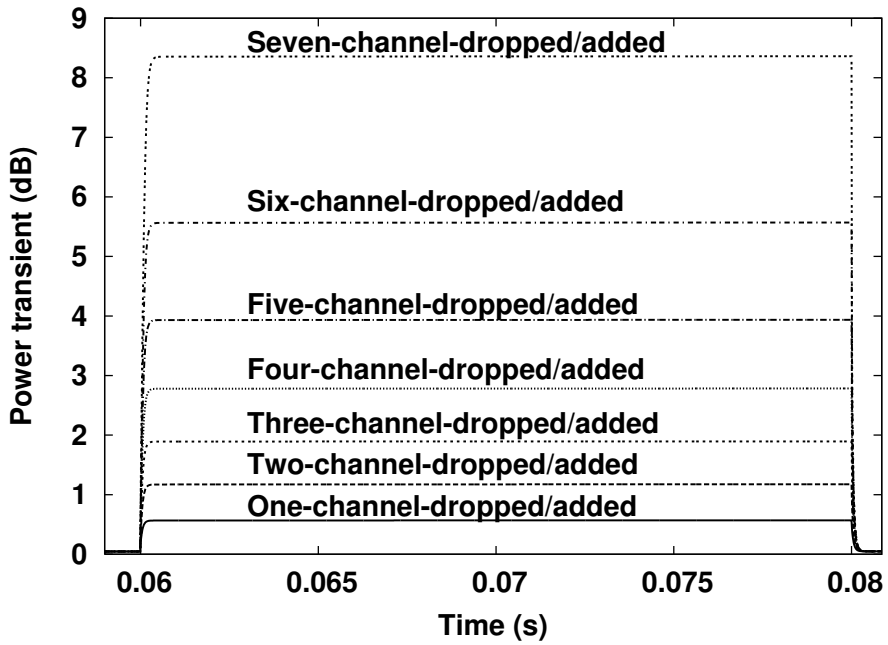

Figure 3.6: The power transients while 1 to 7 channels are dropped at 60 ms and 1 to 7 channels are added at 80 ms of the simulation run-time.

The term input power ratio is used in this thesis. This term refers to the ratio between the input power of the lost or added channels and the total input power of the EDFA before the power transient occurs. In Figure 3.7, when one channel was dropped the total output power transient was 1.132 dB corresponding to an input power ratio of 0.25, the time required by the power transient to reach 1 dB was 122.1 μs, and the rate of power transient was 0.0082

dB/μs. When six channels were dropped the total power transient corresponding to an input power ratio of 0.75 was 5.51 dB, the time needed by the power transient to reach 1 dB was 17.3 μs, and the rate of power transient was 0.0578 dB/μs.

The power transient is small and the rate is slow when a small proportion of total input power is lost, the power transient and the rate increases when a larger value of the total input power is lost.

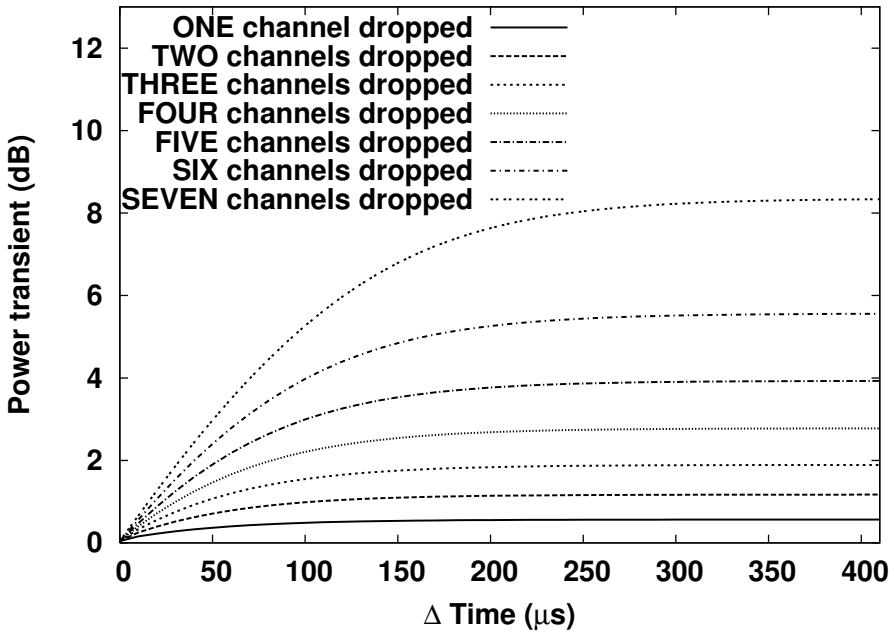

Figure 3.7: The power transients of the surviving channels due to the loss of 1 to 7 channels out of 8 WDM channels in a single EDFA, this figure shows the period when channels are dropped at 60 ms, see Figure 3.6.

Another example is shown in Figure 3.8, we incrementally added channels to the link, up to the full target of 8 channels which were originally in the system. The power transient was 4.42 dB corresponding to a total input power ratio of 0.25, and the time needed by the power transient to decrease 1 dB was 8.2 μs, the rate of the power transient at the input power ratio of 0.25 was 0.1219 dB/μs. When the power transient was 7.7 dB corresponding to a total input power ratio of 0.75, and the time required by the power transient to fall 1 dB was 2.26 μs, and the rate of the power transient at the input power ratio of 0.75 was 0.4424 dB/μs. The simulation results in Table 3.3 show that there is a good agreement with the original model's simulation results reported in [119]. The small difference between our numerical simulation results and the results reported in the literature is simply due to the values of parameters used in the simulation model, such as Giles parameters and geometric parameters shown in

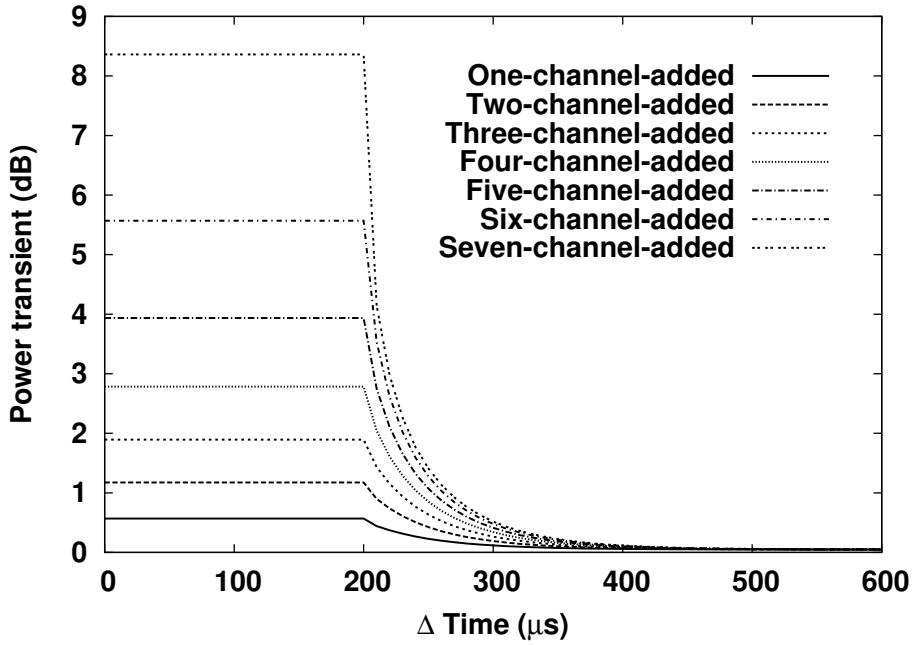

Figure 3.8: The power transients of surviving channels due to the addition of 1 to 7 channels to 8 WDM channels in a single EDFA, this figure shows the period when channels are added at 80 ms, see Figure 3.6.

Table 3.2.

$Input_{ratio}^{pow}$	$1dB_{time}^{rise}$	$\Delta - P_{transient}^{rise}$	$1dB_{time}^{fall}$	$\Delta - P_{transient}^{fall}$	Ch-no
Ratio	μs	dB	μs	dB	Num.
0.125	NA	NA	NA	NA	1
0.25	122.1	1.132	8.2	4.42	2
0.375	50.1	1.86	6.02	5.57	3
0.5	32.6	2.72	4.71	6.46	4
0.625	25.9	3.89	3.6	7.16	5
0.75	17.3	5.51	2.26	7.7	6
0.88	13.8	8.2	1.12	8.3	7

Table 3.3: Simulation results of C-band EDFA.

The results plotted in Figures 3.6 to 3.8 indicate that when less than half of the channels are dropped, the power transients are less than 2 dB. These power transients are identical with the power transients obtained in the numerical simulation and the analytical results of the original model [119].

For further verification of the model, the power transient in the probe channel and the related saturation-factors are plotted from our simulation results after 1 to 7 channels out of 8 WDM channels were dropped, as shown in Figure 3.9. The channels are dropped in

order of descending wavelength in the optical network. The formula used for computing the saturation factor in the numerical simulation is given in Equation (3.2) and these results show a good agreement when compared with the saturation factors of the original model [119].

$$\gamma = -\sum_{i=1}^{N} \frac{P_i^{in}}{P_i^{IS}} \exp(G_{i0}L) = \sum_{i=1}^{N} \frac{P_i^{out}}{P_i^{IS}} \tag{3.2}$$

$$P_i^{out}(t) = P_i^{in} \exp(G_i(t)L) \tag{3.3}$$

Where P_i^{in} and P_i^{out} are the input and the output power in the WDM network system respectively. P_i^{IS} and G_{i0} are the intrinsic saturation power and the gain at steady-state respectively, where L is the length of EDF of the EDFA. It is also possible to define the saturation factor in terms of the spontaneous lifetime of the upper level, τ, and effective upper level lifetime, τ_e, as shown in Equation 3.4. The effective upper level lifetime, τ_e, is the effective decay time of the upper level averaged over the EDF length [119].

$$\tau_e = \frac{\tau}{1+\gamma} \tag{3.4}$$

Where the saturation factor, γ, or alternatively the effective upper level lifetime, τ_e, is used as a fitting parameter to obtain best fit with experimental results as mentioned in the original model [119].

Verification of the original model results was also achieved when saturation factor was plotted against the number of channels dropped. Figure 3.9 shows the saturation factor calculated using Equation (3.2) when less than a quarter of the channels were dropped. The total power transient of the surviving channels is small and the saturation factor is large, whilst the total power transient is high and saturation factor is small when more than three quarters of the channels are dropped. In other words, if more system channels are dropped simultaneously, the total input power decreases as does the saturation factor. Then the total power transient of the survived channels increases. These curves demonstrate agreement with the original model [119].

Figure 3.10 (a) shows that the profile of the power transients in the networks link with EDFAs is similar to the profile of intrinsic saturation power of the EDFA which is calculated using Equation (2.33). Figures 3.9 and 3.10 (b) show that the profiles of the power transients

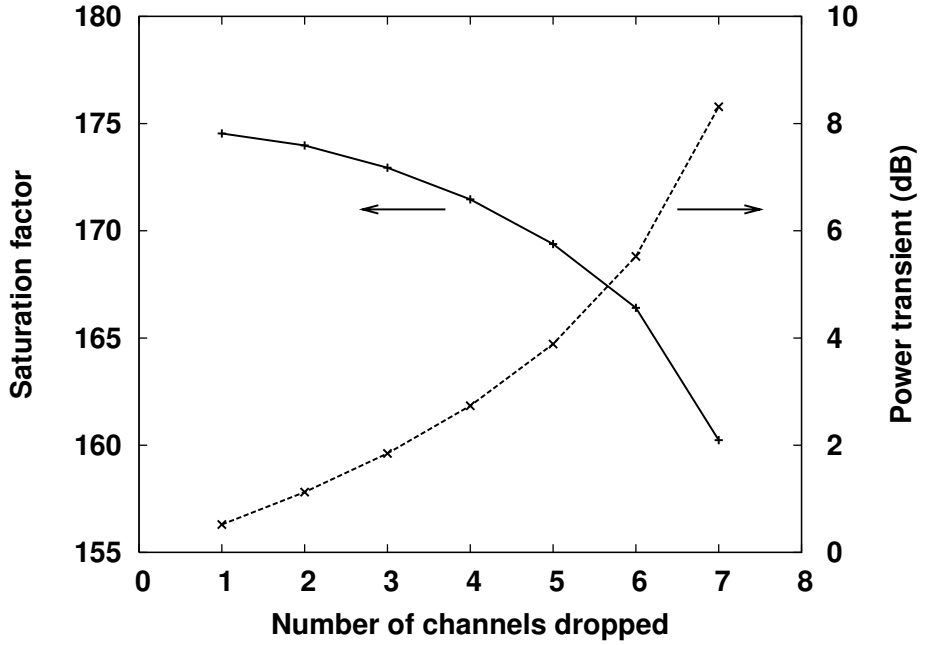

Figure 3.9: The saturation factor and the power transients of the EDFA total output power after the loss of 1 to 7 channels out of 8 WDM channels.

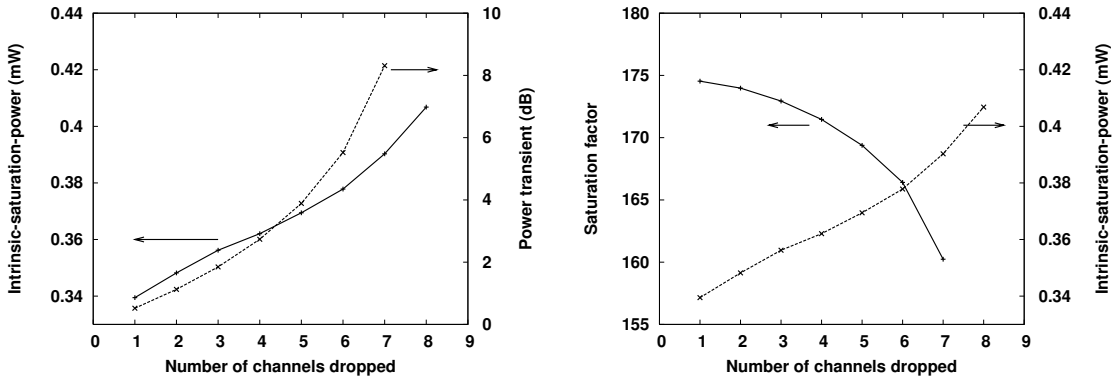

(a) (b)

Figure 3.10: (a) The intrinsic saturation power and the power transients after the loss of 1 to 7 channels out of 8 WDM channels. (b) The saturation factor and the intrinsic saturation power after the loss of 1 to 7 channels out of 8 WDM channels. These parameters are obtained for EDFA total output power.

and the intrinsic saturation power in the networks link with EDFAs are the inverse of the profile of saturation power factor of the EDFA calculated by Equation (3.2), since the intrinsic saturation power is a term in the denominator of the Equation (3.2).

3.2.3 Analysis of numerical simulation results

From the simulation results mentioned in Section 3.2.2, it can be concluded which of the tested parameter variations; input power (lost or added channels), and/or wavelengths, affect the speed of the EDFA response. The simulation results of Figures 3.7 and 3.8 are used for computing the effect of the input power on a 1 dB increase- or decrease-time in addition to the effect of input power on the total output power transient of the surviving channels. The increase-time, decrease-time and total power transient performances versus the dropped/added channels wavelength are shown in Figure 3.11 and the increase-time, decrease-time and total power transient versus the total input power ratio are shown in Figure 3.12. As mentioned earlier, there is good matching with the original model [119] used in this thesis for studying the transient response of the EDFA, the slope or rate in dB/μs of the power transient is proportional to the value of the power loss or addition. Thus, the 1 dB increase-time or decrease-time becomes smaller as the ratio of the input power increases, as shown in Figure 3.12, this indicates that both the rate of power transient and the magnitude of the power transient increase as the ratios of the input power increase, as shown in Figure 3.12.

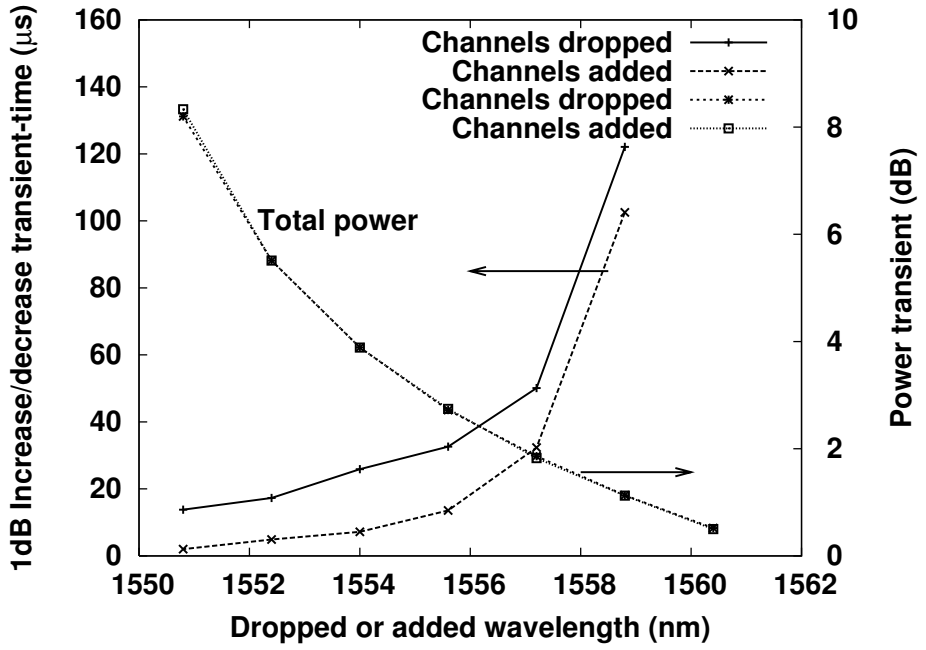

Figure 3.11: 1 dB increase-time, 1 dB decrease-time of the total power transients and the total power transients versus the dropped and added input signal wavelengths.

Figure 3.11 shows the 1 dB increase-time and decrease-time of the surviving channel

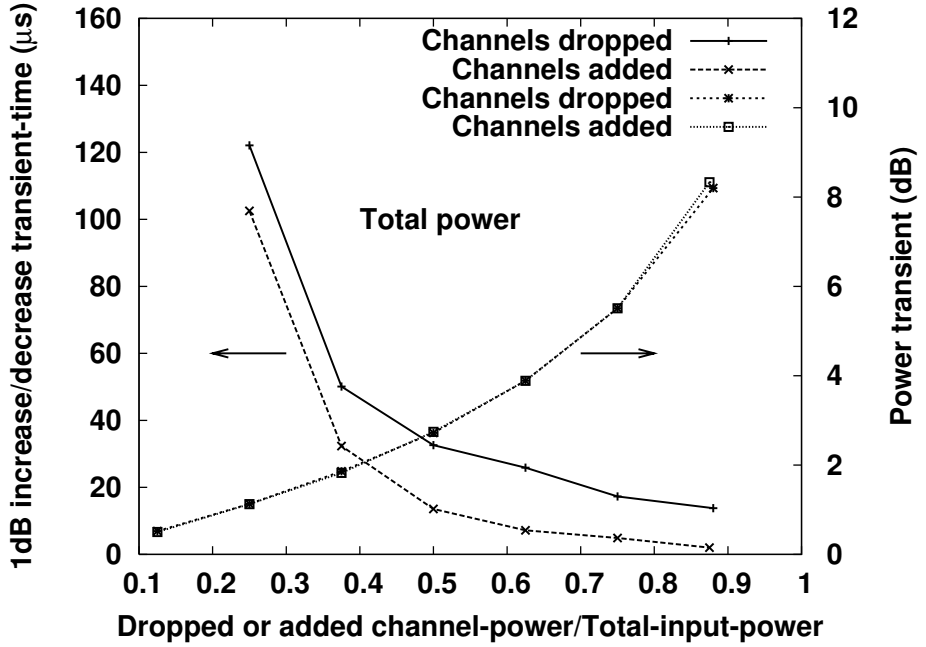

Figure 3.12: 1 dB increase-time, decrease-time of the total power transients, and the total power transient versus different ratios of the total input power.

versus the various surviving channel wavelengths as calculated from the numerical simulation results. For example, it is seen that the 1 dB increase-time for a wavelength of 1557.2 nm is 50.1 μs, whilst the 1 dB increase time for a wavelength of 1550.8 nm is 13.8 μs. Therefore, the increase/decrease-time in the channel with a wavelength of 1550.8 nm is more than three times faster than for the channel with a wavelength of 1557.2 nm. In another example, it is seen that the 1 dB decrease-time for a wavelength of 1557.2 nm is 6.02 μs, whilst the 1 dB decrease-time for a wavelength of 1550.8 nm is 1.12 μs. Therefore, the channel of wavelength 1550.8 nm is more than five times faster than channel of wavelength 1557.2 nm.

It can be seen by differentiating the equation of the second-level population inversion (N_2), shown in Chapter 2, that the power transient depends on the steady state inversion and the sum of the absorption and emission constants. The value of steady state inversion is of the order of a few percent for different surviving channels. Thus, the sum of the absorption and emission constants, is more than two hundred percent higher in the 1550.8 nm domain than it is in the 1557.2 nm and this is the reason for the observed responses. In other words, as the channel wavelengths are dropped in descending order, the amplification of EDFA is wavelength dependent. Thus, the 1 dB increase-time or decrease-time increases as the wavelength of the channel dropped increases, as shown in Figure 3.11. The total power

transient decreases as the magnitude of the channel wavelength that is dropped increases.

In both Figures 3.12 and 3.11, the 1 dB decrease-times are smaller than 1 dB increase-times because the gain of EDFA prior to restoration of the input channel is larger than it is before its subtraction. Adding the input channel at the higher gain creates a larger value for the difference between the output and the input photon numbers, according to the gain dynamic model equation, the change in the averaged population inversion will be higher. In other words, the fast dynamics shown in the channel signal add process are related to the time it uses the added channel signal to deplete the excited ions. One signal photon can 'eat' many excited ions in the stimulated avalanche process, and hence it is enough to have a relatively weaker channel signal to have much faster system dynamics.

3.3 Transient phenomena in WDM networks using cascaded EDFAs

In this section, we use the same simulation parameters and simulation techniques for investigating power transient phenomena as in the network link of a single EDFA, only the simulation resolution has been modified from 10 μs to 2 μs in order to have clear resolution in the overshoot peak region. The cascaded EDFA diagram which is used for studying transient phenomena in WDM networks is shown in Figure 3.13. The phenomena of fast power transients in cascaded EDFA was investigated by Sun et al [105, 106]. Figure 3.14 shows the effect of dropped channels on the surviving channel power in a cascaded EDFA. When 4 out of 8 WDM channels are dropped, the output of each EDFA in the link drops from 64 mW to 34 mW, a power drop of 30 mW. The power in the surviving channel then increases to almost twice the original channel power to conserve the saturated EDFA output power. The consequence of the effect of the collective performance in chains of EDFAs is fast power transients at the output of the link.

The output of the first EDFA is used as an input to the second EDFA after it has been attenuated by a span loss of 11 dB, due to using SMF fibre of length 50 km and attenuation coefficient of 0.22 dB/km [13, 14]. Both the output power of the first EDFA and the output power of the second EDFA increases with time. The output power of the second EDFA has a higher rate of increase than the first EDFA. The increase in the number of EDFAs in the

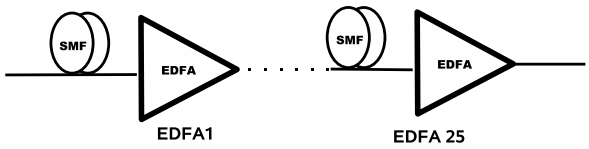

Figure 3.13: Cascaded EDFA model for simulation. Span length is 50 km which causes the span loss of 11 dB by using SMF fibre of attenuation coefficient 0.22 dB/km [13, 14]

.

chain results in faster transients. To avoid performance deterioration in a large-scale WDM optical network, power transient of the surviving channels must be limited to certain values depending on the system receiver threshold.

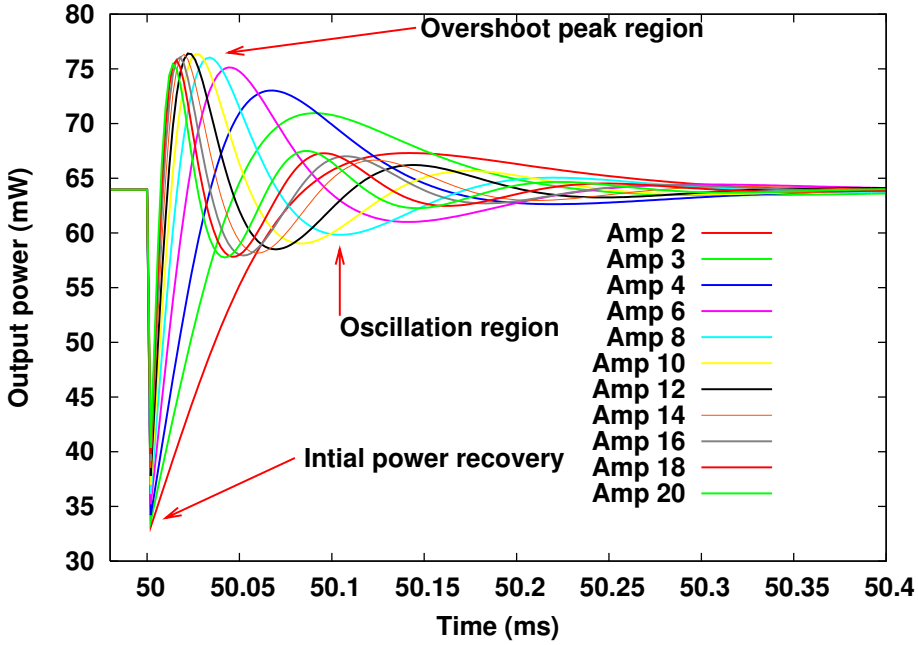

Figure 3.14: The total output power transients at the output of the second to twentieth EDFAs after 4 channels dropped out of 8 WDM channels at simulation run-time of 50 ms.

.

The power transient response of a chain of the EDFAs can be divided into three regions. The first region is called the initial transient and recovery region, the second region known as the intermediate oscillation region, and the third the steady-state region, see Figure 3.14. In the initial transient and recovery region, the gain of the EDFA increases linearly with time and the output power increases at a rate proportional to the number of EDFAs. The time of the power transient after the loss of 4 out of 8 WDM channels for the surviving channels to reach 1 dB is as shown in Figure 3.15. The gradient to overshoot peak power

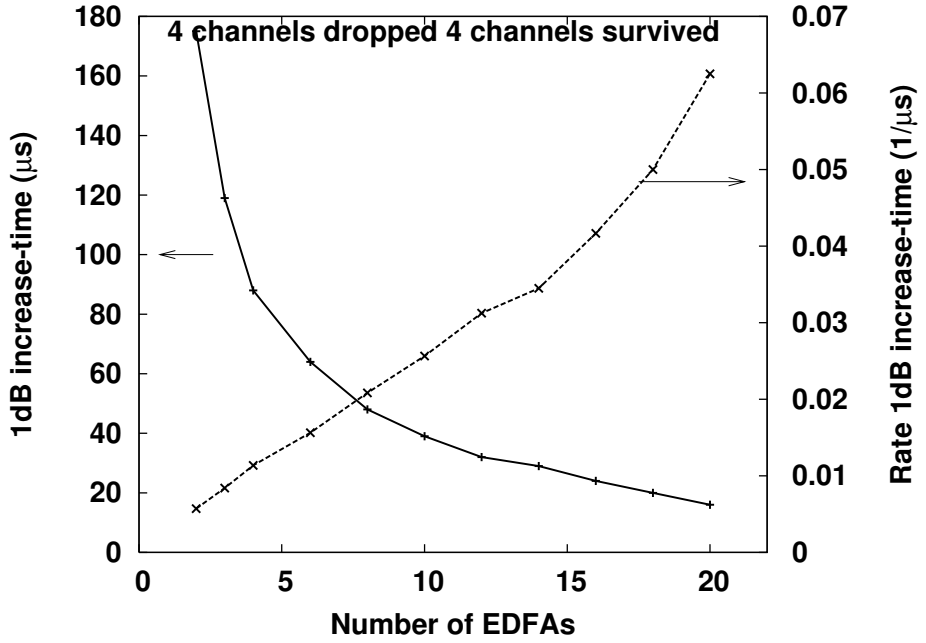

Figure 3.15: 1 dB increase-time and the rate of 1 dB increase-time of the power transients for surviving channels after the loss of 4 channels out of 8 WDM channels.

and rate of a 1 dB power transient in the initial transient region after dropping 4 of 8 WDM channels is as shown in Figure 3.16. We make the assumption that all EDFAs are operating in identical conditions, and the rate of change of the gain at each EDFA is the same, and it is proportional to the total input power dropped. The rate of power transient is plotted in Figure 3.16, it shows that both the rate and the reciprocal of time-delay to peak overshoot power increase linearly with the number of EDFAs in the links.

In the intermediate region or second region, an overshoot spike can be detected in the second EDFA in the link as clearly shown in Figures 3.14. The first overshoot peak is the maximum power transient, since the oscillation peaks that appear subsequently are smaller than the first peak. From the numerical simulation results of WDM networks with M EDFAs, the time to reach the peak is shown to be inversely proportional to M, and the rate to the peak is proportional to (M-1). This indicates that the overshoot peaks are controlled by two main parameters, the operating condition of the EDFAs and the dropped signal power. The specifications in the initial transient and oscillation regions can be used to predict the power transients in large scale optical networks. The same discussion is applied to the case of 4 channels added to the existing system channels to reach the target of 8 channels in a link with a chain of EDFAs.

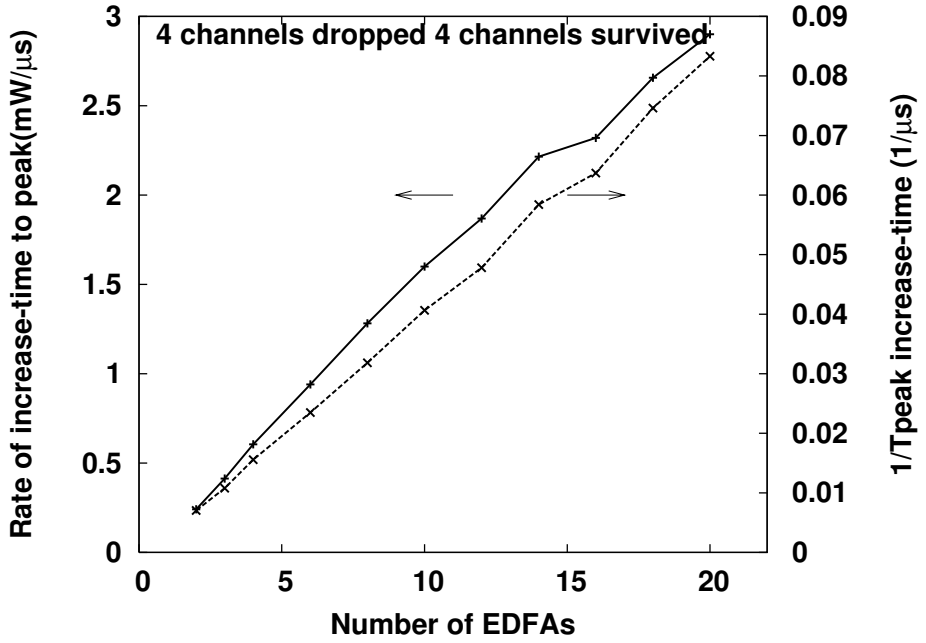

Figure 3.16: The gradient to overshoot peak power and the rate of 1 dB increase-time of the power transients after dropping 4 out of 8 WDM channels.

3.4 Assumptions and limits of the adopted EDFA model

The model which is used for our simulation and shows agreements with the original model of Sun et al [74], is valid under a number of assumptions:

First, the three Stark split energy bands shown in Figure 2.1, are responsible for the amplification process using pump wavelengths of 980 nm and 1480 nm. For 1480 nm two energy levels are related with the amplification process while three energy levels are involved with the 980 nm pumping wavelength. The 1480 nm pumping wavelength behaves as two levels due to the fast thermalisation process that takes place within each energy band. Using two energy levels is a good assumption, since the pumping rate is less than 1 W in the EDFA. This is due to the small life time of approximately 1 μs of the energy level 3 [78].

Second, the excited state absorption is neglected. The excited state absorption affects the pump absorption along the fibre. The effect of erbium ion pair-induced quenching is also neglected since the effect is not powerful in the concentration levels of Er^{3+} that are used in the EDFA [124]. The fibre background impurity loss, of approximately 5 dB/km, is also neglected, because the EDFA fibre length is less than 50 m [87]. The fibre background impurity loss assumption is not applicable for L-band amplifiers, which is specified for fibre

of length more than 100 m [125]. The polarisation dependent gain (PDG) is also neglected. This phenomenon is due to the spatial asymmetry of the spontaneous emission and absorption cross-sections of the erbium ion in its glass host. The PDG effect is significant when the polarisation of the pump and signal fields are orthogonal and of a high power. In the single EDFA in the link in the networks, PDG can produce measurement error of few tenths of a dB. In cascaded EDFAs link, PDG can produce time dependent signal fluctuations, which deteriorates the network performance [126].

Third, the rapid thermalisation process mentioned in the first assumption, produces a homogeneously broadened gain spectrum of the EDFA, and the time rate of such broadening is in the order of picoseconds. This time is faster than any optical process performed during light amplification in the EDFA. This assumption is a very close approximation for most of the glass materials applied in available EDFA models [8, 78]. A result of a residual inhomogeneity of the EDFA gain is Spectral Hole Burning (SHB) which is explained in more detail in Appendix B.1.5. The effect of SHB has been reported in recent studies and could range from few tenth of a dB in the range 1536-1565 nm to almost 1 dB in the 1525-1535 nm band. Generally, the SHB effect depends on the degree of gain compression and the region of the EDFA spectrum. The SHB sets a limit to the ability of both the steady state and dynamic models to properly estimate the EDFA gain characteristic. These models are mostly dependent on the homogeneous gain approximation. The SHB effect in the L-band is more obvious than in C-band EDFAs if the length of EDF in the L-band is longer than the one in C-band [127].

Fourth, the ASE induced gain saturation is neglected. This is true in WDM systems in which the total input power of the channels is large ($>$10 dBm). This is a very good approximation [74]. The amount of ASE generated in L-band EDFAs is much larger than the amount generated for the C-band EDFAs and significantly affects the saturation of the amplifier if the length of EDF in L-band longer than the one in C-band [128].

Fifth, the optical powers of the signal and pump vary slowly compared to the transit time of light along the EDF [129]. It is taken that the speed of light in the fibre is about $(2.988x10^8)/n$ m/s where n is the refractive index of fibre core, the transit time for a 20 m EDF is about 100 ns. The evolution speed of the tested power transients usually complies with this requirement.

Finally, the confinement or over-lap factors are assumed constant and independent of the signal or pump optical powers [78]. This is because the cross-sectional area of the Erbium-doped active region is small compared to the optical mode for all signals and pump wavelengths. The condition of a well confined erbium ion concentration allows the use of the Giles parameters for modelling purposes, and the mathematical formulation of the model.

3.5 Power transient phenomenon in self-saturated C-band EDFAs

The six assumptions, listed in Section 3.4, have been used to develop a dynamic model with which to study the power transients in the WDM networks [74]. In this model, the pump photons that are converted to ASE photons are neglected. Inclusion of the ASE power into the dynamic model is necessary if the EDFA does not operate in the saturated-conditions defined in Chapters 1 and 2 [75, 87]. However, the number of ASE photons and their impact in computing the average population inversion can be negligible in cases when a small number of the input channels is being dropped or added. The dynamic behaviour of EDFAs possesses a large influence over the performance of multichannel optical communication systems and networks with wavelength routing. A model of self-saturated EDFAs is required to analyse the power transient behavior in WDM networks.

In this section, the self-saturated EDFA model is used for the investigation of power transient phenomena as a single EDFA and cascaded EDFAs in the WDM circuit switched networks. The 1 dB increase-time, decrease-time and rate of power transient due to dropping and adding channels to the network are compared with similar cases obtained for the non-self-saturated EDFAs for single and cascaded EDFAs in the WDM networks. The effects of the power transients in both cases (self-saturated and non-self-saturated) on the network performance are analysed.

3.5.1 Computation of the ASE power

The ASE model is added into the non-self-saturated EDFA model in order to be used in the investigation of the power transient phenomena in the self-saturated EDFA networks. The

ASE power model is derived using the model introduced in [87–89]. This ASE model provides a way of computing the rate at which photons of the pump are converted into ASE photons. P_{ASE} is equivalent in physical significance to the term $(P_{out} - P_{in})$. Equation (3.7) [87] is accurate for uniform population inversion along the length of the fibre. When the EDFA is saturated, Equation (3.7) underestimates the total amount of the generated ASE. When the population inversion decreases from the input to the output, the forward propagating ASE is less than half the value of Equation (3.7) and the backward propagating ASE is more. The sum of backward and forward ASE is in general smaller than the actual total value of the ASE as the error in the computation of backward propagating ASE is greater than the error in the computation of the forward propagating ASE. Nevertheless, Equation (3.7) suggests a useful amount of pump photons that are converted to ASE, and the remaining amount of pump photons are known as capture photons which are computed by Equation (3.6). The non-self-saturated dynamic model, ASE power model, and captured-photon model give what is known as a self-saturated dynamic model shown by Equation (3.5).

$$\frac{d}{dt}G_k(t) = -\frac{1}{\tau}(G_k(t) + A_k)$$

$$-\frac{1}{P_k^{IS}\tau}\sum_{j=1}^{M} P_j^{in}(t)\left\{\exp\left[\frac{P_k^{IS}G_k(t) - \left[G_{kj}^0 + A_{kj}\right]\exp\left(\frac{-t}{\tau}\right) + A_{kj}}{P_j^{IS}}\right] - 1\right\}$$

$$-\frac{1}{P_k^{IS}\tau}\left(P_{ASE}(t)\right) - \frac{1}{P_k^{IS}\tau}\left(P_{cpn}(t)\right). \tag{3.5}$$

$$P_{cpn}(t) = 2\gamma_k\left[\frac{G_k(t) + \alpha_k}{\alpha_k + \gamma_k}\right]d_\lambda \tag{3.6}$$

$$P_{ASE}(t) = 4\int (exp^{G_{ASE}} - 1)\left[\frac{\sigma_{ASE}^e}{\sigma_{ASE}^T}\frac{(G_{ASE} + A_{ASE})}{G_{ASE}}\right]d_{\lambda_{ASE}} \tag{3.7}$$

$$\sigma_{ASE}^T = \sigma_{ASE}^e + \sigma_{ASE}^a \tag{3.8}$$

$$n_{sp} = \left[\frac{\sigma_{ASE}^{e}}{\sigma_{ASE}^{T}} \frac{(G_{ASE} + A_{ASE})}{G_{ASE}} \right] \tag{3.9}$$

$$G_{ASE} = \left[\frac{P_k^{IS} G_k(t) - \left[G_{kj}^{0} + A_{kj} \right] \exp\left(\frac{-t}{\tau}\right) + A_{kj}}{P_j^{IS}} \right] \tag{3.10}$$

$$d_{\lambda_{ASE}} = \frac{(ASE_{gB})(c)}{\lambda_{ASE}^{2}} \tag{3.11}$$

Where, all terms in the equations above with the subscript ASE are calculated at ASE wavelength, σ_{ASE}^{e}, σ_{ASE}^{a} are emission and absorption cross-section, σ_{ASE}^{T} is the total cross-sections, G_{ASE} is the log-gain, and A_{ASE} is the absorption loss, c is light speed, and the ASE spectrum starts from 1494 nm to 1573 nm, divided into 200 bins with spacing of 0.4 nm and denoted by (ASE_{gB}), n_{sp} is the spontaneous emission factor, and the factor *4* in the Equation (3.7) accounts for two different polarisations and two different directions of propagation of the ASE. In case of SNR calculation, this factor is halved because it only represents the forward ASE. All these terms are calculated after calculating gain and absorption loss of the probe channel or probe wavelength λ_k using Equations (3.12) to (3.22). The value of $d_{\lambda_{ASE}}$ is calculated using Equation (3.11) [1] because it is required to be converted to the frequency domain for P_{ASE} calculation in Equation (3.7). This frequency conversion is required for numerical simulation.

$$G_j(t) = \frac{P_k^{IS} G_k(t) - \left[G_{kj}^{0} + A_{kj} \right] \exp\left(\frac{-t}{\tau}\right) + A_{kj}}{P_j^{IS}} \tag{3.12}$$

$$P_k^{IS} = \frac{A}{\Gamma_k \left(\sigma_k^{e} + \sigma_k^{a} \right) \tau} \tag{3.13}$$

$$G_k(t) = ln \left[\frac{P_k^{out}(t)}{P_k^{in}(t)} \right] \tag{3.14}$$

$$A_k = \alpha_k L \tag{3.15}$$

$$E_k = \gamma_k L \tag{3.16}$$

$$\alpha_k = N\Gamma_k \sigma_k^a \tag{3.17}$$

$$\gamma_k = N\Gamma_k \sigma_k^e \tag{3.18}$$

$$G_{kj}(t) = P_k^{IS} G_k(t) - P_j^{IS} G_j(t) \tag{3.19}$$

$$A_{kj} = P_k^{IS} A_k - P_j^{IS} A_j \tag{3.20}$$

$$G_{kj}(t) = \left[G_{kj}^0 + A_{kj}\right] \exp\left(\frac{-t}{\tau}\right) - A_{kj} \tag{3.21}$$

Where

$$G_{kj}^0 = P_k^{IS}\, G_k^0 - P_j^{IS} G_j^0 \tag{3.22}$$

In Equation (3.5) for ASE modelling, M represents the number of WDM channels, channel 1 represents the pump, τ is the EDFA fluorescence life-time, P_k^{in}, P_k^{out}, P_k^{IS} are the input, output, and intrinsic saturation fluxes (photons/s) at wavelength λ_k, $G_k \equiv \ln(\frac{P_k^{out}}{P_k^{in}})$ is the logarithmic gain, $A_k = \alpha_k L$ is the loss parameter, L is the length of the EDF, α_k is the absorption constant at wavelength λ_k, and $P_{ASE}(t)$ is the statistical average spontaneous emission flux of the amplifier in photons/s. ASE power is computed assuming a constant inversion as stated in [86, 88].

Equation (3.22) is determined by the initial conditions. Where the term P_k^{IS} is the intrinsic saturation power of the k^{th} channel, $G_k(t)$ is over-all gain parameter at a time t, $P_k^{out}(t)$ is the output power of the k^{th} channel at a time t, $P_k^{in}(t)$ is the input power of the k^{th} channel at a time t, A_k is the absorption coefficient for the whole length of doped-fibre, L, N is the population of the erbium ions in the fibre core, α_k is the absorption coefficient of the k^{th} channel, $P_j^{in}(t)$ is the input power for each channel, and $G_k(0) = G_k^0$ is the initial condition for all channels k =1, 2,..., M. The gain in the j^{th} channel of the ASE-spectrum can be expressed in terms of the gain in the k^{th} channel using Equation (3.12). In other words, once the gain is calculated for k^{th} channel by solving Equation (3.5), the gain of other channels can be obtained from Equation (3.12). If the EDFA is originally in the steady state at *t = 0*, the term $G_{kj}^0 + A_{kj} = 0$.

The fourth term on the right side of the Equation (3.5) is included to model and simulate the power transient phenomena of self-saturated EDFAs in optical WDM networks, and is

described as the captured photons. The physical interpretation of this term is related to the 1st, 2nd and 3rd terms in Equation (3.5). The total output photon flux which is represented by the first three terms is less than the total input photon flux. The captured-photon term represents the number of photons emitted spontaneously in the direction of one of the guided modes, being coupled to the mode. Those photons although emitted spontaneously and couple to the guided modes are measured as part of the total output power, this term is introduced and used for the population inversion calculation in [89]. In our simulation, to the best of our knowledge, this term is being used for the first time for computation of the power transient.

Earlier in this section, we described how the effect of the ASE can be included in Sun's model [74] by the addition of the generated ASE photons. Under the assumption of uniform population inversion along the fibre length, the ASE power is given by Equation (3.7). It was also mentioned that this ASE model provides an overestimation of the forward propagating ASE and underestimation of the backward propagating ASE by an unequal amount when the population inversion along the length of the fibre is not uniform. The forward propagating ASE is needed to study the evolution of the OSNR during dynamic channel configuration in the optical links and WDM networks.

A more accurate computation of the total and forward propagating ASE is possible only if the distribution of the inversion along the fibre is available. In fact, such information is possible by dividing the EDF in small sections of about 0.1 m length, this results in more comprehensive but much slower numerical models [130]. An alternative method, which minimises the error in the computation of the forward propagating ASE, can be achieved when the input signal power is in the limit of non-self-saturated conditions which is defined in Chapter 2. In these conditions, the saturation along the fibre is generated mainly by the input channel signals and the effect of the backward propagating ASE is small [75, 87]. It is possible to simulate short pieces of EDF using the dynamic model described by Equation (3.5) and it is safe when population inversion is uniform. For each piece of EDF the average population inversion or gain can be computed and provide forward or backward propagating ASE power in bandwidth of $\Delta\nu$, centered at frequency ν, can be achieved using Equation (3.7). The forward propagating ASE power is computed and used as input signal to the next fibre piece. This method requires simulation of the dynamic model as many times as there are

EDF subdivision for a single EDFA. This method results in a large increase of the simulation time. For instance, for an EDF of length 20 m, the dynamic model would have to be run 200 times for a single EDFA if a fibre piece length of 0.1 m was chosen, which is sufficient for achieving accurate results for a forward propagating ASE. This method is not reasonable when the link or network contains more than about ten EDFAs.

3.5.2 Numerical simulation parameters

The same simulation parameters for a non-self-saturated EDFA are used. The difference in this case was that the number of channels was 200, input signal channels was 8, one channel for pump signal, and 191 channels for ASE signal from a wavelength of 1494 nm to 1573 nm, provide forward or backward propagating ASE power in bandwidth of $\Delta\nu$, which is equivalent to 50 GHz (0.4 nm). The ASE spectrum including 8 signal channels is shown in Figure 3.17.

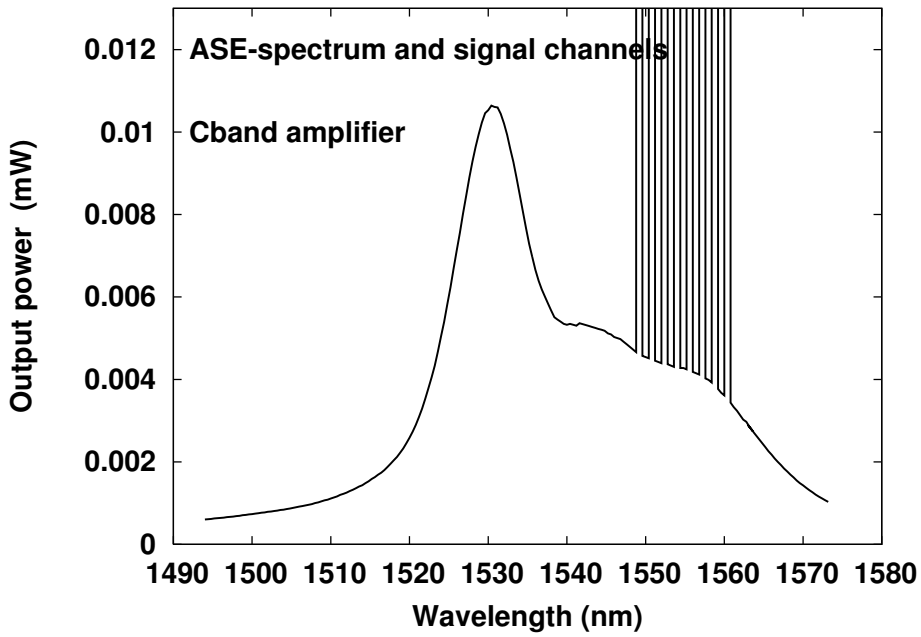

Figure 3.17: The EDFA ASE spectrum with 8 input signal channels.

3.5.3 Numerical simulation results and analysis

In self-saturated (with ASE) EDFAs system, the effect of different input power ratios on the power transients of the surviving channels was examined, both during the loss of channels

and the addition of channels as shown in Figure 3.18 (a, b). The simulation results of both the self-saturated and non-self-saturated (ASE is not included) EDFA systems are compared as shown in Figure 3.19 (a, b).

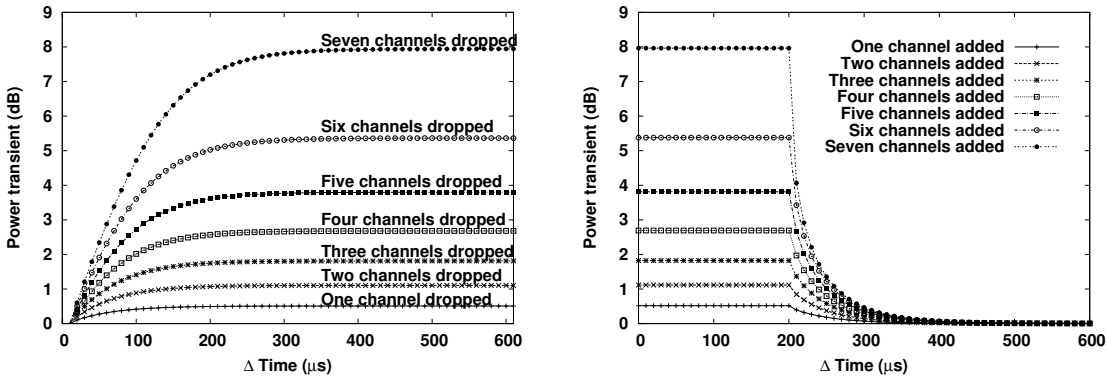

(*a*) (*b*)

Figure 3.18: The power transients of the surviving channels in the self-saturated EDFA when 1 to 7 channels out of 8 WDM channels in a single EDFA, (a) dropped, (b) added.

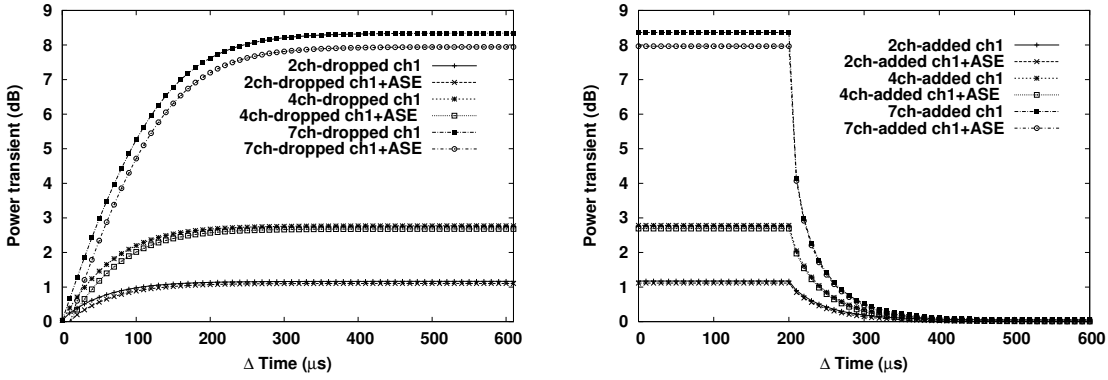

(*a*) (*b*)

Figure 3.19: Comparison of the power transients of the surviving channels in the self-saturated (with ASE) and non-self-saturated (without ASE) EDFAs when 2, 4 and 7 channels out of 8 WDM channels in a single EDFA, (a) dropped, (b) added.

The difference in the power transient between the self-saturated and non-self-saturated EDFAs is negligible when less than four channels are dropped or added. However, the difference increases when the number of dropped or added channels becomes more than four. Even though the highest magnitude may be around 0.5 dB this magnitude may be within the

receiver threshold and so will not affect the performance of the networks [131–133]. For example, when two or four or seven of the channels are dropped equivalent to the input power ratios of 0.25, 0.5, 0.875 respectively, the power transient of the non-self-saturated EDFA is greater than the self-saturated EDFA cases for 2, 4, 7 channels dropped or added by 0.05, 0.1 and 0.5 dB respectively. This proves that when EDFA is in the saturation regime, there is no significant effect for ASE on the transient phenomena of EDFA. As we have seen, ASE has been neglected by Sun et al in their first model [74] because the network they considered operated in the saturation regime.

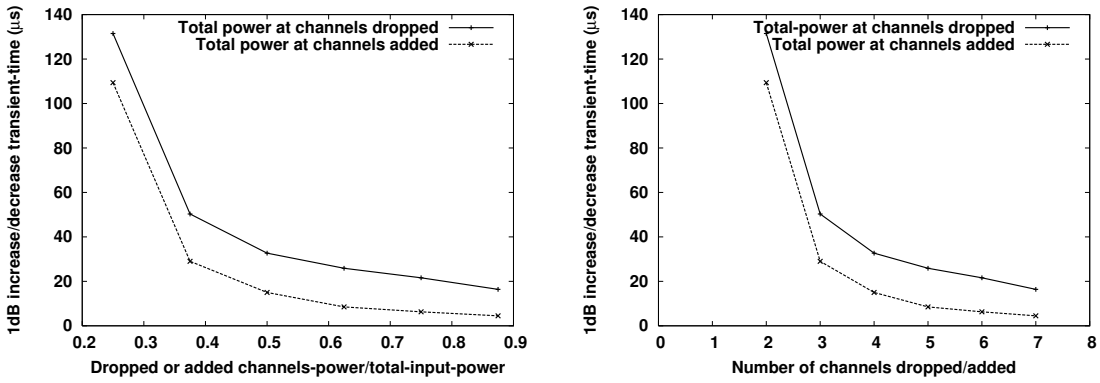

(*a*) (*b*)

Figure 3.20: (a) 1 dB increase-time or decrease-time for different ratios of the input powers caused by dropped or added channels, (b) 1 dB increase-time or decrease-time for different number of dropped or added channels.

From the simulation results for self-saturated EDFA shown in Figure 3.18 (a, b), it is observed that the power loss/addition affects the EDFA response. The 1 dB increase-time or 1 dB decrease-time are also used in this section for analysis of simulation results. The effect of the input power ratios as well as the number of added or lost channels on the 1 dB increase-time/decrease-time and the rate of the power transients of the surviving channels is demonstrated in Figure 3.20 (a, b). The rate (1dB/μs), are also plotted to analyse the effect of the input power ratios on the response of the EDFAs as shown in Figure 3.21 (a, b). The decrease-time is smaller than the increase-time because the gain of the EDFA before the addition of the input channel is larger than it is before its loss. Adding the input channel at the higher gain creates a larger value for the difference between the output and the input photon number, according to the model shown in Equation (3.5) the rate of change of the averaged

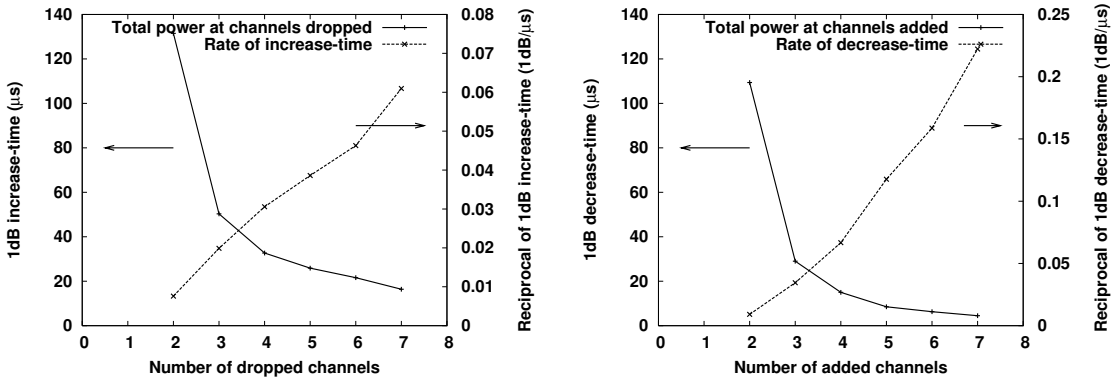

(*a*) (*b*)

Figure 3.21: (a) Comparison between 1 dB increase-time and their slope (rate) when different numbers of channels are lost. (b) Comparison between 1 dB decrease-time and their rate when different numbers of channels are added.

population inversion will be higher. This is obvious in the Figure 3.21 (a, b), for example the rate when 7 channels are dropped is seen to be 0.06 dB/μs whilst the rate when seven channels are added is 0.22 dB/μs. The behaviour of the power transients and its recovery times is smaller with channel addition than for channel loss as shown in Figure 3.22 (a, b). However the power transient in both addition and loss are the same as shown in Figures 3.23 and 3.22 (a).

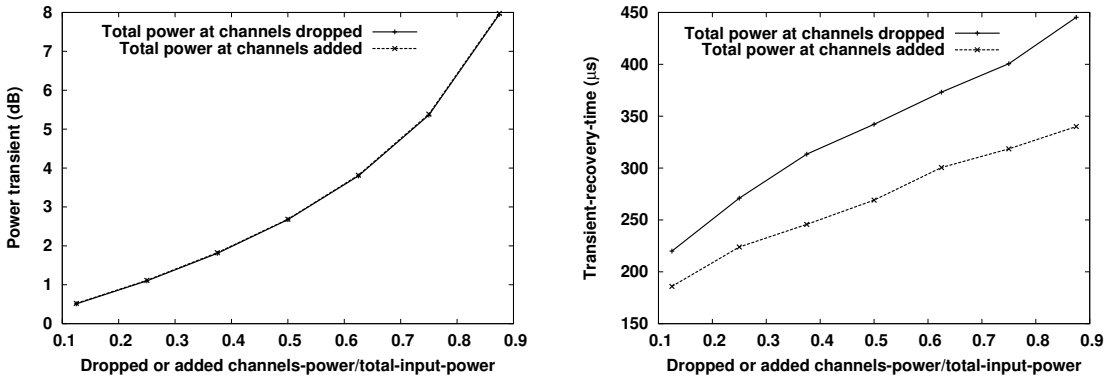

(*a*) (*b*)

Figure 3.22: (a) The power transients at different input power ratios obtained when dropping or adding of channels. (b) The power transient recovery times for the different input power ratios which are caused by dropping or adding of channels in a self-saturated EDFA.

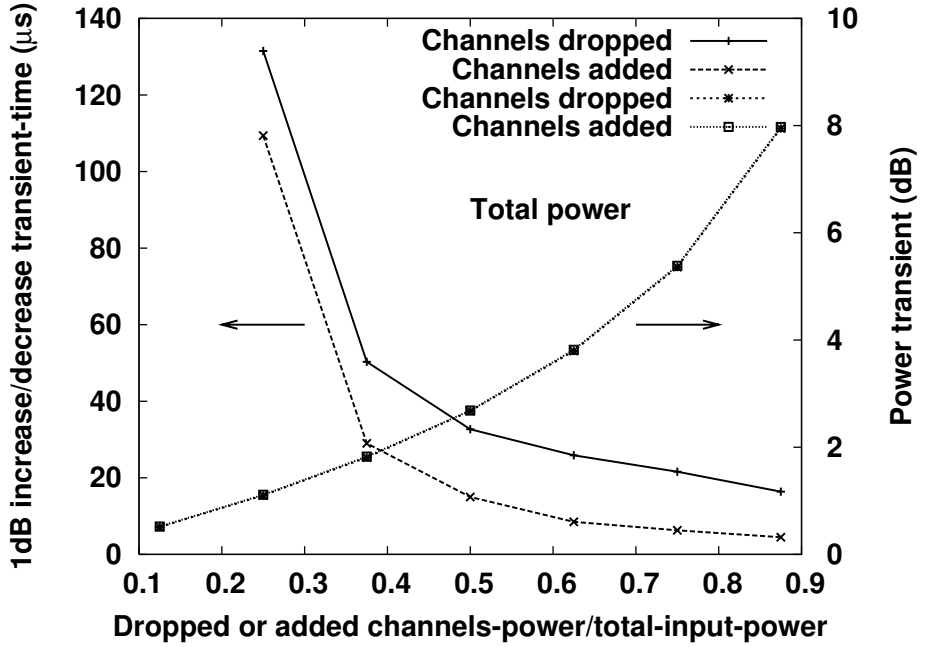

Figure 3.23: Comparison of 1 dB increase-time, decrease-time and total power transients for different input power ratios which obtained from the loss or addition of the system channels.

It has been stated that the transient gain saturation and recovery time constants depend on the metastable level lifetime and also on the total saturated output power of the EDFA [56, 97]. This is because at saturation the gain and the output signal power as well as the average population inversion goes to higher values. When channels are dropped the difference between the input and output photons becomes greater. This increases the rate of change of the gain and population inversion. It is shown in Figure 3.20 (a, b) that the 1 dB increase/decrease-time for the simulated EDFA output powers are in the region of a few tens to hundreds of microseconds.

These simulation results of self-saturated (with ASE) EDFAs are compared with non-self-saturated (without ASE) EDFAs, it is obvious from the 1 dB increase/decrease-time and the power transient curves shown in Figures 3.24 and 3.25, there are good agreements between both cases. This illustrates that the effect of ASE is almost negligible while the EDFA operates under non-self-saturated conditions [74]. The case where a channel is dropped shows better agreement than the case of channels added because, as mentioned earlier, the decrease-time is smaller than the increase-time because the gain of the EDFA before the addition of the input channel is larger than its gain before the loss. Adding the input channel at the higher gain creates a larger value for the difference between the output and the input

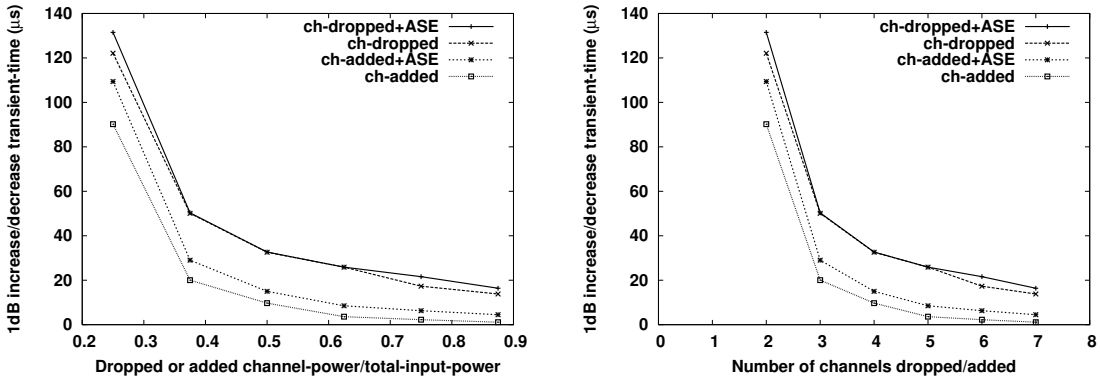

(*a*) (*b*)

Figure 3.24: Comparison of 1 dB increase-time or decrease-time for the self-saturated (with ASE) and non-self-saturated (without ASE) EDFAs, when (a) different input power ratios applied, (b) different number of channels are added or dropped.

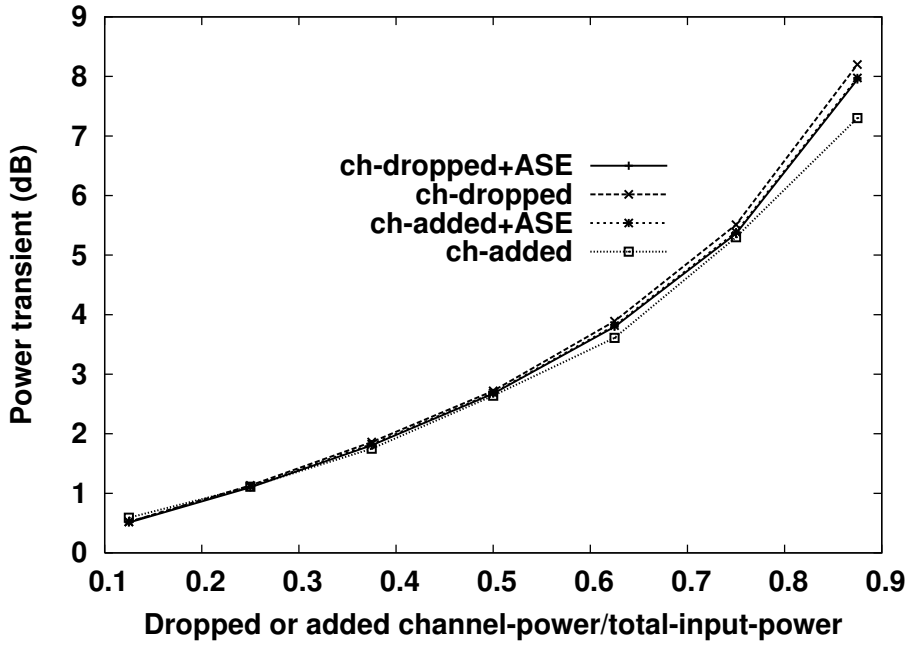

Figure 3.25: Comparison of power transient when different input power ratios are used for the self-saturated (with ASE) and non-self-saturated (without ASE) gain dynamic models of the EDFA.

photon numbers, according to the model shown in Equation (3.5) the rate of change of the averaged population inversion will be higher.

3.6 Power transient in gain-shifted C-band EDFAs

The gain-shifted C-band EDFA is modelled by variation of the geometric parameters of C-band EDFA, keeping the EDF length and ion concentration the same as in the C-band. The EDF length of 20 meters and ion population of $0.7\text{x}10^{25}$ ions/m^3 are used for modelling and simulating the C-band and gain-shifted C-band EDFAs in this work. The C+L-band EDFA is also modelled and simulated in this work by increasing the length of EDF and the erbium ion concentration (to certain extent) [55].

3.6.1 Simulation parameters for gain-shifted C-band EDFAs

The parameters used for simulation of the gain-shifted C-band EDFAs are the same as in the C-band, the difference is in only three geometrical parameters; overlap factors of signal (Γ_s) and pump (Γ_p) and the cross-section of effective area (A_{eff}) as shown in Table 3.2 [6]. The EDF length and ion population are kept the same as in the C-band. The ASE spectrum and 8 signal channels are as shown in Figure 3.26. In Figure 3.26, the peak-power of the spectrum at wavelength of 1560 nm is 22 μW, and the peak power of C-band EDFA spectrum at wavelength of 1530 nm is 12 μW as shown in Figure 3.17. The difference in the peak power value results from the gain of gain-shifted C-band being higher than the C-band EDFA, this gain is due to the variation in the mentioned geometrical parameters. To the best of our knowledge this use of the gain-shifted C-band EDFA with the geometry parameters of Table 3.2 is a first for investigation of power transients phenomenon. The non-self-saturated condition [74] is used for modelling and analysis of the power transients in the gain-shifted C-band EDFAs. The wavelengths for 8 channels are chosen the same as in the C-band EDFA mentioned in Section 3.2.1. The ASE is neglected in this study since the non-self-saturated condition is applied, this condition is defined in Chapter 1.

3.6.2 Simulation results of gain-shifted C-band EDFAs

Prior to the occurrence of power transient phenomenon, the steady-state gain performance for all 8 signal channels of the gain-shifted C-band EDFA are plotted as a result of simulation of the non-self-saturated model in Figure 3.27. The saturated gains of all 8 channels as shown in the figure are between 7.5 dB and 14dB. The gain in the probe channel of wavelength

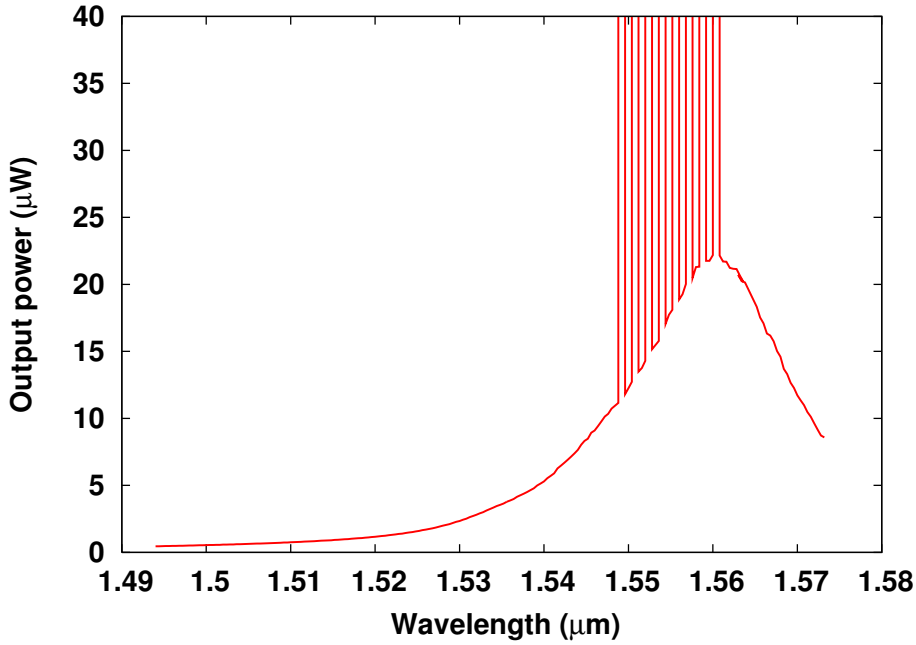

Figure 3.26: The ASE spectrum includes 8 input signal channels of gain-shifted C-band EDFA, we observed that the peak of the spectrum is at wavelength of 1560 nm.

1549.2 nm is around 7.75 dB and in 8th channel of wavelength 1560.4 nm is around 13.75 dB.

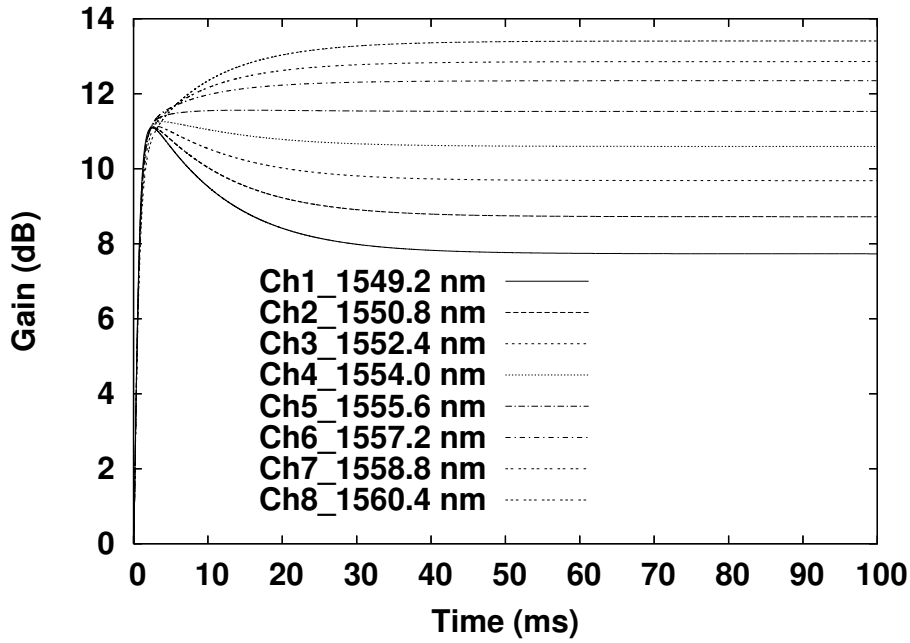

Figure 3.27: The gain of 8 signal channels as a function of time prior to any power transients in the gain-shifted C-band EDFA link.

3.6.3 Analysis of numerical simulation results of gain-shifted C-band EDFAs

We simulated the transient response of the gain-shifted C-band EDFA caused by variation in the input power of the EDFA due to dropping or adding of input channels of different wavelengths. Figure 3.28 (a, b) shows the total power transients and the power transients in the probe channel of wavelength 1549.2 nm respectively after 1 to 7 channels are dropped at 50 ms of simulation run-time. The 1 dB increase-time or decrease-time (defined in Section 3.2.3) is used to study and compare time response of the power transients of the EDFA.

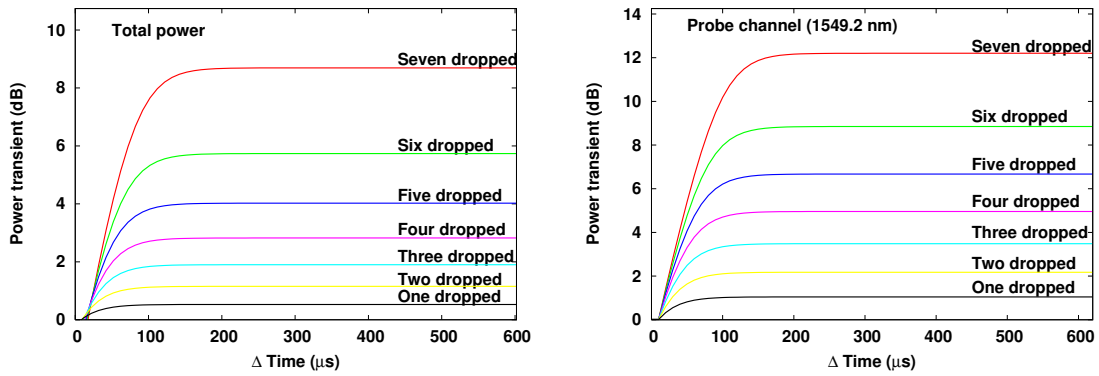

(a) (b)

Figure 3.28: The power transients of the surviving channels when 1 to 7 channels are dropped from the 8 WDM channels in the gain-shifted C-band EDFA, observed at (a) total output power, and (b) probe channel (1549.2 nm).

We noticed from Figure 3.28 (a, b) that the total power transients are 2, 4, and 8.8 dB and power transients of probe channel are 3.5, 6.5 and 12.3 dB respectively when 3, 5, and 7 channels are dropped. This is also the case in the C-band EDFA, i.e. the power transient in the probe channel is higher than the total output power. The total power transients of the C-band are 1.9, 3.95, and 8.5 dB when 3, 5, and 7 channels are dropped as shown in Figure 3.7.

The comparison of C-band and gain-shifted C-band power transients shows very little difference, which is because the total gain and individual channel gain in the gain-shifted C-band is higher than the C-band due to the gain-shifted C-bands EDFA having higher geometric parameters, such as confinement factors of the signal and pump as well as higher

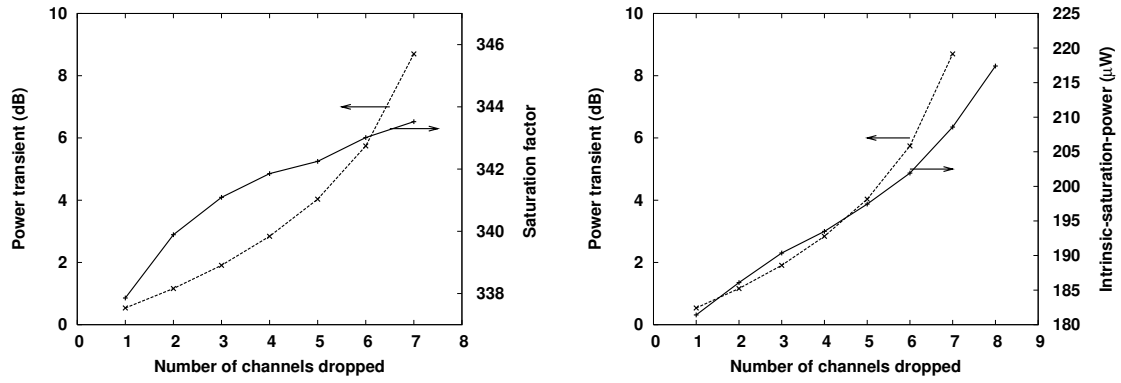

(*a*) (*b*)

Figure 3.29: The gain-shifted C-band EDFA when (a) the power transient and saturation factor of the total output power plotted versus number of channels dropped, (b) the power transient and intrinsic saturation power plotted versus different number of channels dropped.

effective area.

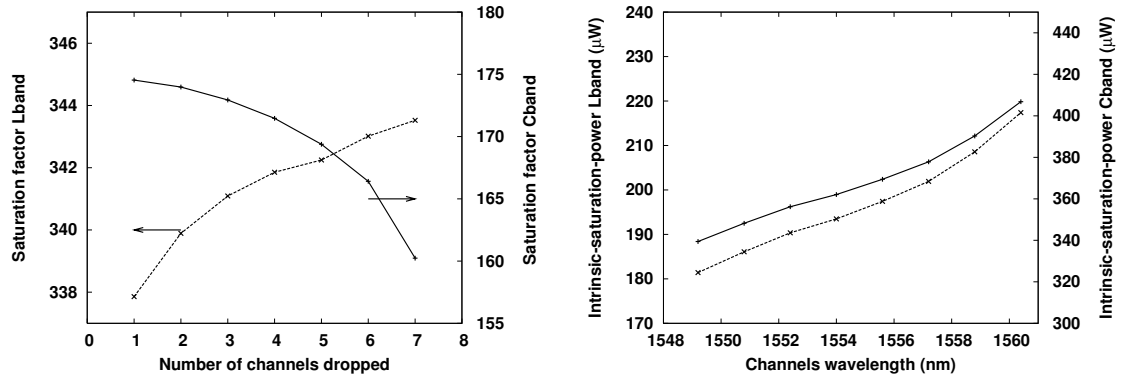

(*a*) (*b*)

Figure 3.30: Comparison between the C-band (solid) and gain-shifted C-band (dashed) EDFAs when different number of channels are dropped, (a) saturation factors, (b) intrinsic saturation powers.

Figure 3.29 (a) shows that the total power transients increase when 1 to 7 channels are dropped (i.e. the input power to the EDFA decreases). The power transient is small when a small proportion of total input power is lost, but increases when a large proportion of total power is lost as shown in Figure 3.29 (b). The saturation factor is calculated using the same Equation 3.2 used for the C-band EDFA stated in Section 3.2.2. The value of saturation

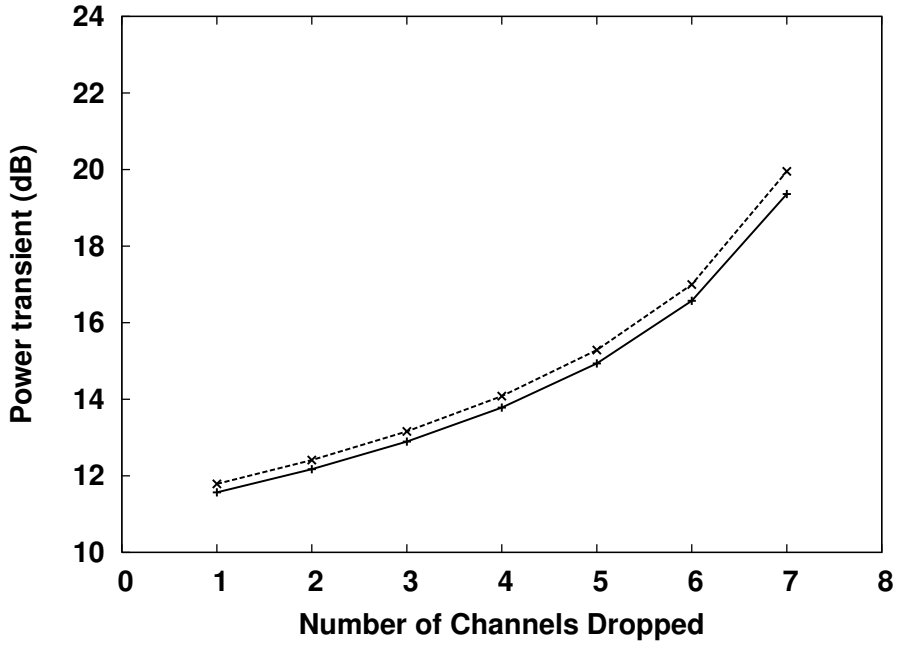

Figure 3.31: Comparison between the C-band (solid) and gain-shifted C-band (dashed) EDFAs in the total output power transients versus different number of channels dropped.

factors are 342.5 and 343.5 when 5 and 7 channels are dropped in the gain-shifted C-band EDFAs respectively. We noticed from Figures 3.9 and 3.30 (a), that in the C-band EDFAs, the saturation factors are 169 and 160 when channels 5 and 7 are dropped respectively. The comparison shows that the saturation factor decreases as the number of dropped channels in the C-band increase but the saturation factor increases when the number of dropped channels increased in the gain-shifted C-band EDFAs. This difference between C-band and gain-shifted C-band EDFAs as shown in Figure 3.30 (a) is due to the difference in value of intrinsic saturation power which in the C-band has twice the value as in the gain-shifted C-band as shown in Figure 3.30 (b), where the intrinsic saturation power is in the denominator of the Equation 3.2.

The power transient for 1 dB increase- or decrease-times and the transient rate are examined for different ratios of the input signal powers in the gain-shifted C-band EDFA at the probe channel as shown in Figure 3.32. The curve of 1 dB increase-time or decrease-time decreases very sharply when 0.125 or 0.25 of total power is dropped or added. As the input power ratios increase, the curve decreases less rapidly and approached an asymptotic value at maximum power loss. The transient rate of 1 dB increase-time or decrease-time rises as the input power ratios increase as shown in Figure 3.32, the rate of increase appears constant

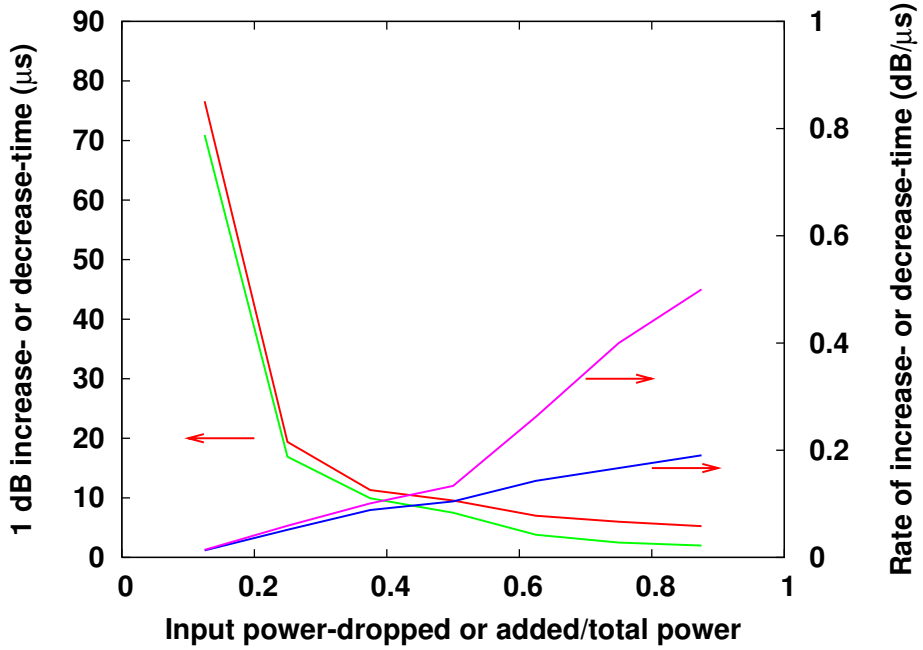

Figure 3.32: 1 dB increase-time or decrease-time (y-axis at left) versus different ratios of the input signal powers when channels are dropped (red) and added (green) in the gain-shifted C-band EDFA observed at the probe channel (1549.2 nm). Also the rate of the power transients (y-axis at right) versus different ratios of the input signal powers when channels dropped (blue) and added (pink).

with a gradient of about 0.6 for dropped channels for all input power ratios. With added channels there is the same rate of increase for input power ratios between 0.2 and 0.5, but at 0.5 there is a sudden increase in the rate of increase of the power transients. This strange increase occurs in the case of channel addition because the gains in the channels are different from each other, see Figure 3.33, and the addition of input power to the EDFA causes the photons to lose their energy in larger amounts than the case when the input signal power is dropped.

The 1 dB increase-time and decrease-time and their rate for the gain-shifted C-band are compared with C-band as shown in Figure 3.33 (a, b). We noticed that the values for 1 dB increase-time/decrease-time for gain-shifted C-band are within the range of variation of the increase-time and the decrease-time of C-band EDFAs. This supports network management use of the same receiver for C-band and gain-shifted C-band EDFAs. This is because the threshold of receiver is applicable for both types of amplifiers [131–133].

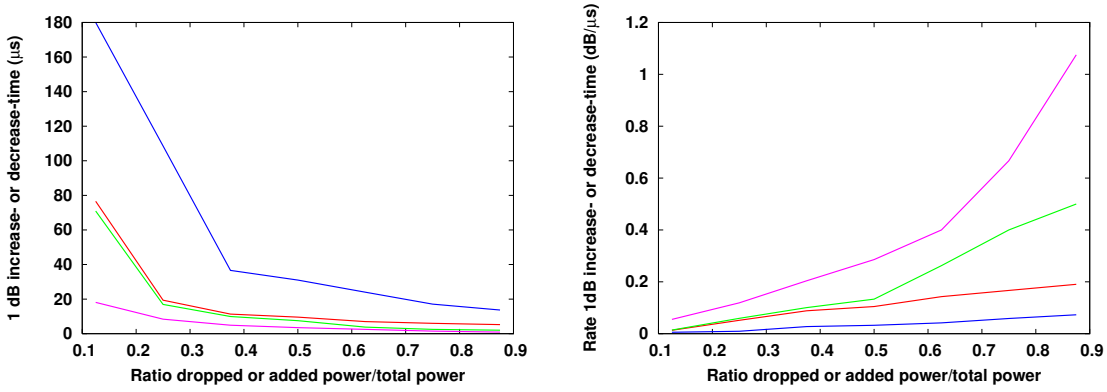

(*a*) (*b*)

Figure 3.33: Comparison between the C-band and gain-shifted C-band EDFAs using different ratios of the input signal power: (a) 1 dB increase-time or decrease-time of the power transients in gain-shifted C-band, when channels dropped (red) and channels added (green), in C-band when channels dropped (blue) and channels added (pink), (b) the transient rate of 1 dB increase-time or decrease-time of the power transients in gain-shifted C-band when channels dropped (red) and channels added (green), and in C-band when channels dropped (blue) and channels added (pink).

3.7 Summary

In this chapter the validation of the EDFA model used for the simulation of power transients in WDM optical networks is explained. The conditions under which the model of Sun et al [74] is valid are explained. Sun's model is the basis of the simulated mode which was constructed by the addition of the terms corresponding to the ASE and captured-photons which are generated by EDFA.

The extended model has been investigated carefully using an extensive set of numerical simulations and compared with similar ones in the literature. There was a good agreement between the results of the model in this thesis and those found in the literature. The numerical simulation results of non-self-saturated (without ASE) EDFAs and self-saturated (with ASE) EDFAs in WDM networks are compared, based on numerical simulation results of a 1 dB increase-time and decrease-time of the surviving channels power transient. There was good agreement between the results which show that the ASE and captured-photon terms can be neglected when the EDFAs run in saturated conditions, which are defined in Chapter 1.

The gain-shifted C-band EDFA is modelled by variation in geometric parameters (ef-

fective area of fibre core and confinement factors) of C-band EDFA, then the model was examined through extensive sets of simulations. It was noticed that the power transients in the gain-shifted C-band are worse than in the C-band, because the gain of the gain-shifted C-band is higher than the gain of the C-band EDFAs for the same input signal and pump powers. This gain is a result of the higher effective area of the fibre core and higher confinement factors of signal and pump than in the C-band EDFA. Since the gain-shifted C-band EDFAs have a fibre length and ion concentrations similar to the C-band EDFA, we avoid behaviour arising from the fibre length, such as ASE noise accumulation, and inhomogeneous characteristics as mentioned in Section 3.4 [6, 127]. Thus, the gain-shifted C-band EDFA is convenient for building network links consisting of both of C-band and gain-shifted C-band. This supports amplification of wide bands of wavelengths. In other words, the C-band and gain-shifted C-band EDFAs can be used together in parallel to build two stage EDFAs, these EDFAs can be applied as an in-line amplifier for long haul communication systems.

Chapter 4

Effects of Poisson traffic on EDFA power transients

4.1 Introduction

Contemporary multimedia applications generate different types of traffic, such as voice, video and data. The voice and real-time video traffic, mentioned in Chapter 1, are very sensitive to loss, jitter and packet delay in network routers or switches. Video traffic also requires high-bandwidth. However data traffic, such as video games and web browsing is less sensitive to delay and loss. Voice traffic is Poisson distributed, whereas video and data traffic follow a Pareto distribution and are self-similar in nature. Recent research has shown that Ethernet traffic is self-similar in nature [111, 134, 135] and that variable-bit-rate video traffic shows long-range dependence [112].

In spite of ATM-IP traffic being self-similar and following a Pareto distribution, this chapter models ATM-IP traffic with a Poisson distribution, because voice traffic is originally Poisson traffic - voice and video communications traffic (such as voice over IP [VoIP], and voice and video over instant messaging) had reached 2 percent of all traffic by 2011, up from less than 1 percent in 2010 [136]. Packet error rate and latency requirements for a mobile wireless access system in an IP Network is mentioned in [137]. The bit error rate (BER) of conversational voice ((AMR codec)/ 4.75-12.2 kpbs) and audio streaming is 10^{-4} [137]. For acceptable QoS, BER must be better than 10^{-4} [136,137]. Voice traffic alters the statistics of

networks. The effect of Poisson traffic on the power transients phenomena is worthy of study in order to show the specification of PDF using non-Pareto traffic. The non-self-saturated (without ASE) dynamic model and the simulator, which are described in Chapter 3, are used. The output power transients (i.e. output power includes power transients) are examined using numerical and statistical analysis.

4.2 Traffic types and models

Multimedia applications in the WDM packet-switched optical networks use ATM-IP packets. There is a rapid fluctuation of the input power when the channels of the networks are fed by these ATM-IP packets. In fact, the role of high variability in inter-arrival and packet times from the EDFA gain saturation view is that long periods of inactive traffic (burst-OFF) or active traffic (burst-ON) give enough time to the EDFA to respond to the variations of the input power. The resulting variations in the output power, gain and OSNR lead to deterioration of both the system performance and QoS of the networks.

For investigation of the effect of ATM-IP traffic behaviour on the power transients of EDFA traffic of bit-rate 2.5 Gb/s with Poisson distribution in burst-ON and burst-OFF periods is used. The burst-OFF period is a sequence of time slots that do not carry packets, the mean time of empty slots is 50. Similarly, the burst-ON period is a set of time slots that all carry packets, the mean time of slots occupied with a packet is 5. In the following section, we explain the Poisson distributed traffic model and verify the input traffic sources accordingly. Then we perform a numerical and statistical analysis for the output power transient behaviour in the WDM links at two different regions of the EDFA gain spectrum performance: one in an EDFA saturated gain regime and the other in the small signal gain regime.

4.2.1 Poisson distribution traffic model

The Poisson distribution model in a telephony context was developed by Erlang [138]. It is the oldest known traffic model in use and this model can be expressed [138] as:

$$P(n) = \frac{e^{-\lambda}\lambda^{n}}{n!} \tag{4.1}$$

Where $P(n)$ is Poisson probability density function of n. The mean and variance of which are given by:

$$E(n) = Var(n) = \lambda \tag{4.2}$$

The equation for the Poisson cumulative distribution function is:

$$F(n) = \sum_{j=0}^{n} \frac{e^{-\lambda}\lambda^{j}}{j!} \tag{4.3}$$

We analyse the traffic and verify the model by plotting the PDF of the burst-ON and burst-OFF periods for the input traffic sources as shown in Figures 4.1 and 4.2. Figure 4.1 is obtained from generating random instances of more than 1 million packets. Similarly, Figure 4.2 is from generating random instances of more than 2 million empty slots. As seen in Figure 4.1 the traffic sources follow a Poisson distribution with an exponentially decaying function for burst-ON periods, the mean of the histogram is 5.07 slots per packet. Figure 4.2 shows that the burst-OFF periods traffic also follows a Poisson distribution, the mean of this histogram is 50.1 empty slots. The means of both burst-ON and burst-OFF indicate a good agreement with the corresponding analytical model.

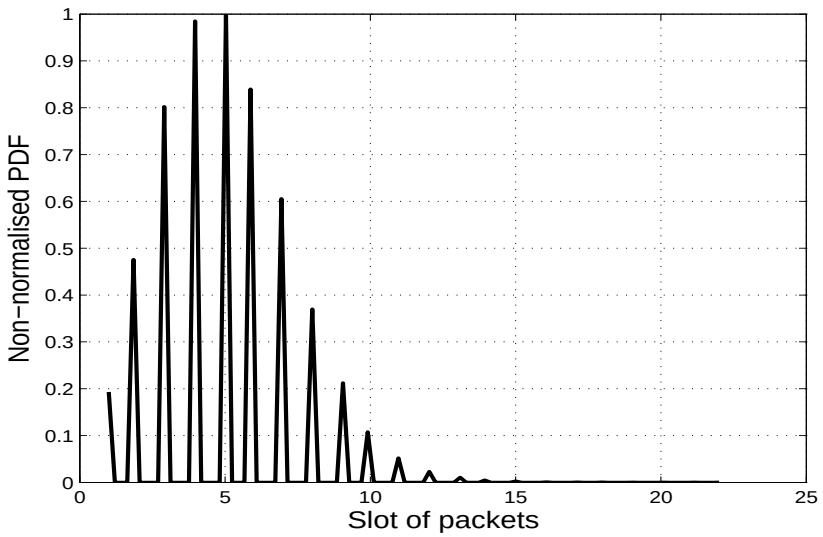

Figure 4.1: PDF of packet slots (burst-ON) of input source traffic of Poisson distribution.

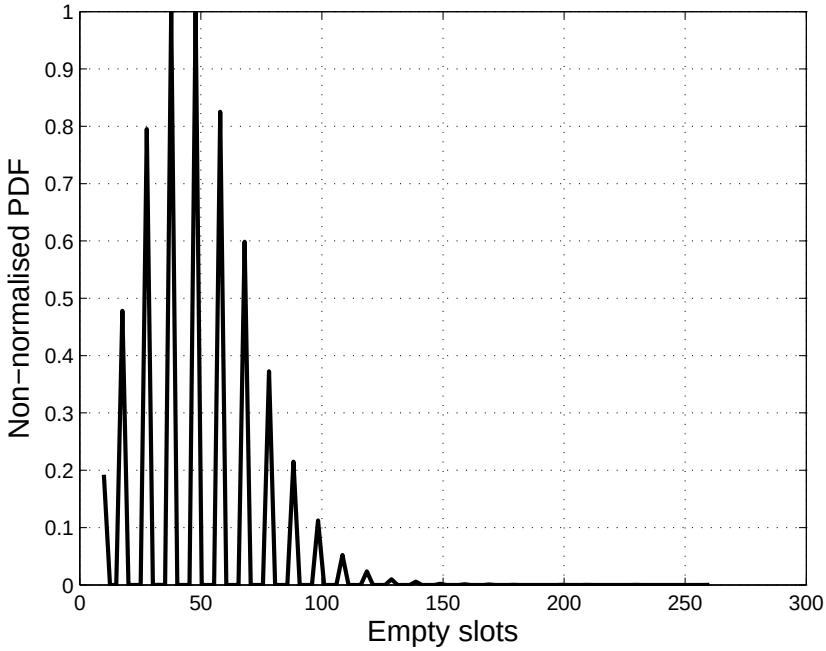

Figure 4.2: PDF of empty slots (burst-OFF) of input source traffic of Poisson distribution.

4.3 Impact of the Poisson traffic on the power transients of the EDFA

In this section, we use a non-self-saturated (without ASE) gain dynamic model of the EDFA [74] to analyze the power or gain transients in wavelength division multiplexed (WDM) optical networks. As mentioned earlier in Section 3.4, this model is valid under certain conditions which are fulfilled when the input signal power values or the gain of EDFA are according to the non-self-saturated conditions defined in Chapters 1 and 2.

4.3.1 Simulation parameters

The link in our simulation consists of three signal channels of different wavelengths and three cascaded EDFAs. The input to channel 1 is CW at wavelength of 1549.2 nm. The input to channel 2 and channel 3 are ATM-IP traffic sources of Poisson distribution at wavelengths 1550.8 nm and 1552.4 nm respectively. The Poisson distributed ATM-IP traffic source is shown in Figure 4.3. The input peak power of -2 dBm (630 μW) is used in all three signal channels. The EDFAs are pumped at 980.0 nm, with pump peak power of 19 dBm as input to

channel 0. We use a C-band EDFA and all simulation parameters are the same as described in Section 3.2.1. All EDFAs in the link are identical and operate in the non-self-saturated conditions for simulation run-time 250 ms.

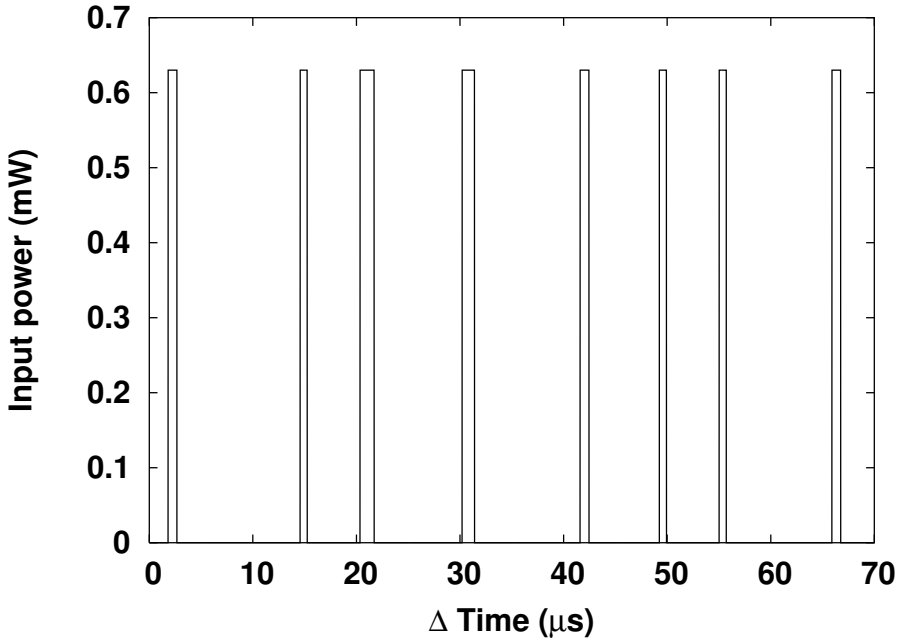

Figure 4.3: Poisson distributed traffic of means 5 and 50 at burst-ON and burst-OFF respectively, using input traffic sources for channel 2 and channel 3.

The output power transient of each channel at the output of each EDFA will be the input for the next EDFA after a span-loss of -19.36 dB, as the gain of each EDFA is 19.36 dB. The span length for such a link is 88 km using a single mode fibre of attenuation coefficient 0.22 dB/km [13, 14].

4.3.2 Results and analysis

In this section, we numerically analyse the EDFA power transients of WDM packet switching networks in two parts. In the first part, we numerically analyse the power transients of ATM packets, where the burst-OFF and burst-ON periods are random variables of Poissonian distribution. The second part deals with the statistical analysis for the output power transients of each channel in the cascaded EDFAs. This statistical analysis is performed by studying PDFs of output power transients and their associated Gaussian fit.

4.3.2.1 Power transient numerical analysis

Any variation of the total input power of WDM signals is echoed in the total number of excited ions. In some cases the packetized channels are in burst-OFF for a certain time, and the total EDFA input power decreases. From the system point of view, the decrease of input fluxes under constant pump power will produce an increase in the total number of excited ions. On the contrary, if some ATM-IP packets based channels become burst-ON for a long period, the total input power increases and the total number of excited ions falls. EDFA gain transients are a direct result of these variations [139]. The burst-ON and burst-OFF in one or more input channels in the EDFA of WDM systems affect the output power of other surviving channels, leading to output power transients in the individual channel even though the input of the individual channel is a continuous wave [108]. This is known as a cross-gain-modulation and is shown in Figure 4.4.

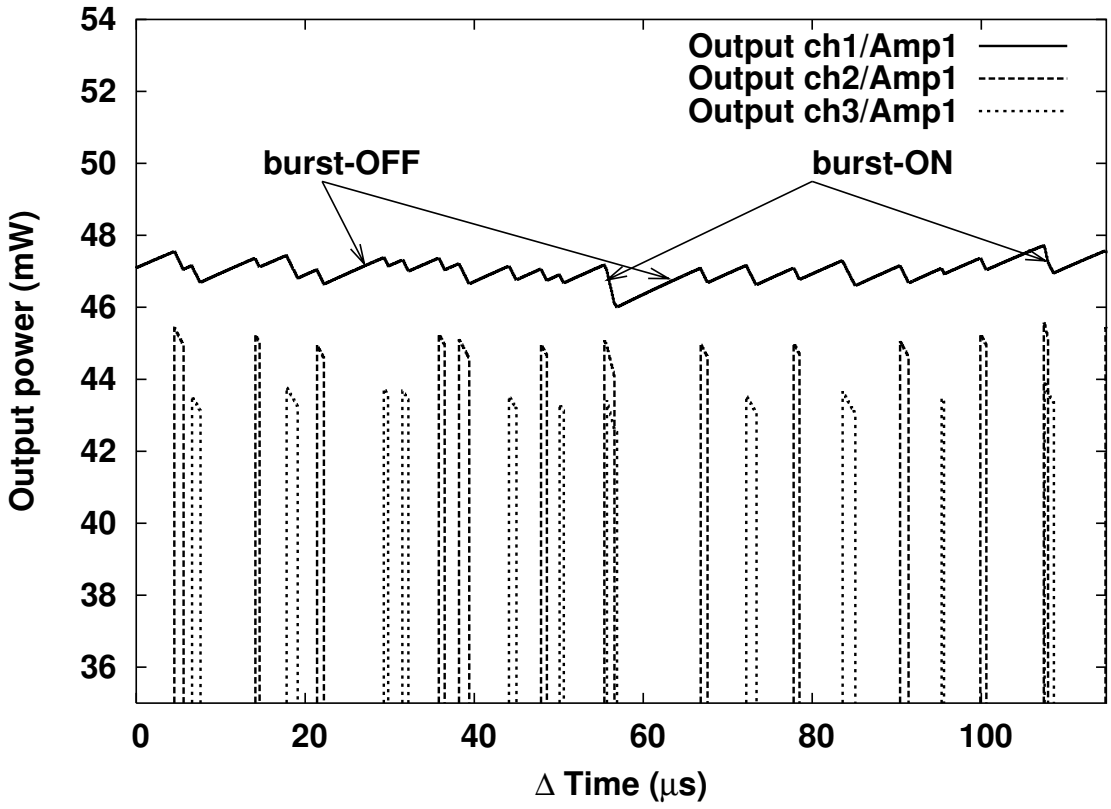

Figure 4.4: The output power transients of channel 1 using CW signal, channel 2 and channel 3 using Poisson distributed ATM-IP traffic.

The power transients for channel 1, channel 2 and channel 3 are shown in Figure 4.4. When channel 2 and channel 3 are at burst-OFF period, the power of channel 1 increases

above the average level. In Figure 4.4, for instance, the time duration between 22.34 μs to 29.18 μs no packets have arrived in channel 2 and channel 3, so the power level in channel 1 increases during this 6.84 μs from 46.6578 mW to 47.3957 mW, the increase in power is 0.7379 mW. This period of time allows the EDFA to achieve a gain or power exceeding the average power. After this, a packet in channel 3 arrives (channel 2 receives no packets) and this causes a reduction in channel 1 power level to 47.1849 mW at a time of 29.7858 μs, the drop in the power is 0.2108 mW. Then another packet arrives at channel 3 (channel 2 again receives no packets) and this causes a further drop in the power level of channel 1 to 46.974 mW at a time of 32.199 μs.

Another example of the power transient in channel 1 occurs between 56.7369 μs and 66.7933 μs, (a longer period than in the first example) when for channel 2 and 3 the burst-OFF period is 10.05 μs. The power transient in channel 1 increases from 45.9725 mW to 47.1322 mW, the increase in the power is 1.1597 mW.

As mentioned earlier in this section that the longer the burst-OFF period, the more time for the ions in the EDFA to achieve higher energy to produce higher output gain. For the second example we have seen in Figure 4.4 the increase in power was 1.1597 mW while in the first example it was 0.7379 mW for the burst-OFF durations of 10.05 μs and 6.842 μs respectively. These power increases that we have observed in both examples are due to the higher inversion achieved following a long OFF period. Thus, the EDFA provides a higher power than the average output power level.

Likewise, we also analyze channel 1 at the burst-ON period for different overlap periods of packets of channel 2 and channel 3, in the first example we have seen in Figure 4.4 the packets from channel 2 overlap completely with packets from channel 3 for a duration of 1.2068 μs and this causes the output power in channel 1 to drop from 47.2376 mW at a time of 55.5301 μs to a power of 45.9725 mW at a time of 56.7369 μs, the drop in power in this case is 1.2651 mW. In the second example, packets from channel 2 overlap partially with packets from channel 3 for a duration of 0.603 μs and this causes the output power in channel 1 to drop from 47.8174 mW to 47.0794 mW, the drop in power is 0.738 mW, then at the end of packets from channel 3, the output power in channel 1 drops to 46.9213 mW, the drop in power level for duration of 1.106 μs is 0.896 mW. The power drop in the second example is less than the first because in the first example channel 2 and 3 are both active for

the duration of 1.2068 μs, while in the second example channel 2 and channel 3 are only both active for duration of 0.603 μs. These power drops that we have noticed with both examples are because of low ion energy. Thus, the EDFA provides lower power in channel 1 than the average output power level.

4.3.2.2 Power transient statistical analysis

In order to investigate the output power transient effect in the cascaded EDFAs in packet-switched networks, we analyse the PDFs of output power transients of each channel in the link at the output of each EDFA in the chain as shown in Figures 4.5, 4.6 and 4.8. For the statistical analysis we make use of the PDF of the output power transients compared to its associated Gaussian fit. The mean and the standard-deviation of the output power transients, and the power-swing of each channel at the output of each EDFA are analysed.

The power-swing is the difference between No-load power or max(p(t)) and full-load power or min(p(t)) (i.e. max(p(t)) - min(p(t))). The output power-swing is calculated with probability of 10^{-03}, at which this point is more than three standard deviations from the mean of the PDF. For the normal distribution, this includes 99.9% of the data. The Gaussian fit of the output power transients in each of Figures 4.5, 4.6 and 4.8 is plotted using Equation (5.7). Figures 4.5, 4.6 and 4.8 illustrate the PDFs of the output power transients of channel 1 of CW signal, channel 2 and channel 3 of Poisson-distributed ATM-IP traffic.

In Figure 4.5 (a), the profile of the PDF of the output power transient of channel 1 fits well with the related Gaussian distribution, where ATM-IP source traffic of channel 2 is in the burst-ON period, whilst the traffic in channel 3 is in burst-OFF period, the mean of the output power transients is 47 mW, and the standard deviation is 7.5103×10^{-4} mW, the corresponding values of max(p(t)) is 49.59 mW, and min(p(t)) is 44.04 mW, thus the power swing is 5.55 mW. Figure 4.5 (b) shows the PDF of output power transient of channel 1 when both channel 2 and 3 are in the burst-OFF period, the mean of the output power transients is 47.1 mW and the standard deviation is 7.48×10^{-4} mW, the related max(p(t)) is 49.69 mW, and min(p(t)) is 44.15 mW, thus the power swing is 5.54 mW.

Figure 4.5 (c) shows the PDF of the output power transients of channel 1 when channel 2 and 3 are in mixed burst-OFF and burst-ON periods, the mean of the power transients is 47 mW and the standard deviation is 7.49×10^{-4} mW, the corresponding of max(p(t)) is 49.67

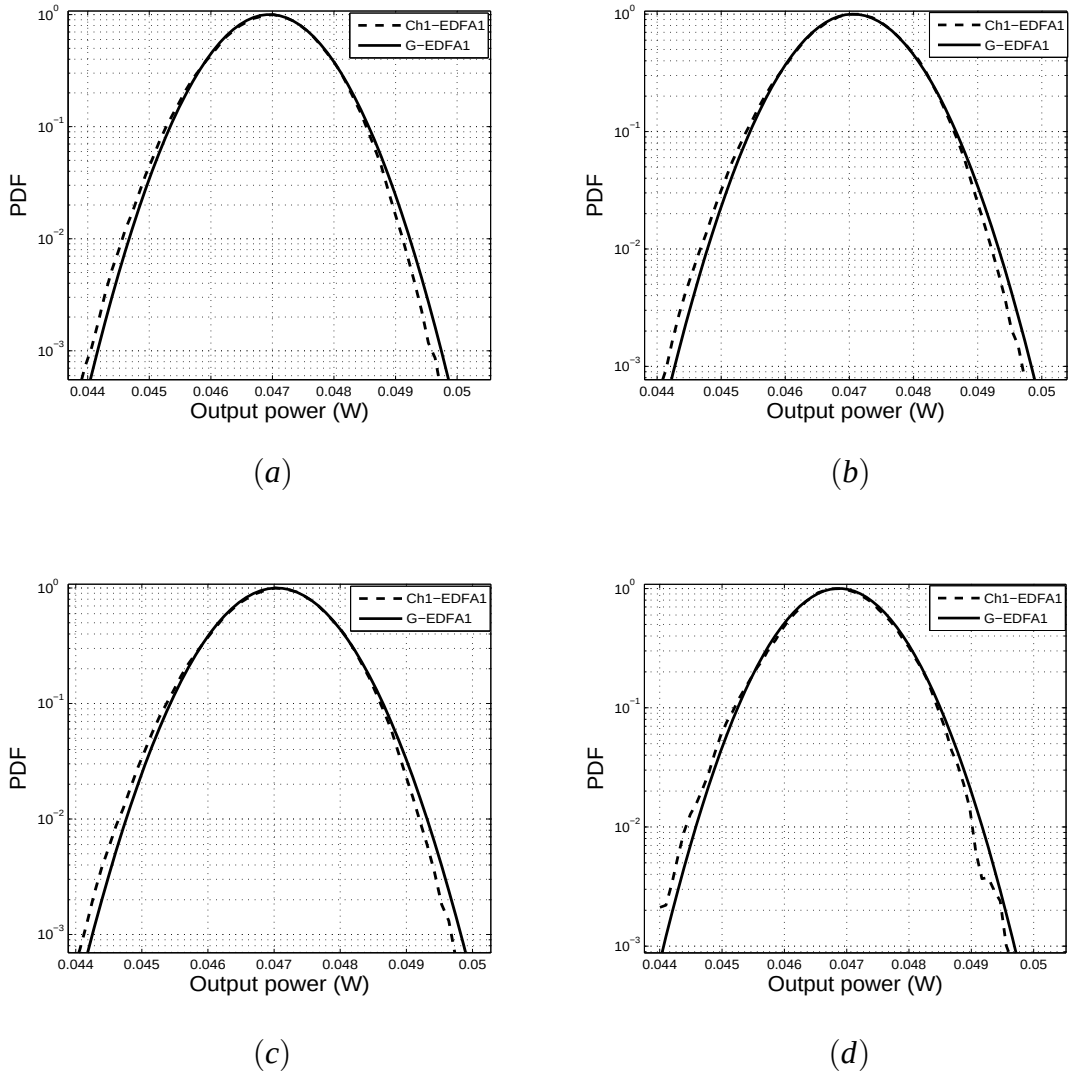

Figure 4.5: PDFs of the output power transients and related Gaussian fits (denoted by G-EDFA1) of channel 1 at the output of the first EDFA, whilst Poisson distributed ATM-IP traffic in (a) channel 2 is in burst-ON periods and channel 3 is in burst-OFF periods, (b) both channels 2 and 3 are in burst-OFF periods, (c) both channels 2 and 3 are in mixed burst-ON with burst-OFF periods, (d) both channels 2 and 3 are in burst-ON.

mW, and min(p(t)) is 44.14 mW, thus the power swing is 5.53 mW. Figure 4.5 (d) shows the PDF of power transients of channel 1 when channel 2 and 3 are both in the burst-ON periods, the mean of the output power is 44.9 mW and the standard deviation is 6.97×10^{-4} mW, corresponding max(p(t)) is 49.59 mW, and min(p(t)) is 44.04 mW, thus the power swing is 5.55 mW.

If all three channels are active, the input power to the EDFA is 100%, the PDF is shown in Figure 4.5 (d). If one of the three channels are not active the input power to the EDFAs

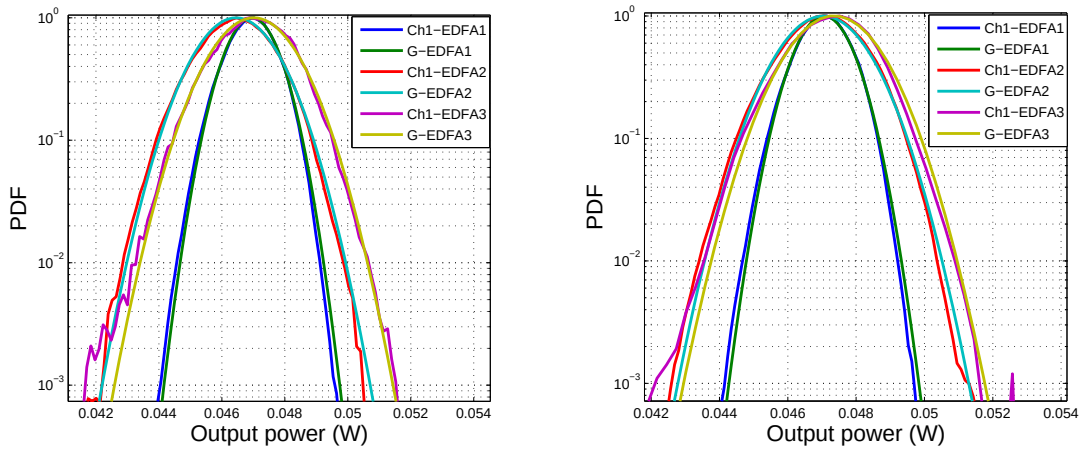

Figure 4.6: PDFs of the output power transients and related Gaussian distribution (denoted by G-EDFA*) of channel 1 at the output of the first to third EDFAs, whilst the Poisson distributed ATM-IP traffic in channels 2 and 3 are in (a) burst-ON periods, (b) burst-OFF periods.

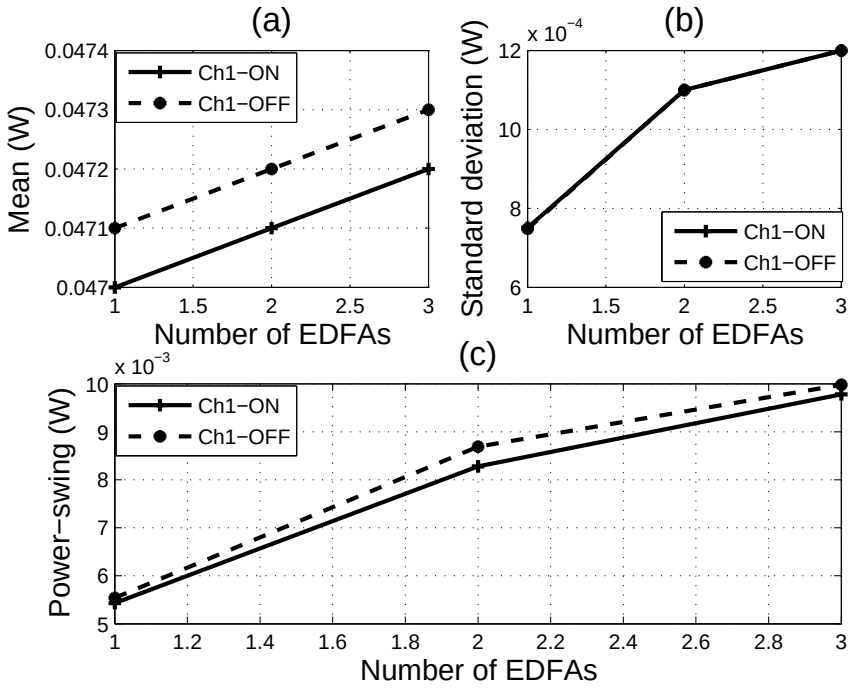

Figure 4.7: (a) Mean, (b) standard deviation and (c) power-swings of the output power transients of channel 1 versus number of EDFAs in the chain.

drops by 33%, the PDF is shown in Figure 4.5 (a), and if two channels traffic are not active the input power to the EDFA drops by 66%, the PDF is shown in Figure 4.5 (b). The latter (two channels are not active) gives the EDFA enough time to achieve gain greatly above the

average value. As the probability of concurrent occurrence of simultaneous long periods of burst-OFF in several channels decreases, the gain fluctuations also decrease [108].

Figure 4.6 (a, b) shows that the standard deviation and power swings in channel 1 increase at the output of the first EDFA more significantly than the output of the second or third EDFA or the rest of the EDFAs in the chain. This is clear from the slope of the curves in Figure 4.7 (b, c). The slope of the curve in Figure 4.7 (c) is 0.6 at the output of the first EDFA in the chain while the slope is 0.29 at the output of the second EDFA, approximately half the slope at the output of the first EDFA.

These statistics which are discussed are compared in Figure 4.7. Label ch1-OFF represents the output power transients of channel 1 while channel 2 and channel 3 are in burst-OFF periods. Label ch1-ON represents the output power transients of channel 1 while channel 2 and channel 3 are in burst-ON periods.

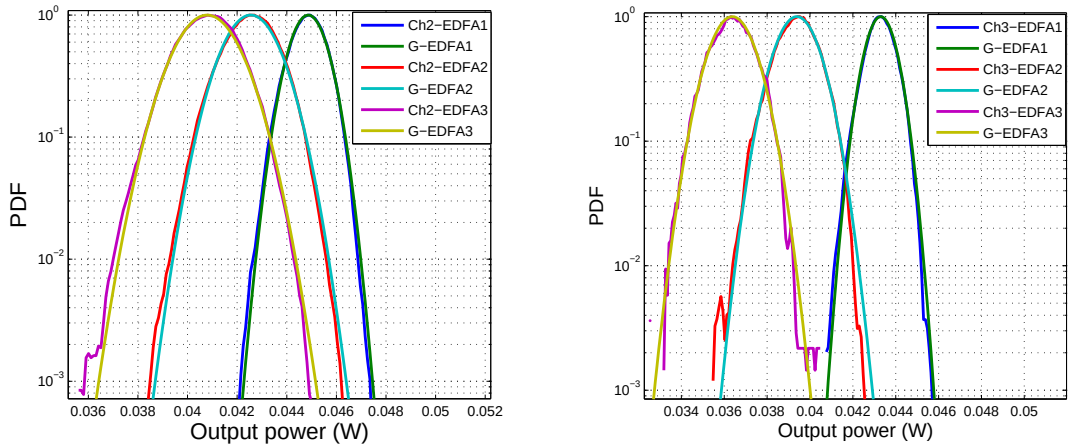

(*a*) (*b*)

Figure 4.8: PDFs of the output power transients and related Gaussian fits (denoted by G-EDFA*) at the output of the first to third EDFAs in (a) channel 2 , (b) channel 3, whilst the Poisson distributed ATM-IP traffic is in burst-ON periods.

The PDFs of the output power transients of channel 2 and channel 3 are plotted for burst-ON periods as shown in Figure 4.8 (a, b) respectively. The PDF of the output power transients have bell-shape or Gaussian profiles in all figures, however, the mean, standard-deviation and power swings vary as shown in Figures 4.7 and 4.9. These statistical parameters vary at the output of each EDFA in the chain of network links. Thus, we conclude that the standard-deviation and power swings for all three channels increase along the cascaded EDFAs as

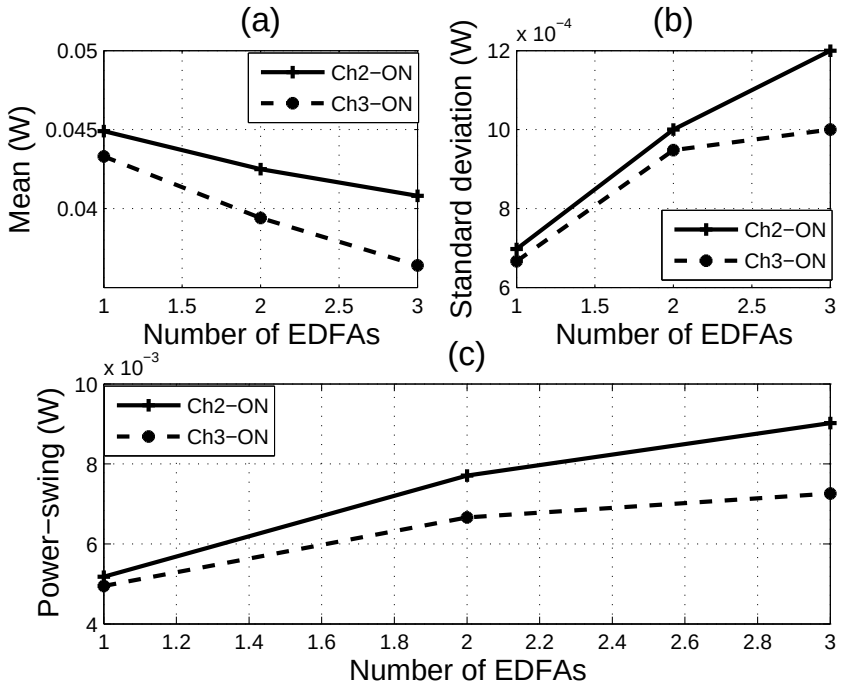

Figure 4.9: (a) Mean, (b) standard deviation and (c) power-swings of the output power transients of channels 2 and 3 versus number of EDFAs in the chain.

shown in Figures 4.7 (b, c) and 4.9 (b, c) respectively.

Figure 4.9 (a) shows that the mean of channel 2 and channel 3 decreases as the number of EDFAs increase in the cascaded EDFAs link. Label ch2-ON or ch3-ON represents the output power transients of channel 2 or channel 3 while channel 3 or channel 2 are in burst-ON period respectively. Figure 4.9 (b, c) shows the standard deviation and the power swings of the output power transient of channel 2 and 3 increase as the number of EDFAs increase. It is observed from the slope of the curves in Figure 4.9 (b, c) that the standard deviation and the power swings increase at the output of the first EDFA more than the standard deviation and the power swings at the output of the other EDFAs in the chain. The slope of the curve in Figure 4.9 (c) is 0.26 at the output of the first EDFA, the slope is 0.125 at the output of the second EDFA, about half the slope at the output of the first EDFA.

We conclude that in the saturated EDFAs chain, the output power transient increases at the output of each amplifier as the number of EDFAs increase. However, the increase in standard deviation and output power swings along the cascaded EDFAs at the output of the first amplifier is twice the increase in the standard-deviation and the output power-swings at the output of the second or the other EDFAs in the chain. The increase of output power

transients take such behaviour (discussed above) along the chain if the EDFA operates in a saturation condition while the output power transients of the small signal input power at cascaded EDFAs have different behaviour, as we explain in Section 4.4.

4.4 Power transients at small signal power

In this section, two small input signal powers are used for the Poission distributed ATM-IP traffic, -16 dBm (25 μW) and -26 dBm (2.5 μW). In previous simulations, EDFAs operated in saturation regimes using peak input power of -2 dBm (0.63 mW). The effects of these three input powers on the output power transients are investigated. We first discuss parameters for the numerical simulation and then in the following subsection, we analyze the power transients of each channel in the link. A statistical analysis of the power transient also follows later in this section.

4.4.1 Simulation parameters

These parameters are the same as the ones used with the numerical simulation of the EDFA at non-self-saturated conditions except for the input power, which is chosen from the linear region of the EDFA spectrum. We simulate the network link for two different values of input power. One of these small signal values for input power for each channel is -16 dBm. The span loss which is calculated for this case is -31 dB and it corresponds to a span length of 125 km. Another smaller value for an input power is -26 dBm. The span loss for this case is -34.7 dB and it corresponds to a span length of 173.5 km. As mentioned earlier, the input power for the saturated EDFA is -2 dBm, the span loss is -19 dB, and its equivalent span length is 88 km using a single mode fibre of attenuation coefficient 0.22 dB/km [13, 14].

4.4.2 Results and analysis

In the first set of results, we discuss the power transient analysis which clearly shows the effects of output power transients of individual channels and their relationship with the total input power level, and the number of cascaded amplifiers in the link. In the second set of results, the statistical analysis of the power transient in each individual channel is detailed.

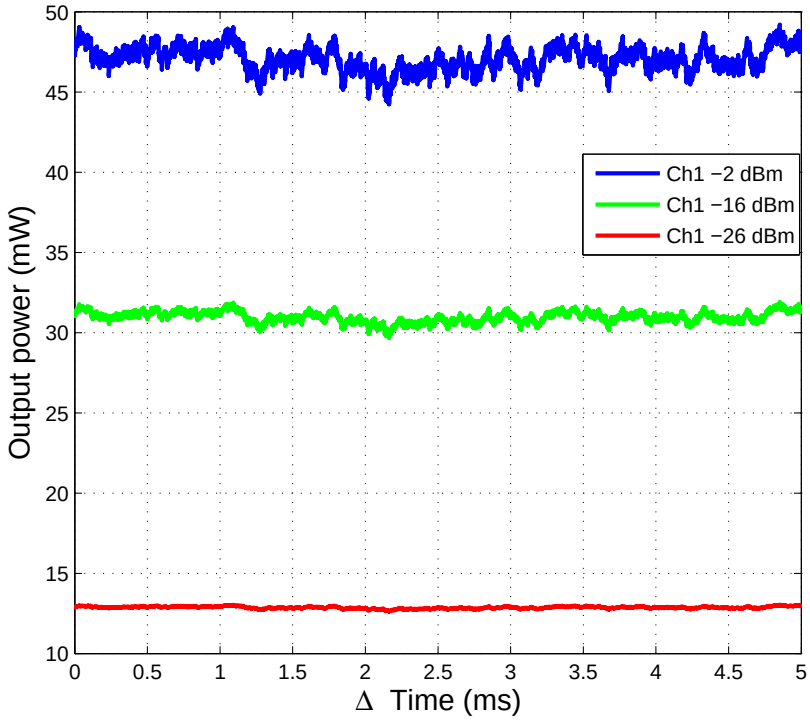

Figure 4.10: The output power transients of the CW channel at the output of the first EDFA for different input powers -2 dBm, -16 dBm and -26 dBm, are compared on the same scale.

The dependence of mean, standard deviation and power swing on the number of cascaded EDFAs in the link are analyzed.

4.4.2.1 Numerical analysis of the power transients

The response of EDFAs to random variation of the input power of channels due to randomized times of packet arrival and variation in packets size is of prime importance in this thesis. The changes of input power into the EDFA leads to a wide output power transient, and because the gain of an EDFA is wavelength dependent this leads to different gains in different WDM channels. Therefore, signals along cascaded amplifiers will experience an increasing output power spread among individual channels which will depends on the ON and OFF periods of the input signal in the specific channels.

Figure 4.11 (a, b, c) highlights the power transients for channel 1 at the output of the first amplifier for three different input powers -2 dBm, -16 dBm and -26 dBm respectively. The output power transients for each input power are 0.53, 0.41, 0.37 mW respectively. This difference is clearly shown in the Figure 4.10 which has the three different outputs plotted

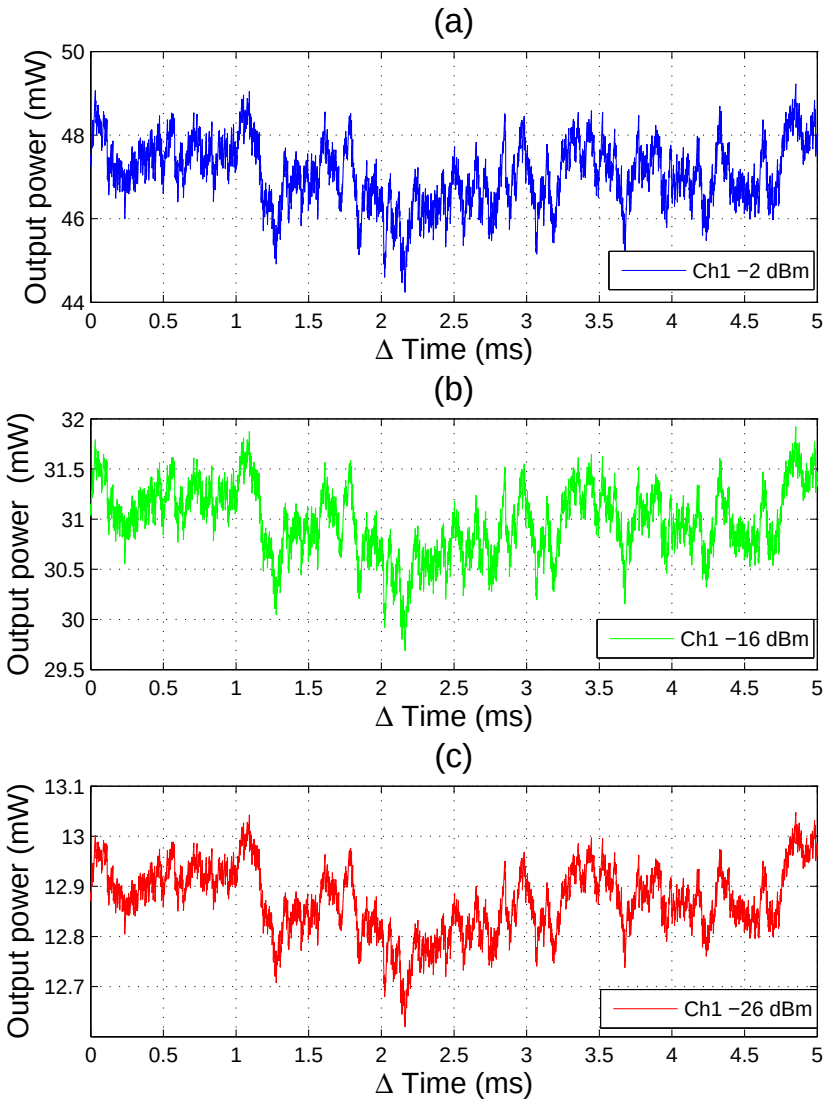

Figure 4.11: The output power transients of the CW channel at the output of the first EDFA for different input powers (a) -2 dBm, (b) -16 dBm and (c) -26 dBm.

in one figure. The output power transients of the link decrease as the input power decreases. This results from the high sag in the upper part of the packets with high input power to the EDFA while the packet sag is low with low input power to the EDFA, as was previously explained in Figure 3.4 (b). Figure 4.12 (a) shows the sag (on the top of packets) clearly with input power -2 dBm, in Figure 4.12 (b), the sag is less than in Figure 4.12 (a) with smaller input power of -16 dBm, and the sag has almost disappeared in Figure 4.12 (c).

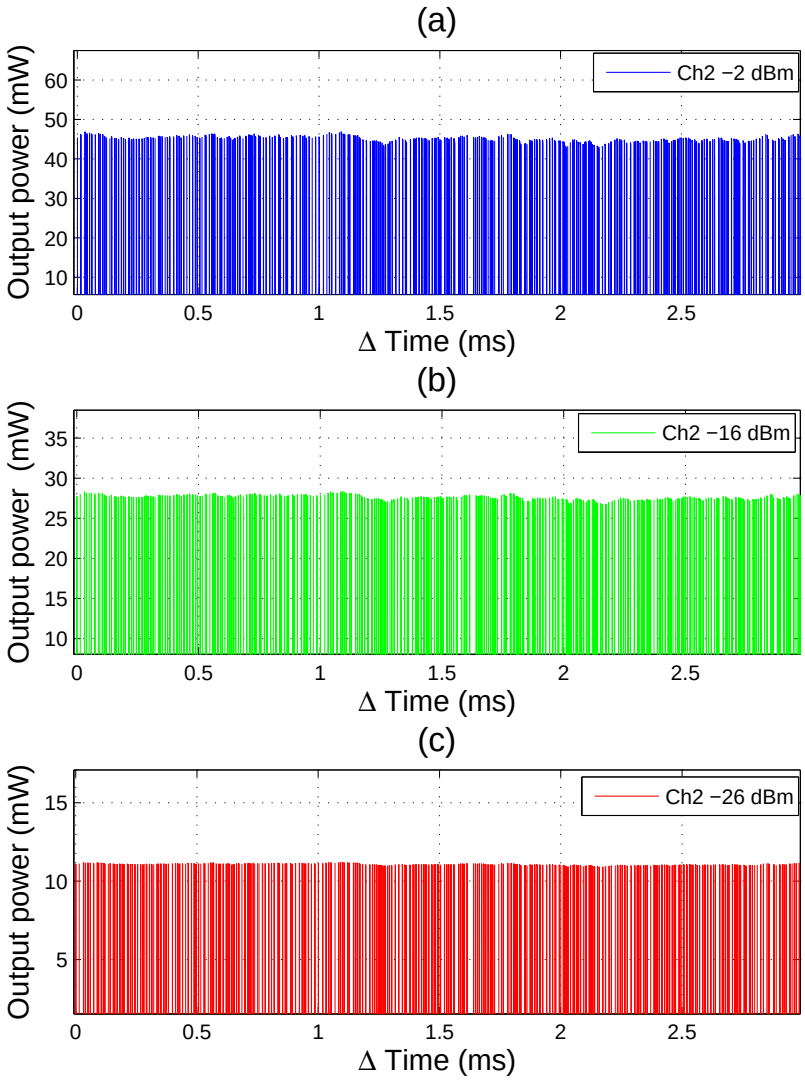

Figure 4.12: The output power transients of channel 2 at the output of the first EDFA for ATM-IP traffic for input peak powers of (a) -2 dBm, (b) -16dBm and (c) -26dBm.

4.4.2.2 Statistical analysis of power transients

The simulation was performed using a chain of EDFAs. The PDFs of the output power transients of channel 1 at the output of the first EDFA in a chain for the input powers -16 dBm are shown in Figure 4.13 (a, b) while both channel 2 and 3 are in burst-OFF and burst-ON periods respectively. Figure 4.13 (c, d) shows the PDFs of the output power transient of channel 2 and 3 while their traffic is at the burst-ON periods.

The output power transient of each channel along the cascaded EDFAs for the input of -

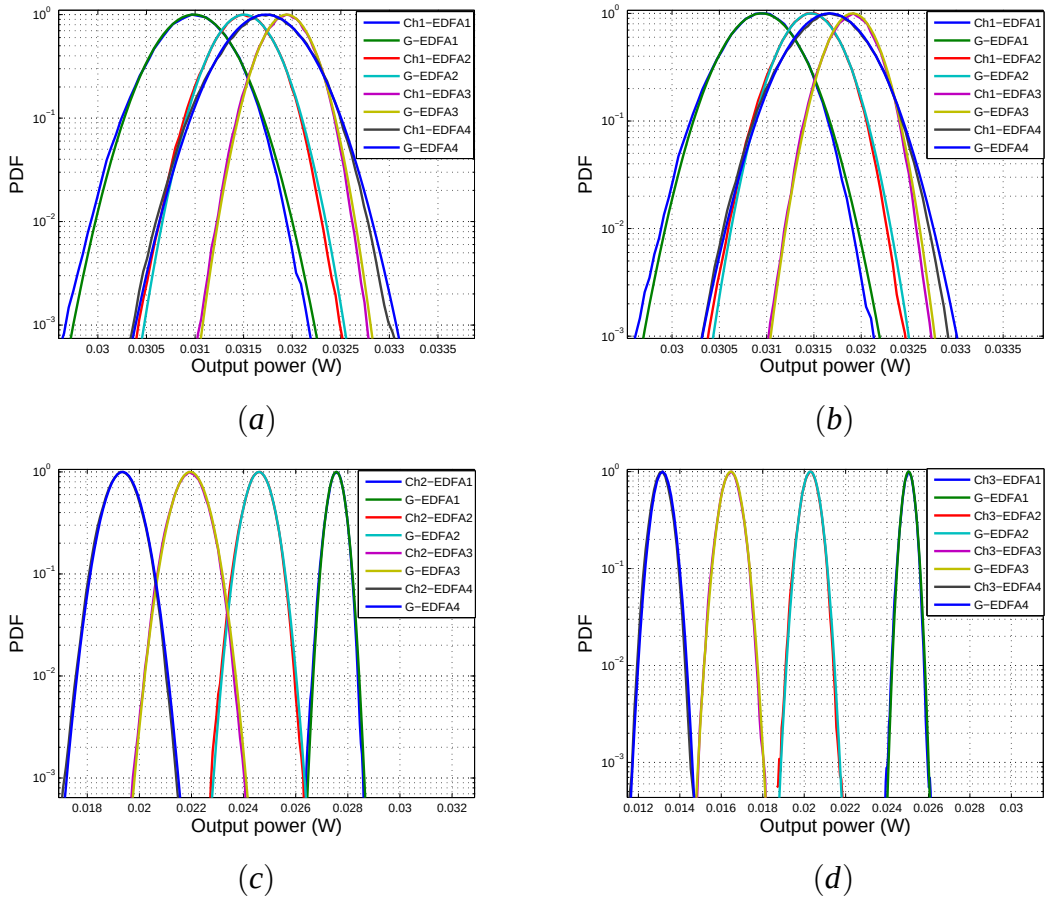

Figure 4.13: PDFs of the output power transients and related Gaussian fits (denoted by G-EDFA1/2/3/4) of channel 1 at the output of the first to fourth EDFAs when the input signal power is -16 dBm while the traffic in channels 2 and 3 are in (a) burst-OFF periods. (b) burst-ON periods. PDFs of the output power transients and related Gaussian fits (denoted by G-EDFA1/2/3/4) at the output of the first to fourth EDFAs while the traffic in burst-ON periods and using input signal power of -16 dBm in (c) channel 2, (d) channel 3.

16 dBm increases as shown in Figure 4.13 (a, b, c, d). The mean of the output power transient of channel 1 increases as shown in Figure 4.14 (a) but the mean of channels 2 and 3 decrease as shown in Figure 4.15 (a). The standard deviation and power swings of all channels along the cascaded EDFAs increase as shown in Figures 4.14 (b, c) and 4.15 (b, c) respectively.

The simulation was performed using an input power of -26 dBm. The PDFs of the output power transients of channel 1 at the output of the first EDFA in a chain are shown in Figure 4.16 (a, b) while both channel 2 and 3 are in burst-OFF and burst-ON periods respectively. Figure 4.16 (c, d) shows the PDFs of the output power transient of channel 2 and 3 while their traffic is in burst-ON periods.

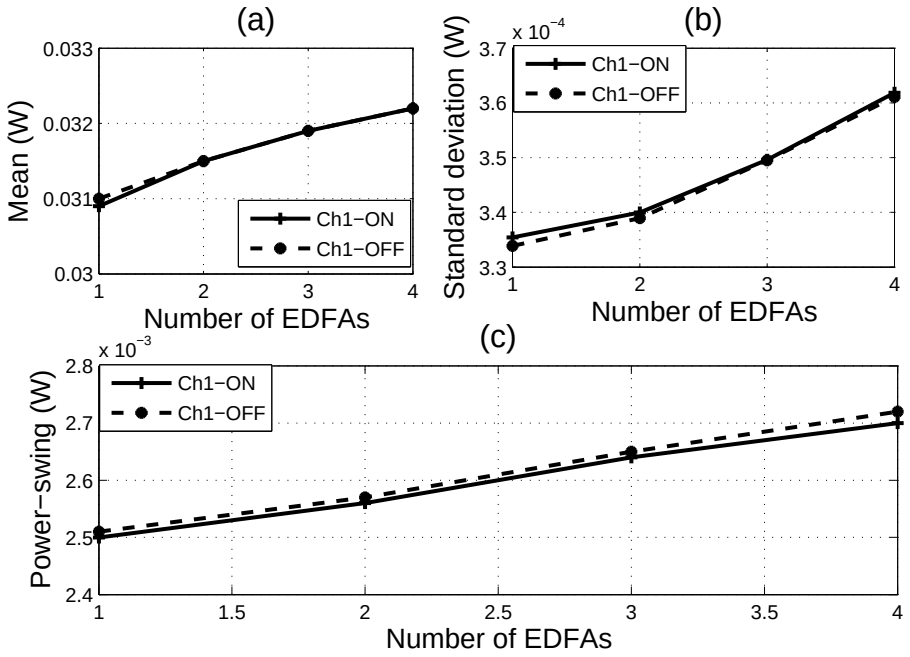

Figure 4.14: (a) Mean (b) standard deviations and (c) power swings of the output power transients of channel 1 when the input signal power is -16 dBm.

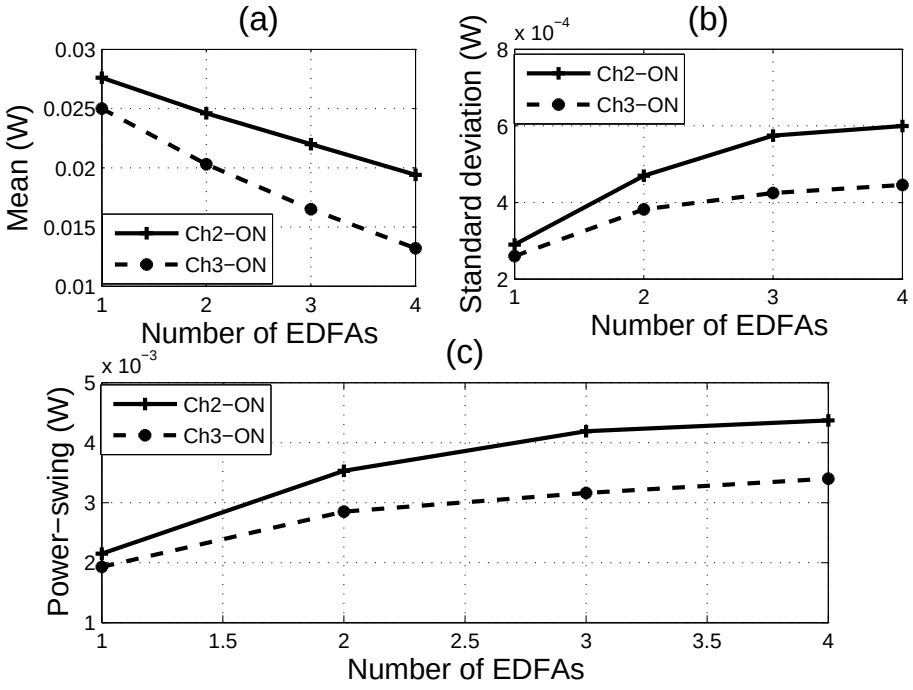

Figure 4.15: (a) Mean (b) standard deviations and (c) power swings of the output power transients of channel 2 and 3 when the input signal power is -16 dBm.

The output power transient of each channel along the cascaded EDFAs increases for the input -26 dBm as shown in Figure 4.16 (a, b, c, d). The mean of the output power transient

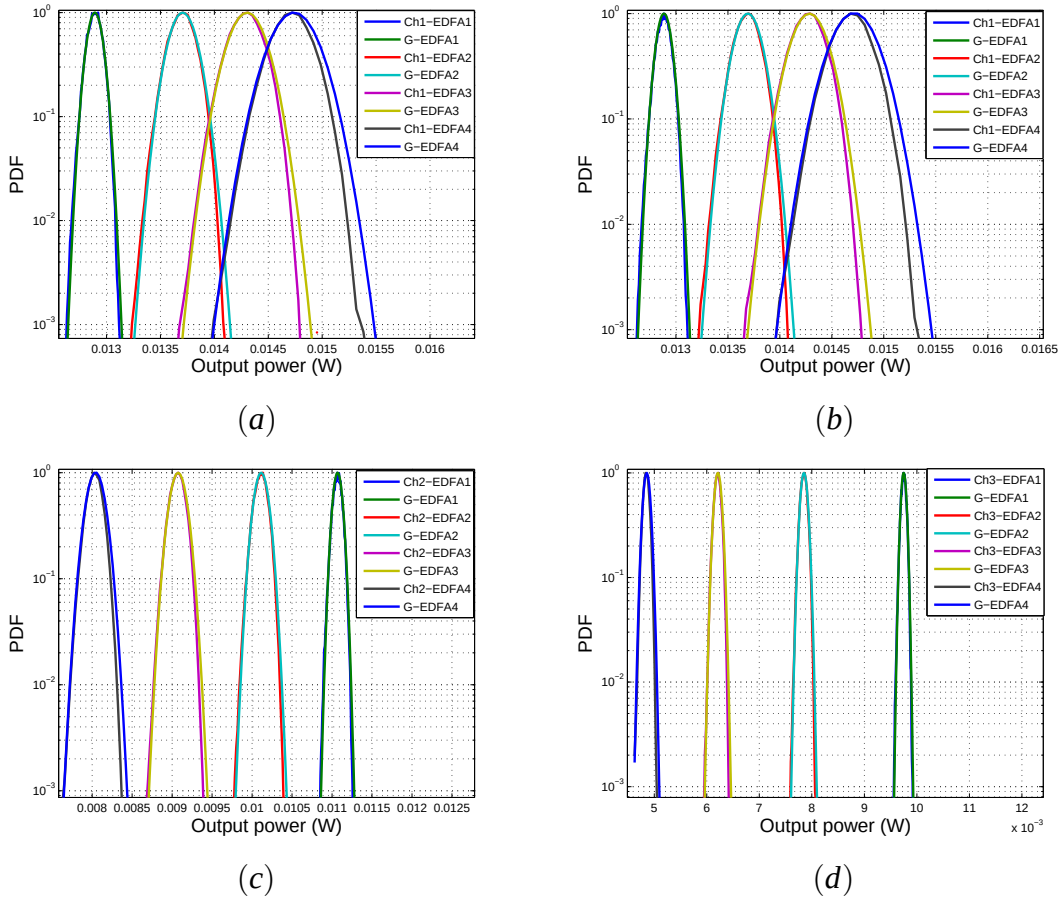

Figure 4.16: PDFs of the output power transients and related Gaussian fits (denoted by G-EDFA1/2/3/4) of channel 1 at the output of the first and fourth EDFAs when the input signal power is -26 dBm while the traffic in channels 2 and 3 are in (a) burst-OFF periods. (b) burst-ON periods. PDFs of the output power transients and related Gaussian fits (denoted by G-EDFA1/2/3/4) at the output of the first and fourth EDFAs during burst-ON periods using input signal power of -26 dBm in (c) channel 2, (d) channel 3.

PDFs of channel 1 along the cascaded EDFAs increases as shown in Figure 4.17 (a) but the mean of the output power transient of channel 2 and channel 3 decreases as shown in Figure 4.18 (a). The standard deviation and power swings of all channels along the cascaded EDFAs increases as shown in Figures 4.17 (b, c) and 4.18 (b, c). The PDFs of the output power transients of channel 1 at the output of the first EDFA in a chain for three different input powers, -26, -16 and -2 dBm are shown in Figure 4.19 (a, b) while both channel 2 and 3 are in burst-OFF and burst-ON periods respectively. Figure 4.19 (c, d) shows the PDFs of the output power transient of channel 2 and 3 at the output of the first EDFA for three different input powers, -26, -16 and -2 dBm while their traffic is in burst-ON periods.

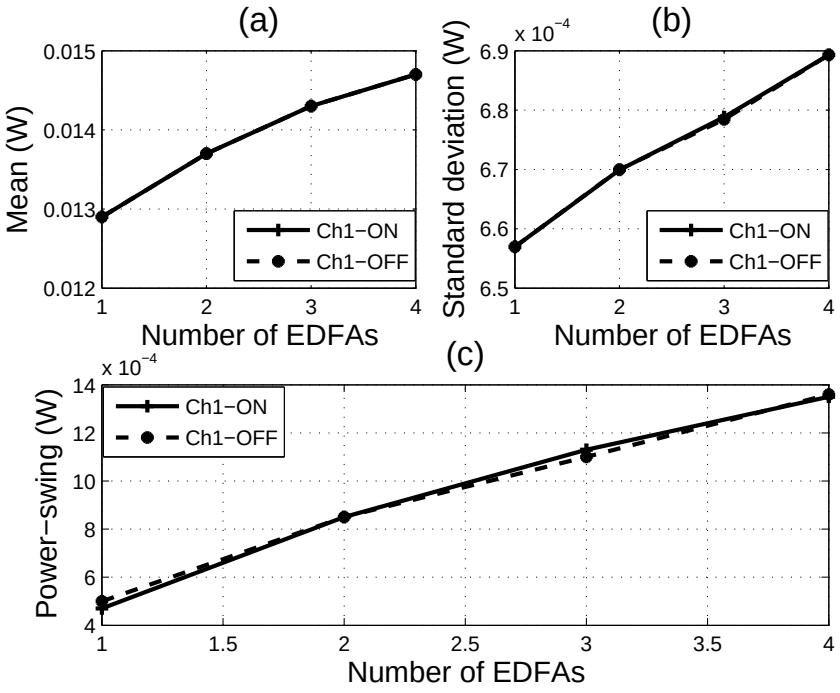

Figure 4.17: (a) Mean (b) standard deviations and (c) power swings of the output power transients of channel 1 when the input signal power is -26 dBm.

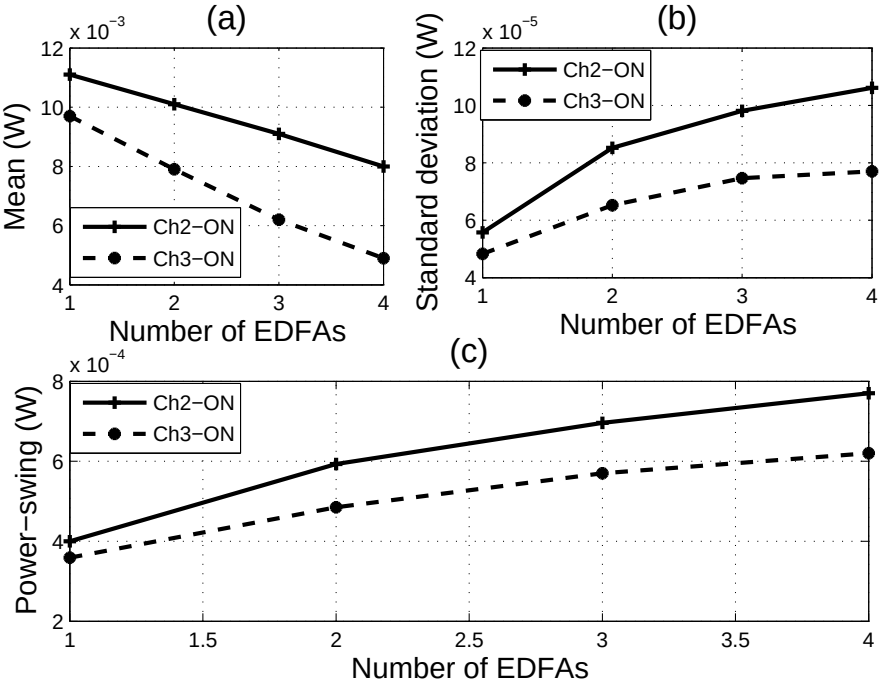

Figure 4.18: (a) Mean (b) standard deviations and (c) power swings of the output power transients of channel 2 and 3 when the input signal power is -26 dBm.

For Figures 4.19, the location of the output power PDFs are: PDF for -2 dBm to the right,

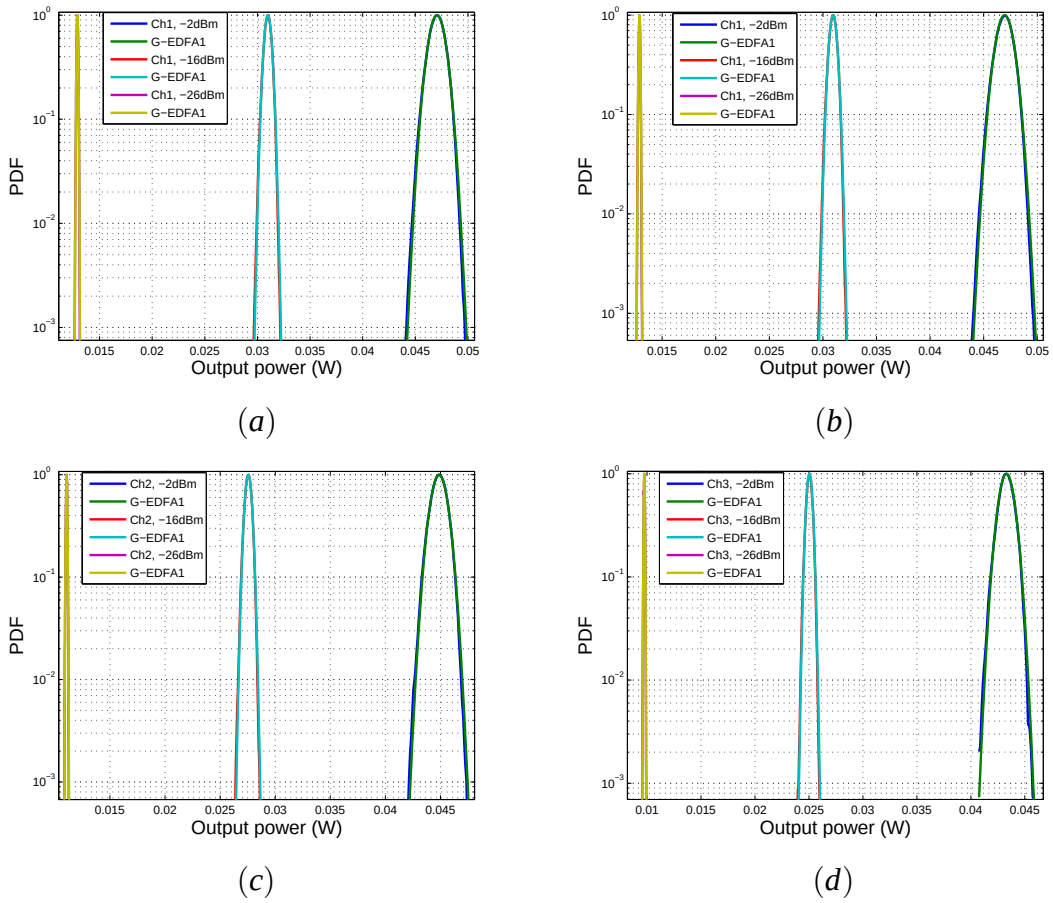

Figure 4.19: PDFs of the output power transients and related Gaussian fits (denoted by G-EDFA1) for three different input powers, -26, -16 and -2 dBm (from left to right) of channel 1 at the output of the first EDFA in a chain, while both channel 2 and 3 are in (a) burst-OFF periods, and (b) burst-ON periods. PDFs of the output power transients and related Gaussian fits (denoted by G-EDFA1) of (c) channel 2, and (d) channel 3, for three different input powers, -26, -16 and -2 dBm, while the traffic of channels 2 and 3 are in burst-ON periods.

PDF for -16 dBm at the middle, PDF for -26 dBm to the left. Analysis and observation confirm, the narrower the PDFs, the less the output power transients are. The mean, standard deviation and power swings of channels 1, 2 and 3 for three different input powers, -26, -16 and -2 dBm are plotted for comparison as shown in Figures 4.20 and 4.21. It is observed that the mean, standard deviation and power swing of all channels increase as the input power increases.

We conclude from our simulation results that, in the packetized channels, the mean decreases while the standard deviation and the power swings increase versus the number of EDFAs in both cases of saturated and small signal power. However, the power swing's mag-

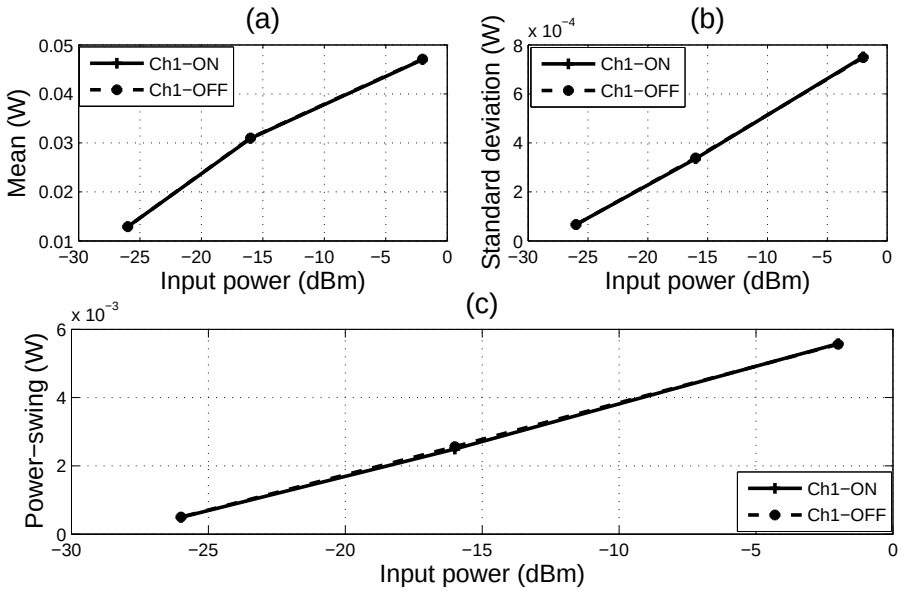

Figure 4.20: (a) Mean, (b) standard deviation and (c) power-swings of the output power transients of channel 1 versus different values of the input powers.

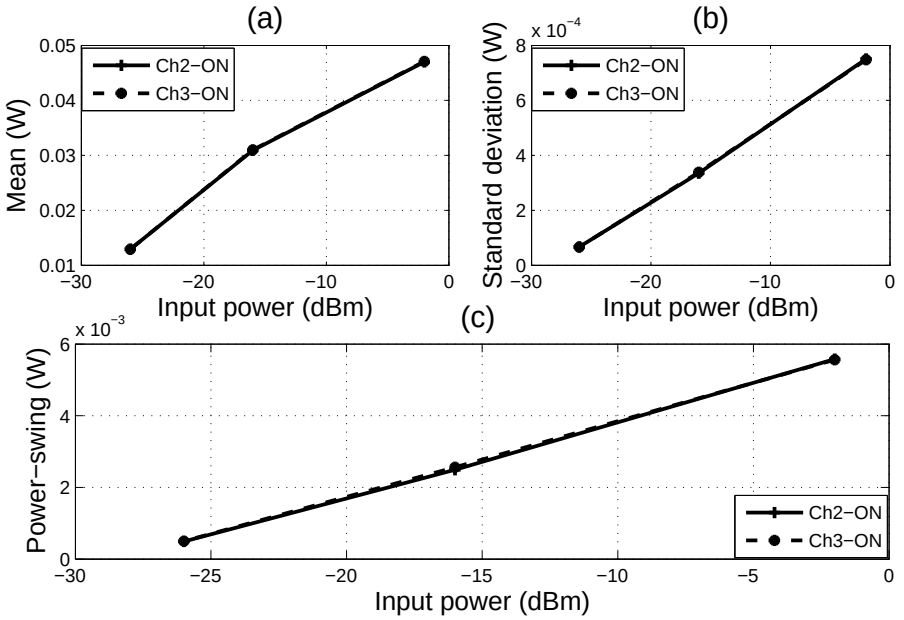

Figure 4.21: (a) Mean, (b) standard deviation and (c) power-swing of the output power transients of channel 2 and 3 versus different values of the input powers.

nitude becomes smaller in the saturated case after the second amplifier as with the small input power, the power-transient increases with the different magnitudes at the output of each EDFA in the chain.

4.5 Summary

This chapter examined the effect of Poisson traffic on output power transient phenomena using non-self-saturated (without ASE) model. The magnitude of the output power transients are examined using numerical and statistical analysis. The oldest known traffic model in use in a telephony context, the Poisson distribution model, is used. We verified the traffic model by plotting the non-normalised PDFs of the burst-ON and burst-OFF periods for the input traffic sources. The traffic sources follow the Poisson distribution with an exponentially decaying function for burst-ON and burst-OFF periods. These values show good agreement with the corresponding analytical Poisson distribution.

To analyse the effect of the small signal packetized input on power transient phenomenon, we simulated the network link for two different values of small signal powers of -16 dBm and -26 dBm which were chosen from the linear regime of the EDFA spectrum, using the non-self-saturated model.

The response of EDFAs to random variation of the input power of channels due to randomized times of packet arrival and variation in packet size are effective parameters of the power transients. The changes of input power in EDFA leads to large output power transients. Moreover, the gain of an EDFA is wavelength dependent and this leads to different gains in WDM channels. Therefore, signals along cascaded amplifiers will experience an increasing output power spread among individual channels and this depends on the ON and OFF periods of the input signal in the specific channels. The standard deviation and power swings are sufficient for clearly indicating the increase in the output power transients.

From our simulation results, we observed that the output power transients of each channel represented by the related PDF broaden. The broadening of PDF depends on EDFA parameters, such as the traffic type and the number of the EDFAs in the chain in the network. The PDFs show a good Gaussian fit. Therefore, the mathematical manipulation rules mentioned in Chapter 1, which are applied to Gaussian distribution data, are also applied to output power transients in this chapter. If the power transient is high, then the output power will be outside the limit of the receiver and this produces a bit error rate which is not acceptable for networks performance (i.e. higher than 10^{-4} for voice traffic).

Chapter 5

Effect of ATM-IP traffic on EDFA power transients in optical networks

5.1 Introduction

In this chapter, the dynamic model of the non-self-saturated EDFA, described and validated for the circuit-switched WDM networks in Chapter 3, is used to investigate the transient behaviour in packet-switched WDM optical networks.

Packet sources are modelled as ATM-IP traffic [140], known as bursty traffic, which has burst-ON and burst-OFF periods. The burst-OFF period is a sequence of time slots that do not carry packets. Similarly, the burst-ON period is a set of time slots that all carry packets.

In this study, three scenarios have been examined. In the first scenario, a periodic train of pulse traffic at a bit rate of 4.24 Mb/s is examined. In the second scenario, a train of ATM-IP packets of different repetition times for each channel is examined. In the final scenario, ATM-IP traffic of Pareto distribution with variation parameter of 1.2 at burst-ON and burst-OFF periods is implemented at bit rate of 2.5 Gb/s. The output power of the non-self-saturated (without ASE) EDFAs chain for three study cases is used for numerical analysis of the output power transients (i.e. output power plus power transients). The Probability Density Function (PDF) is used for statistical analysis of these output power transients.

5.2 WDM network traffics

In the context of networks, this research concentrates on developing traffic models which can be applied to any communication network, specifically to the Internet. The idea behind such traffic models is to achieve two objectives. First, traffic models are used as input sources in network simulations. These simulations are performed to study and analyse how traffic behaviour affects the particular network conditions (e.g. congestion, output power and SNR swings in circuit- and packet-switched optical networks, etc.). It is very important that the applied models behave with the characteristics of the traffic it is supposed to describe. Second, a genuine traffic model will provide an insight into a better understanding of the network traffic characteristics. In turn, this will lead to a better QoS. For instance, a model which has been validated and shows some correlation between traffic arrivals, can be used for better understanding and developing solutions to some network problems, or to design devices and packet handling strategies.

The oldest traffic model, which was initially developed in a telephone context, was based on Poisson processes, and call arrivals could be identically and independently distributed, and the call holding times have an exponential distribution with parameter λ, the mean and variance are equal to λ. Poisson traffic can be characterized by assuming that the packet arrivals are independent or have temporal correlations that decay exponentially, i.e traffic distribution has an exponentially decaying tail. In spite of initially being analytically simple and successful, the Poisson model has been proved insufficient to simulate data traffic in modern LANs and WANs [112, 135, 141].

Data networks are characterized by high variability in burst-OFF and burst-ON, that is a self-similar traffic which repeats itself at many time scales. Many traffic measurement studies in data communication networks such as the Internet have found long-tailed distributions. Research proved that Ethernet traffic has a self-similar nature [111, 134] and the variable-bit-rate video traffic has been shown to possess long-range dependence [112]. This means that the characteristics of these data clearly diverge from the conventional telephone traffic and its related Markov models with short-range dependences. Such traffic can be described through long-tailed distributions such as the Pareto and Lognormal distributions [135].

5.3 Packet traffic model

Modelling different classes of WAN traffic generated by such different application protocols as TELNET (Teletype Network), FTP (File Transfer Protocol), SMTP (Simple Mail Transfer Protocol) and NNTP (Network News Transfer Protocols) will depend on context. However, only the TELNET connection and FTP session arrivals for short time periods can be modelled by a Poisson process, independent of the protocol generating it. The Pareto distribution is applied to all WANs traffic because of the bursty and heavy-tailed nature of the traffic [142–144]. In addition, the FTP data bursts and TELNET packet inter-arrivals were modelled with the Pareto distribution because of the traffic nature implied [145]. The Pareto distributions are especially attractive for their simple analytical form.

The long-tailed distributions suffer from the weakness of not having finite moments of all orders and this weakness has limited their use in data communication networks. This weakness in Pareto distribution is overcome by introducing a truncated version of the Pareto distribution.

5.3.1 Pareto distribution traffic model

The Pareto distribution is a simple model for positive data with a power law probability tail. It is natural to consider an upper bound that truncates the probability tail, and the truncated Pareto distribution has a wide range of applications in different fields of data communication networks analysis. The truncated Pareto distribution is used for our traffic modelling in this thesis [146]. In the truncated Pareto distribution, the probability of a random variable x is given by [147]:

$$P(x) = \left(\frac{x}{x_m}\right)^{-k} \tag{5.1}$$

$$x = \frac{x_m}{P^{1/k}} \tag{5.2}$$

where P(x) is the probability of variable x. The Pareto distribution is specified by two quantities, x_m and k. x_m is the minimum possible value of x, and k is a positive parameter called the Pareto index and is an indicator of the degree of variability of the traffic. The value of P will be given with a uniform distribution from zero to one.

In our simulations, we used $x_m = 1$ in order that the burst-ON and burst-OFF periods of

the packet can alter between 1 and ∞ time-slots. The PDF for the truncated Pareto distribution is:

$$P(x;k,x_m) = k\frac{x_m^k}{x^k} \tag{5.3}$$

We use the truncated Pareto distribution shown in Equation (5.3) to produce the random variable, x. Then, we rounded x to the smallest integer which is required to make the burst-ON or burst-OFF periods of the packets a multiple of the ATM packet size. The expected mean value of a random variable x for $k > 1$ for the truncated Pareto distribution is:

$$E(x) = \frac{kx_m}{k-2} \tag{5.4}$$

The variance of x for k > 2 is:

$$Var(x) = -\left(\frac{k\,x_m^3}{3-k} + \frac{2\,x_m^4}{k} + \frac{k^3\,x_m^5}{(k-2)^2(1-k)}\right) \tag{5.5}$$

If $k \leq 2$, the mean and variance are infinite. It was proved by Taqqu [134] that simultaneously input of ON-OFF traffic sources of degree of variability $k \leq 2$, with each source having infinite variance, achieves self-similar traffic.

The total network utilization factor, u, is achieved by:

$$u = \frac{E(T_{ON})}{E(T_{OFF}) + E(T_{ON})} \tag{5.6}$$

Where $E(T_{ON})$ is the mean of the burst-ON period of the packets, $E(T_{OFF})$ is the mean of the burst-OFF period of the empty cells, k_{ON} is the Pareto index or variability term for burst-ON periods, and k_{OFF} is the variability term for burst-OFF periods.

For verification of the Pareto traffic source, the Log-Log normalised PDF for the burst-ON and burst-OFF traffic, used as input sources of ATM-IP traffic to channels 2 and 3 in scenario 3, are plotted in Figure 5.1 (a) and (b). The PDF of the analytical truncated Pareto traffic is also plotted in Figure 5.1 (a) and (b) for the purpose of fitting using Equation (5.3).

Figure 5.1 (a) shows the PDF for normalized burst-ON periods versus cell or packets. It is obtained by simulating the arrival of more than 28 million packets. Figure 5.1 (b) shows the PDF for normalized burst-OFF periods. It is achieved by simulating the arrival of more than 33 million empty cells.

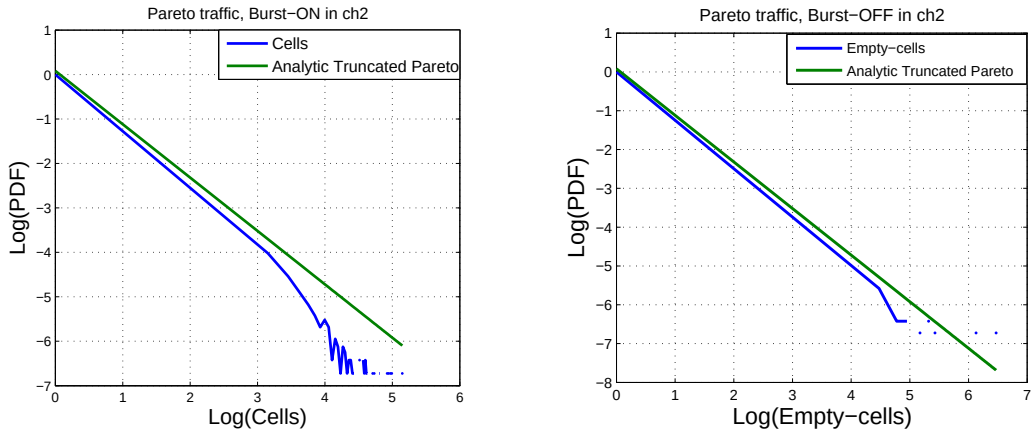

(a) (b)

Figure 5.1: Log-Log PDF of the normalised ON-OFF periods with truncated Pareto distribution of variability degree, $k_{OFF} = k_{ON} = 1.2$: (a) PDF of the burst-ON periods, and (b) PDF of the burst-OFF periods. Blue line - simulation of the truncated Pareto distribution traffic; green line - analytical truncated Pareto distribution.

From Figure 5.1 (a) and (b), the slope of the analytical truncated Pareto PDF is calculated as = - (variability degree) = - 1.2, this is equivalent to $k_{ON} = k_{OFF} = 1.2$, which is used in our traffic simulations. Although the number of cells used in this simulation was more than 33 million empty slots for burst-OFF and more than 28 million packets for burst-ON, this was not sufficient to illustrate the heaviest tail of the distribution. Thus, the number of cells used to generate Figure 5.1 (a) and (b) leads to noise in the tail at around $10^{(}-4)$.

5.4 Cascaded EDFAs for Pareto distribution traffic

This section focuses on numerical and statistical analysis of the three case studies, each of which has different traffic characteristics, such as traffic bit rate and traffic distribution. The network configurations and EDFA parameters are identical for all three cases.

The network topology considered was the bus type, and a span length of 88 km was used to provide span loss of 19.36 dB using SMF fibre of attenuation coefficient of 0.22 dB/km in C-band EDFAs, and span length of 90 km was used to provide span loss of 19.94 dB using SMF fibre of attenuation coefficient of 0.22 dB/km in the gain-shifted C-band EDFAs [13, 14].

5.4.1 Scenario no.1

We present in this scenario the results of numerical simulations performed for 2 signal channel systems and the output power was observed at the first EDFA in the network link. Channel 1 was fed with CW and channel 2 with ATM cells or packets. The CW signal is a good indicator of the output power transients. Thus, the CW signal is used as an input source to channel 1 in all our simulation scenarios. The motivation behind these numerical simulations is analysis of the effects of the output power transients or the gain dynamics obtained from rapid variations of the input power on the output power at the output of the first EDFA. The discussion of results is done in two parts. In the first part, we present the simulation parameters. In the second part, the critical analysis of the power transients is presented.

5.4.1.1 Simulation parameters

In our simulation, we use the simulator developed for the C-band and gain-shifted C-band EDFAs based on the non-self-saturated model [74]. This model is described in Chapter 3. The simulation parameters of this scenario which uses the C-band EDFA are the same as discussed in Section 3.2.1. The EDFAs operate in the non-self-saturated conditions as defined in Chapter 2.

In this numerical simulation, two channels for the input signal and one channel for the pump are used. The input to channel 1 is CW at wavelength 1549.2 nm, with signal peak power of -2 dBm. The input to channel 2 is ATM-IP traffic source with peak pulse power of -2 dBm at a wavelength of 1550.8 nm, using a channel spacing of 1.6 nm. The system runs for 100 ms (i.e. the transmission lasts for 100 ms in the link). At transmission time of 40 ms a packet of duration of 100 μs arrives in channel 2, corresponding to an ATM cell of 424 bits at the bit rate 4.24 Mb/s. ATM cell consist of 424 bit (53byte). One bit time = 1/(4.24) = 0.235 μs. Thus, one packet time = 424 x 0.235 = 100 μs.

In the current simulation scenario, the model has been implemented using 10 points per packet, resulting in a simulation time resolution of 10 μs. The sharp edges of the transient recovery curve in Figure 5.2 is due to this low simulation resolution. The resolution was changed in all of the following scenarios to 10 ns, because of the higher bit-rate of 2.5 Gb/s. The latter's fine resolution can capture the output power and OSNR transients much less than 0.1 dB [52, 113].

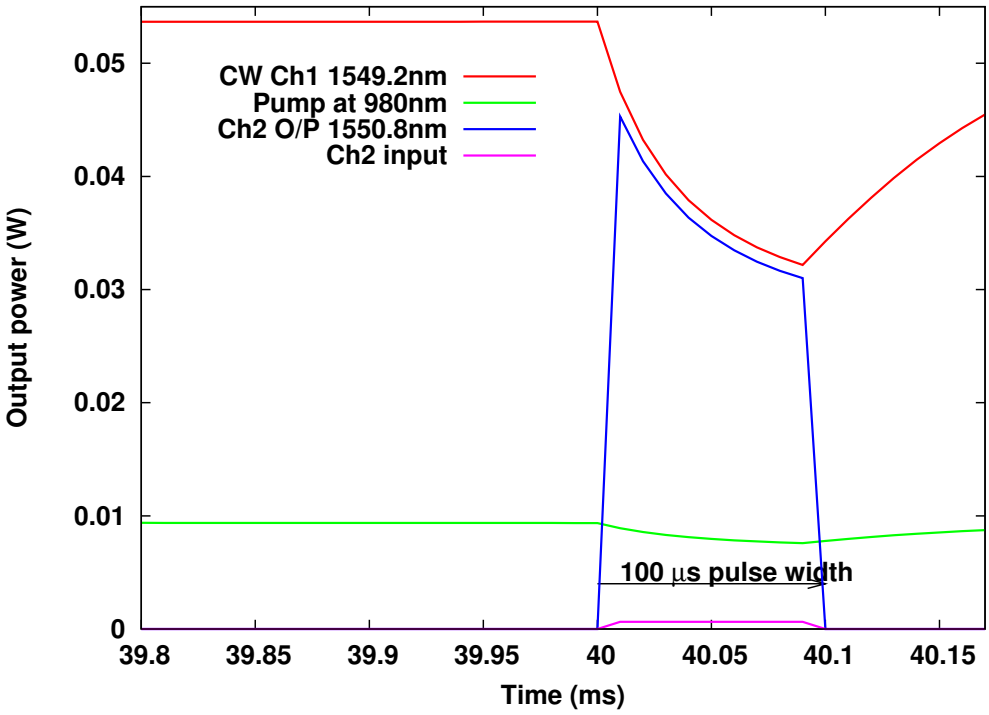

Figure 5.2: Output power transients at the output of the first EDFA for pump signal, channel 1 using CW signal and Channel 2 using packetized traffic.

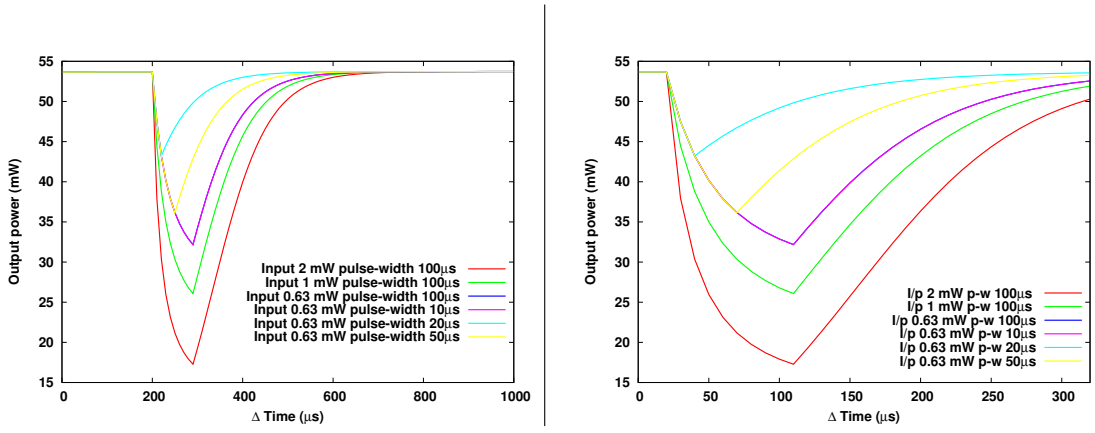

(*a*) (*b*)

Figure 5.3: The output power transients of channel 1 at the output of the first EDFA while different input powers and packet durations are used for the input traffic of channel 2. (a) output power transient in large time scale (0 - 1 ms), (b) output power transient in smaller time scale (0-350 μs) magnified.

5.4.1.2 Results and discussion

In this scenario, we can see from Figure 5.2, the output power transients start with arrival of a packet in channel 2. The output powers of the pump channel, channel 1 and channel 2 all

decrease. This phenomenon is caused by the fast depletion of excited ions. In Figures 5.2 and 5.3, with the arrival of a packet in channel 2 of input peak power of 0.63 mW and duration 100 μs at 40 ms the output power of channel 1 drops from 53.9 mW to 32.10 mW during 100 μs (packet interval), so the power transients in channel 1 is 21.8 mW. Then the output power in channel 1 after channel 2 goes inactive (burst-OFF), increases to its original steady state magnitude of 53.9 mW in 480 μs and total time (transient and recovery times) is 580 μs as shown in Figure 5.3 (a), the transient recovery time depends on pump power. The phenomenon of the power transient in channel 1 due to train of packet traffic in channel 2 is known as "cross-gain modulation effect in the packetized EDFA" [108].

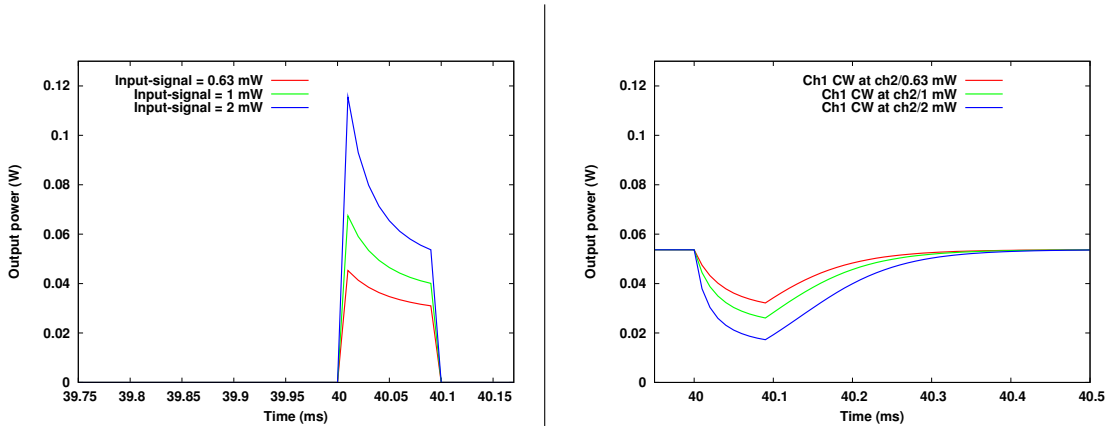

(a) (b)

Figure 5.4: The output power transients at the output of the first EDFA observed at (a) channel 2, (b) channel 1, while different input powers (0.63 mW, 1 mW and 2 mW) are used for the input traffic of channel 2.

In Figure 5.2 the output power in channel 2 decreases from 45.4 mW to 31.0 mW during the duration of the packet (100 μs), so the power transient in the packet is 14.4 mW. This phenomenon occurs when the first packet arrives at channel 2 where it finds a large number of excited ions, the EDFA operates in a small signal gain regime because the pump power is high, and the input signal exists for the duration of the packet (100 μs). Because of stimulating emission, the ions start depleting quickly, and very fast power transients occur during the time of the packet, in consequence, the last bits will have a lower amplification than the initial bits. We can see in Figure 5.4 (a) the output power sag is greater the higher the input power to channel 2.

As we mentioned the gain dynamics can be very fast in high peak packets due to the

stimulated-emission avalanche depletion of the excited ions. Figure 5.4 (a) illustrates the sag across the output power of the packet for different input powers. When the packet peak power of channel 2 is 0.63 mW, 1.0 mW, or 2.0 mW the power transient in the output power of the packet is 14.4 mW, 27.4 mW or 62 mW respectively.

Figures 5.3 (a), (b) and 5.4 (b) shows the effect of different packet peak powers and different packet durations of channel 2 on the cross-modulation behaviour of the output power of channel 1, the individual input power is used at the individual simulation. With arrival of the packets of channel 2 of input peak power of 2 mW, 1 mW, or 0.63 mW with the same packet duration of 100 μs for all three inputs, the output power of channel 1 decreases from 53.9 mW to 17.35 mW, 25.9 mW, 32.1 mW respectively. When the input peak power of the packets of channel 2 is 0.63 mW and of different packet durations of 100, 50, 20 and 10 μs the output power of channel 1 decreases to 32.10, 36.2, 43.4 and 47.6 mW respectively, so the power transients in channel 1 are 21.8, 17.7, 10.5 and 6.3 mW respectively. We concluded from Figure 5.3 that the transient time and power of channel 1 depends on the input packet duration and peak power of channel 2. However, the output power transient and recovery times in all cases is 580 μs as seen in Figure 5.3 (a).

We can also conclude from our simulation that the sag will double when the input peak power is doubled, as shown in Figure 5.4 (a). The transient time depends on pulse duration, while the transient recovery time depends on the pump power. In the case where the packet repetition is long, then this will provide enough time for the ions to regain their initial energy. Thus, the second packet will behave in the same way as the first packet, but if the packet arrives before restoration of the ions to the initial condition, then the packet will have less initial gain or less power sag across the output packet and require less time to become stable. This means that the initial bits in the packet experience higher gain than the last bits in the packets and less than the leading packet. This will be seen in the next scenario with ATM packets at a bit rate 2.5 Gb/s. As the bit rate increases the slot (packet or empty cell) time will decrease. In the current example, we consider the low bit rate communication link to demonstrate the effect of pulse peak power and the pulse duration or the channel bit rate on the power transient magnitude and duration in channel 2 and adjacent channels in the link [107, 148].

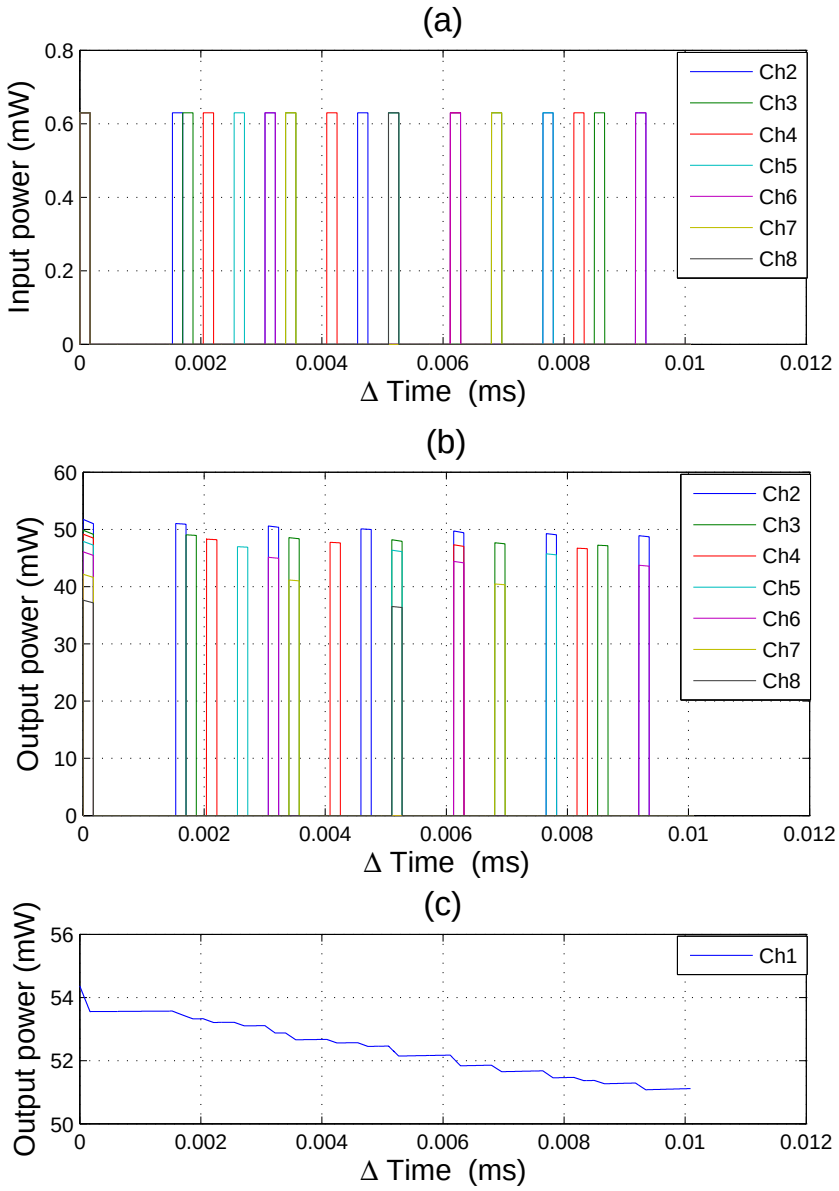

Figure 5.5: (a) Input traffic to all 7 packetized channels, t=0 is equivalent to 75 ms of simulation run-time, (b) the output power transients of 7 packetized channels at the output of the first EDFA, t=0 is equivalent to 75 ms of simulation run-time, (c) the output power transients of channel 1, CW, at the output of the first EDFA. These output power transients are observed prior to the system reaching an equilibrium state.

5.4.2 Scenario no.2

In this section we present the results of numerical simulations performed for the 8 channel system and the output power observed at the first and the third EDFAs in the network link. Channel 1 was fed with CW and channels 2 to 8 were fed with a periodic train of ATM-IP cells or packets of different repetition times [107]. The main idea behind these numerical

simulations is to analyse the effect of rapid variations of the input power and different burst-OFF periods on the output power transients of system channels at the output of the first EDFA.

5.4.2.1 Simulation parameters

In our simulation, we use a traffic source of ATM-IP specification at the bit rate of 2.5 Gb/s [107]. The simulation parameters are the same as in scenario 1. In this scenario, eight signal channels are used and fed with ATM-IP traffic of different patterns of the burst-OFF periods, then amplified with EDFA in the link of the optical network.

5.4.2.2 Results and discussion

The ATM-IP traffic sources provided for channel 2 to channel 8 are: packet duration is 170 ns and denoted by T_p, corresponding to an ATM-IP cell of 424 bits at a bit rate of 2.5 Gb/s. In this simulation, the burst-OFF periods are created manually in each channel and the overlapping of the packets of different channels is likely to occur as shown at the input powers and the output powers prior to the system equilibrium, see Figure 5.5 (a) and Figure 5.5 (b) respectively. We chose the repetition period denoted by T_r, for channels 2, 3, 4, 5, 6, 7 and 8 to be $10\times T_p$(one packet every 10 slots), $11\times T_p$, $13\times T_p$, $16\times T_p$, $19\times T_p$, $21\times T_p$ and $31\times T_p$ respectively as shown in Figure 5.6 (b) to (h) respectively. After the system equilibrium, the burst-OFF periods and the overlapping of the packets of different channels is also shown at the input powers and the output powers in Figure 5.7 (a) and Figure 5.7 (b) respectively.

We can derive a relation for system utility factor, denoted by u, from T_p, and T_r. T_p is the full-load period in each channel in the network because the traffic is in burst-ON periods. (T_r - T_p) is no-load period in each channel in the network because the traffic is in burst-OFF periods. u = full-load/(full-load + no-load). The utility factor of channel 2 is 0.1, and of channel 3 to channel 8 are 0.0909, 0.0769, 0.0625, 0.0526, 0.0476, 0.0323 respectively. This shows that less than 50% of the link is used because of the long burst-OFF periods which are created artificially in each channel. u decreases as (T_r - T_p) increases.

In the first part of this section, the output power transients of cascaded EDFAs resulting from ATM-IP traffic source, was explained. The packet duration of ATM-IP packets is 170

ns and the inter-arrival periods are different in each channel as discussed above. A numerical analysis for the output power transients of each channel in the cascaded EDFAs was performed.

5.4.2.3 Transient analysis

As mentioned, channel 1 was fed with CW while channel 2 through to channel 8 were fed with ATM packets of duration 170 ns. The transmission in this scenario lasts for 100 ms. We fed a pump and channel 1 with an input power commencing at t = 0 simulation time, while the other channels were fed after the system stabilized. When feeding the pump signal and channel 1 at t = 0, the equipment following the EDFA in the link was protected from damage. This idea is used in the experimental set-up for the protection of devices from high peak signals into the link. This idea is also one of the channel protection techniques to mitigate power transient effects in the packet-switched optical networks discussed in Section 1.9. In contrast, feeding the pump and all eight channels with power simultaneously at t =0, and there would be a very high output power in the channels because all the ions which have been transferred to the metastable level by pump power would be available photons to the input signal when the signal suddenly arrives at t = 0, and this would result in an initial very high peak power in the amplified signal, the equipment following the EDFA in the link would be in danger of being subject to a high peak power.

The first packet in all 7 channels arrives at the same time, t = 75 ms, at the input of the first EDFA. The packet signals of all 7 channels absorb available photons of the excited ions. The excited ions quickly start depleting by stimulated emission, thus causing a very sharp power transient across the packets of channel 2 to channel 8 and a sharp decline in the slope of the CW signal of channel 1. The final bits in the packetized channels will experience less amplification than the initial bits as shown in Figure 5.5 (b), this phenomenon is more clear in Figure 5.7 (b).

Since the first packet from all channels overlap at 75 ms of simulation run-time as shown in Figure 5.5, the excited ions deplete faster, and the output power curve of channel 1 sharply declines for a duration of 170 ns. The output power of channel 1 decreases from 54.36 to 53.56 mW, the drop in power is 0.80 mW, the output power of channel 2 decreases from 51.66 to 50.99 mW, a drop in power of 0.67 mW, and so on for the other channels. Channel

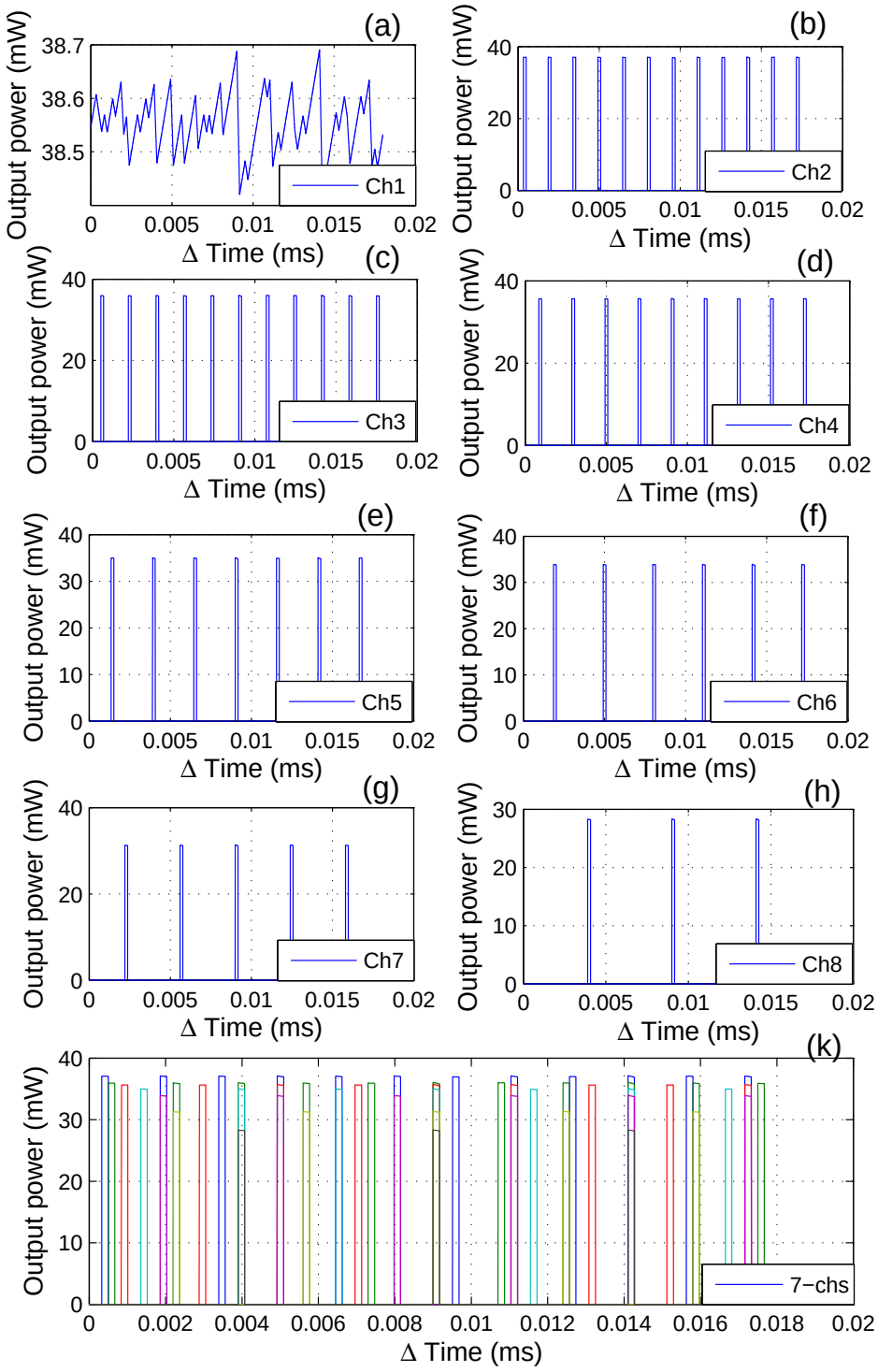

Figure 5.6: (a) to (h) illustrate the individual output power transients for channels 1 to 8, (k) illustrates the output power transients of the 7 packetized channels together. These output power transients are observed at the output of the first EDFA when the system is in equilibrium state.

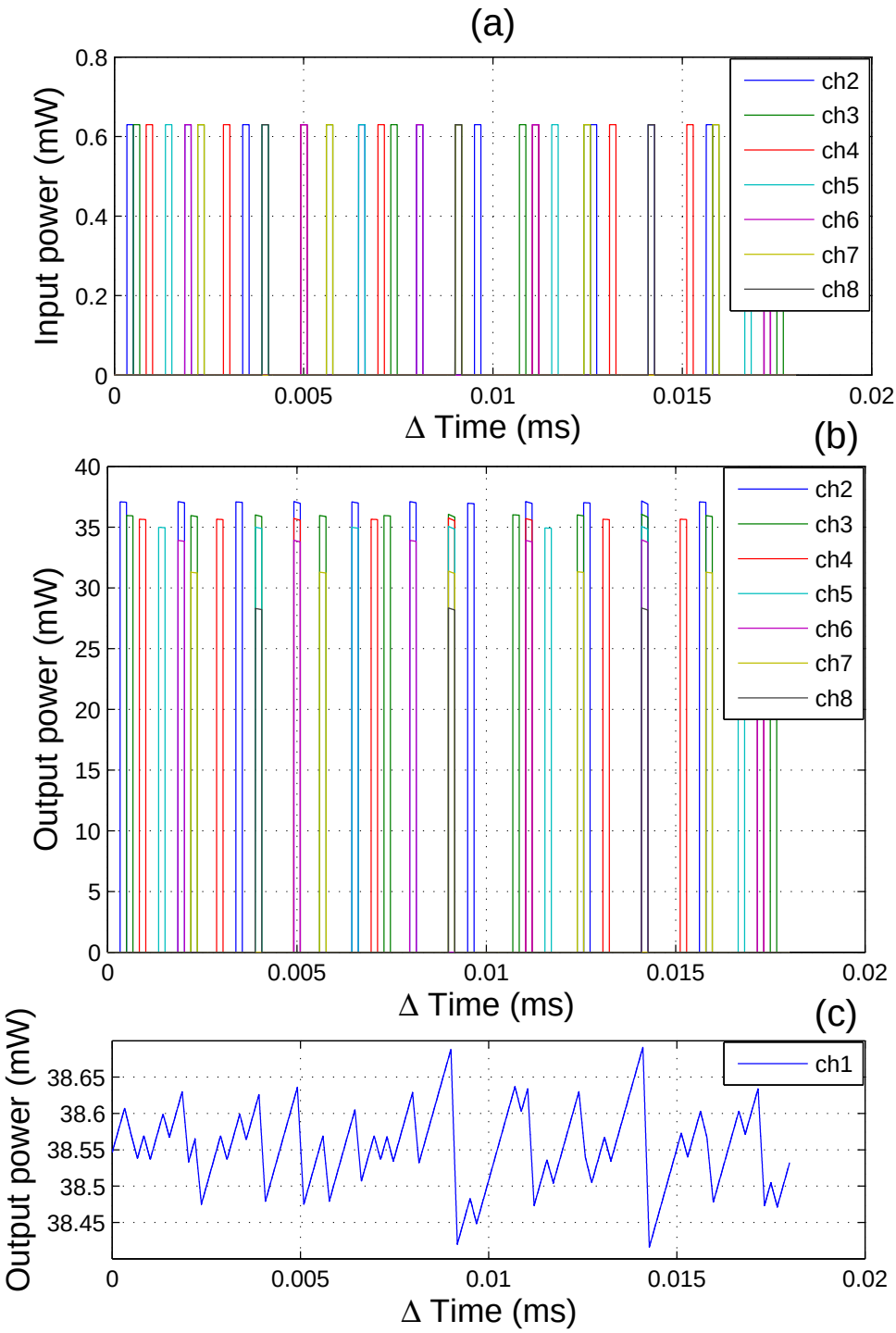

Figure 5.7: (a) Input traffic to all 7 packetized channels, (b) the output power transients of all 7 packetized channels, (c) the output power transients of channel 1. These output powers are observed at the output of the first EDFA when the system is in equilibrium state.

2 to channel 8 are in burst-OFF mode for the time interval of more than 1500 ns. The slope of the output power of channel 1 relaxes in this period, and the output power of channel 1 stays at 53.5607 mW, since the next packet arrives and there is insufficient time for excited ions to

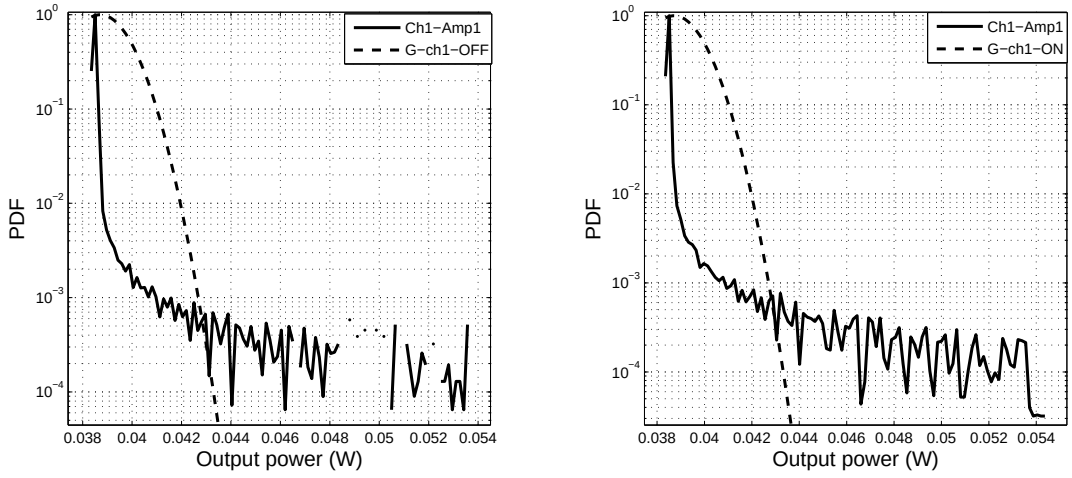

(a) (b)

Figure 5.8: PDFs of the output power transients (full line) and related Gaussian fit (dashed line) of channel 1 at the output of the first EDFA while traffic in the other 7 channels is in (a) burst-OFF periods, (b) burst-ON periods.

restore their energy, as the next packet of channel 2 arrives 1500 ns after the initial simulation start-time, the remaining excited ions are depleted further. In fact, the excited ions can hardly restore their initial energy, as shown by the small increase of the output power of channel 1 in the time between packets. As each packet arrives, it receives less amplification, until the power amplification reaches a dynamic equilibrium level. In our simulation, the equilibrium level is achieved after 3 ms of simulation run-time as shown in Figures 5.6 and 5.7, compared with Figure 5.5 which illustrates the system before equilibrium.

As seen from Figure 5.5, the first packet of channel 2 has a strong output power sag, but as the amplified power decreases, the subsequent packets experience less amplification. Thus, the sag on the output power amplification decreases, and it disappears at the dynamic equilibrium in the case of short packets. The flat gain at equilibrium is not always there, and the duration of the packet is the effective parameter. When the duration of the packet is 100 μ, the power sag at dynamic equilibrium is six times higher than the power sag when the packet duration is 10 μ [107].

In Figure 5.8 (a) and (b), the PDFs of the output power transients of channel 1 at the output of the first EDFA and related Gaussian fit are plotted for both burst-OFF and burst-ON periods respectively. The labels G-ch1-OFF or G-ch1-ON defines the output power

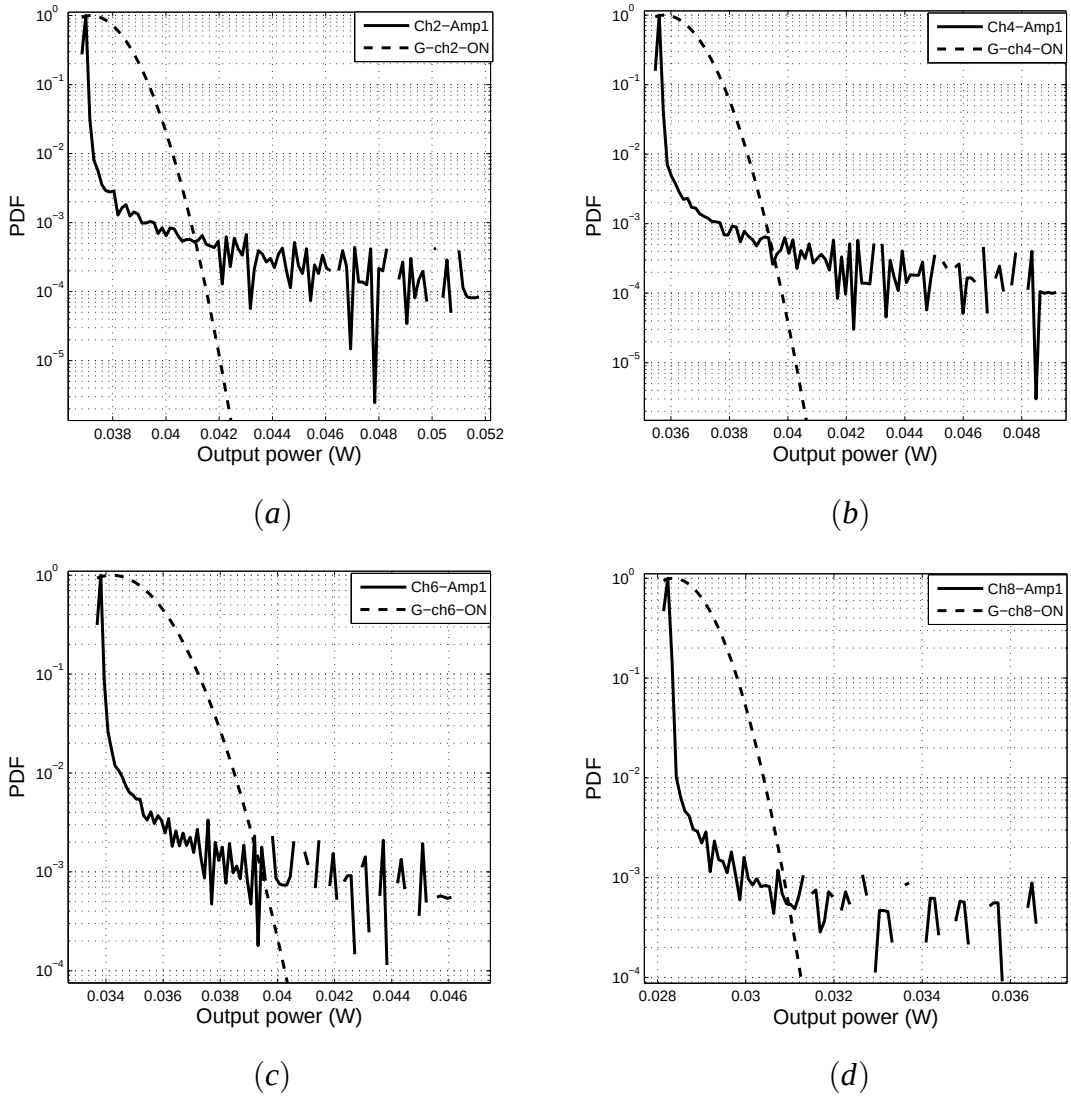

Figure 5.9: PDFs of the output power transients (full line) and related Gaussian fits (dashed line) of (a) channel 2, (b) channel 4, (c) channel 6, (d) channel 8 respectively, observed at the output of the first EDFA while the traffic is in burst-ON periods.

transients and related Gaussian distribution of channel 1 while channel 2 to channel 8 are in burst-OFF period or burst-ON period respectively. The normalized associated Gaussian distribution is plotted using Equation (5.7):

$$Px = \frac{1}{\sigma\sqrt{2\pi}} \exp\left\{ -\frac{(x-\bar{x})^2}{2\sigma^2} \right\} \tag{5.7}$$

Where x is the output power transient which has a mean of $\bar{x}$ and the standard deviation of σ. Figure 5.9 (a), (b), (c) and (d) show the PDFs of the output power transients of channel 2, 4, 6, and 8 respectively at the output of the first EDFAs in the chain. The PDFs do not fit

the associated Gaussian distribution. These PDFs illustrate the long-tail distributions for all channels in the link. The mean of the output power transients of channel 1 at burst-ON and burst-OFF are the same, 0.0387 W. The standard deviation of the output power transients of channel 1 at burst-ON and burst-OFF are the same, 0.0011 W. The output power swings occur due to power transient phenomenon in the link. The power swings are difference between the maximum output power transients, which is defined by max(p(t)), and the minimum output power transients, which is defined by min(p(t)). The max(p(t))of channel 1 at burst-OFF and burst-ON traffic are 0.053, 0.0544 W respectively. The magnitude of max(p(t)) related to burst-OFF periods is smaller than the magnitude related to burst-ON periods because the burst-OFF periods are no-load periods of the system where empty slots are transmitted in channels 2 to 8. However, there is an output power transient in channel 1 due to the long transient recovery time, the magnitude of this output power transient is not as in burst-ON periods, which are the full-load periods of the system. The min(p(t)) of channel 1 at burst-OFF and burst-ON traffic are the same, 0.0384 W. As mentioned in Section 5.4.2.2, the system utility factor is less than 50%, since the number of packets transmitted is very small compared with number of empty slots, thus, the no-load area of PDFs has a large deviation from the mean while the full-load area of PDFs has a small deviation from the mean. This discussion applies to all channels in the link.

We can derive a relationship between the packet peak power and repetition period of each channel in the network link. Assume the input peak power of the packet is *pin*, the average of *pin* ($\overline{pin}$) for a given packet duration T_p with the repetition rate of frequency $F_r \cong 1/T_r$ can be found [$\cong (T_p/T_r)pin$] as can the standard deviation and power swings. At low repetition rates the sag across the output packet is larger because the excited ions have sufficient time to restore their energy after each packet [107]. The mean of the output power transients of channel 2 and channel 8 are 37.20 and 28.40 mW respectively, and the standard deviation of channel 2 and channel 8 are 1.00 and 0.67 mW respectively, the decrease in mean and standard deviation is because the gain of channel 8 is less than that of channel 2, because the gain of EDFA is wavelength dependent.

The power swing (i.e. max(p(t))- min(p(t))) of the output power transients as calculated from the PDF of channel 2 is 15 mW while the power swing of channel 8 is 9.5 mW, this is because the EDFA gain is wavelength dependent and the gain of channel 8 is less than

the gain of channel 2, the repetition rate of channel 2 is 6 packets/s while repetition rate of channel 8 is 2 packets/s.

If the repetition rate is varied for each individual channel, we will see that the lower the repetition rate of the channel the higher is the power swing. We conclude from our simulation results that the gain dynamics can give large power swings across the packets if EDFA experiences long burst-OFF periods. This gives the excited ions enough time to restore their energy [107].

5.4.3 Scenario no. 3

We present in this section the results of numerical simulations performed for the 3 channel systems with cascaded EDFA links which are fed by Pareto distribution traffic described by the model in Section 5.3.1 and shown in Figure 5.10. The main idea behind this numerical simulation is to analyse the effect of the power transients obtained from rapid variations of the input traffic on the output power. The PDFs of power transient with associated Gaussian fits from two different simulation run-times, 250 and 600 ms, are compared. It is shown from the curves of standard deviation and mean of PDF versus time in the Figures 5.11 (a) and (b) respectively, that as the numerical-simulation run-time increases the PDFs of power transient become more stable. The discussion of results is in two parts. In the first part of this section, the power transients of cascaded EDFAs caused by ATM-IP traffic sources are explained. The statistical analysis for the output power transients of each channel in the cascaded EDFAs is performed in the second part. The statistical analysis is performed by plotting PDF of output power transients and their Gaussian fits.

5.4.3.1 Simulation parameters

In our simulation, we use the same simulation parameters mentioned in scenario number 2 except the number of signal channels are reduced to 3 due to the long simulation run-time. The output power transients are obtained from numerical simulation performed on the chain of EDFAs for transmission duration or run-time of 600 ms. The input traffic fed to this network link is shown in Figure 5.10. As mentioned earlier, the input traffic bit rate is 2.5 Gb/s. Thus, the bit time of the ATM cell has the duration of 169.6 ns $\approx$ 170 ns. We use 17 points per ATM-cell to implement the non-self-saturated model described in Chapter 3. The

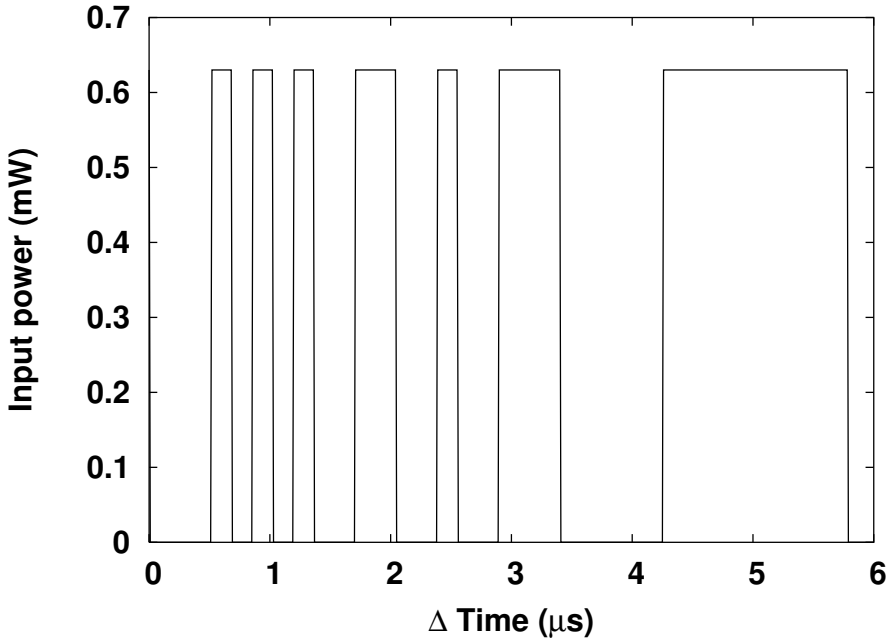

Figure 5.10: Sample of the ATM-IP traffic source of truncated Pareto distribution with variation parameter k = 1.2 for burst-ON and burst-OFF periods.

simulation resolution was 170 ns/17 points = 10 ns. Thus, this 0.01 μs time resolution is fine enough to capture power transient much less than 0.1 dB as shown in 1 dB increase-time or decrease-time of output power transients in Figure 3.12.

5.4.3.2 Numerical analysis of the power transients

There are many parameters related to the PDF of the output power transients. These parameters require clear definition, thus a sample-diagram is presented for this purpose. The sample-diagram of the output power transients is shown in Figure 5.12. In this figure the steady-state power is at the middle of the bell-shaped curve and the mean of the output power transient denoted by $\overline{S}$. The values surrounding $\overline{S}$ represent the slowly varying ATM-IP traffic. As the durations of the burst-ON and burst-OFF periods increase the curve broadens. For this bell shape curve, two limits or conditions are available. The first limit is presented by the left-side of the curve and this is the full-load condition. The full-load condition appears when all channels in the link were transmitting the ATM cells or packets for a long period of time or in burst-ON periods. The second limit is presented by the right-side of the curve, and this is the no-load condition. The no-load condition appears when all channels in the link have empty cells or in burst-OFF periods. The latter condition gives time to the EDFA to

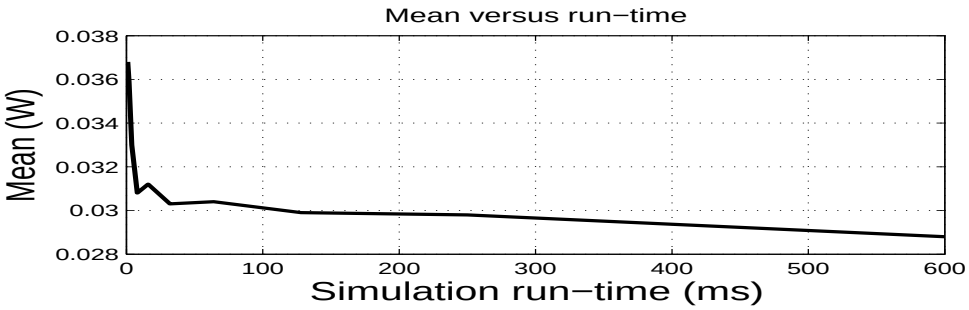

(*a*)

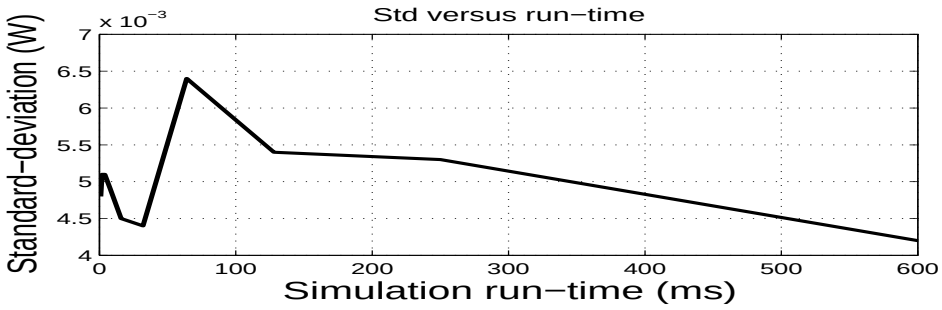

(*b*)

Figure 5.11: (a) Mean of the output power transients of channel 1 at the output of the first EDFA versus the simulation run-time, (b) standard deviation of the output power transients of channel 1 at the output of the first EDFA versus the simulation run-time.

increase the output power to high levels. In other words, the excited ions gain enough energy to amplify the next input signal. In terms of channels, the ATM cells or packets which were followed by burst-OFF periods were exposed to extreme decay or sag. The amount of broadening in no-load or full-load depends on the variability of burst-ON and burst-OFF periods of the burst mode traffic and on the speed of transients [113].

As illustrated in the PDF sample-diagram shown in Figure 5.12, the full-load power limit is around 0.02 W and the no-load power limit is around 0.06 W, and the $\overline{S}$ output power is oscillating around 0.04 W which depends on the channel wavelength because EDFA gain is wavelength dependent. In Figure 5.13, the mean of PDFs of the output power and their related no-load and full-load powers are shown. The full-load power limit results from the output power transients due to the long periods of burst-ON in both channel 2 and 3. The output power transient decreases from 0.04 W to 0.02 W as shown in Figure 5.14. In Figure 5.14 (a), the output power transient was 0.02 W for periods of time that follow the burst-ON periods in channel 2 while the bursty traffic in channel 3 varies between long

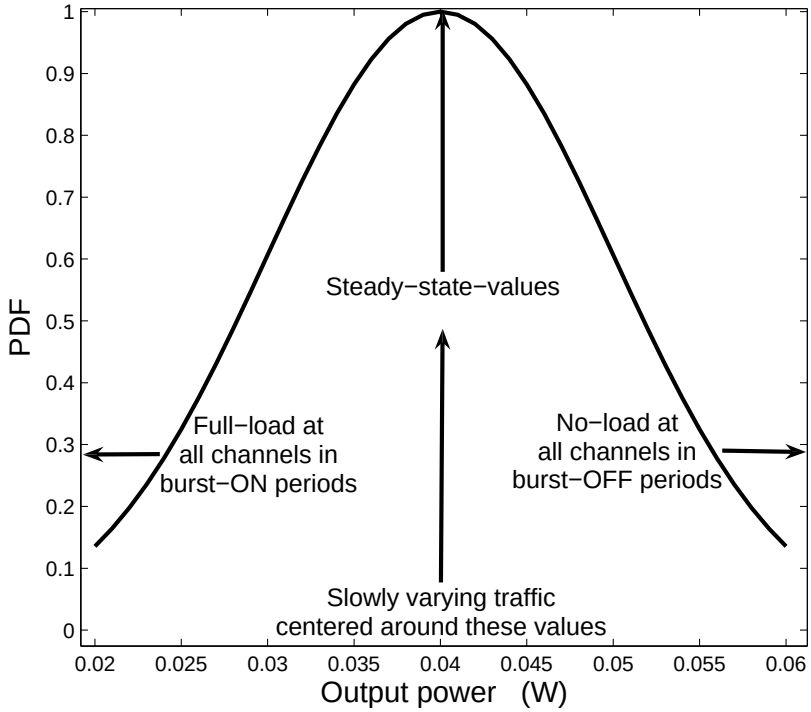

Figure 5.12: Sample diagram of the PDF plot with related parameters.

periods of burst-ON and short periods of burst-OFF. Thus, this resulted in a power transient between 0.026 W and 0.014 W in channel 1 as shown in Figure 5.16 (b) (at left side or full-load area of PDF) and in channel 2 as shown in Figure 5.16 (c)(at left side or full-load area of PDF), the behaviour of channel 3 is similar to channel 2.

In Figure 5.14, the simulation period is when the burst is ON in channel 2 and OFF in channel 3, then the power increased to a certain value because the burst-OFF periods in channel 3 gave time for the excited ions to gain energy, which is shown as an increase in power of input signal, this amplification happens during the preceding 10.87 ms. Then the power increased to 0.02 W in steps as a result of a train of packets in channel 3. The simulation period between 10.834 ms (1.0834×10^7 ns) and 10.864 ms (30 μs) in Figure 5.14 explains the peak power of 0.02 W with probability above 10^{-1} in the full-load area of all PDFs as shown in Figures 5.13 (a), (b), (c), and (d). This probability variation above and below 10^{-1} at the full-load limit around the values of 0.02 W increased and became more obvious in cascaded EDFAs as shown in Figure 5.16 (a), (b), and (c) (at left side or full-load area of PDF). The transient period for sag from 0.022 W to 0.020 W is from 10.864 ms

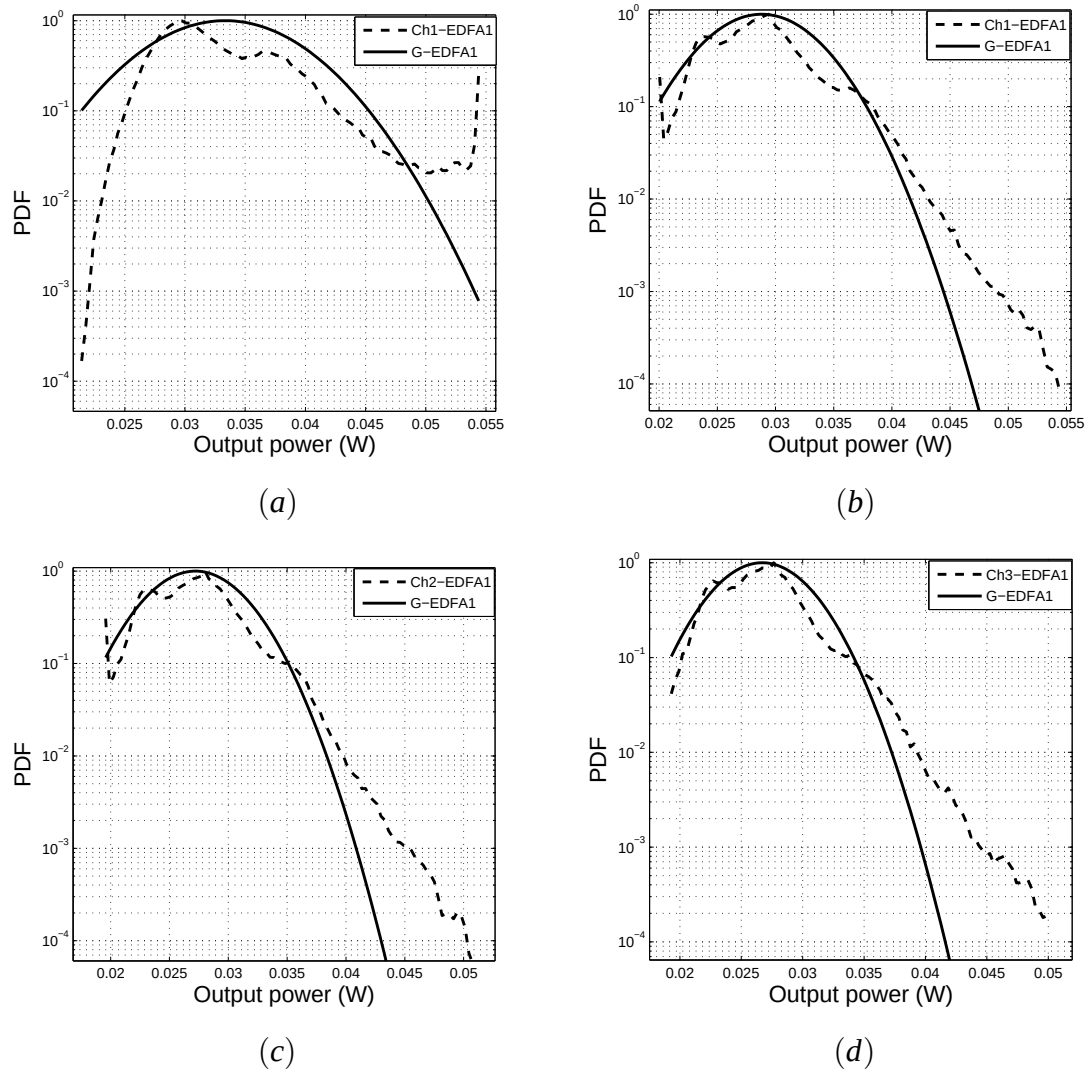

Figure 5.13: PDFs of the output power transients (dashed line) and associated Gaussian fits (full line) of channel 1 at the output of the first EDFA while channel 2 and 3 at (a) burst-OFF periods, (b) burst-ON periods. PDFs of the output power transients and related Gaussian fits at the output of the first EDFA for (c) channel 2, (d) channel 3, while their traffic is in the burst-ON periods.

(1.0864×10^7 ns) to 10.838 ms (26 μs), then to return to the power 0.022 W required a period from 10.872 ms to 10.864 ms (8 μs).

Regarding the no-load area of the power transient PDFs, the ATM-IP traffic is in burst-OFF for this area. The opposite phenomena was observed compared to the full-load condition. A long burst-OFF period transmitted in channel 2 and channel 3, caused an increase in the output power of channel 1 to 0.055 W at the output of the first EDFA and to 0.065 W at the output of the cascaded EDFAs because the excited ions had enough time to gain

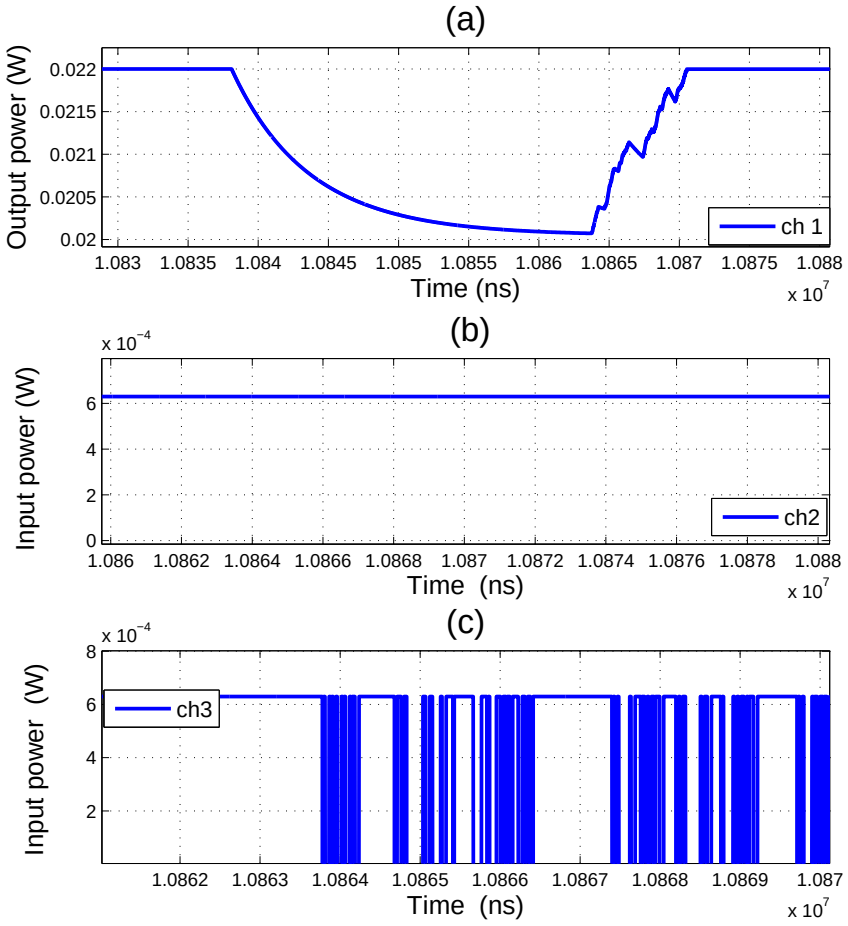

Figure 5.14: The output power represents a sample from power transients at full-load area of the PDFs, (a) channel 1 of CW signal while both (b) channel 2 of packetized traffic at burst-ON periods, and (c) channel 3 of packetized traffic at burst-ON or burst-OFF periods. This plot gives the reason for the heavy-tail of the PDFs that are observed in Figures 5.16 (a), (b) and (c) (at left side or full-load area of PDF), the x-axis scale can also be read in ms (10.834 ms = 1.0834×10^7 ns).

energy from the pump power while the burst is in the OFF periods in the other two channels as shown in Figure 5.15. Figure 5.15 also explains the peak value with probability more than 10^{-1} at no-load area of the PDF of channel 1 for burst-OFF periods and is shown in Figure 5.13. This oscillation around the probability of 10^{-1} at no-load area of the burst-OFF PDFs of channel 1 was more obvious for cascaded EDFAs as shown in Figure 5.16 (a) (at right side or no-load area of PDF).

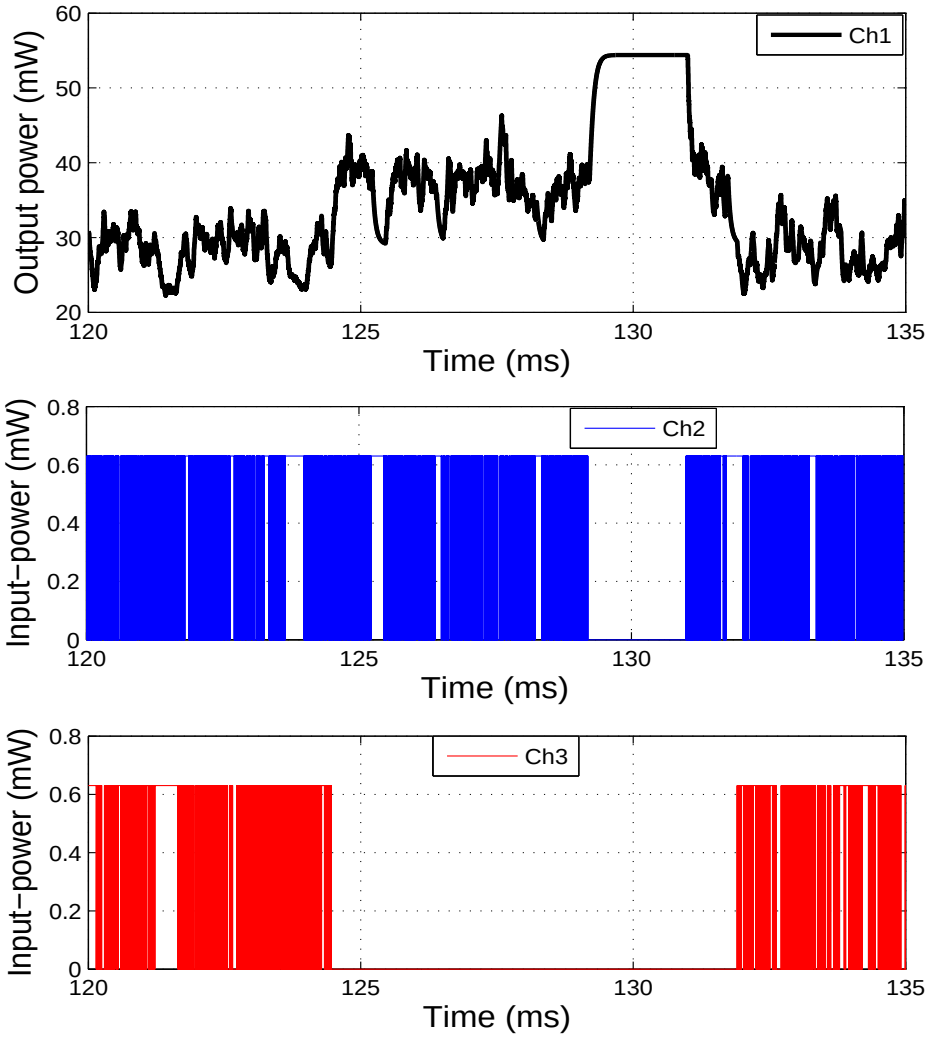

Figure 5.15: The output power transients in channel 1, CW, caused by long burst-OFF periods at channels 2 and 3. This power transient is shown as the high peak at the right-side of the PDF of channel 1 in Figure 5.13 (a). This plot gives the reason for the long-tail of the PDFs observed in Figure 5.16 (a), (b), and (c) (at right side or no-load area of PDF)

.

5.4.3.3 Statistical analysis of the power transients

The analysis of the transients caused by burst-mode traffic are shown through information illustrated in Figure 5.13 (a), (b), (c), and (d) for single EDFA and Figure 5.16 (a), (b), (c), and (d) for 5 cascaded EDFAs in the WDM optical networks link.

The output power transients of the burst-OFF and burst-ON periods are used for PDF calculation. The PDFs are calculated on 100 bins, each bin of 0.4 mW width. The power

swings in the PDF were between maximum load and minimum load of the networks link. The steady-state value $\overline{S}$ is the mean value of the PDF. These power swings range between $\overline{S}$ + 20 mW and $\overline{S}$ - 20 mW. The $\overline{S}$ can be obtained by dG/dt = 0 using Bisection methods for solving transcendental or non-linear equations as explained in Chapter 2. In this scenario, the non-self-saturated model is used, so for $\overline{S}$ we use the value used in [74].

We analysed the PDF of the output power transients of each channel in the link as shown in Figures 5.13 and 5.16. For statistical analysis, the power transient PDF and its Gaussian fit are plotted and compared. The PDF mean, standard deviation and power swing for each channel at the output of each amplifier are analysed. Equation (5.7) is used for plotting the normalized Gaussian distribution.

The power-swing is difference between no-load power or max(p(t)) and full-load power or min(p(t)) (i.e. max(p(t)) - min(p(t))). The output power swings are calculated with probability of 10^{-1}. This is because there was not enough data to calculate for higher probability.

It was observed from the results, that there was an increase in the output power swing along the EDFA chain. This indicates that for longer EDFA chains, a large output power swing at the end of the chain. These power swings might exceed the receiving threshold of the receiver, thus causing optical non-linearity or an insufficient eye-opening.

Term	Mean250	Mean600	Std250	Std600	P-swings250	P-swings600
ch1-OFF	0.0328	0.0333	0.0054	0.0056	0.0108	0.0112
ch1-ON	0.0286	0.0288	0.0040	0.0042	0.0080	0.0084
ch2-ON	0.0272	0.0272	0.0036	0.0037	0.0072	0.0074
ch3-ON	0.0267	0.027	0.0035	0.0039	0.0070	0.0078

Table 5.1: Mean, standard deviation and power swings of the output power transients for traffic duration of 250 ms and 600 ms at the output of the first EDFA (power swings is measured with probability larger than 10^{-1}).

We started with the statistical analysis of the output power with transients in channel 1, CW, at the output of the first EDFA. Now we examine the output power transients caused by the burst-OFF period of the ATM traffic which is used as traffic source for channels 2 and 3. The PDF for such power transients is shown in Figure 5.13. The transient is not very significant at the first amplifier as discussed in Chapter 3. However, the mean = 33.3 mW, the no-Load limit is 60 mW, and the full-load limit is 20 mW. Thus the range of power swings covers almost 40 mW with a probability more than 10^{-4}, the broadening of the curve

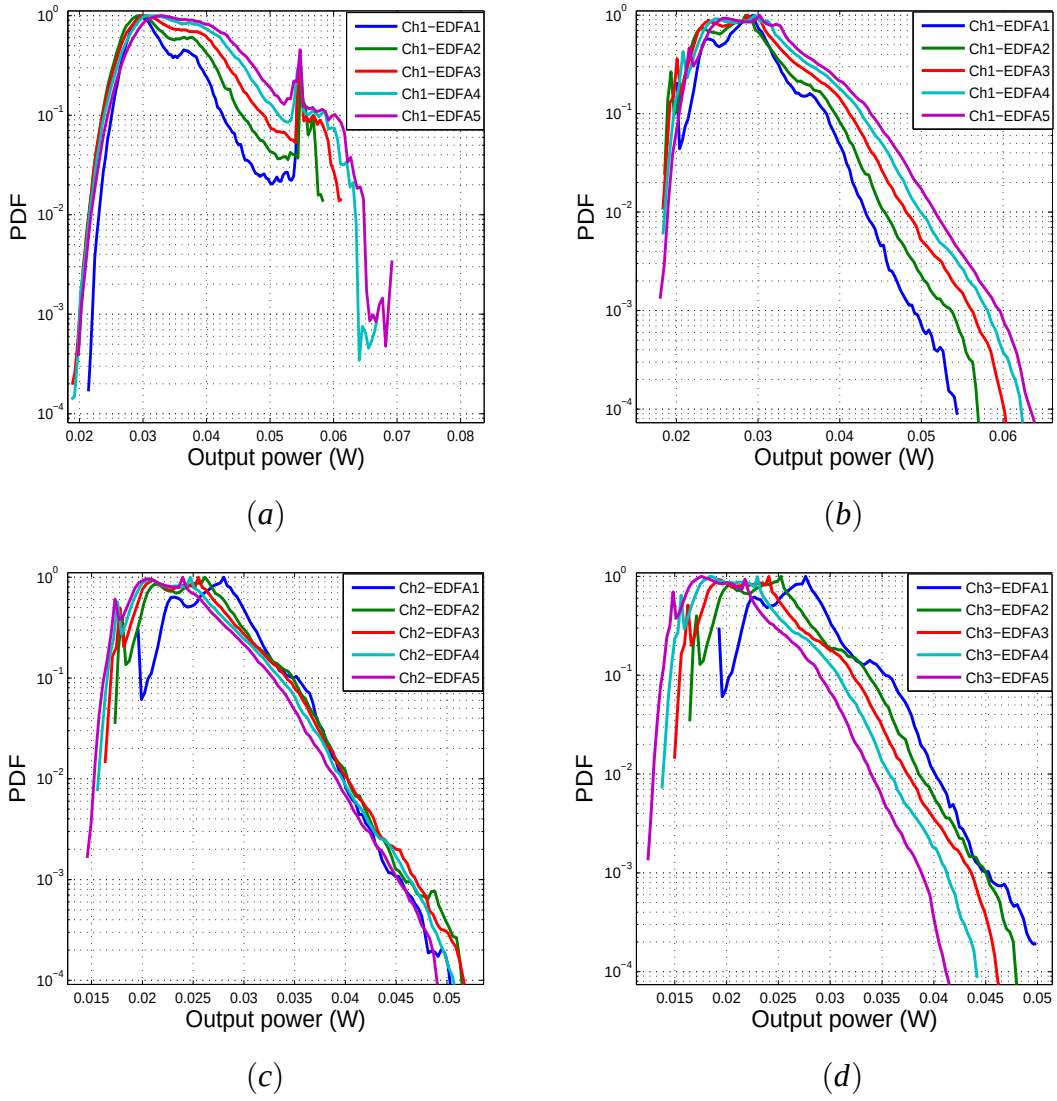

Figure 5.16: PDFs of the output power transients of channel 1 at the output of the first to fifth EDFAs while channel 2 and channel 3 are in (a) burst-OFF periods, (b) burst-ON periods. PDFs of the output power transients at the output of the first to fifth EDFAs for (c) channel 2, (d) channel 3, while their traffic is in burst-ON periods.

happens on both sides of the steady state (mean) due to the infinite variance of both burst-ON and burst-OFF periods. The profile of the PDF of the output power transients does not fit with a related Gaussian distribution for all three channels. In other words, all PDFs have non-Gaussian profiles, they are heavy tail Pareto distributions.

In addition, the output power PDFs have different statistics, such as mean, standard deviation and power swings for each channel and each EDFA in the network link even though all EDFAs in the chain are identical. Figures 5.17 and 5.18 show these parameters for channels

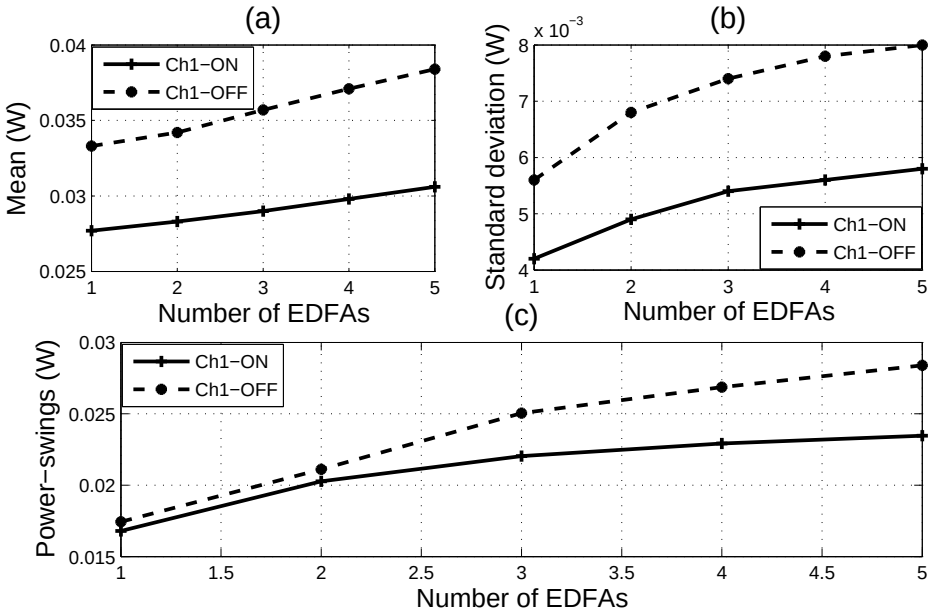

Figure 5.17: Statistics of channel 1 versus number of EDFAs in the chain (a) mean, (b) standard deviation, and (c) power swings.

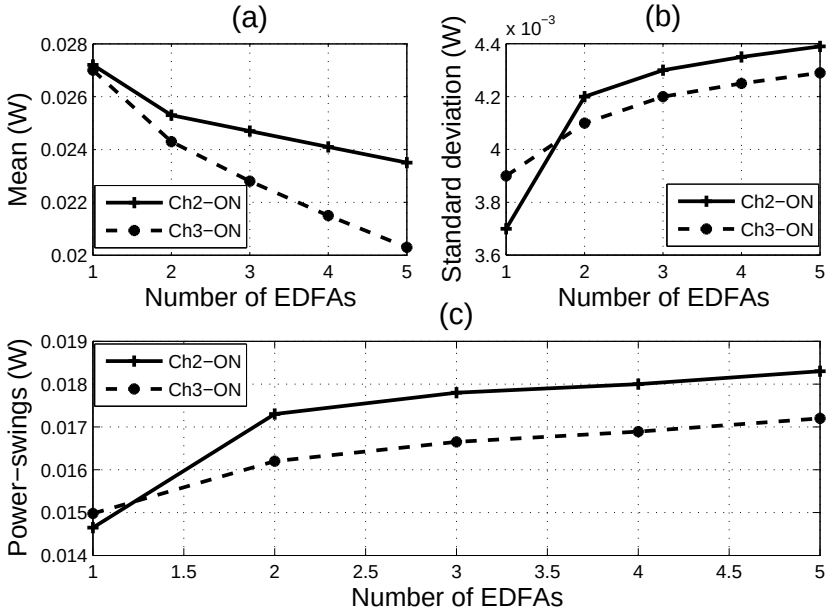

Figure 5.18: Statistics of channel 2 and channel 3 versus number of EDFAs in the chain (a) mean, (b) standard deviation, and (c) power swings.

1, 2, and 3 respectively.

The legends of Figures 5.17 and 5.18 are ch1-OFF, ch1-ON, ch2-ON, and ch3-ON. The label ch1-OFF represents the output power transients of channel 1 while channel 2 and channel 3 are in burst-OFF periods. Label ch1-ON represents the output power transients of

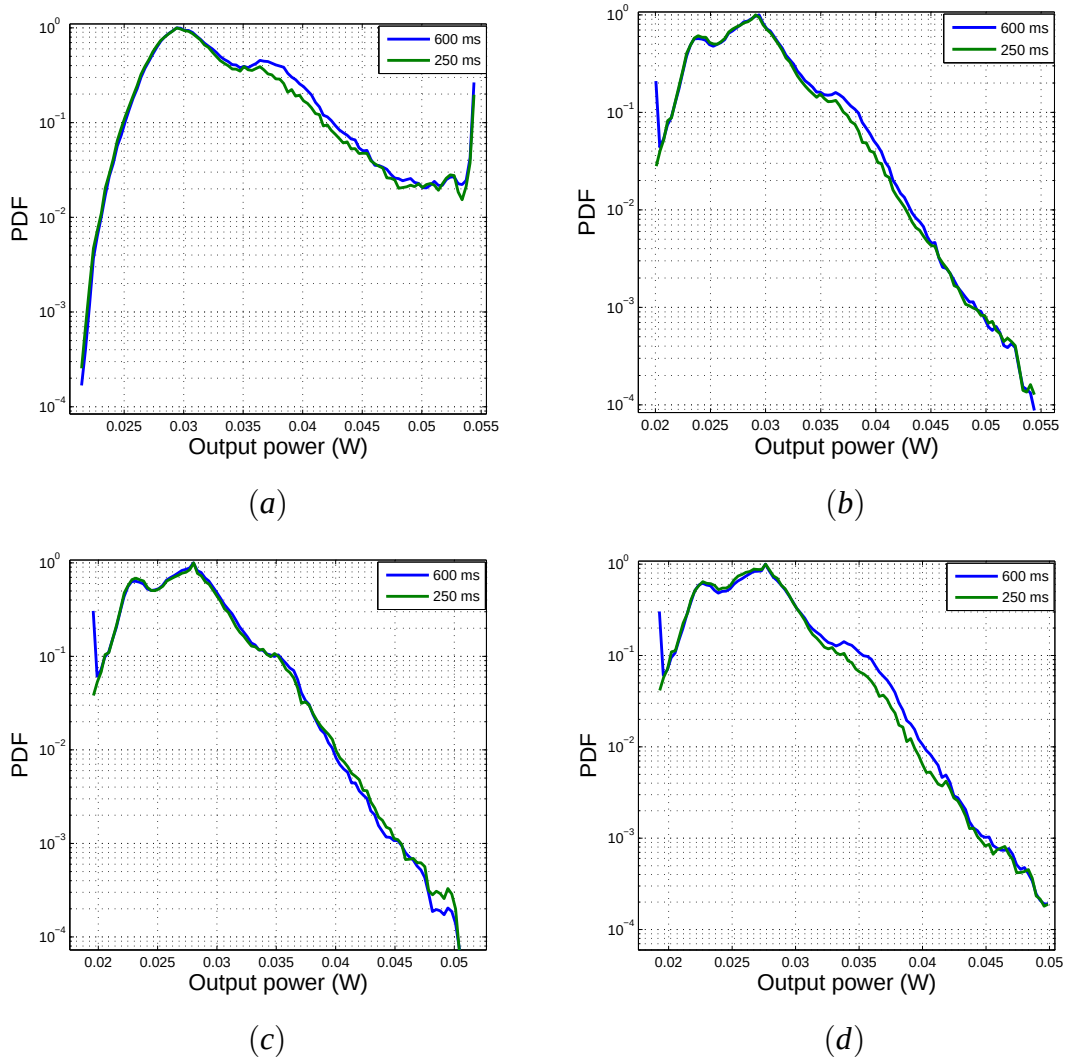

Figure 5.19: Comparison between the PDFs of the output power transients of Channel 1 at the output of the first EDFA for simulation run-time 600 ms and 250 ms while the traffic of channels 2 and 3 is in (a) burst-OFF periods, (b) burst-ON periods. Comparison between the PDFs of the output power transients at the output of the first EDFA of simulation run-time 600 ms and 250 ms for (c) Channel 2, and (d) channel 3, while their traffic is in burst-ON periods.

channel 1 while channel 2 and channel 3 are in burst-ON periods. Where ch2-ON or ch3-ON represents the output power transients of channel 2 or channel 3 while channel 2 or channel 3 are in a burst-ON period respectively.

It is shown that the mean, standard deviation and power swings increase for channel 1 along the cascaded EDFAs as shown in Figure 5.17(a) (b), and (c). However, the mean for channel 2 and 3 decreases as the number of EDFAs increase in the chain, the standard deviation and power swing of the output power transients of channel 2 and channel 3 increase

along the cascaded EDFAs as shown in Figure 5.18. These variations in statistical parameters of channels 2 and 3 are due to the fact that the traffic of ATM-IP is of Pareto distribution and their PDF has a power law specification [149].

The PDFs of channel 2 and channel 3 are plotted for burst-ON periods as shown in Figure 5.13 (c) and (d), and Figure 5.16 (c) and (d). Figure 5.18 (a) shows that the mean decreases when we compare the first amplifier of channel 2 (27.2 mW) with the fifth amplifier of channel 2 (23.5 mW). The same happens with the mean of channel 3 where both channels 2 and 3 use identical ATM-IP traffic sources. This is due to skewness [149] in the PDF due to the power law distribution of the traffic. Figure 5.18 (b) shows the standard deviation for channel 2 and channel 3, we conclude from our results that the standard deviation of power transients increases as the number of amplifiers increases. The same conclusion applied to power swings (difference between max(p(t)) and min(p(t))) which are shown in Figure 5.18 (c). The output power swings increase as the number of amplifiers increase in the cascaded EDFAs. These power transients will affect the network performance through being out of the specification limit of the system receivers.

We conclude from our results that the power transient increases at the output of each saturated amplifier as the number of amplifiers increase. However, the increase in the standard deviation and power swings at the output of the first amplifier is higher than the increase in the standard deviation at the output of the second or the third amplifier for cascaded EDFAs. This is clear from the slope of the curves in Figure 5.18 (b) and (c) as well as the slope of the curves in Figure 5.17 (b) and (c). The behaviour of this increase is because the first EDFA input power for each channel in the link is -2 dBm, while the input power to the second EDFA is calculated from total output power considering span loss in the link of 19 dB using SMF fibre of 88 km with attenuation coefficient of 0.22 dB/Km. In addition, the EDFAs are operating in the saturation regime, the most important statistical consequence is the self-similar nature of the ATM-IP traffic. The PDF of the output power transient at cascaded EDFAs demonstrated in Chapter 4 proved this behaviour for Poissonian traffic.

Finally, we have compared simulation run times, Figure 5.19 shows that the 250 ms and 600 ms simulation run-times do not clearly differentiate between the corresponding PDFs, and they show the same profile. This is also obvious from Table 5.1 for the mean, the standard deviation and the power swings. Thus, a longer run time may not be the solution to

make Pareto distribution traffic with heavy tails fit the Gaussian distribution profile, but can with tails at lower probability. The heaviness of the tail can be quantified using the Kurtosis (which is the normalized fourth central moment as defined in [149]). For short simulation run-times the multi-canonical simulation technique is required [150–152] to provide tails of the PDF at lower probability. Due to the long run-times requirements in our simulation, the first five EDFAs were the only ones simulated in the network link. For example, a link consisting of 3 channels and 5 EDFAs, simulation run times of 80 days are required using the CRAY fast server.

5.5 Effect of Pareto distribution traffic on power transients in gain-shifted C-band EDFA

The design and parameters of gain-shifted C-band EDFA are discussed in Sections 3.2.1 and 3.6. The simulator developed for the non-self-saturated EDFA, in Chapter 3, is used for investigation of the output power transients in this section. In our simulation, a network link of three channels and five cascaded EDFAs is considered, running for a duration of 250 ms. Channel 1 is fed with CW signal, whereas channel 2 and channel 3 are fed by ATM-IP traffic which are Pareto distributed, the traffic sources used for transient investigation of C-band cascaded EDFAs previously discussed in this chapter, are used in this section.

5.5.1 Results and discussion

In this section, the output power transients from the simulations of the gain-shifted C-band and C-band EDFAs are analysed numerically and compared. The statistical analysis of the power transients of the gain-shifted C-band EDFA is performed and compared with that of the C-band EDFA.

5.5.1.1 Numerical analysis of the power transients

We investigate the output power transient of channel 1, CW signal. Figures 5.20 and 5.21 show that the output power transients exhibit similar patterns for gain-shifted C-band and C-band. This is because the network utilization factor and the number of channels in the

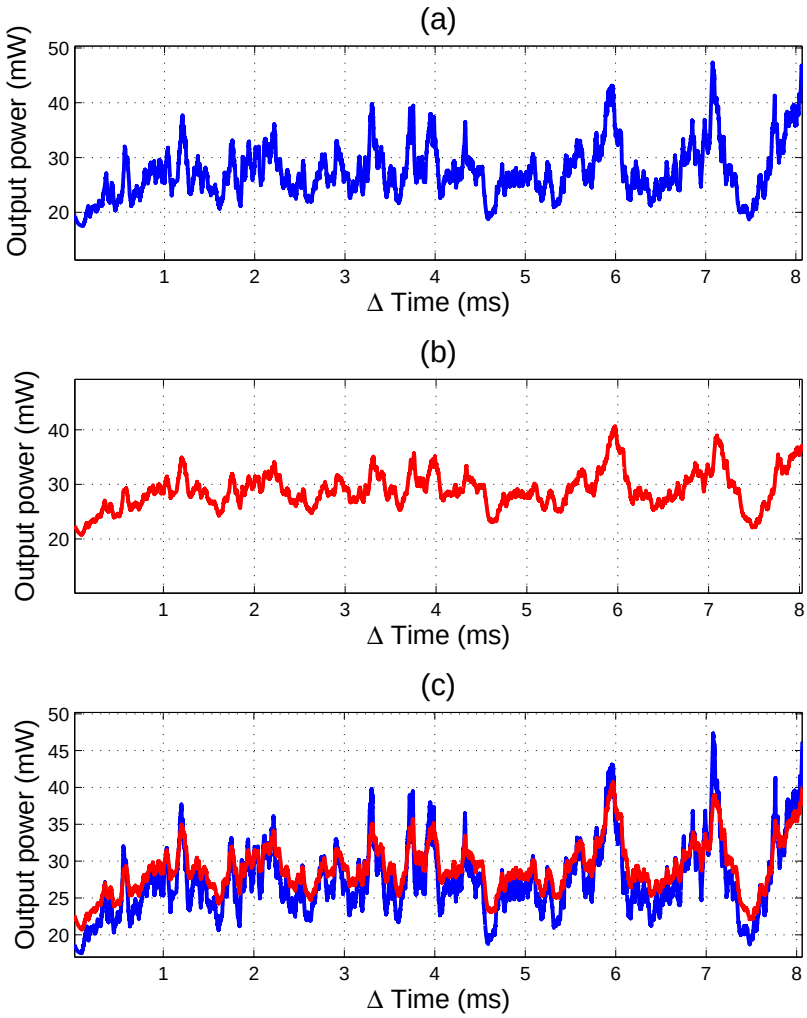

Figure 5.20: The output power transients of channel 1 (a) at the output of the first gain-shifted C-band EDFA, (b) at the output of the first C-band EDFA, and (c) at the output of both types of EdFAs.

gain-shifted C-band EDFA link is the same as in the C-band EDFA link. However, the swing of the power transient for gain-shifted C-band is higher than in the C-band and this is because the amplification or gain in the gain-shifted C-band (initial gain value is 20 dB) is higher than the C-band (initial gain value is 19 dB) for the same input signal power of -2 dBm. As mentioned earlier, the higher the power or gain of the EDFA, the higher the fluctuation will be in the CW signal and the higher the sag will be in ATM-IP packets. This is shown in Figures 5.20 and 5.21, where the gain-shifted C-band output power transients are shown in blue and the C-band in red.

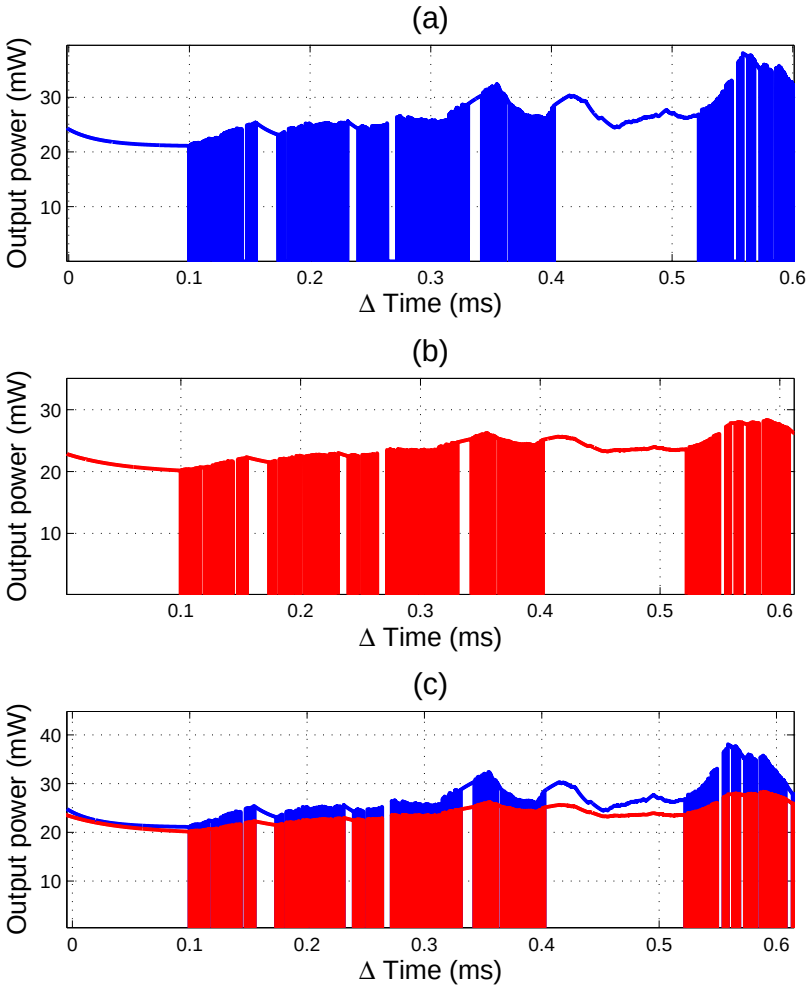

Figure 5.21: The output power transients of channel 2 (a) at the output of the first gain-shifted C-band EDFA, (b) at the output of the C-band EDFA, and (c) at the output of both types of EdFAs.

5.5.1.2 Statistical analysis of the power transients

The PDFs of the output power transients of the cascaded EDFAs for each channel are shown in Figures 5.22 and 5.23. As shown in Figure 5.22 (a), (b), (c) and (d), the PDFs of channel 1 at the output of the first EDFA during burst-OFF period and burst-ON period have different profiles. The mean, the standard deviation and the power swings are found to be different for burst-ON and burst-OFF as illustrated in Figure 5.25 (a), (b) and (c) for channel 1. Therefore, we can generally conclude that the mean of output power PDFs decrease for channel 1 while the mean increases for packetized channels, channel 2 and channel 3, along the cascaded

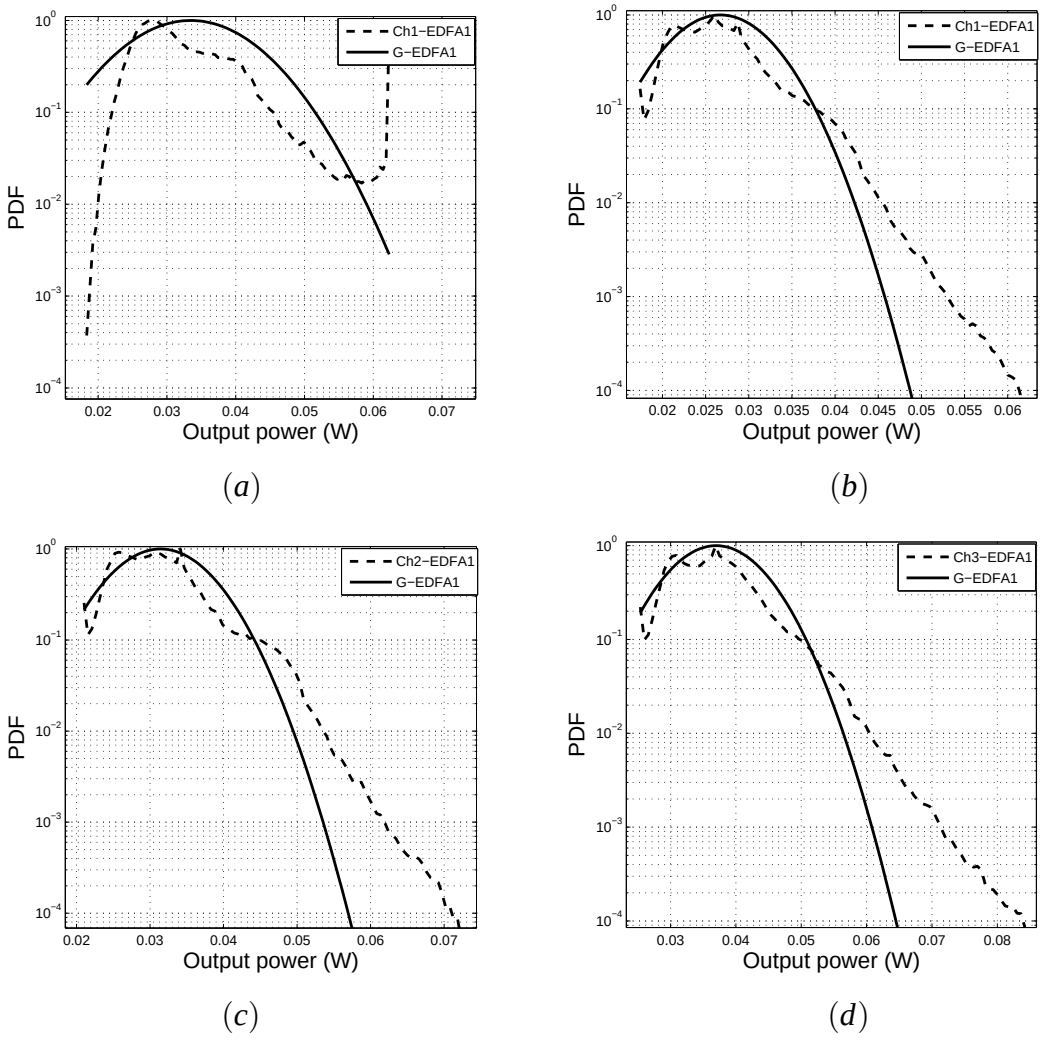

Figure 5.22: PDFs of the output power transients (dashed line) and related Gaussian fits (full line) of channel 1 at the output of the first gain-shifted C-band EDFA during (a) burst-OFF periods, (b) burst-ON periods. PDFs of the output power transients at the output of the first gain-shifted C-band EDFA for (c) channel 2, (d) channel 3 while their traffic is in burst-ON periods.

EDFAs as shown in Figure 5.26 (a). However, the standard deviation and power-swing increase for all channels along the cascaded EDFAs as shown in Figures 5.25 and 5.26. If the standard deviation or power swing increase above a certain limit, it will cause the network performance to deteriorate when the power swings exceed the threshold level of the receiver. These variations in statistics are due to the self-similar nature of ATM-IP traffic.

The legends of Figures 5.25 and 5.26 are ch1-OFF, ch1-ON, ch2-ON, and ch3-ON, and these have the same meanings as given in Section 5.4.3.3. As can be seen in Figures 5.23 (a) and 5.24 (a) channel 1 during burst-OFF period has a high tail to the right side of the PDFs.

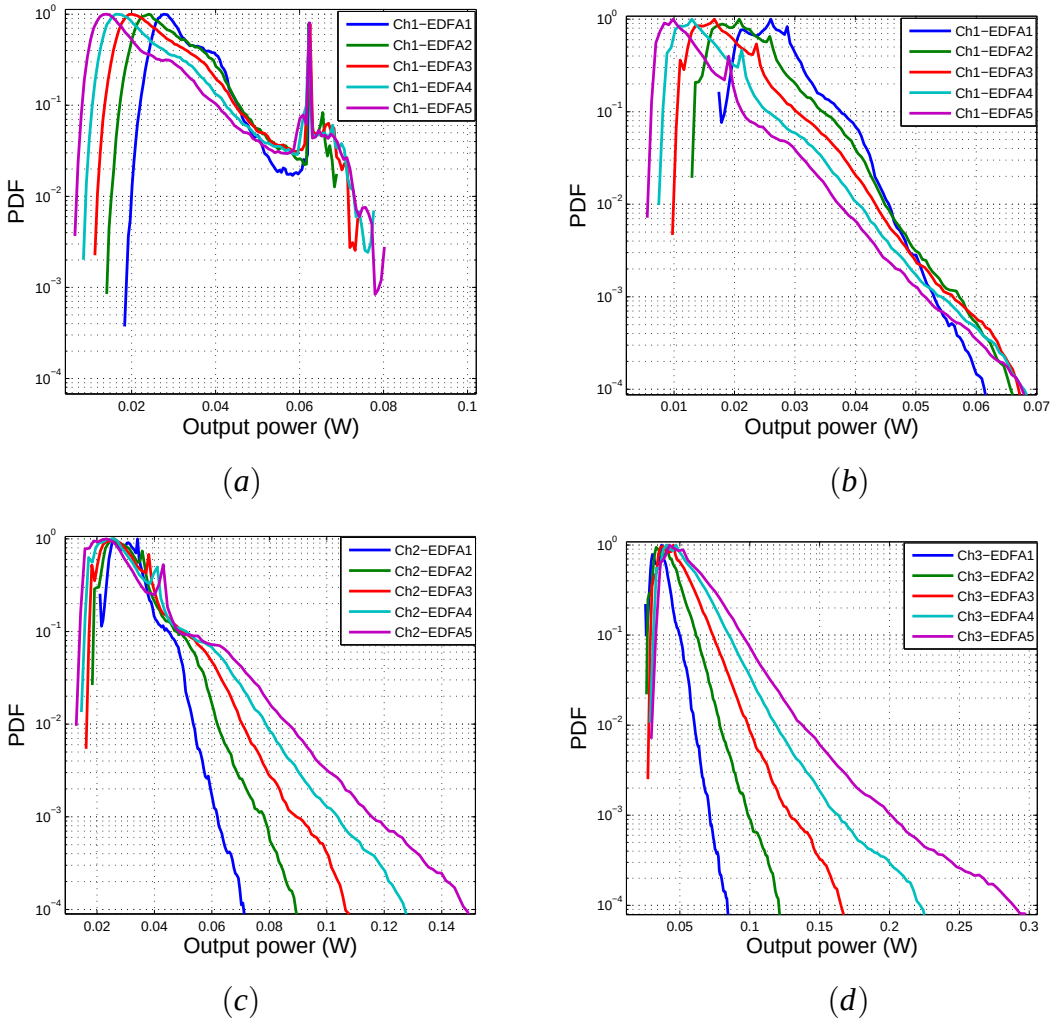

Figure 5.23: PDFs of the output power transients of channel 1 at the output of the first to fifth gain-shifted C-band EDFAs during (a) burst-OFF periods, (b) burst-ON periods. PDFs of the output power transients at the output of the first to fifth gain-shifted C-band EDFAs for (c) Channel 2, (d) Channel 3 while the traffic is in the burst-ON periods.

This is due to the long burst-OFF periods in the input power of channel 2 and channel 3. In other words, the input to the EDFA drops by 60%. This allows the EDFA to achieve a gain much higher than the average. This is the same with the PDF of the power transient of the C-band EDFA since the same traffic sources are used for both type of EDFAs.

Regarding packetized input channels, in Figure 5.22 (c) and (d), the PDFs of the output power transients for channel 2 and channel 3 have little difference in the mean, standard deviation and power swings. This is due to the difference in the wavelengths used in these channels as it is known that the gain of the EDFA is wavelength dependent. This is shown

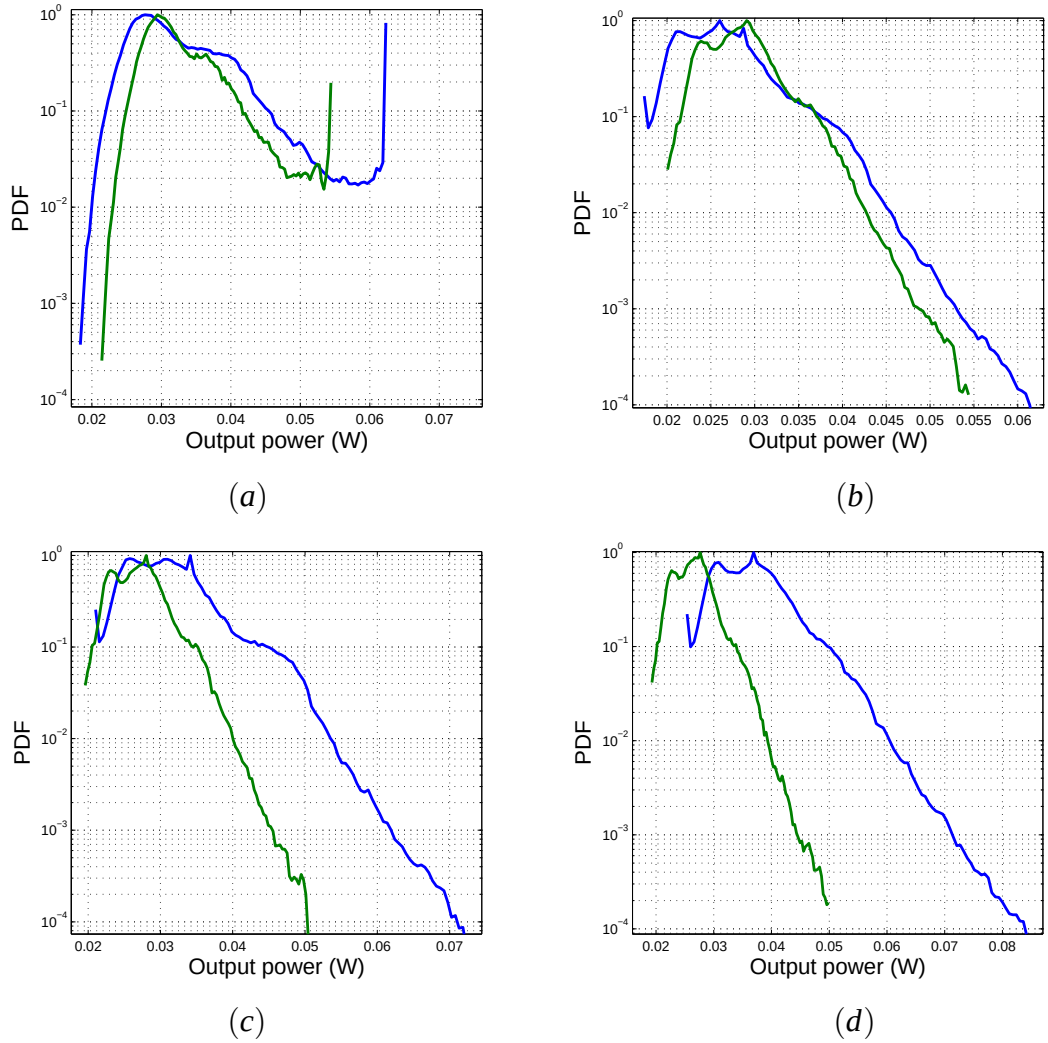

Figure 5.24: PDFs of the output power transients of channel 1 at the output of the first EDFA for gain-shifted C-band (blue) and C-band (green) EDFAs while channel 2 and 3 are at (a) burst-OFF periods, (b) burst-ON periods. PDFs of the output power transients at the output of the first EDFA for the gain-shifted C-band (blue) and C-band (green) EDFAs in (c) channel 2, (d) channel 3 while their traffic is in the burst-ON periods.

in Figure 5.26. The general observation for channel 2 and channel 3 with input source of ATM-IP packets is that the mean output power transient increases as well as the standard deviation and the power swing increases along the cascaded EDFAs. However, the increase in the standard deviation and power swings along the cascaded network link at the output of the first EDFA is higher than the standard deviation and the power swing at the output of the second and third EDFAs because the system operates in saturation. The input to each channel at the first EDFA is -2 dBm while the input to each channel at the input of the second

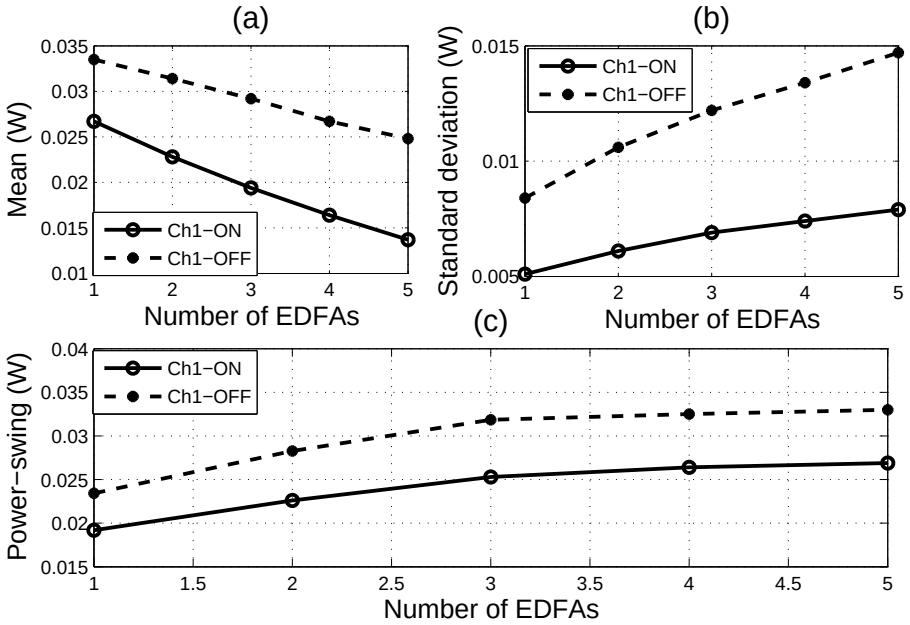

Figure 5.25: Mean, standard deviation and power swing of the output power transients of channel 1 (CW) at the output of the first to fifth gain-shifted C-band EDFAs in the chain.

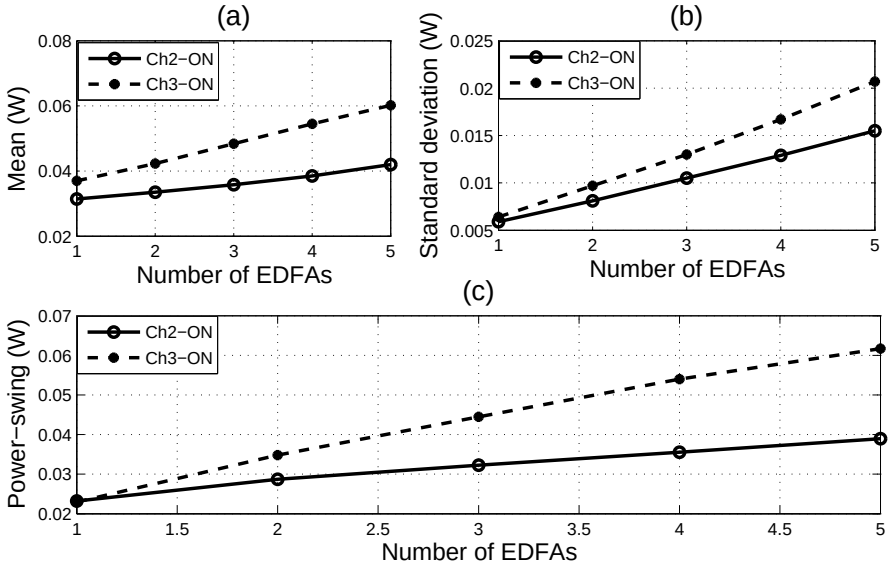

Figure 5.26: Mean, standard deviation and power swings of the output power transients of channel 2 and 3 in gain-shifted C-band at the output of the first to fifth gain-shifted C-band EDFAs in the chain.

and third EDFAs is calculated from total output power considering span loss in the link to be 19.9 dB using SMF fibre of 90 km with attenuation coefficient of 0.22 dB/km.

Figure 5.24 shows the comparison of the output power transients of C-band with gain-shifted C-band using the same traffic source and the same number of channels in the network

link. This figure shows that the PDFs of the output power transients of gain-shifted C-band have the same characteristics as that of C-band. In other words, PDFs of gain-shifted C-band have non-Gaussian distribution. The standard deviation and the power swings increase along the cascaded EDFAs.

When we compared the mean of PDF of channel 3 from the first EDFA to the fifth EDFA, we observed, due to its non-Gussian nature (power law distribution [149]), the PDF which in the C-band varied from 27 to 20.5 mW was skewed in the direction of full-load area of PDF by 6.5 mW, and in gain-shifted C-band varied from 37 to 60 mW was skewed in the direction of no-load area of PDF by 23 mW. Thus the standard deviation and power swings are increased based on these changes in the means of the PDF. However, the mean, standard deviation and power swings are higher in the gain-shifted C-band than in C-band EDFAs. This draw-back is due to the higher gain provided by the gain-shifted C-band EDFA over the C-band EDFA in steady state conditions as shown in Chapter 3. In other words, the output power transients in the gain-shifted C-band EDFAs are different from C-band EDFAs, however both variations in range will affect the system performance if it is beyond the threshold of receiver sensitivity,

5.6 Summary

As mentioned, Internet and LAN traffic follow a Pareto distribution and is self-similar in nature. Thus modelling problems in data communication networks include long-tailed distributions, but such distributions do not have finite moments (i.e. they do not have a finite mean and/or a finite variance) at all orders and this limits their use in data networks. Therefore, we modelled the traffic sources for ATM-IP traffic with a truncated Pareto distribution which possesses finite moments of all orders and therefore could be a suitable model for video and data traffic. We used the truncated Pareto distribution model, which provided self-similar traffic distribution to simulate the ATM-IP packet traffic with degree of variability of 1.2 at bit rate of 2.5 Gb/s. The degree variability of 1.2 (or shape parameter which determines the concentration of data toward the mode) gave the best self-similar traffic pattern.

An extensive number of simulations of the model have been used for investigating the effect of the ATM-IP packet traffic on the output power transients (where output power in-

cludes the power transients) at the single and cascaded C-band and gain-shifted C-band EDFAs. The simulation was divided into three case studies. In the first case study, two signal channels are used in the link, one channel was fed with a CW signal and the other channel fed with packetized traffic of bit rate of 4.24 Mb/s. In this scenario, the output power transients start with arrival of a packet in channel 2. Then the output powers of pump channel, channel 1 and channel 2 decrease. This phenomenon is caused by the fast depletion of excited ions. At a simulated time of 40 ms a packet arrives in channel 2 with input peak power 0.63 mW and duration of 100 μs, the output power of channel 1 drops from 53.9 mW to 32.10 mW during the packet interval (100 μs), so the power transients in channel 1 is 21.8 mW. After channel 2 goes inactive (burst-OFF) the output power in channel 1 increases to 53.9 mW in a time of 480 μs - this transient recovery time will depend on pump power. Total transient and recovery time is 580 μs. This scenario shows the power transients phenomena in packetized traffic with low bit rate (4.24 Mb/s).

The second simulation case study includes 8 signal channels, one fed with CW signal and the other seven channels fed with periodically varying burst-OFF periods. If the repetition rate is varied for each individual channel, we see that the lower the repetition rate of the channel the higher is the power swing. We conclude from our results that gain dynamics can give large power swings across the packets if the EDFA experiences long burst-OFF periods. This gives the excited ions enough time to restore their energy. The PDFs for these 8 channels do not fit the Gaussian distribution. These PDFs illustrate the long-tail distributions for all channels in the link. These long-tail PDFs are due to the repetition rate which is varied for each individual channel. This explains the power transients phenomena in packetized traffic with long burst-OFF periods which provides skewed long-tail PDFs of non-Gaussian distribution.

In the third case study, three signal channels are used, one channel fed with CW signal and the other two channels fed with truncated Pareto traffic, this is applied to both the C-band and gain-shifted C-band. Because of the extremely lengthy simulation run times involved in Pareto distributions, for instance for a link consisting of 3 channels and 5 EDFAs a simulation run time of 80 days was required using the CRAY fast server. Therefore, we limit the time of the ATM-IP traffic in our simulation to 600 ms. However, we measured the output power transients with a simulation resolution of 0.01 μs leading to accurate statistics of the output

power transients as low as 0.06 dB.

The non-self-saturated model of EDFA is used for investigating power transients in this chapter. The statistical analysis has been performed in terms of the power swings, standard deviations and skewness (the mean of PDFs shifts to the no-load or full-load area) which are achieved from the PDFs of the output power transients at the output of each EDFA in the chain, as discussed in Section 5.4.3.3. It has been observed from the results, for C-band EDFA at the output of the first, second and third EDFA the power swings for channel 2 are 14.8, 17.2 and 17.3 mW respectively, while for gain-shifted C-band EDFA at the output of the first, second and third EDFA the power swings for channel 2 are 23, 30, and 32 mW respectively, this shows that there is an increase in the output power swing along the EDFA chain. It also indicates that for longer EDFA chains, a larger output power swing and a higher skewness will occur at the end of the chain. For instance, SONET specifies that the BER must be 10^{-10} or better. Gigabit Ethernet and fibre channel specifications require a BER of 10^{-12} or better, which requires a receiver sensitivity of -18.6 dBm. This BER is the foundation for determining a receiver's sensitivity. It has been observed from our simulation results, such as when the traffic in the burst-ON mode for channel 2 the mean of the power transient PDF decreases at the output of the second EDFA by 1.5 dBm, and from the third to the fifth EDFA by 0.37 dBm. Thus, at the end of fifth EDFA the mean of PDF is skewed to the left by 1.83 dBm, and at the thirtieth EDFA will be skewed by 5.2 dBm from the mean of the first PDF. This gave an indication of the heavy tail of the PDFs being on the left side since the mean is skewed to the left. The standard deviation for channel 2 increases from 3.6 dBm at EDFA1 to maximum of 6.3 dBm at the third EDFA. The output power swings described above might not be within the receiving threshold of the receiver, causing insufficient eye-opening which at the end deteriorates the optical network performances.

However, in channel 1 (CW), the mean increases and skews to the no-load power area, especially in burst-OFF periods, thus causing optical non-linearity in the system. Because of the high peak power of the signal packets, the nonlinearity in EDFAs, such as SPM, may become a limiting factor. Furthermore, other nonlinear effects like FWM and XPM will also occur, causing interference amongst different WDM channels. Additionally, the amount of dispersion in an EDFA can also cause detrimental pulse broadening effects due to all these separate performance problems. Thus, the length of the communication link is determined

by the receiver sensitivity at the destination.

Therefore, if at the thirtieth EDFA the power transient is out of receiver sensitivity limit, then for instance, the longest link which will operate within the acceptable bit error rate for Gigabit Ethernet (10^{-12}) is 2640 km (we used in our simulation span length of 88 km for C-band EDFA, then the link length is 88x30 km). Thus it is necessary to investigate the magnitude of power transients in the link in order to apply a convenient channel protection scheme as mentioned in Section 1.9.

Chapter 6

Effect of power and OSNR transients on optical receiver in cascades of self-saturated EDFAs for optical networks

6.1 Introduction

In Chapter 3 we discussed the simulation model for non-self-saturated and self-saturated gain dynamics for both single and cascaded EDFAs and provided confirmation of the validity of the model against available literature. In this chapter the self-saturated model is the core for investigating the evolution of OSNR transients in EDFA amplified links. The simplest type of WDM system configuration is a point-to-point optical fibre link and these links are the main units of optical wavelength routed networks. The power and OSNR transients during transient phenomena along amplified optical links are analyzed. It has been shown that as the number of EDFAs increase in the network link, the OSNR is further degraded, thus providing lower QoS due to network performance deterioration.

There are different factors affecting the speed and behaviour of optical power transients in chains of gain-saturated EDFAs. Most of the factors that depend on the dynamics of the cross-gain saturation in individual EDFAs have been mentioned in Section 3.2.2. In general,

the evolution of the gain transients of a single EDFA is specified by a time constant ranging from tens to hundreds of microseconds depending on the total output saturated power of the EDFA. However, it is possible that the interconnected or interdependent gain saturated EDFAs might cause multiplication of the speed of evolution of the optical power and OSNR transients to the sub-microsecond timescale [106]. This phenomenon would affect the gain stabilisation procedure in systems that consist of many EDFAs. In the following, the dynamic EDFA model shown in Chapter 3 is used to investigate the optical power and OSNR transients in a chain of self-saturated EDFAs.

6.2 Investigation of power and OSNR transients in cascades of EDFAs for optical networks

The evolution of the signal power and OSNR transients along EDFA chains is simulated using Equation 3.5 which is described in Chapter 3. This equation numerically simulates each EDFA in the chain. The input power values of the signal channels and the spectrally resolved ASE were represented in the form of signal and ASE matrices. The initial value of the gain was calculated by setting the derivative in Equation (3.5) equal to zero and solving the resulting equation numerically for the input signal and ASE powers in the first row of their corresponding matrices. The calculated gain represented the gain of the network at the steady state (i.e. before any transient occurs). Beginning from this point, successive steps of numerical integration were used to calculate the output power, then the gain per channel was calculated from the output power and generated the forward propagating ASE as a function of time. The signal and ASE values representing the output power of an EDFA were multiplied by fibre loss and used as the input signal for the next EDFA.

The simplest method to analyse a chain of EDFAs used for long haul transmissions systems, is to assume that all EDFAs have the same gain and that the loss between EDFAs exactly compensates the EDFA gain. The output power at the last EDFA of the chain is assumed to be equal to the output power at the first EDFA of the chain. This is a relatively accurate assumption if the ASE generated by EDFA is small compared to the input signal power. Each EDFA produces an equal amount of ASE as the other EDFAs, and ASE propagates to the output of the chain, the same way as the signal does. The total ASE of the link is

the linear addition of the ASE produced by each EDFA. In our simulation, we calculate the OSNR at the output of each EDFA by Equation (6.1).

$$OSNR = \frac{P_k^{out}(t)}{P_{ASE}(t)} \tag{6.1}$$

Where the output signal power is denoted by $P_k^{out}(t)$ and computed from Equation (3.14), the output ASE power is denoted by $P_{ASE}(t)$ and computed from Equation (3.7), then $P_{ASE}(t)$ is divided by two because the forward ASE power is considered for OSNR calculation as explained in Chapter 3.

For large gain the OSNR is independent of the gain, and this is a useful outcome that controls the system performance of in-line EDFAs. This independence is explained by Equations (6.2) and (6.3). The OSNR for a single EDFA is given by Equation (6.2) [1, 6].

$$OSNR = \frac{G\,P_{in}}{2\,h\upsilon\,n_{sp}\,B_o\,(G-1)} \tag{6.2}$$

Where P_{in} is the optical input signal and assumed to be continuous at the input to the EDFA. Thus, provided G is reasonably high, the SNR is determined only by the input power and the inversion parameter n_{sp}. More specifically, the SNR is independent of the gain. All terms in the equations are defined in Chapter 3. The OSNR at the output of the EDFA chain is obtained by replacing n_{sp} by n_{sp} N, where N is the number of EDFAs in the chain. The OSNR at the output of the chain is given by [1, 6]

$$OSNR = \frac{P_{in}}{2\,h\upsilon\,N\,n_{sp}\,B_o\,(G-1)\,L} \tag{6.3}$$

Where the gain G is given in terms of the input signal power P_{in} and the bandwidth B_o of the optical filter assumed to be placed after each EDFA, the span loss is denoted by L, and GL $\cong$ 1. Thus, it is clear that for large G, OSNR $\approx$ constant [1, 6].

The OSNR is the most important system design parameter for optically amplified systems. The OSNR is observed for each signal channel at the output of the last EDFA in the chain. The accumulated ASE at the output of the last EDFA degrades the output optical signal. End-to-end system performance can be estimated from the OSNR and the model of total noise in the receiver. Study and analysis of OSNR transients is important for enhancing the performance of the WDM optical networks.

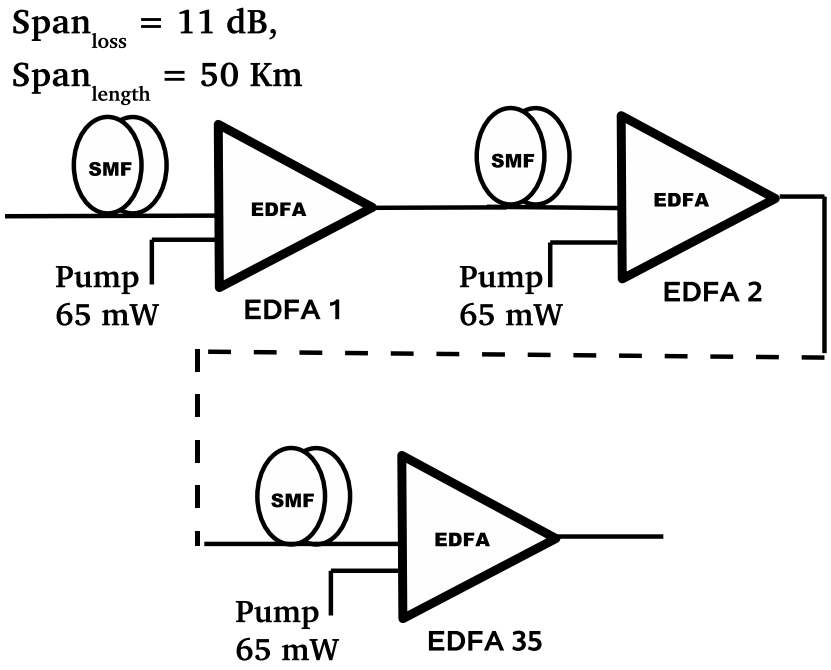

Figure 6.1: Cascaded EDFA simulation model for OSNR investigation

6.2.1 Analysis of OSNR transients in EDFAs chain

We considered an EDFA chain containing 35 identical single stage EDFAs, as shown in Figure 6.1. Simulation parameters used in this section are the same as used for the self-saturated EDFA explained in Chapter 3.

The ASE spectrum begins at wavelength 1490 nm and extends to the wavelength 1570 nm. This spectrum is divided into 200 bins with spacing of 0.4 nm (equivalent to 50 GHz). The forward ASE power is calculated using Equation (3.7) and treated in the same way as each input signal channel was treated in the subsequent EDFAs.

Two case studies were tested: In the first case, 4 channels are dropped and 4 channels survive. In the second case, 4 channels are added to 4 already existing channels. In both cases the dropped and the added channels consisted of high wavelength channels. The dropped or added channels are 8, 7, 6, and 5 and are of wavelengths 1560.4 nm, 1558.8 nm, 1557.2 nm, and 1555.6 nm respectively. The resolution used for the simulation is 2 μs in order to provide the accuracy needed to show the evolution of the overshoot peak power region of the wavelengths, at the output of a long chain of EDFAs the overshoot region of the peak power can vary at a high rate. Most interesting to our investigation is the case of channels added,

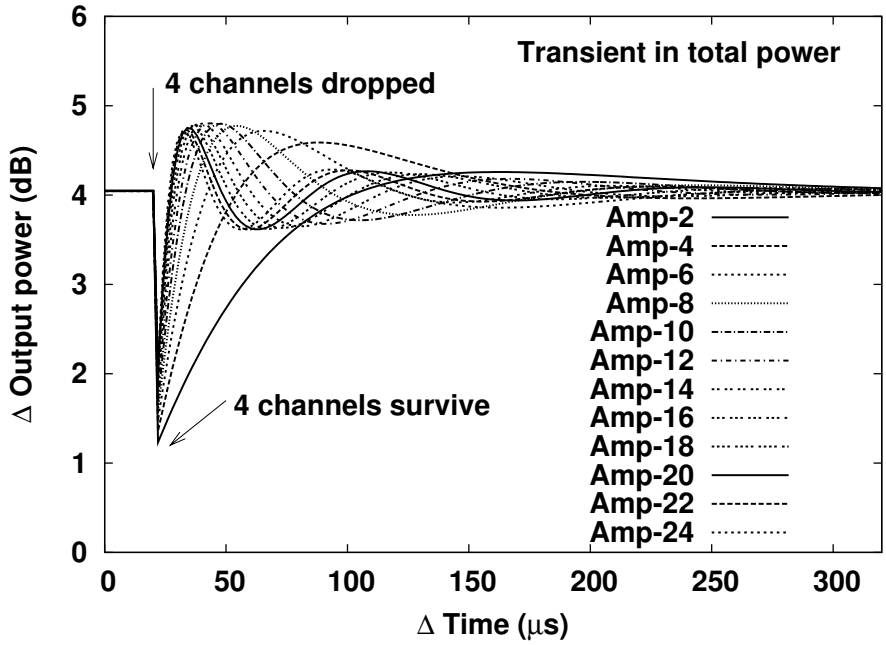

Figure 6.2: The total output power transients when 4 channels are dropped simultaneously and 4 channels survive.

where the OSNR is reduced to a certain level due to output power transients.

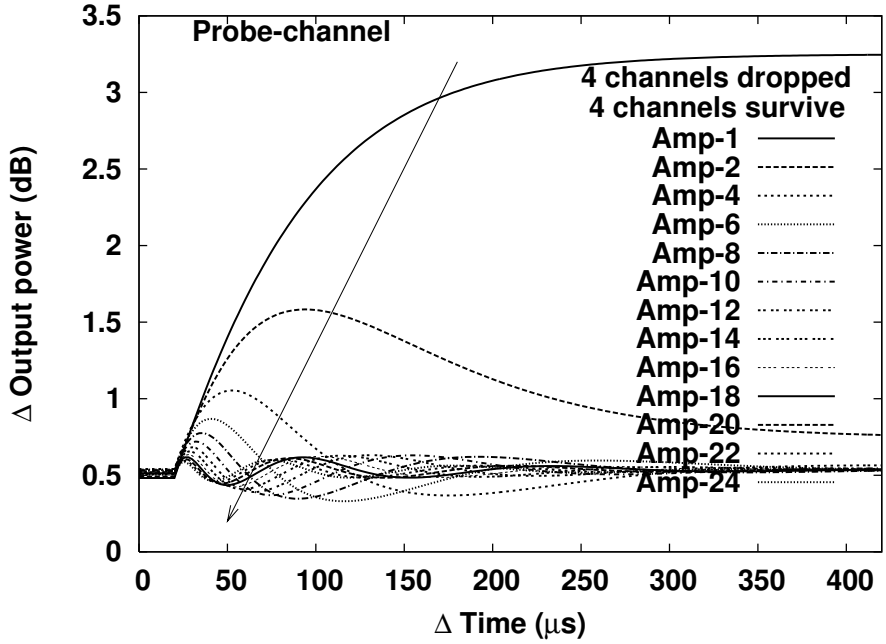

Figure 6.3: The output power transients observed at probe channel (wavelength of 1549.2 nm) when 4 channels are dropped simultaneously and 4 channels survive.

Figure 6.2 shows the evolution of the total output power transients (i.e. the total output power including power transients) of the surviving channels from the output of the second to

the twenty fourth EDFAs in the chain. Figure 6.3 shows the evolution of the power transient in the probe channel when 4 channels are dropped and 4 channels survive. We observed that the angle of the initial gradient of the power transients in all EDFAs, from the first to twenty fourth in the chain, is the same, which is illustrated by the direction and gradient of the arrow in the figure.

Figure 6.4 clearly shows the rate of evolution of the OSNR when 4 channels are dropped at the input of the first EDFAs is the same as for the corresponding power transients as shown in Figure 6.3 at the outputs of the same EDFAs. The time is calculated relative to the instant when the power loss or addition starts at each EDFA. We define the power and OSNR swings in our simulations as the difference between upper limit and lower limit of the output power and OSNR transients, [max(p(t)) - min(p(t))] and [max(OSNR(t)) - min(OSNR(t))] respectively. We observed that in the case when four channels are dropped the swings in the upper limit of the output power and OSNR in the probe channel, denoted by max(p(t)) and max(OSNR(t)) are +3.6 dB and +4.2 dB respectively.

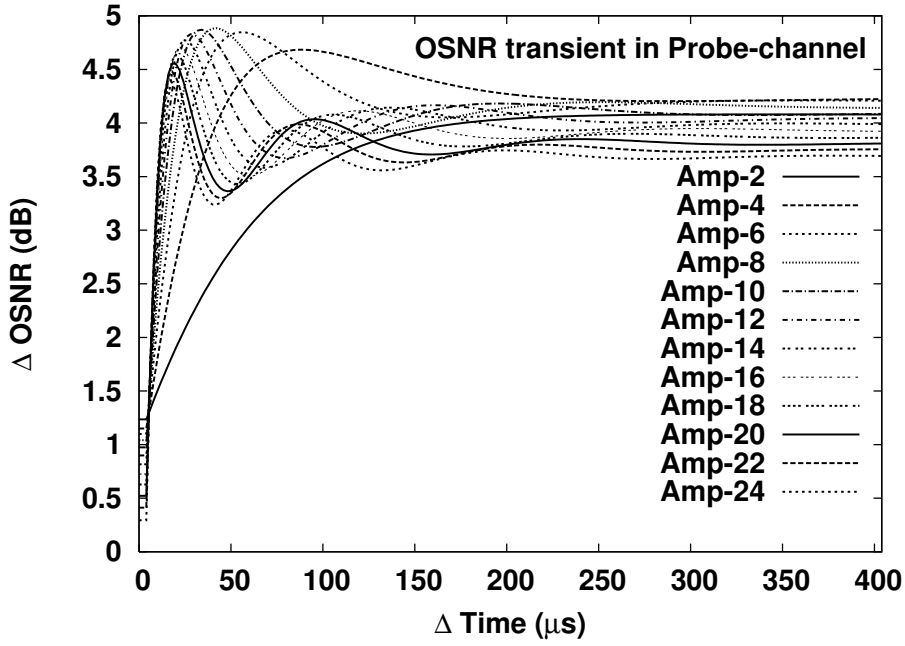

Figure 6.4: The OSNR transients observed at probe channel when 4 channels are dropped simultaneously and 4 channels survive.

In the second case study, we simulate the self-saturated model for the network link when 4 channels are added simultaneously to 4 existing channels in the system. The output power and the OSNR transients are as shown in Figures 6.5 and 6.6 respectively. The lower limit of

the output power and the OSNR swings in the probe channel which are denoted by min(p(t)) and min(OSNR(t)) are -5.0 dB and -5.5 dB respectively.

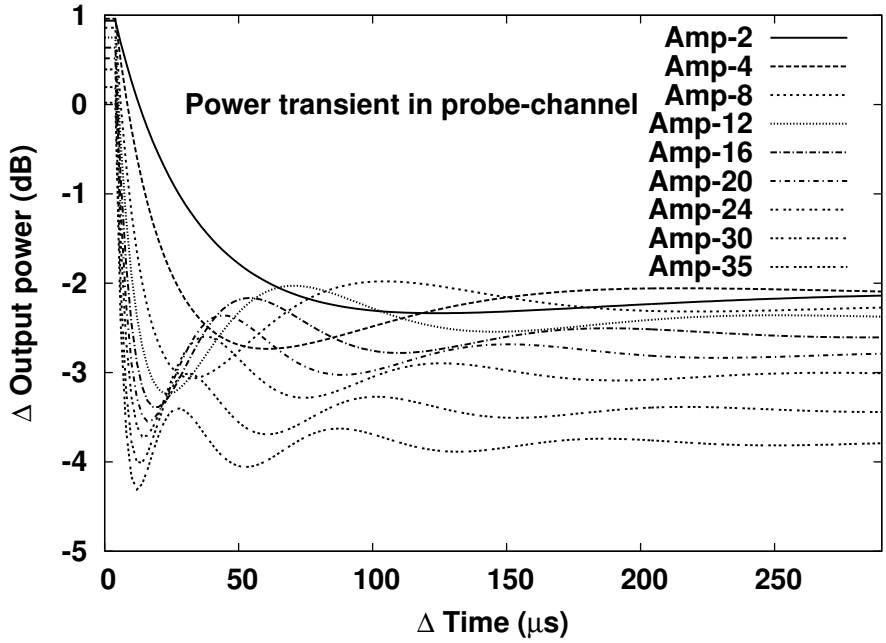

Figure 6.5: The power transients observed at probe channel when 4 channels are added simultaneously to 4 existing channels in the network link.

In Figures 6.3 to 6.5, the power and OSNR transients after the channels were dropped or added were observed in the probe channel of wavelength 1549.2 nm. The other surviving channels follow a similar evolution but with less power and OSNR transients. The wavelength with the least power and OSNR transients was 1554.0 nm, which is the longest surviving channel wavelength. These values are consistent with the differential gain of the EDFA decreasing from 1549.2 nm to 1554.0 nm. In fact, the differential gain of EDFA is proportional to the sum of the absorption and emission constants.

As mentioned earlier, the evolution of the optical power transients can be divided into three regions: the initial or linear region, the oscillatory region and the final steady state region [101,129]. The initial region follows the change in wavelength number and the power of the surviving wavelength increases or decreases gradually and linearly with time.

It can be seen in Figure 6.2 that the rate of change of the optical power increases as the number of amplifiers increases. This is because all EDFAs in the chain experience the same change of the input power since they are identical and have equal gain. The average population inversion changes for each EDFA in the chain. The gain of each EDFA depends on the

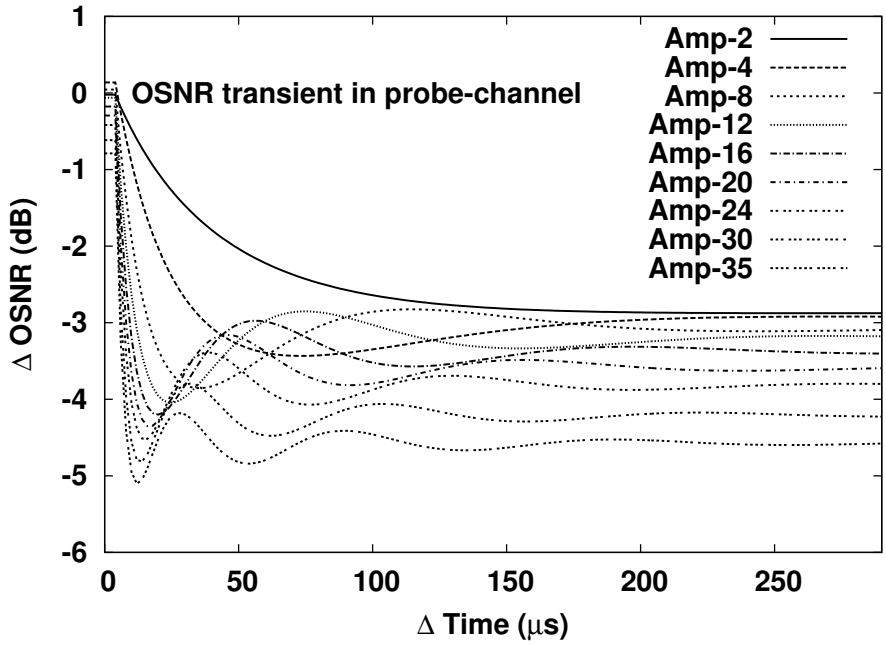

Figure 6.6: The OSNR transients observed at probe channel when 4 channels are added simultaneously to 4 existing channels in the network link.

average population inversion and will increase or decrease by the same amount. Therefore, the power of each surviving wavelength will be multiplied by the same amount of change of the differential gain at each EDFA. Consequently, the power of the surviving channel will change in proportion to this differential gain raised to the power of the number of amplifiers. In logarithmic units this corresponds to a power change that is proportional to the number of EDFAs. The rate of change of the power of the surviving wavelength in an EDFA chain is a multiple of the rate of which the gain of each EDFA changes.

Nevertheless, the OSNR transients, which are shown in Figures 6.4 and 6.6, are the result of the rate of change of both the input optical power and the ASE power. The OSNR transients increase or decrease at a rate which is slower than that of the optical power transients. This is clearly demonstrated in Figure 6.7 where the 1 dB decrease-time is plotted as a function of the number of EDFAs in the chain both for the optical output power and the OSNR transients.

Normally, when the EDFAs in the chain do not have equal gain, the slope of the 1 dB increase-time which is the initial region of the transient will not be a constant. For example, in a non-equal gain EDFA chain, the loss of channels will produce different input power for each of the chain EDFAs and as a result the initial gain change of each EDFA will be

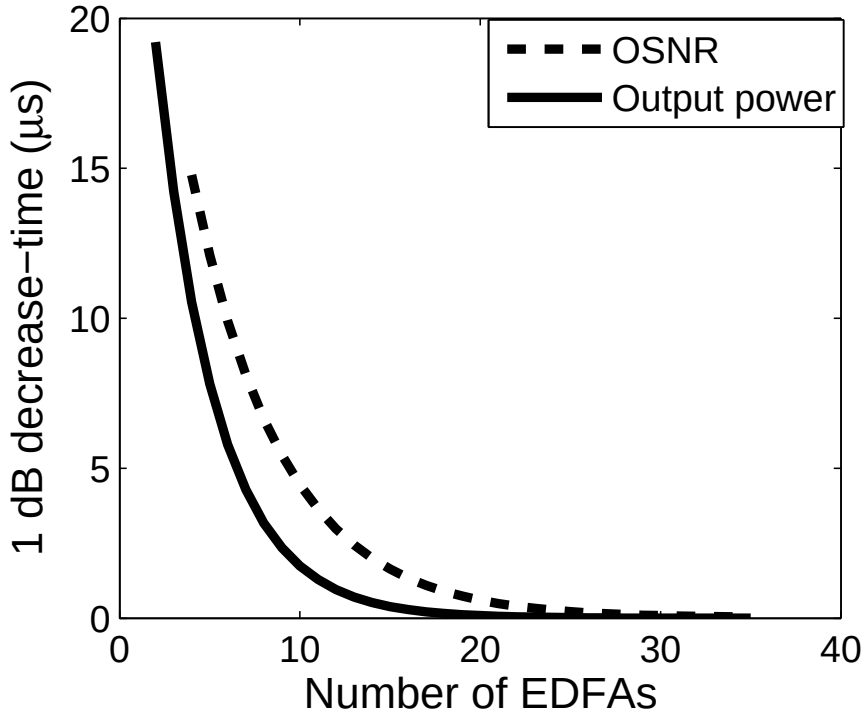

Figure 6.7: 1dB increase time for power and OSNR transients versus 35 cascade EDFAs in the chain.

different. Nevertheless, the rate of change of the dynamic power transients increases at each EDFA, even though by a non-equal amount.

In, for example, Figures 6.2 and 6.4, at the end of the initial region, the power transients of the surviving channels at the previous EDFAs increase enough to start decreasing the gain of the subsequent EDFAs, and this stops the increase in the overshoot of the optical output power transients. Figure 6.2 clearly shows the overshoot at the end of the initial region and the beginning of the second region converge to a single maximum value as the number of EDFAs increases. The third region is the oscillatory region, and the damped oscillations represent the balance between the signal photons and the amplification throughout the chain as the power of the surviving channels provides a new steady state. In this region the oscillatory aspects dominated the evolution of the OSNR transients due to the oscillation behaviour of the ASE power and were identical to the optical signal power.

Figure 6.2 shows that the power of the surviving channels at the new steady state after the transient stage, converge to almost the same level from the first EDFA to the last EDFA in the chain. The power transients of the remaining surviving channels follow the same behaviour.

The power difference between the channels of different wavelengths with maximum and the minimum power transient (1549.2 nm and 1554.0 nm) was shown in simulation results to have the same value of about 1 dB throughout the chain. This is due to the total power change, subsequently being compensated for by the increase or decrease in the surviving channel power. For the first one or two EDFAs, the average population inversion of the subsequent EDFA goes back to the initial value. The imbalance of the power at the output of the chain is mainly due to the first and second EDFAs. The amount of the imbalance power depends on the bandwidth of the spectral area of the EDFA used and on the proportion of the channel wavelengths that are lost or added [101, 129, 153].

Figure 6.4 shows that the new steady state OSNR transient varies slightly at the output of the first EDFA, and as the number of EDFAs increase it slowly converges to the value of the optical power transients, as shown in Figure 6.7. This is a consequence of the self-regulating action of the chain of saturated EDFAs. The rate at which the OSNR changes as a function of amplifier number depends on the initial value of the OSNR. The same considerations apply to the second case study in which 4 channels are added to 4 existing channels in the networks link.

6.2.2 Effect of power and OSNR transients of cascaded EDFAs on the optical receiver for WDM networks

In order to quantify the result of power transients with output signal quality at the end of the cascaded EDFAs, the bit error rate of the output signal of the system ought to be estimated. In accordance with Forghieri [154], two independent quantities, the optical quality of signal (Q_{OSNR}) and the back-to-back receiver quality (Q_{RX-BB}) can be used for estimation of the quality factor (Q) of the received signal:

$$Q = \frac{1}{\sqrt{\frac{1}{Q^2_{OSNR}} + \frac{1}{Q^2_{RX-BB}}}} \tag{6.4}$$

Where (Q_{OSNR}) is a function of the OSNR as obtained by Marcuse [155]:

$$Q_{OSNR} = \frac{OSNR}{\sqrt{OSNR+1}+1}\sqrt{\frac{B_o}{B_e}} \tag{6.5}$$

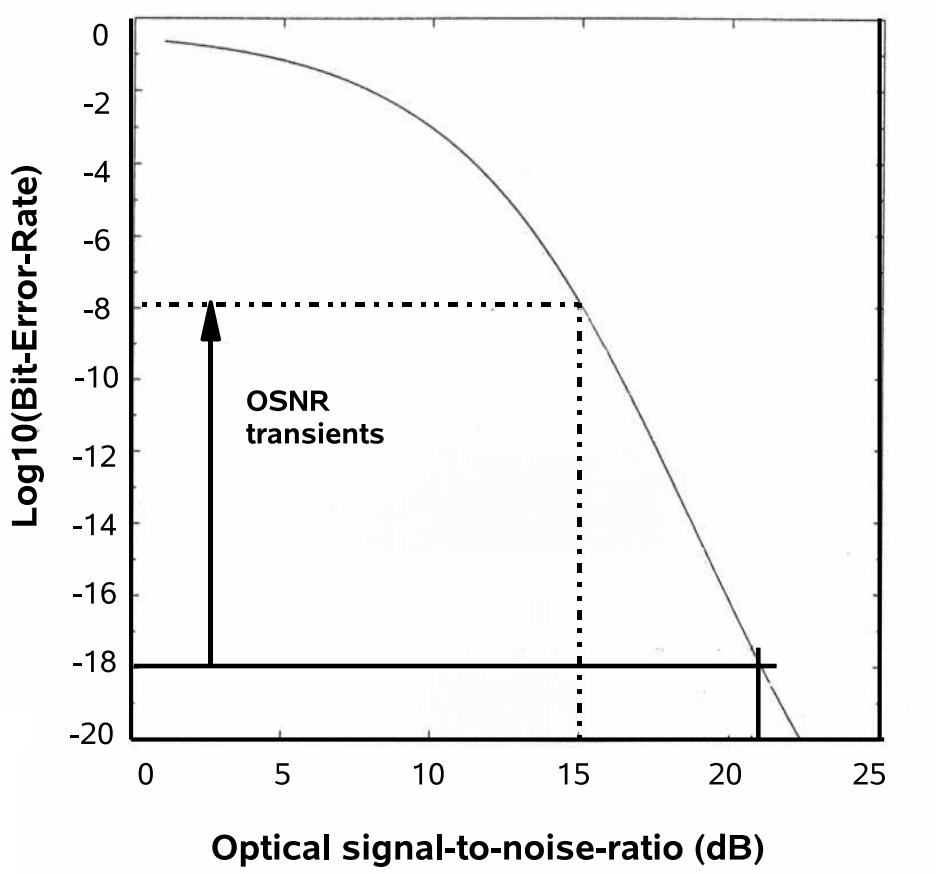

Figure 6.8: Bit-error rate versus the OSNR (dB).

Where B_o represents the optical bandwidth and B_e represents the electrical filter bandwidth at the receiver. B_o and B_e are assumed to be 0.2 nm and 0.7 times the bit rate, respectively. In our simulation, we assume the (Q_{RX-BB}) = 21 dB. This supports the evaluation of the BER as:

$$BER = \frac{1}{2}\, erfc(\frac{Q}{\sqrt{2}}) = \frac{1}{\sqrt{\pi}} \int_{Q}^{\infty} e^{-t^2/2} dt \tag{6.6}$$

This relation between BER and OSNR is shown in Figure 6.8. This figure allows us to determine the BER range corresponding to any achieved OSNR range [108, 156]. As can be seen from Figure 6.6 the OSNR(t) decreased by 5.5 dB at the output of the thirty fifth EDFA in the chain. Using Figure 6.8, we can see that the BER can reach 10^{-8} for this case. Thus, it is required that the OSNR(t) must not be decreased more than 3.5 dB in order the BER can be within the permissible limit of 10^{-9}, which is the experimental standard limit for acceptable system performance. Strictly BER should be $<< 10^{-9}$ [136].

6.2.3 Effect of the abrupt input power on the power and OSNR transients in the EDFAs chain

Figure 6.2 shows the total output power transient rate and Figure 6.4 shows OSNR rate at the probe channel, we observed from our simulation results that the transient rate increased as the number of EDFAs increased. The transient in Figure 6.2 was a consequence of the steep variation in the input power from 5.4 mW to 2.7 mW over a duration of 2 μs. The behaviour of power transients was examined when the input power to the first EDFA drops from 5.4 mW to 2.7 mW over different time intervals, 2 μs, 5 μs and 10 μs respectively, as shown in Figures 6.9 and 6.10.

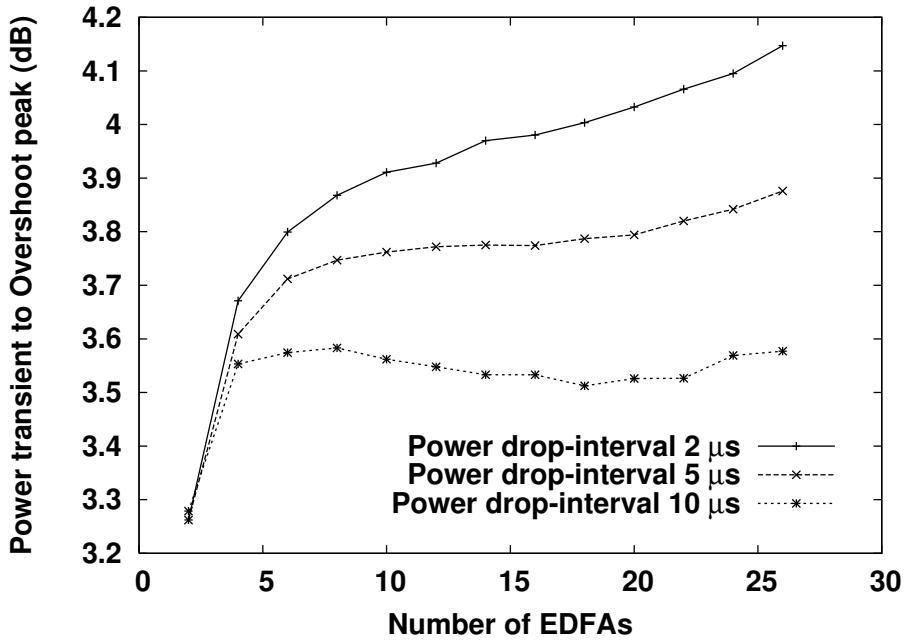

Figure 6.9: The power transients from initial to overshoot regions versus number of EDFAs in the chain and observed when the input signal drops at different time intervals (i.e. the input signal drops at different speeds)

Figure 6.9 illustrates the overshoot behaviour of the output power transients for the probe channel at the output of the different EDFAs of the simulated chain for the different time intervals when 4 channels out of the 8 channels are dropped. It is clear that a more gradual change in input power reduces both the peak power of the overshoot and the rate of increase-time or decrease-time of the output power transients [73, 157, 158]. This is also shown in Figure 6.10.

The 1 dB slope (reciprocal of 1 dB increase-time) or the rate of the power transient was

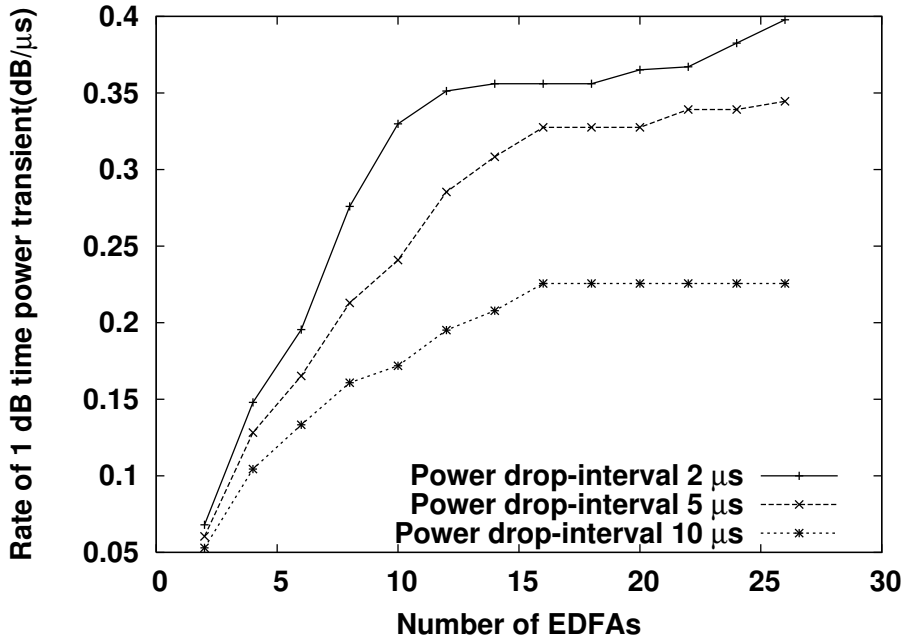

Figure 6.10: Rate of 1 dB increase-time of the power transients versus number of EDFAs in the chain and observed when the input signal drops at different time intervals (i.e. the input signal drops at different speeds).

plotted when the input power drops at three intervals, 2, 5 and 10 μs respectively, as shown at the output of the simulated EDFA chain in Figure 6.10. It can be seen in Figure 6.10 that the rate of 1dB increase-time varies according to the input power drop time-interval. With a more gradual drop-off of the input power, the rate of 1 dB increase-time not only increases more slowly but can reach a saturation or stable value at EDFA number 16 for a power drop interval of 10 μs.

The rate of input power drop puts a limit on the gradient of the 1 dB increase-time or decrease-time. The rate of 1 dB increase-time of the OSNR transients follows the same behaviour as the power transients and also reaches a saturation or stable level at EDFA number 16. For the output power and OSNR, as the time of the power drop interval increases the overshoot peak decreases as shown in Figure 6.11 (a, b), the overshoot value decreasing is very important because the output power in the overshoot region may exceed the limit of the receiver threshold, then the OSNR and bit error rate will deteriorate. In Figure 6.11 (b) when the number of EDFAs is greater than 10 we observe fluctuations in the curve representing the drop-interval of 10 μs.

The optical input power can possibly vary faster than the response of the switching-gate,

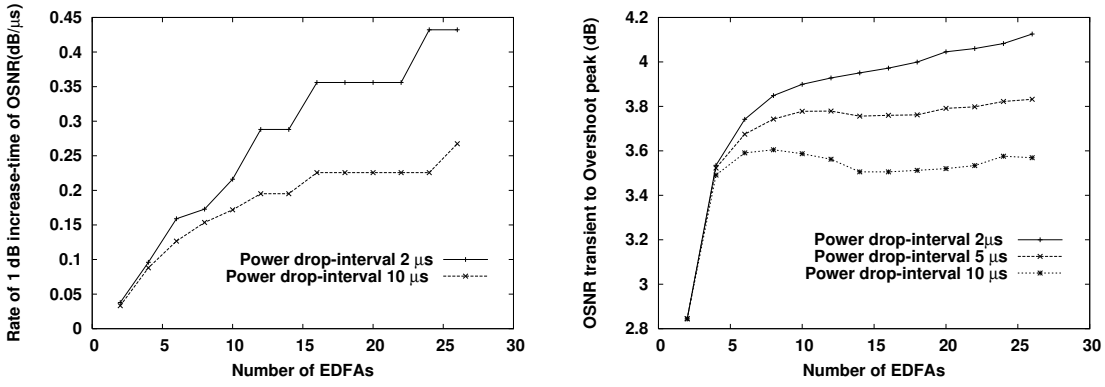

(a) (b)

Figure 6.11: (a) Rate of 1 dB increase-time of the OSNR transients versus number of EDFAs in the chain, (b) OSNR transients to overshoot peak versus number of EDFAs in the chain, observed when the input signal drops at different time intervals.

which was developed using a semiconductor optical amplifier (SOA) with switch time in nanoseconds [159]. Very fast changes in the input power (Δ t $<<$ τ (metastable state life-time)) will not affect the EDFA output power and not deteriorate the network performance. If the speed of variation of the input powers of the EDFA is in a comparable range with τ, i.e. variation frequency is in comparable range to 100 Hz, then the input power variation generates transient phenomena and deteriorates the network performance.

Consequently, it is obvious from these simulation results that the rate of variation of the input power in a chain of EDFAs may be controlled in a way that will relax the timing requirements for gain stabilisation or other channel protection schemes. It is important for channel protection design to specify all time intervals related to: network reconfiguration, or addition/removal of channels for increasing the capacity of the network, or regarding network maintenance and equipment failure time intervals. This is because they can possess values close to the required speed of response of the channel protection scheme.

6.3 Summary

In this chapter the output power and OSNR transients of the cascaded EDFA link was investigated. The self-saturated dynamic model which was developed and described in Chapter 3 was used for numerical simulations. It was shown that the OSNR transient has the same

behaviour as the output power transient, since the OSNR transient is a function of output power transient. The power transient deteriorates and its speed increases proportionally to the number of the cascaded EDFAs in the link. The 1 dB increase-time/decrease-time is used to compare both output power and OSNR transients. It was found that the speed of evolution of the OSNR transients is slower than the output power transient. This behaviour is a consequence of the automatic control or self-regulation of the gain of saturated EDFAs as discussed in Chapter 2. Moreover, it was observed that the power instability between surviving channels when transients occur was due to the instability at the first EDFA. This latter is also the result of the self-regulating characteristic of gain saturated EDFAs in the network link.

For our simulations, to determine the effect of power transients on system performance at the end of the cascaded EDFAs, the bit-error rate of the output signal of the system was assessed. This allowed us to determine the BER range corresponding to any achieved OSNR range [108]. We observed that the min(OSNR(t)) is -5.5 dB at the output of the chain with the addition of four channels to the four existing channels in the link, and that the BER can reach 10^{-8} for this case. Thus, it is required that the min(OSNR(t)) $\geq$ -3.5 dB in order that the BER can achieve the experimental standard limit of 10^{-9}. For acceptable system performance, the BER is required to be $<< 10^{-9}$ [136].

As mentioned above, as the number of EDFAs increases, the rate of the optical power transient will become faster due to the fast power variation in the input of the cascaded EDFAs. It is possible that cascaded EDFAs will face faster variation in the input power than this as the bursty traffic in the packet switching networks can easily be in nanoseconds or less as the bit rate of the transmissions increase.

The effects of a more gradual variation of the input power on the behaviour of the power and OSNR transients in the cascaded EDFAs was investigated. Three intervals for the input power drop, 2, 5 and 10 μs were used in this investigation. It was found that a more gradual input of the power variation decreases the rate of the power transient and the amplitude of the overshoot. It was observed that if the rate of variation of the input power in a cascaded EDFA can be regulated, this will provide sufficient time for gain stabilisation.

Our simulation results demonstrate that swing, which is represented by the amplitude of the overshoot in both the output power and the OSNR, can be reduced in the cascaded

EDFA links when a more gradual variation of the input power is applied. For instance, OSNR transient overshoot peaks are around 3.5, 3.8 and 4 dB at power drop-intervals 10, 5 and 2 μs respectively. Our simulation results show one term that we can use in the gradual input power technique for mitigating the effects of EDFA power and OSNR transients, and another term - the increase in the speed of drop-interval of the input power - which results in a larger swing which is the condition that the EDFA faces with bursty traffic. Very fast changes in the input power (Δ t $<<$ τ (metastable state life-time)) will not affect the EDFA output power and not deteriorate the network performance. If the speed of variation of the input powers of the EDFA is in a comparable range with τ (i.e. variation frequency is about 100 Hz) then the input power variation generates transient phenomena and deteriorates the network performance.

In contrast to other transient mitigating methods, the input power shaping or gradual variation method is simple and easy to implement but requires a special electronic switch to decrease or increase input power gradually, and this is the drawback of this method. However, all transients mitigating techniques have advantages and disadvantages as mentioned in Section 1.9 and Chapter 7. For instance, one of the methods described in the literature for mitigating EDFA transients is called power shaping and here heads and tails are added to traffic blocks in order to gradually increase or decrease the average power on the channel [73].

Our simulation work shows, that for better, faster and longer network designs, it is necessary to investigate the link between the amount of power and OSNR transients under the different circumstances of the network. The design of suitable channel protection methods for mitigating power and OSNR transient problems is essential to enhance the quality of the network.

Chapter 7

Gain Locking System for EDFA in WDM Optical Networks using PID Controller

7.1 Introduction

The power transient phenomenon that occur in such saturated gain optical amplifiers as the EDFA [74, 160, 161] and Raman [162, 163], represents a services problem in multi-wavelength optical networks. As mentioned in Chapter 1, there are three main techniques used to mitigate the effect of this phenomenon and the basic idea behind each is to clamp the saturated gain of the EDFA.

It is obvious from literature survey that the gain controlled and transient suppressed EDFAs were all designed and developed for specific field requirement. For example, for long-reach passive optical networks using bursty traffic, hybrid electro-optical feedback gain stabilized EDFAs were developed as this approach avoids any oscillation in the burst envelopes, and provides accurate adaptation for receiver threshold, efficient pump power scheme compared with optical feedback approaches (i.e. the approach gives no useless heavy loading on the network) [164].

A high efficiency automatic-power-controlled and gain-clamped EDFA for broadband passive optical networking systems is presented by Jyi-Lai et. al. [165] in order to compensate for phase and amplitude variation due to different distances between the optical line terminal (OLT) and optical network units (ONU).

Many feedback approaches have been reported to stabilize the gain of an EDFA based on sampling and detecting output light and using it to control the pump laser. Vijayakumar and Sreeja [166] have used a feed-forward technique to stabilize the output gain of an EDFA. A lithium niobat based Mach-Zehnder interferometer is used to modulate the intensity of pump light in accordance with the input signal power in order to maintain constant output power.

It was also reported that automatic gain controlled EDFA for the burst-mode signals is one of the useful device in new generation WDM [167]. All-optical gain clamped EDFA was developed by Ting-Tsan et. al. [168] using a DWDM. In this approach, one output channel of the DWDM demultiplexer is connected into the ring cavity to provide the lasing oscillation for gain clamping while the other output channels are used as the signal output channels of the EDFA.

Several other techniques have been proposed in the literature to stabilize the average inversion in the EDFA. Electronic and all-optical feedback are the two main types of gain control methods widely reported in recent years. An approach reported by Li et. al. [169], related to design and analysis of gain clamped EDFA using a fixed all optical feedback system which shows superior static and dynamic performance. Other methods have also been used for changing pump laser to keep the signal output power or gain constant [170–172].

7.2 PID controller for the EDFA

In order to lock the saturated gain of the EDFA for variable input power due to the addition or removal of channels caused by network reconfiguration or link failure, the input signal Ps_{pin} or the input pump power Pp_{pin} must be changed. The signal gain is determined by the level of population inversion in the EDFA which is related to the amount of absorbed pump power and so the control system relies, in this work, on fixing the pump power, here a PID (Proportional, Integral, and Derivative) controller, as shown in Figure 7.1 is used to update the pump power. The response time of the update depends on the technology used in the design of the PID controller in the EDFA and that affects the response of the network physical layer. The fast response controller is the most efficient system for WDM optical networks, in particular for packet switched optical networks.

The PID controller transfer functions used in the design of the controller are shown in

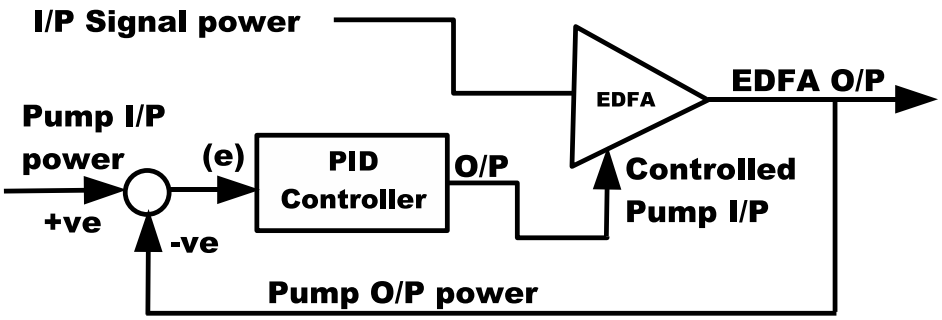

Figure 7.1: The schematic diagram for EDFA and controller, illustrating the negative feedback loop for updating the pump power.

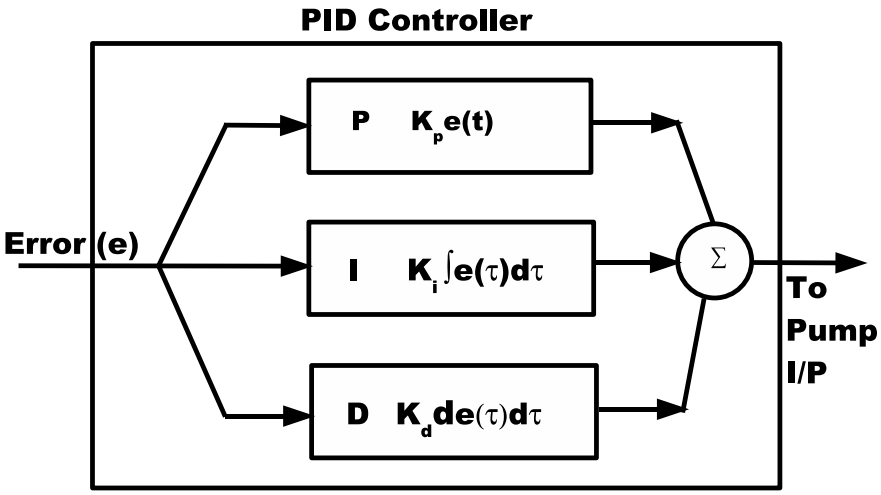

Figure 7.2: PID controller schematic diagram using functions described in equation (7.1).

Figure 7.2 [160, 173]. The error (e) is obtained from subtraction of the actual output power from the desired input power and this magnitude is the power transient. The term (e) defines the tracking error, this error signal passes through the controller which computes the proportional, the integral and the derivative of this error signal.

The output at the controller is equal to two main terms, the instantaneous pump input and the controlled gain error. The controlled gain error is the sum of proportional gain (K_p) multiplied by the magnitude of the error, the derivative gain (K_d) multiplied by the derivative of the error, the integral gain (K_i) multiplied by the integral of the error, as shown in Equation (7.1). The selection of the controller functions is according to the requirements

of the application, it is not necessary to implement all three controllers in a single system. Keeping the controller system in this application as simple as possible was achieved by testing each controller alone and then pairs of controllers together in order to find which controller gives an optimum response [174].

The main components in a controller unit are the optical receiver and components that performs the functions of integrating, proportioning and differentiating. The optical receiver consists of a photodetector (PD), transimpedance amplifier (TIA), and limiting amplifier (LIM). The response characteristics of the PID controller mainly depend on the photodetector characteristics which should be high sensitivity and wide dynamic range of input signal power, and a fast response to signal variation to cope with fast power transients in cascaded EDFAs. Also the receiver cost should be low to allow for use in each EDFA. The short response time will improve the efficiency of the controller unit. For photo-detectors an avalanche photodiode (APD), which requires a bias and control circuit is used to obtain high sensitivity and wide dynamic range of input signal power. However, using a PIN-photodiode (PIN-PD) for photo-detector can reduce the cost of the receiver with no need for a bias circuit but with less sensitivity than the APD. The TIA and LIM also affect the design of the receiver regarding sensitivity, dynamic range, bandwidth and thermal noise. These specifications of the components all together affect the efficiency and response time of the controller [131, 132, 175], which is a point that must be considered in the PID controller design for the circuit switched network and for the WDM optical packet-switching systems [131, 133].

7.3 Simulation parameters

The parameters in this numerical simulation are for: an EDF of length 20 m, co-propagated direction pump at wavelength of 980 nm, pump power, P_{pin} = 65 mW (18.12 dBm), a multi-wavelength signal consisting of eight channels which start at 1549.2 nm with 1.6 nm channel spacing, input power of -2 dBm per channel is used, the effective area of doped-fibre is $1.5742 \times 10^{-12}\ m^2$, the erbium ion concentration is 7×10^{24} ions/m^3, and the life-time of the metastable level is 10.5 ms. The simulation resolution for all numerical simulations is 0.1 μs. To illustrate transient phenomena in the surviving channels the input signal was modulated

at a frequency of 1 kHz. That defines the dropping of 4 channels at 80 ms and addition of 4 channels at 81 ms.

In all simulations four channels are dropped or added unless it otherwise stated. The updating interval for pump power in this investigation in all simulations is 5 μs, corresponding to a 200 kHz controller bandwidth. The controller bandwidth and specifications were varied in an accordance with components (all-optical or electronic) used for building (all-optical or electronic) the transient controlled EDFAs as mentioned in Section 7.2.

7.4 Numerical simulation

These sections discuss the characteristics of each of the proportional (P), the integral (I), and the derivative (D) controllers, and how to tune them to obtain a desired response. In our implementation, we controlled the input power of the pump in the EDFA, since the pump input power and signal input power are the two fundamental input powers which affect the response of the EDFA. Therefore, the ratio of the instantaneous pump output power to instantaneous pump input power, $P_{out}(t)/P_{pin}(t)$, has been introduced. Equation (7.1) [160, 161, 173] represents the numerical model used for the negative feedback loop system for updating the pump power in an interval equivalent to the updating cycle of the electronic controller [165, 168].

$$P_{pin}(t+dt) = P_{pin}(t) + K_p\left(\frac{P_{pout}(t)}{P_{pin}(t)} - \frac{P_{pout}(0)}{P_{pin}(0)}\right)$$

$$+K_d\frac{d}{dt}\left(\frac{P_{pout}(t)}{P_{pin}(t)} - \frac{P_{pout}(0)}{P_{pin}(0)}\right) + K_i\int\left(\frac{P_{pout}(t)}{P_{pin}(t)} - \frac{P_{pout}(0)}{P_{pin}(0)}\right) \tag{7.1}$$

$P_{pout}(t)/P_{pin}(t)$ is the ratio of instantaneous output power to instantaneous input power of the pump, $P_{pout}(0)/P_{pin}(0)$ represents the ratio of the output to input pump power when all eight channels are amplified or prior to perturbation of the system, and K_p, K_d and K_i represent the proportional, derivative and integral gain parameters used in the negative-feedback system as shown in Figure 7.2.

Figure 7.3 shows the evolution of output power in both the signal channel of wavelength 1549.2 nm and the pump during the steady-state and the transient periods prior to the gain controller being applied.

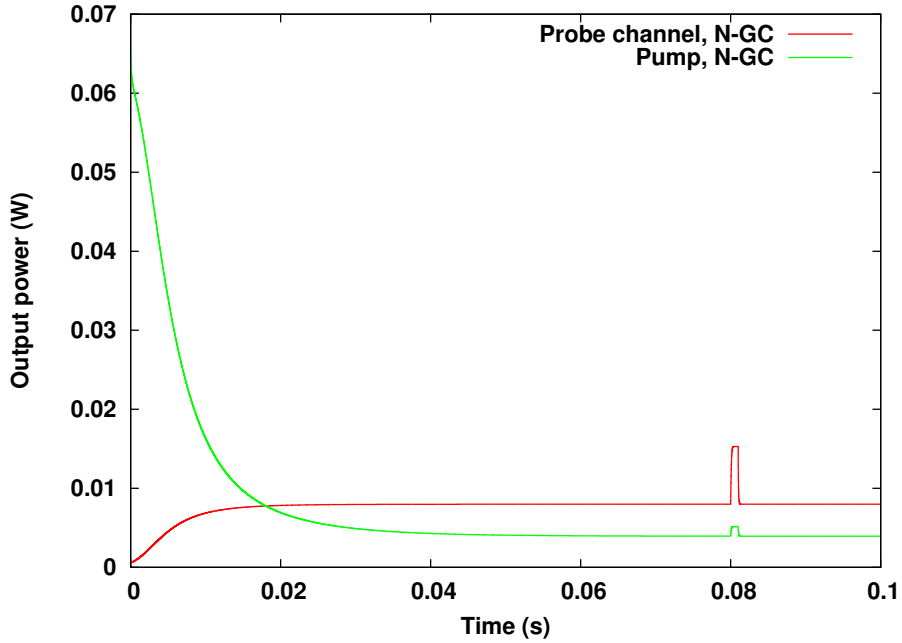

Figure 7.3: Power evolution in the pump and probe channel in the EDFA during steady-state and transient periods when there is no gain controller (N-GC).

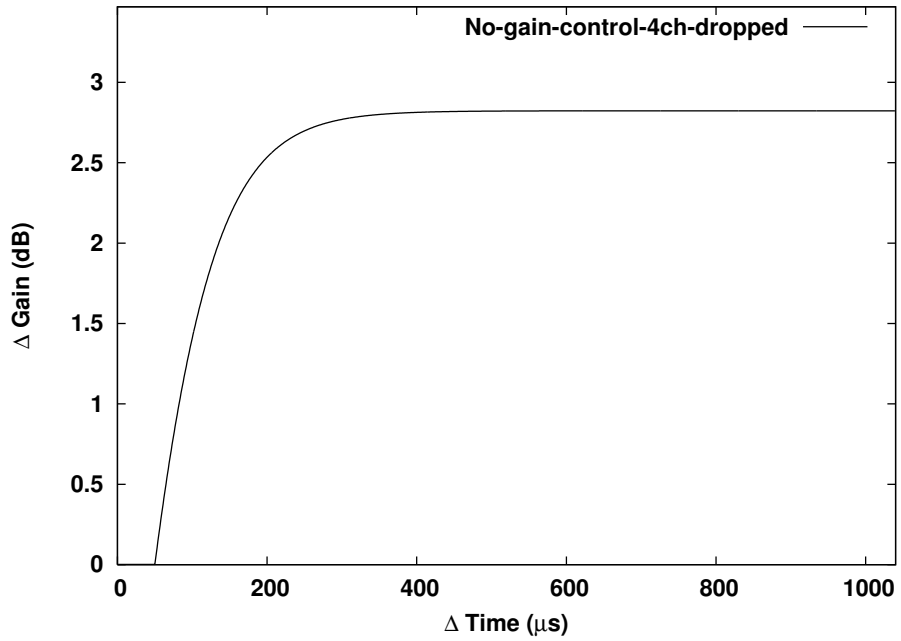

Figure 7.4: Output power transients at signal channel of wavelength 1549.2 nm as a function of time when four out of eight channels are dropped.

Proportional controller (P-controller), we began by investigating the proportional numerical model shown in Equation (7.2), for clamping the saturated gain of EDFA to mitigate the power transients due to the loss of 50% of input power, for the 4 input signal channels of

wavelengths 1555.6 nm, 1557.2 nm, 1558.8 nm and 1560.4 nm.

$$P_{pin}(t+dt) = P_{pin}(t) + K_p \left(\frac{P_{pout}(t)}{P_{pin}(t)} - \frac{P_{pout}(0)}{P_{pin}(0)} \right) \tag{7.2}$$

Figure 7.4 shows the power transient for wavelength 1549.2 nm in the absence of the gain controller, the magnitude of the power transient is 2.8 dB. The rise time of the power transient is the time from transient point to transient overshoot, The relaxation time of the power transient is the time from the transient overshoot to the stabilisation level (restored reference level, 0 dB). The total transient time = the rise time of the power transient + the relaxation time of the power transient. When the proportional controller is applied, the output power transient is suppressed. We began with K_p = 0, as shown in the green curve in Figures 7.5 and 7.6, the power transient is 2.8 dB, as expected when the controller is switched off. We changed K_p to values greater or less than zero, and observed that when K_p is greater than zero, such as K_p = 0.08 the power transient approaches 3.05 dB that is equivalent to 14.081 dB (at relative time of 600 μs), this value is with input pump power of 0.0685 W, as shown in Figure 7.6. As expected this represented positive feedback and is detrimental. When K_p is less than zero, such as K_p = -0.4, the transient power is 1.84 dB, this value corresponded to an input power of 0.043 W. It was also observed that when K_p = -0.6, the power transient overshoot is 1.77 dB as shown in Figure 7.5, this value corresponds to an input pump power of 0.027 W, as shown in Figure 7.6.

This increase and decrease in the pump input power produces different levels of photons in the metastable level, causing an increase or decrease in the amplifier output power, by these steps the required gain reference level is adjusted as shown in Figures 7.5 and 7.6. The steps in pump input power in Figure 7.6 are related to the updating period of the pump input power at intervals of 5 μs.

When K_p = -0.523, the transient power reduced to 1.79 dB and the gain was restored to the reference level, 0 dB, the time from transient point to gain-overshoot was 80 μs, the time from gain-overshoot to the restored reference level was 470 μs, so the total transient time was 550 μs, as shown in Figure 7.5. The required pump input power for restoring the gain of the probe channel to 11.03 dB was 0.0337 W. From this observation it was concluded that the proportional gain error model on its own can provide control of the cross-gain saturation of EDFA, since it can restore the gain of the surviving channels to the reference level because the main requirement of the automatic gain controller is to decrease the power transient

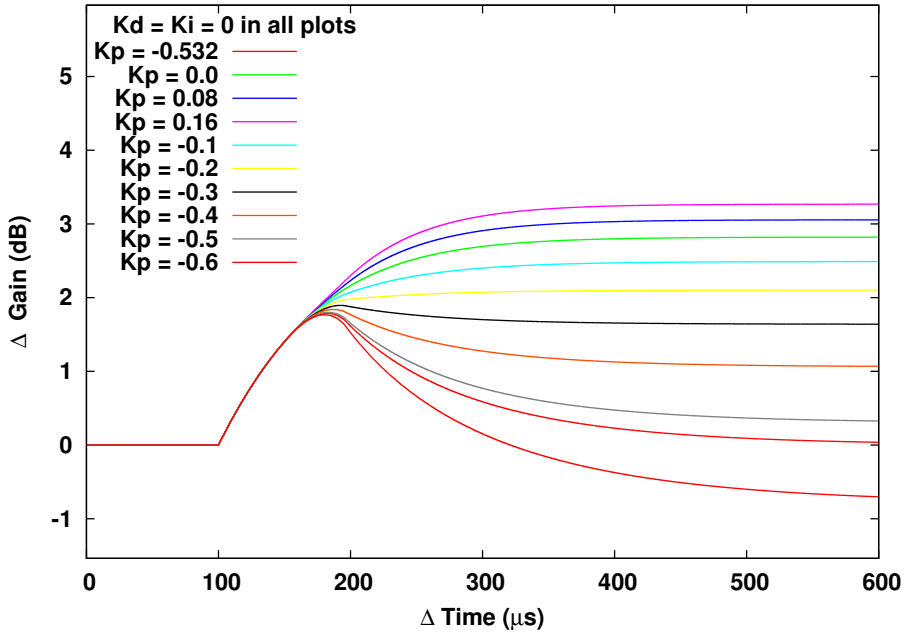

Figure 7.5: Output power transient when the proportional controller is applied to EDFA with $K_i = K_d = 0$. K_p is varied as stated in the plot. When K_p = -0.523, the transient power was reduced to 1.79 dB and the gain restored to its reference level 0 dB (red curve).

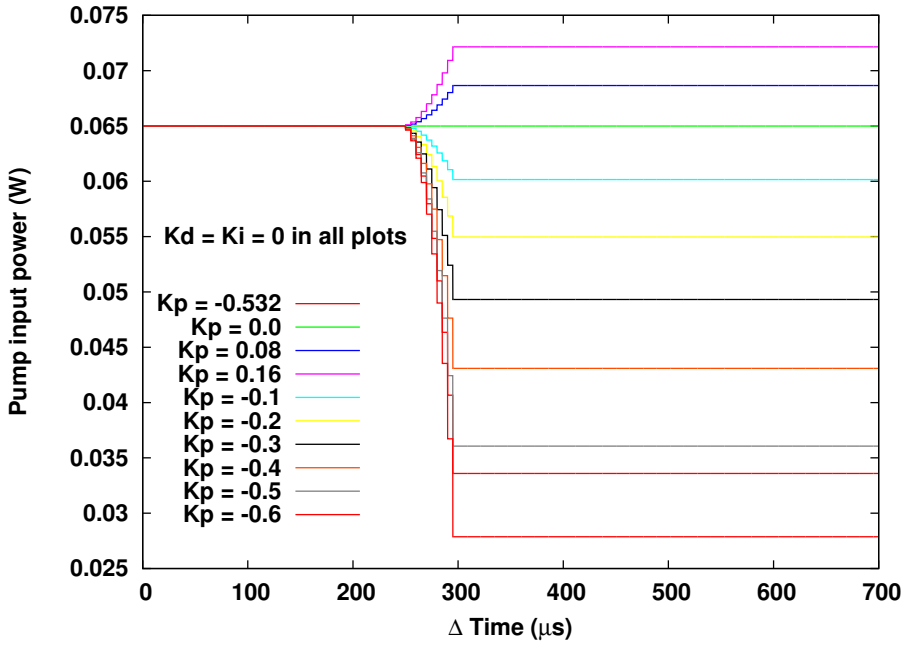

Figure 7.6: Input power of the pump channel when only the proportional controller is applied to the EDFA, with $K_i = K_d = 0$. K_p was varied as stated in the plot. When K_p = -0.523, the transient power reduced to 1.79 dB and the gain restored to its reference level 0 dB (red curve).

overshoot and total transient time and so mitigate the power transient phenomenon.

The *Integral controller (I-controller)*, was numerically simulated by the model shown in

Equation (7.3), the power transient was suppressed by the integral controller. This controller provides the instantaneous pump input power and integral of the ratio of the instantaneous pump output power to the related pump input power at intervals of 5 μs. When K_i was assigned the value 0, the output power transient overshoot was maintained at 2.8 dB, thus demonstrating that the controller was switched off. Then K_i was set to values above and below zero, while $K_p = K_d = 0$, this was done to suppress the transient overshoot and to restore the gain to the reference level. It was observed that when $K_i = 1.0\times10^{-4}$, the power transient approaches 3.2 dB i.e. higher than normal magnitude (2.8 dB) as shown in Figure 7.7. The pump power required for this power transient was 0.0708 W as shown in Figure 7.8. When K_i = -4.21$\times10^{-4}$, the power transient became 1.18 dB, the transient rise time was 70 μs, the time between gain overshoot and relaxation at the reference level, 0 dB, was 430 μs, the total transient time was 500 μs as shown in Figure 7.7. The input pump power for achieving this target was 0.0337 W as shown in Figure 7.8.

$$P_{pin}(t+dt) = P_{pin}(t) + K_i \int \left(\frac{P_{pout}(t)}{P_{pin}(t)} - \frac{P_{pout}(0)}{P_{pin}(0)} \right) \tag{7.3}$$

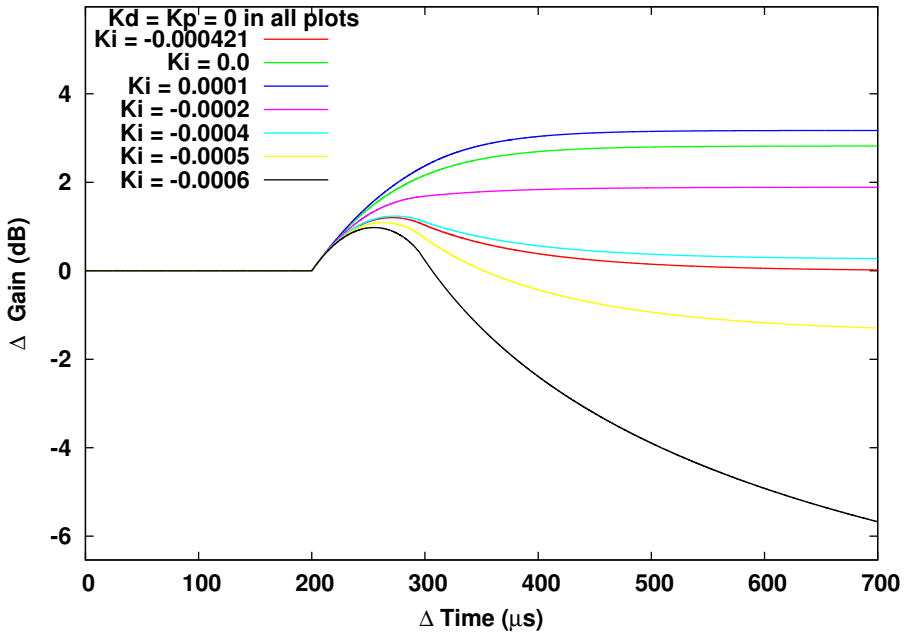

Figure 7.7: Output power transient using integral controller, $K_p = K_d = 0$ and K_i is varied as stated in the plot. When K_i = -4.21$\times10^{-4}$, the power transient became 1.18 dB, and the gain level relaxes at reference level, 0 dB (red curve).

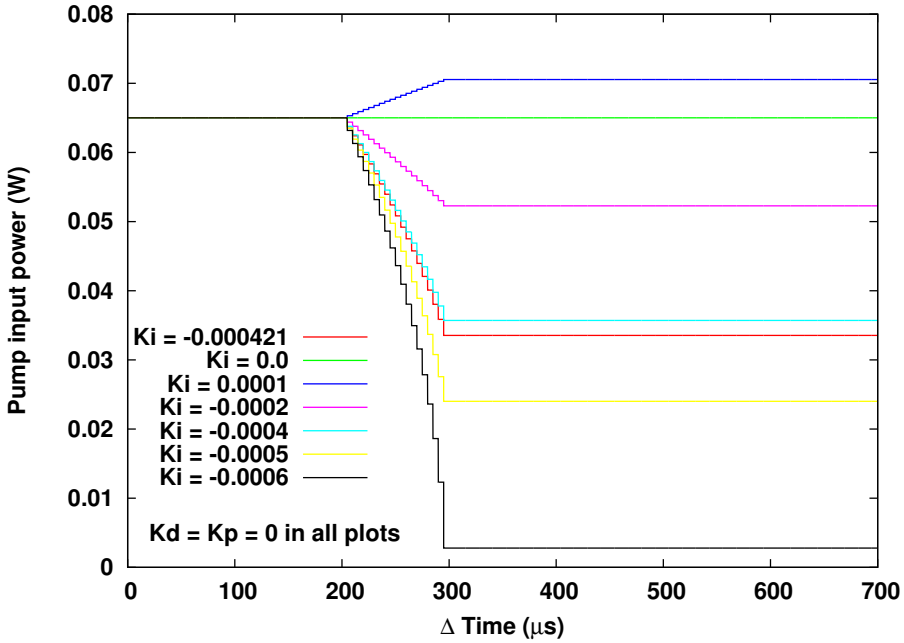

Figure 7.8: Input pump power only using integral controller, K_p = K_d = 0 and K_i is varied as stated in the plot. When K_i = -4.21$\times 10^{-4}$, the power transient become 1.18 dB (red curve) the required pump power for this was 0.0337 W.

It was observed from the simulation results of the integral controller, that when K_i = -6.0$\times 10^{-4}$, the power system appears to be unstable. From the results of the above simulation we concluded that the integral controller alone can clamp the cross-gain saturation of the EDFA without support tuning of the proportional or derivative controllers. The steps of the input pump power, as shown in Figure 7.8, at 200 μs where the transient started were due to the 5 μs interval for updating of input pump power by the I-controller.

The *derivative controller (D-controller)*, was the third part of the investigation of the PID controller, and the simulation of the derivative gain error is shown in Equation (7.4). This was undertaken to asses the value of K_d that clamped the cross-gain saturation of the EDFA.

$$P_{pin}(t+dt) = P_{pin}(t) + K_d \frac{d}{dt}\left(\frac{P_{pout}(t)}{P_{pin}(t)} - \frac{P_{pout}(0)}{P_{pin}(0)}\right) \tag{7.4}$$

With the derivative controller, when K_d was set to 0, as with the two previous controllers, the power transient overshoot remains at 2.8 dB as shown in Figure 7.9 (green curve). This indicates that the gain-controller is not active, see Figure 7.10 when K_d = 0. The D-controller starts updating the pump power at intervals of 5 μs, and as K_d was tuned to magnitudes greater or less than zero, it was observed that when K_d = 0.02, the power transient = 3.2

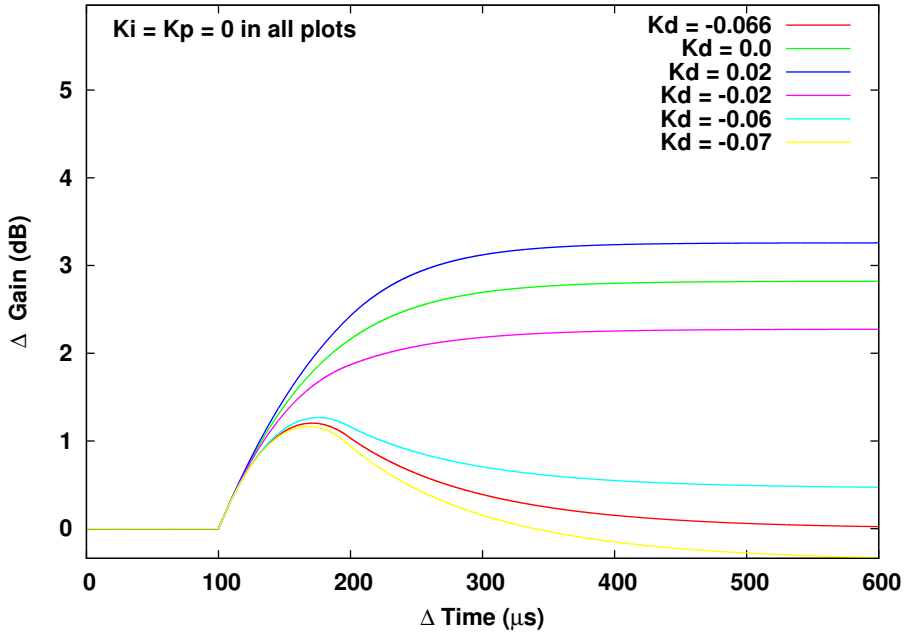

Figure 7.9: Output power transient of probe channel using only derivative controller, K_p = K_i = 0 and K_d is varied as stated in the plot. When K_d = -0.066 the power transient overshoot reduced to 1.18 dB and the gain level relaxes at reference level, 0 dB (red curve).

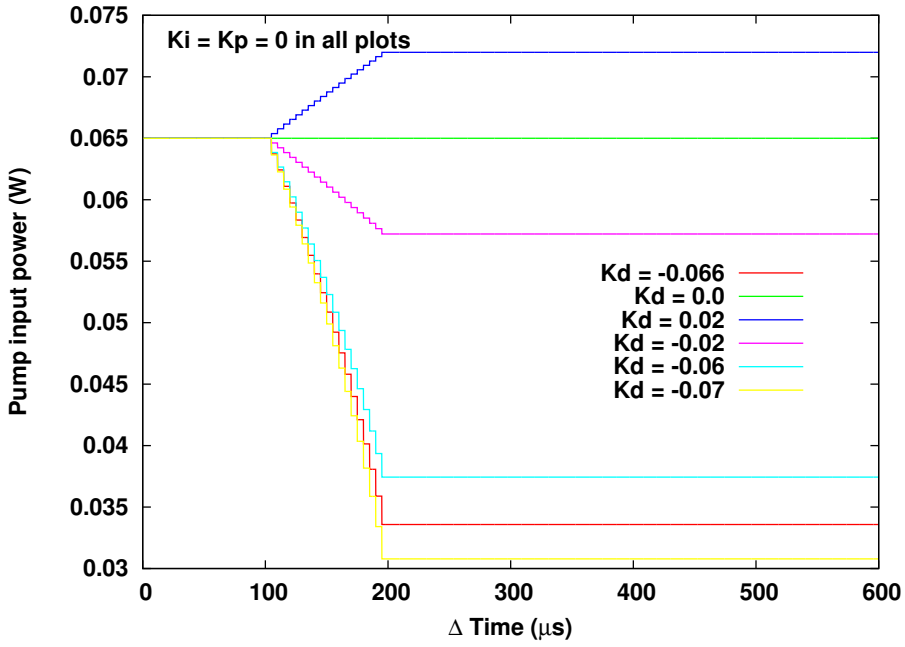

Figure 7.10: Input pump power only using derivative controller, K_p = K_i = 0 and K_d is varied as stated in the plot. When K_d = -0.066 the power transient overshoot reduced to 1.18 dB (red curve) the required pump power for this was 0.0337 W.

dB which is higher than the system without gain controller, and when K_d = -0.02, the power transient = 2.268 dB. We noticed that when K_d = -0.066, the power transient overshoot = 1.18

dB, and the gain relaxes at reference level, 0 dB. The transient rise time = 70 μs, the time between gain overshoot and relaxation at reference level was 430 μs, so the total transient time was 500 μs. The pump input power was 0.0337 W as shown in Figure 7.10 and this was the pump power for restoring the gain of the probe channel to 11.03 dB. This indicates that the derivative controller can clamp the cross-gain saturation of the EDFA without being supported by the proportional or integral controllers.

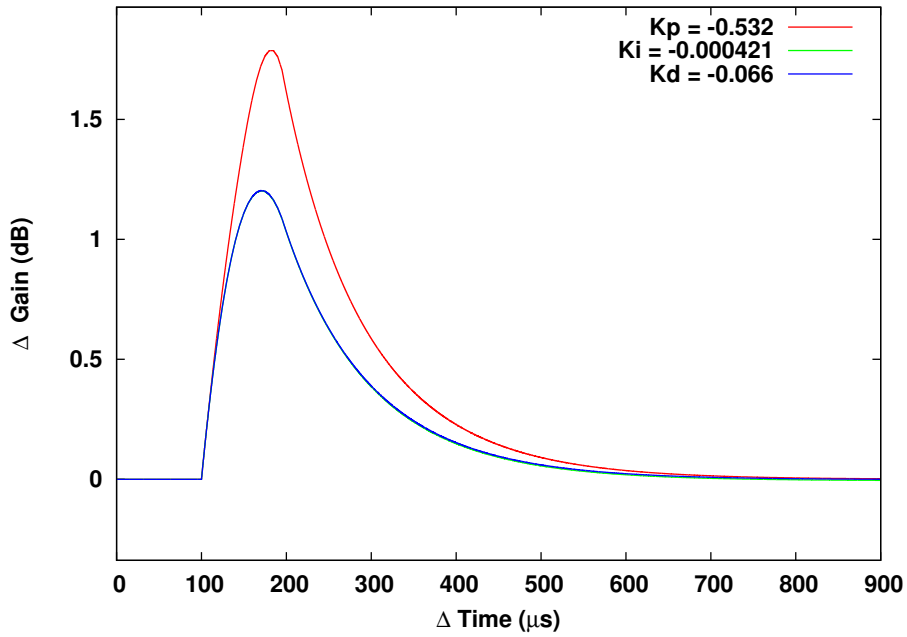

Figure 7.11: Comparison between optimum output power transient of probe channel using integral, derivative or proportional controller, K_i = -4.21$\times$10^{-4}, K_d = -0.066, K_p = -0.532.

Comparison between P, I, and D controller responses derived from the numerical simulation showed that when four out of eight channels dropped, the I- and D-controllers perform better than the P-controller, see Figures 7.11 and 7.12. For the I- and D-controllers the power transient overshoot and total transient time were 1.18 dB and 500 μs respectively, while for P-controller the power transient overshoot and time were 1.79 and 550 μs respectively.

With *integral and proportional controller*, the integral gain parameter was initially set at K_i = -4.21$\times$10^{-4}, then K_p was set to different values, this was done to obtain a better power transient overshoot and time than achieved earlier with the I-controller alone. With K_p = 0, that is the I-controller alone was active, the power transient overshoot and total transient time were 1.18 dB and 500 μs respectively, and the adjusted pump input power = 0.0337 W, as shown in Figures 7.13 and 7.14 (green curve). When K_p = 0.01, the power transient =

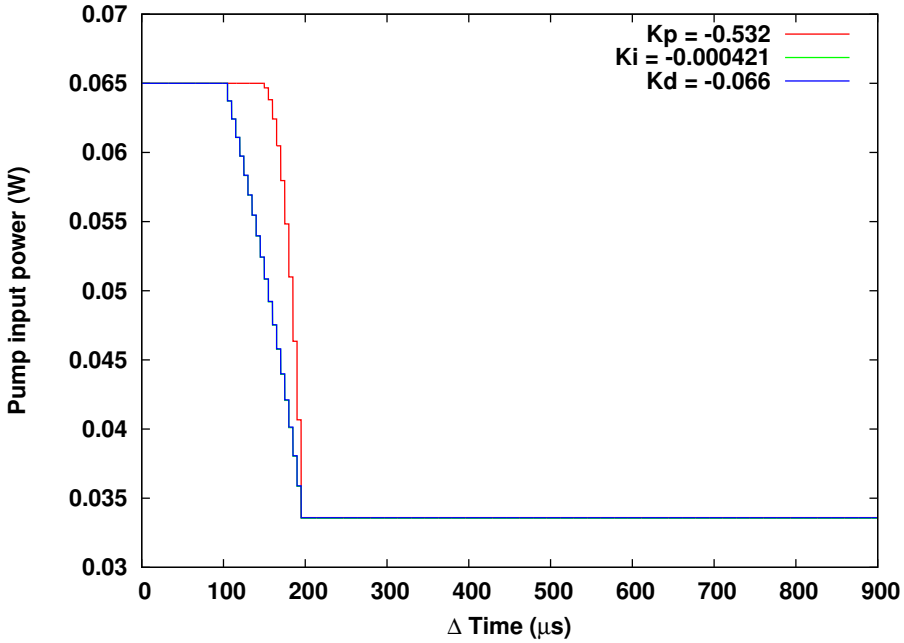

Figure 7.12: Comparison between optimum pump input power for probe channel using integral, derivative or proportional controller, K_i = -4.21×10^{-4}, K_d = -0.066, K_p = -0.532.

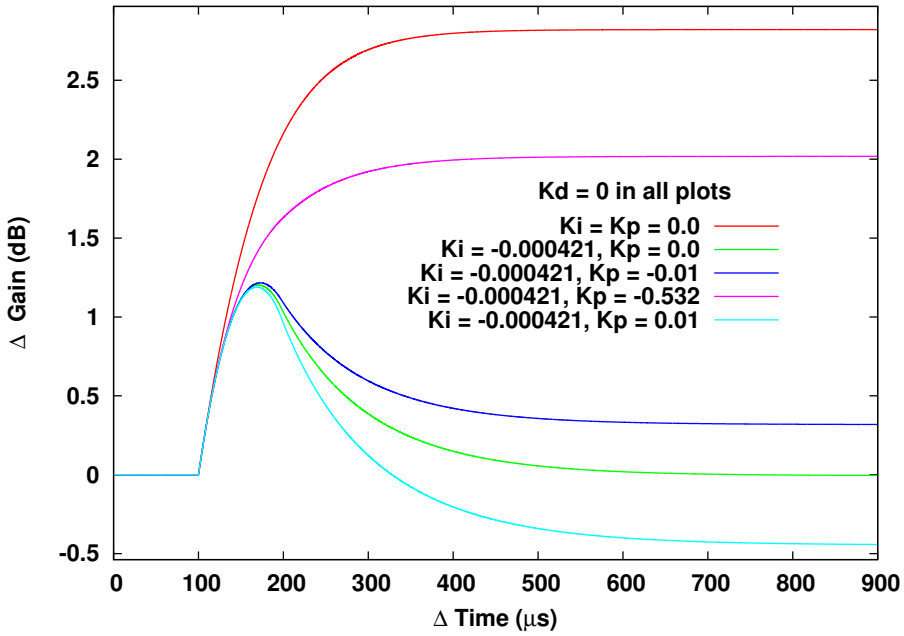

Figure 7.13: Output power of probe channel using integral and proportional controllers, K_i = -4.21×10^{-4}, K_d = 0, K_p is varied as stated in the plot.

1.63 dB measured between power overshoot and power undershoot, the adjusted input pump power was 0.0302 W. The power transient overshoot was 2.02 dB when K_p was -0.532, and the adjusted input pump power was 0.0539 W as shown in Figure 7.14. When K_p = -0.01,

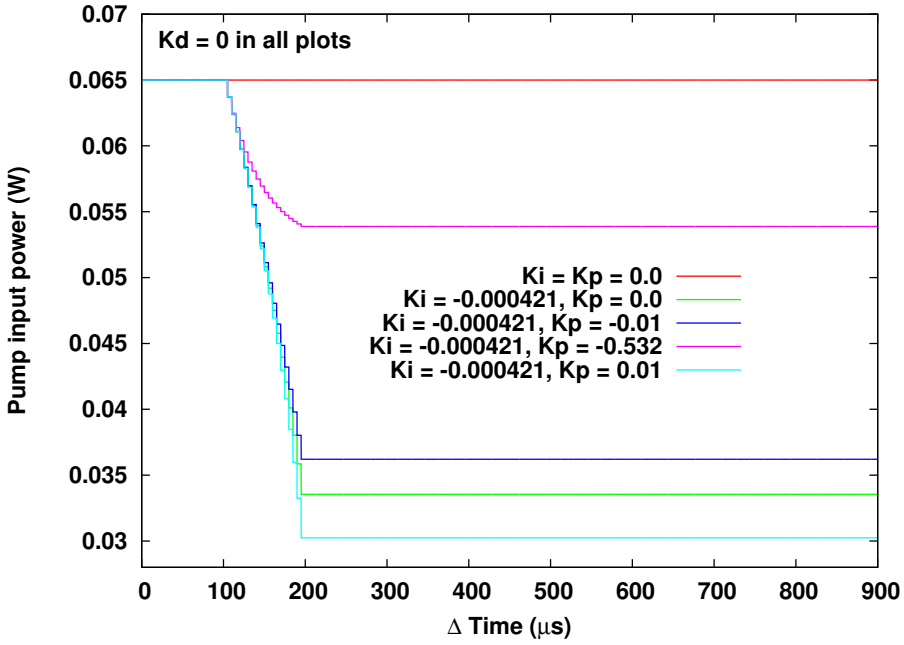

Figure 7.14: Pump input power using integral and proportional controllers, K_i = -4.21$\times 10^{-4}$, K_d = 0, K_p is varied as stated in the plot.

the power transient overshoot was 1.21 dB and the adjusted pump input power was 0.0363 W. It was conclude that the P-controller was not enhancing the transient overshoot nor the transient time which was previously tuned by I-controller.

With *the differential and proportional controllers*, K_i was assigned the value 0, and K_d was assigned -0.066, then K_p was tuned to different values to achieve better optimization in the power transient overshoot and total transient time than achieved earlier with the D-controller alone. We observed the power transient overshoot = 1.18 dB as shown in Figure 7.15 when K_p = 0 or K_p = -0.36 and the adjusted input pump power was 0.0337 W as shown in Figure 7.16. When K_p = -0.532 (which provides optimum power transient overshoot in P-controller), the power transient overshoot increases to 2.02 dB as shown in Figure 7.15 and the adjusted input pump power = 0.0539 W as shown in Figure 7.16. When K_p = -0.7, the power transient overshoot increases to 2.27 dB as shown in Figure 7.15 and the adjusted input pump power = 0.037 W as shown in Figure 7.16. We conclude that the power transient overshoot and total transient time are not optimized further by adding a P-controller to the D-controller.

A *different numbers of channels being dropping or adding was simulated using a P-controller*. It was observed that when 2, 4 and 7 out of 8 channels were dropped, K_p =

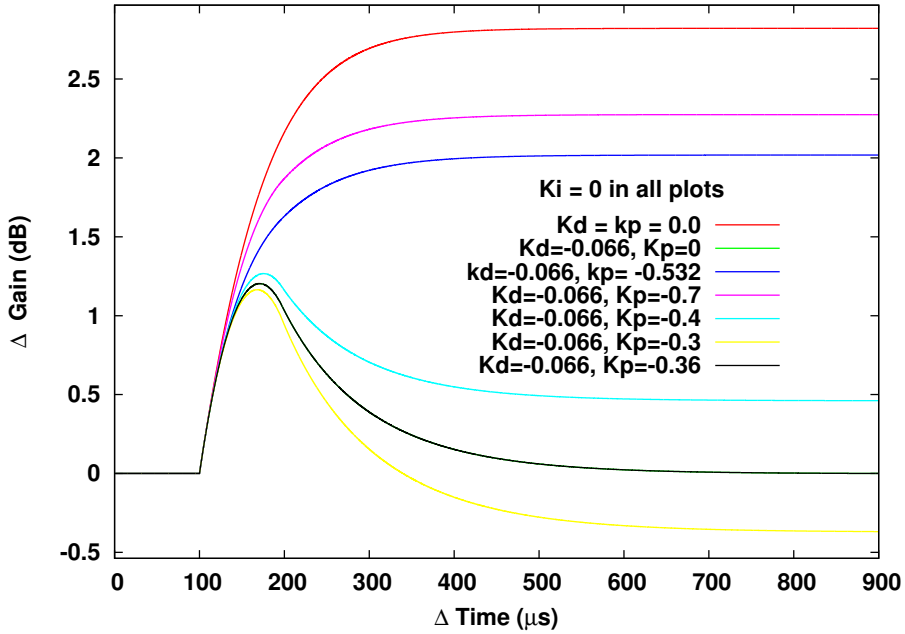

Figure 7.15: The output power transient of the probe channel using D-controller and P-controller, K_i = 0.0, K_d = -0.066, K_p was varied as stated on the plot.

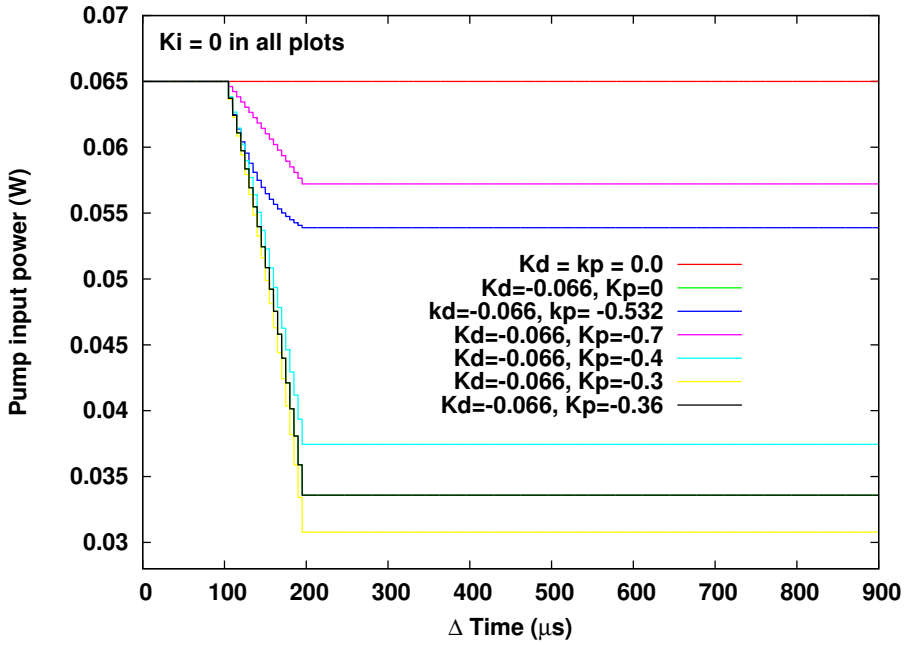

Figure 7.16: The pump input power using D- and P-controllers, K_i = 0.0, K_d = -0.066, K_p was varied as stated on the plot.

-0.6580, -0.5320, and -0.3733, the power transient overshoots were 0.75 dB, 1.79 dB, and 4.33 dB, the transient times were 350 μs, 550 μs, and 1650 μs, the power transient rise time were 78 μs, 80 μs, 92 μs, and the pump input powers were 0.0497 W, 0.0337 W, 0.0098 W respectively as shown in Figures 7.17 (a) and (b). We concluded that the suppressed power

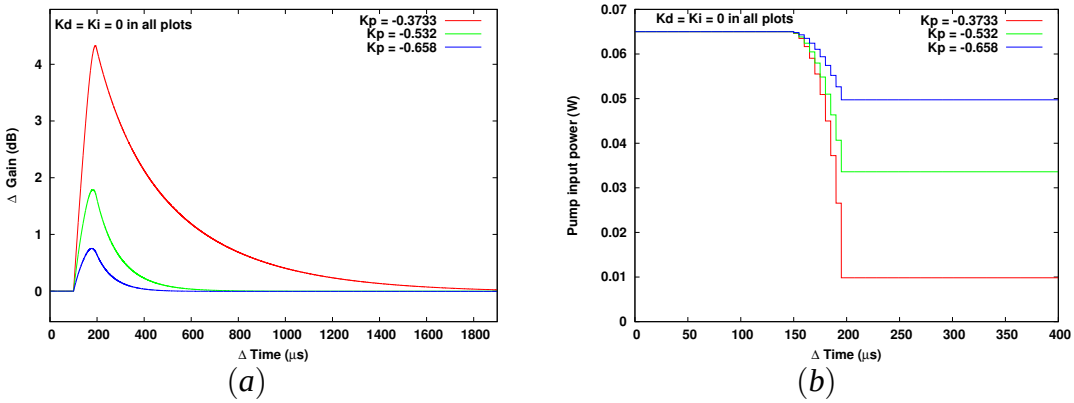

Figure 7.17: The power transient when 2, 4 and 7 channels out of 8 were dropped using the P-controller for suppressing the transient. K_p are -0.6580, -0.5320, and -0.3733 respectively. (a) Output power transient (dB) at probe channel of wavelength 1549.2 nm. (b) Input pump power (W) at wavelength of 980 nm.

transient is also increased as the number of dropped channels increased, this is why it is necessary to test the controller for the worst condition for this system, i.e. when 7 out of 8 channels (equivalent to nearly 90% of the system load) were dropped or added.

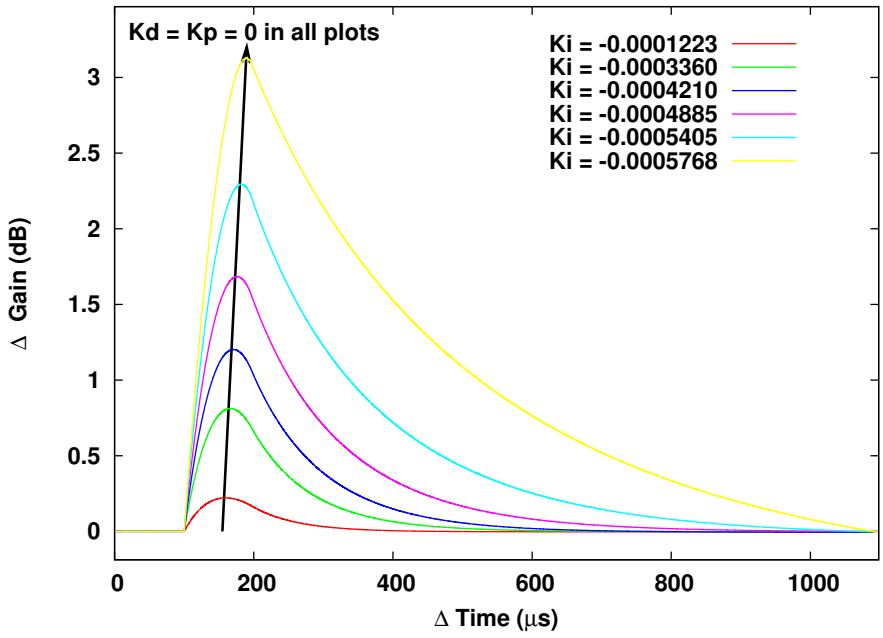

Figure 7.18: Suppressed power transient using I-controller, K_i = -1.223$\times 10^{-4}$ for one channel dropped (red), K_i = -3.360$\times 10^{-4}$ for three channels dropped (green), K_i = -4.210$\times 10^{-4}$ for four channels dropped (dark-blue), K_i = -4.88$\times 10^{-4}$ for five channels dropped (magenta), K_i = -5.405$\times 10^{-4}$ for six channels dropped (light-blue), K_i = -5.678$\times 10^{-4}$ for seven channels dropped (yellow).

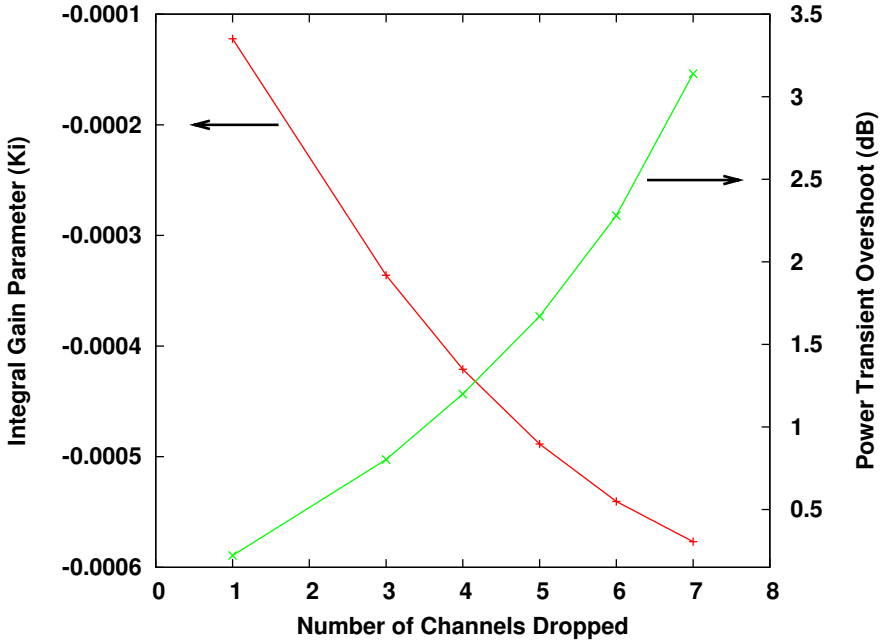

Figure 7.19: Different magnitudes for K_i and power transient overshoot as a function of number of dropped channels in the optical networks using the I-controller.

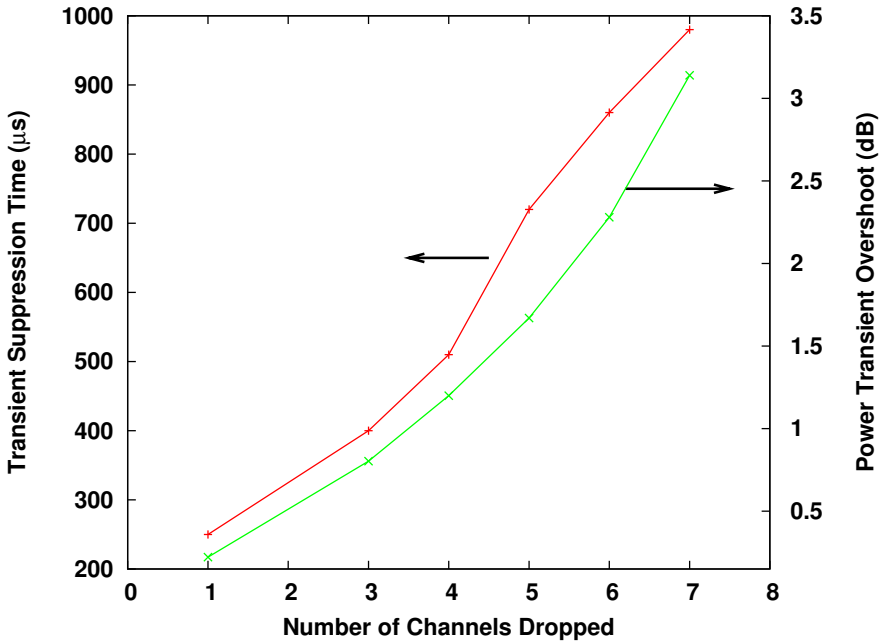

Figure 7.20: Different magnitude of power transient overshoots and transient time as a function of number of dropped channels in the network, using the I-controller.

We also *simulated different numbers of channels dropped or added using an I-controller*. The I-controller was chosen because the response of the D-controller is similar to that of the I-controller for power transient overshoot or undershoot and total transient time as shown in Figures 7.11 and 7.12. As can be seen from Figure 7.18, 1, 3, 4, 5, 6, 7 channels were

dropped and the magnitude of K_i was different for each number of dropped channels. It was observed that the magnitude of K_i was inversely proportional to the number of dropped channels, see Figure 7.19. It was also noticed that the power transient overshoot and total transient times were proportional to the number of dropped or added channels, as shown in Figure 7.20, and this is strongly related to the percentage of dropped or added input power to the EDFA. This is clear when we compare one channel failure with seven channels failure in Figures 7.19 and 7.20.

Optical Power Add/Drop Input	Channels Dropped	Overshoot power	Transient Suppression Time	Integral gain K_i
4.01 dBm	50%	1.18 dB	500 μs	-4.210$\times 10^{-4}$
5.70 dBm	75%	2.28 dB	900 μs	-5.405$\times 10^{-4}$
6.44 dBm	90%	3.14 dB	1000 μs	-5.726$\times 10^{-4}$

Table 7.1: The suppressed transient parameters while the pump input power was updated using the value of K_i given in column five.

Table 7.1 summaries the important factors of a controller considered by designers and manufacturers of PID controllers. Column two shows the percentage loading of the system, whereas columns three, four and five show important parameters: power transient overshoot, total transient times and integral gain parameters respectively. These parameters were measured to evaluate the efficiency of the controller performance.

We investigated the case of when five channels out of eight were dropped or added using I-controller. As can be seen in Figure 7.21, with K_i = -4.880$\times 10^{-4}$ for five channels dropped (dark-blue curve) the power transient overshoot = 1.68 dB, transient rise-time = 76 μs and the adjusted pump input power was 0.0256 W as shown in Figure 7.22. We applied K_i = -3.360$\times 10^{-4}$, as the control parameter for the case when three channels were dropped (red curve), we recorded that the power transient overshoot was 1.85 dB, transient rise-time was 86 μs and the adjusted pump input power was 0.0337 W. We also used K_i = -4.210$\times 10^{-4}$ as the control parameter when four channels were dropped (green curve), and we observed that the power transient overshoot was 2.08 dB, transient rise-time was 92 μs and the adjusted pump input power was 0.0416 W.

From above numerical simulation results, we concluded that neither the value of K_i used when three channels were dropped nor the value of K_i used when four channels were dropped

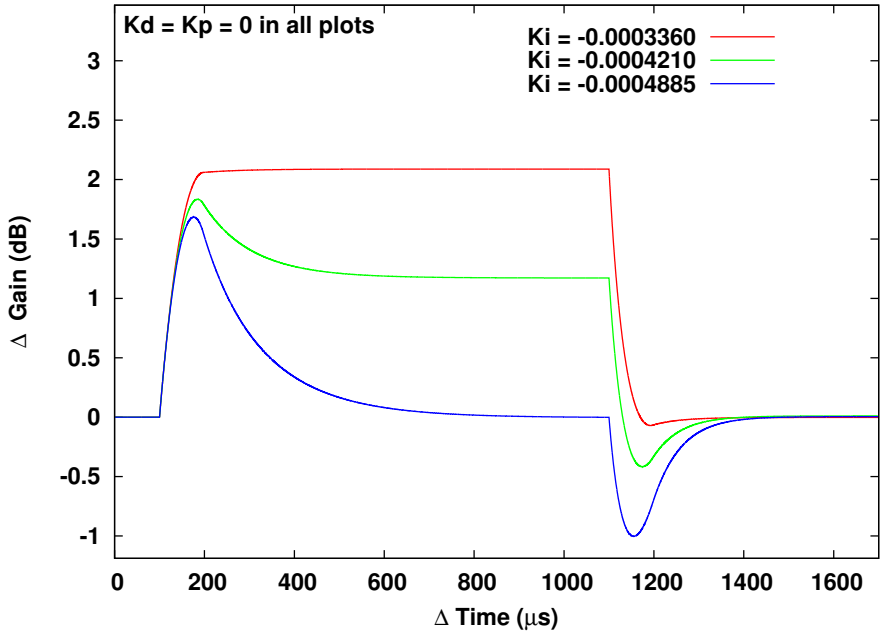

Figure 7.21: The suppressed power transient when dropping and adding of 5 channels using I-controller with: K_i = -3.360×10^{-4} (when three channels dropped (red)), K_i = -4.210×10^{-4} (when four channels dropped (green)), K_i = -4.88×10^{-4} (when five channels dropped (dark-blue)).

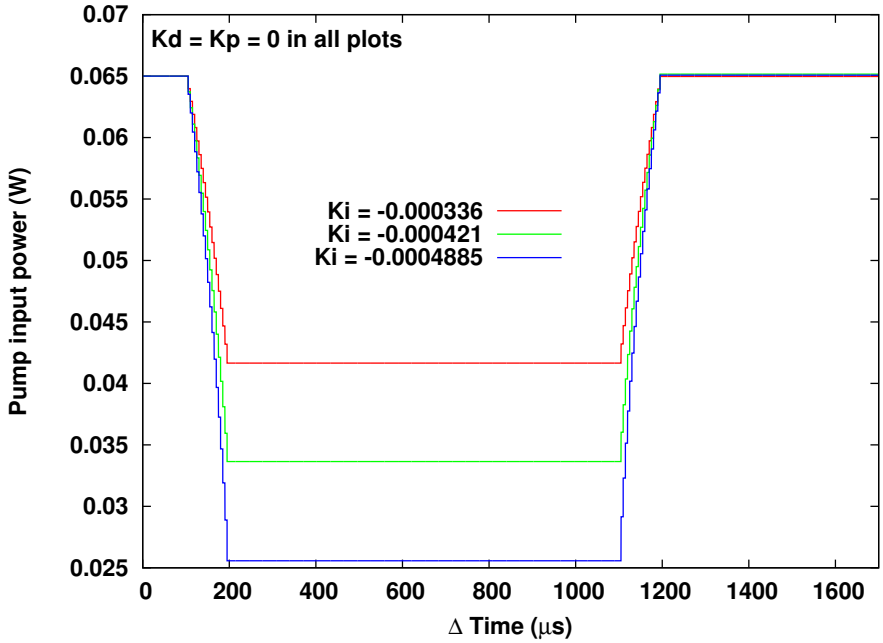

Figure 7.22: Pump input power when dropping and adding of 5 channels using I-controller with: K_i = -3.360×10^{-4}, K_i = -4.210×10^{-4}, K_i = -4.880×10^{-4}.

.

were suitable for use when five channels were dropped, see Figures 7.21 and 7.22. This

means there must be continuous adjustment for the gain parameters; matching each case. It should also be noted that the value of K_i to be used when channels are dropped will not be suitable for use when channels are added. For example, when five channels were dropped K_i-d = -4.880$\times 10^{-4}$, but when five channels were added K_i-a = 4.672$\times 10^{-4}$.

Moreover, if we choose a value for K_i-d (K_i at channels dropped) of -4.178$\times 10^{-4}$ which best stabilised and suppressed the output power transients when 4 channels were dropped, this would not be a suitable value for the recovery of the system if 2 or 7 channels were dropped as shown in Figure 7.23. This shows that one value of the controller gain parameter is not good for all situations.

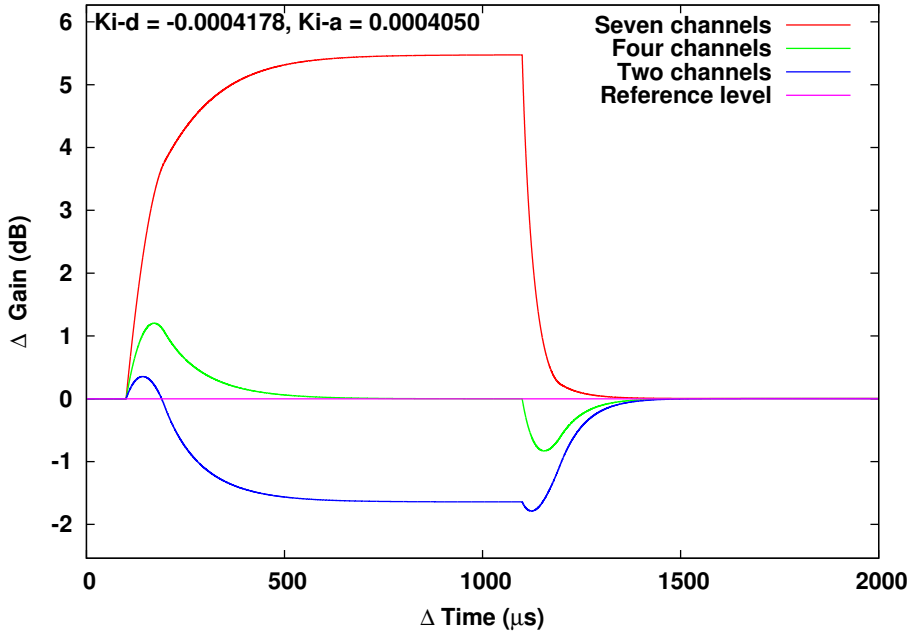

Figure 7.23: The suppressed output power transient when 2, 4 and 7 channels were dropped using value of K_i (K_i-d = -0.0004178, K_i-a = 0.0004050) which were parameters for the best recovery in the case of four channels dropped.

As mentioned the variation in the input power of the EDFA affects the gain parameters of the controller. The speed of variation of the input power as well as the modulation frequency of the input signal affects the gain parameters of PID controller, such as when the dropped-interval (the time interval used for dropping or adding channels) of the channels changed from 1 μs to 100 ns. Using the I-controller, which updated the pump power at regular intervals of 50 μs it was observed that at a dropped interval of 100 ns, K_i = -4.250$\times 10^{-4}$, and at a dropped interval of 1 μs, K_i = -0.421$\times 10^{-4}$, see Figure 7.24. The time-interval or speed at which the channels were dropped or added depended on the speed of the add/drop

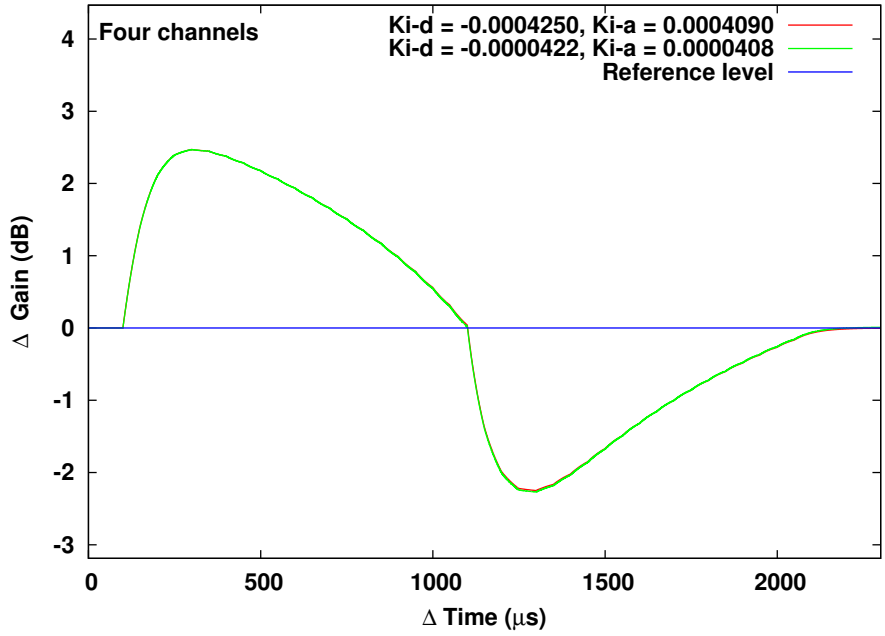

Figure 7.24: The suppressed power transient using I-controller, updating intervals of input pump power = 50 μs. For channel drop-interval of 100 ns, K_i-d = -4.250$\times 10^{-4}$, for channel drop-interval of 1 μs, K_i-d = -0.4220$\times 10^{-4}$.

multiplexer (ADM), or the speed of the link failure. Thus, we can conclude that the performance speed of the ADM will, in turn, affect the values of K_i that control transient power and restore gain to the reference level. The gradual dropping or addition of the channels is one of the techniques used for mitigating the power transient in surviving channels, this approach has been implemented in Chapter 6, and it clearly demonstrated the reduction of the power transient overshoot of the survived probe channel due to gradual dropping of the channels [167].

The modulation frequency affects the controller gain parameters because at very high frequencies the photons in a metastable level do not have sufficient time to regain their energy, so when channels were dropped or added in such circumstances the controller parameter will be different from the case where there was adequate time for photons to regain their original energy from the pump power provided. This was why transient undershoot values and transient fall times were different when the system was modulated at a frequency of 500 Hz than when modulated at 1 kHz.

From the above simulation cases, we concluded that it is necessary to optimise the parameters in columns three and four in Table 7.1 for trading of automatic gain controlled EDFA, and this is why they are the focus of attention by designers and manufacturers [176].

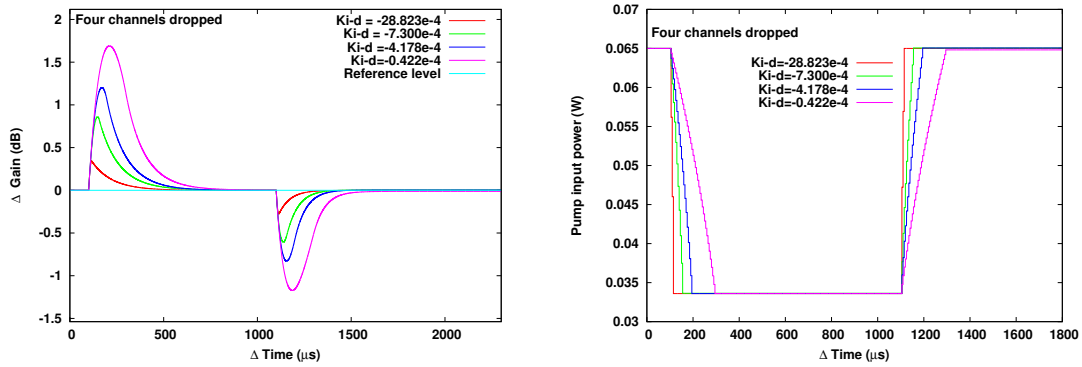

Figure 7.25: The suppressed power transient when the input pump power was updated using K_i = -28.823$\times 10^{-4}$, -7.300$\times 10^{-4}$, -4.178$\times 10^{-4}$, -0.422$\times 10^{-4}$ when four channels out of eight were dropped. (a) Output power transient (dB) at probe channel of wavelength 1549.2 nm. (b) Input pump power (W) at wavelength of 980 nm.

Nevertheless, when the input signal modulated frequency was set to 50, 20, 10 and 5 kHz, four out of eight channels were dropped, and the pump updating interval was 5 μs, then it was observed that for K_i =-28.823$\times 10^{-4}$, K_i = -7.300$\times 10^{-4}$, K_i = -4.178$\times 10^{-4}$, K_i = -0.422$\times 10^{-4}$ the transient overshoots were 0.34, 0.8, 1.2, 1.7 dB respectively, as shown in Figures 7.25 (a) and (b). The modulated frequency of the input signal represents the rate of the dropping or adding of channels. This is similar to the burst-ON and burst-OFF periods in packet switching optical networks, and this rate affects the value of K_i. Thus, using a PID controller for such a variable modulated frequency input signal is not practical because it requires readjusting gain parameters. This is the main issue if this PID controller is to be applied to packet switched optical networks especially with ATM-IP traffic which has the burst-ON and burst-OFF periods of Pareto distribution. This is discussed in Chapter 4.

Optical Power Add/Drop	Channels Dropped	Overshoot power	Undershoot power	Transient Suppression Time	Integral gain K_i
4.01 dBm	50%	0.34 dB	-0.28 dB	362 μs	-28.823$\times 10^{-4}$
5.70 dBm	75%	0.56 dB	-0.36 dB	672 μs	-39.30$\times 10^{-4}$
6.44 dBm	90%	0.67 dB	-0.37 dB	1000 μs	-43.65$\times 10^{-4}$

Table 7.2: Transient control parameters while the pump input power was updated using value of K_i given in column six.

Table 7.2 summaries the important factors for gain control using the value of K_i obtained

for an input signal modulation frequency of 50 kHz. Using a higher value of K_i than when the input signal was modulated at 1 kHz, gave a reduction in the number of updating cycles required to restore the gain to the reference level and reduced the transient power overshoot and undershoot.

In addition to the variation of the gain parameters (K_i, K_d and K_p) with the number of channels dropped or added, as reported by Pachnicke and et. al. [177,178] the cascaded EDFAs in WDM optical networks are not dependent on a single EDFA gain parameters tuning. The controller designer and manufacturer must take all these factors into consideration and, if they use an electronic controller because it is cheaper, they need to use a micro-controller programmed to take all these points into account [179]. The fast suppression of the transient overshoot or undershoot power and the total transient time are the most important considerations, and the developers must use all available optical technology for the design of the transient controller for EDFA.

It was conclude that in a PID controller, the total transient time and the transient overshoot were controlled by two terms: first, the updating interval (which is 5 μs in this application) of the pump input power by the controller; second, the magnitude of the gain parameters (K_i, K_d and K_p) that has been chosen to restore the probe channel gain to the reference level. We observed when four channels were dropped if the updated interval of the pump input power was 50 μs the suppressed power transient was 2.5 dB, while for an updating interval 5 μs for the pump input power, the suppressed power transient was 1.18 dB.

We report the optimised controller parameters under different operating conditions. We show for the first time to our knowledge the effect of modulation frequency, dropped or added speed, different numbers of channels affect on the value of the controller gain parameter for single EDFA.

7.5 Summary

The main idea presented here for mitigating the power transients phenomena, is to restore the gain to the level prior to the occurrence of the perturbation, as well as requiring the transient rise and relaxation times to be minimised, which are the main requirements from the automatic gain controller. The pump control technique, used in this work has the advantage

over other transient controlling techniques of avoiding unnecessary load on the network, which is one of the deficiencies of link control techniques. We used a pump controller to clamp the cross-gain saturation of the EDFA when four out of eight channels in the system were dropped or added.

The controller consisted of proportional, integral, and derivative (PID) controllers, with pump updating interval of 5 μs. First we tested the P-controller with four channels dropped out of the eight channels in the system, K_p was varied between 0.16 and -0.6 while $K_i = K_d =$ 0, and we concluded from the results of numerical simulation that the proportional controller model can provide clamping for the cross-gain saturation of EDFA, since it can restore the gain of the surviving channels to the reference value and it decreased the power transient overshoot from 2.8 dB to 1.79 dB in a transient time of 550 μs. The adjusted input pump power for achieving this target was 0.0337 W.

A second investigation used an integral controller with four channels dropped out of the eight channels in the system to clamp the cross-gain saturation of the EDFA. We simulated the response of the I-controller when K_i was varied from 1.0×10^{-4} to -6.0×10^{-4} while K_p $= K_d = 0$. We observed that when $K_i = -4.210\times10^{-4}$, the transient overshoot decreased from 2.8 dB to 1.18 dB and the gain relaxes to the reference level, 0 dB, at a transient time of 500 μs. The adjusted input pump power for achieving this target was 0.0337 W.

A third investigation used the derivative controller to clamp the EDFA cross-gain saturation with four channels dropped out of the eight channels in the system. We simulated the D-controller when K_d was varied from 0.02 to -0.07 while $K_p = K_i = 0$. We observed that when K_d = -0.066, the transient overshoot decreased from 2.8 dB to 1.18 dB and the gain relaxes to reference level, 0 dB, at a transient time of 500 μs. The adjusted input pump power for achieving this target was 0.0337 W.

From above we concluded that it is possible to use the P-controller or I-controller or D-controller alone to mitigate the power transient phenomenon in a saturated EDFA. However, the performance of I- and D-controllers is better than that of the P-controller since the power transient overshoot and the total transient time is less than for the P-controller.

A fourth investigation simulated the I-controller with P-controller, and the results of simulation were that the P-controller did not reduce the power transient overshoot nor the transient time which was previously attained by the I-controller alone. We also simulated

the D-controller with P-controller, and the simulation results predicted that adding the P-controller did not improve the power transient overshoot nor the power transient time which was previously provided by the D-controller alone. Thus, using each controller alone in gain-controlled/transient suppressed EDFA is more cost effective and design wise.

A fifth investigation considered numerical simulation of the link failure of different numbers of channels. It was predicted that the power transient that occurred when four (50%) of the input channels were dropped was lower than the power transient when six (75%) of input channels were dropped. We applied I-controller using K_i = -4.21$\times 10^{-4}$ when dropping 50% of input channels, and K_i = -5.405$\times 10^{-4}$ when dropping 75% of input channels. Thus, the power transient of the probe channel was reduced. However, the K_i for four channels dropped (50%) was different for the K_i for six channels dropped (75%). The difference in K_i, K_p or K_d magnitudes make a PID controller complicated to design and costly to manufactur since it requires tuning for different percentages of channels dropped or added. It was observed that the magnitudes of K_i varied inversely with number of dropped channels. The suppressed transient power controls the transient rise and relaxation times, and the suppressed transient power is controlled by the time interval used for updating the pump input power, thus if the updating time of the pump input power is reduced from 50 μs to 5 μs, the transient overshoot as well as transient time will be decreased. We observed when four channels were dropped if the updated interval of the pump input power was 50 μs the suppressed power transient was 2.5 dB, while if the updated interval of the pump input power was 5 μs, the suppressed power transient was 1.18 dB. Minimizing the power transient overshoot and transient time is a requirement of all transient controlling techniques. In the case of the pump power controller being used, it depends on the available state of art in the optic and electronic fields for optimising the transient power and time [180–182]. Thus, each EDFA in the physical layer requires an electronic or optical circuit of PID controller that clamps each EDFA gain and suppresses the power transient during cross-gain saturation.

Moreover, we observed that the speed of dropping or adding of channels is another important factor which affects the magnitudes of gain parameters (K_i, K_d and K_p) in controller design. For example, when dropping channels at a time interval of 100 ns, the transient overshoot and total transient time will different from when dropping channels at a time interval of 1 μs. Accordingly the PID parameters will be different for the same percentage of channels

dropped or added [169].

In addition to the above operating conditions, the modulated frequency of the input signal is also another operating condition that affects the gain parameters. It was observed that for K_i =-28.823$\times 10^{-4}$ the transient overshoot was 0.34 dB when the modulated frequency was 50 kHz, whereas for K_i = -7.300$\times 10^{-4}$ the transient overshoot was 0.80 dB when modulated frequency was 20 kHz. This shows that it is not possible to use gain-controlled and transient suppressed EDFAs designed for specific application in circuit switched networks for packet-switched networks. Therefore, the PID controllers will be required to be designed each for specific application or network requirements [131, 164, 166, 167, 180–183].

Nevertheless, some other deficiencies have been shown by researchers [177, 178] which are also related to the optimising of sets of parameters for the controller under different operating conditions. These research works indicate that the gain parameters for a single EDFA may not be optimal for cascaded EDFAs, and depend on the number of cascaded EDFAs, For example, the controller gain parameters for a set of 10 EDFAs will be different from that for a set of 18 EDFAs.

We report the optimised controller parameters under different operating conditions. We show for the first time, to our knowledge, the effect of modulation frequency, speed of dropping or adding different numbers of channels and their affect on the value of the controller gain parameters for a single EDFA.

Chapter 8

Conclusions and future work

8.1 Conclusions

One of the performance limitations to multi-wavelength routed WDM networks using EDFA chains is imposed by the power transients of the EDFA. The power transient phenomenon is a consequence of a network reconfiguration or a failure of a link in the circuit switched networks or is due to traffic patterns such as that of ATM-IP in the packet switched networks. These produce variations in the input signal power and these transfer to EDFA output as power or OSNR transients if the speed of variation of the EDFA input power is in a comparable range with the metastable state life-time (i.e. variation frequency is in a range of about 100 Hz). Power transients are bad for system performance, so we have investigated the magnitude and duration of power transients for different environments on the network.

In this work, the non-self-saturated (without ASE) and self-saturated (with ASE) C-band EDFA models have been validated. Then the models are used to build simulators to investigate the magnitude of the power transients and OSNR in cascaded C-band EDFA links in circuit-switched networks. In addition the power transients have been studied using ATM-IP traffic of Pareto and Poisson distributions in the packet-switched networks. We modelled the non-self-saturated gain-shifted C-band EDFA by variation in geometry parameters, such as effective area of fibre core and confinement factors of the C-band EDFA, then the simulator was built to investigate power transients in non-self-saturated gain-shifted C-band EDFA chains in the networks. These models have been built to study the power transients and

OSNR in the different environments of the networks.

Our simulation demonstrated the output power swings in single and cascaded EDFA links, while dropping and adding different numbers of channels in the circuit-switched networks. The scale used for comparison of power transient and OSNR time and rate is the 1 dB increase- and decrease-time (which is applied in the literature for comparing the time and rate of the power transients since 1 dB power swing is the limit margin of systems). The power swings (power transient overshoots) observed for non-self-saturated C-band EDFA, and the time required to limit the power transient to 1 dB, when two or seven channels were dropped were 1.132 dB and 8.2 dB and 122.1 μs and 13.8 μs, respectively. When EDFAs supported larger number of WDM channels in networks the transient power will be higher than 8 dB and transient time may fall below 10 μs. These transients affect system performance. Therefore, dynamic gain control of the EDFAs with fast response times will be necessary to control the signal power transients.

In our simulation for EDFA chains, When 4 out of 8 channels are suddenly dropped, the output of each EDFA in the chain drops almost by 30 mW and the power in each surviving channel then rises to the original channel power to conserve the saturated EDFA output power. Although the gain dynamics of an individual EDFA is not altered, the increase in channel power at the end of the system accelerates for longer EDFA chains, the accumulated effects of the EDFAs in the chain results in faster and faster power transients as the number of EDFAs in the chain increases. To avoid deteriorated performance in a large WDM optical network, the surviving channel power transients must be limited to certain values depending on the system margin. For instance, in certain networks, the power swing should be within 0.5 dB when channels are added and 1 dB when channels are dropped. From our simulation results, for a chain consisting of 30 EDFAs, the response times required in order to limit the power transients to 0.5 dB and 1 dB would be 5 and 10 μs, respectively. Our simulation results demonstrated that the automatic gain control scheme using pump control minimized the power swing from 2.8 to 1.18 dB using the update interval of 5 μs for pump power. Therefore, it is necessary to investigate the power transient in terms of power and time and then design a mitigating system to satisfy the margin limits of the system.

As we observed from our simulation results in Section 6.2.2, the low power levels could pass under the threshold of the receiver power and inadequate eye opening would indicate

this. Therefore, in this thesis we have focused on investigating the magnitude and speed of power and OSNR transients in EDFA chains. It was observed from our simulation results that the OSNR transient has the same behaviour as the output power transient but that the speed of the OSNR transients is slower than the output power transients. This behaviour is a consequence of the automatic control or self regulation of the gain saturated EDFAs. Moreover, it was observed that the power instability between surviving channels when transients occur was due to the instability at the first EDFA. The latter is also the result of the self regulating characteristic of gain saturated EDFAs in the network links. From our simulation results, as the number of EDFAs increases the rate of the optical power transient will also increase. This is due to fast power variation in the input of the cascaded EDFAs. Since very fast changes (Δ t $<<$ τ (metastable state life-time)) are irrelevant, the speed of variation of the EDFA input powers must be in a comparable range with $1/\tau$.

It was also observed from our simulation results that the OSNR decreases in the case of channel addition to the networks. In order to determine the result of power and OSNR transients over output system performance at the end of the cascaded EDFAs, the bit error rate of the output signal of the system is assessed. We observed that the OSNR(t) decreased by 5.5 dB at the output of thirty fifth EDFA in the chain due to the addition of four channels to the four existing channels, we observed from the OSNR versus BER curve that the BER can reach 10^{-8} for the mentioned OSNR(t) change. Thus, it is required that the OSNR(t) must not be decreased more than 3.5 dB at that EDFA during addition of channels to the network in order the BER can meet the experimental standard limit, 10^{-9}. For acceptable system performance, the BER is required to be $<< 10^{-9}$ [136].

To prevent performance penalties and to mitigate the power transient a gradual variation of the input power was investigated. Three intervals for the input power drop, 2, 5 and 10 μs were used for this investigation. It was observed that a more gradual input power variation decreased both the rate of the power transient evolution and the amplitude of the overshoot. In a link of 20 cascaded EDFAs, the power transient overshoots were 4.05, 3.8 and 3.55 dB respectively when the input signal dropped at 2, 5 and 10 μs, since input regulation can provide enough time for gain stabilisation. This technique is one for mitigating transients.

The effects of ATM-IP traffic on the power transients of C-band and gain-shifted C-band cascaded EDFAs were also studied. From our simulation results, a very fast power transient

occurs during the packet interval, and in consequence the last bits of the packet will have a lower gain than the initial bits. The time to restore its original power level depends on pump power. Therefore, it can be seen that the higher the peak power of the input packet, the more the power sag in the output power of packet. The gain dynamics can be very fast for a strong signal pulse due to the stimulated-emission avalanche depletion of the excited ions. Simulation results demonstrated that the packet peak power, burst-ON and burst-OFF periods affect the magnitude and time of power transients. These swings may deteriorate the system performance if they are outside the network margin.

Statistical analysis of the output power transients of each channel in the cascaded EDFAs using ATM-IP traffic of Poissonian distribution and truncated Pareto distribution was performed. The PDFs for poissonian distributed ATM/IP traffic are well characterised by Gaussian tails. Therefore, the performance of systems with Poissonian traffic can be performed on the assumption of Gaussian statistics. In contrast, the PDF of the output power transients using ATM-IP truncated Pareto distribution does not have a Gaussian profile. Therefore, estimating the performance of ATM/IP networks with Pareto traffic should not be performed on the assumption of Gaussian statistics.

In addition, the non-Gaussian PDFs have different means, standard-deviations and power swings after each EDFA in the network link, For channel 1 of CW signal, channel 2 and channel 3 of packetized traffic, the profile of the PDF of the output power transients, the mean increases for channel 1 along the cascaded EDFAs, the standard deviation and power swing also increase along the cascaded EDFAs in the link. It has been observed that the power swing in channel 1 for the burst-OFF period was 28 mW and in channel 2 and 3 for the burst-ON period were 18.2 and 17 mW, respectively at EDFA number five in the chain. If these power swings are not within the limit of the network margin, this will degrade the network performance. The amount of power swing in the gain saturated EDFAs chain is low in comparison with a small signal gain EDFAs chain and this was studied for links using Poisson traffic.

The gain-shifted C-band EDFA is also fed by ATM-IP packets which are Pareto distributed. Simulation results of the gain-shifted C-band EDFA showed that the PDFs have non-Gaussian distribution and their standard deviation and the power-swing increase along the cascaded EDFAs. However, the standard deviation and power swings are higher in gain-

shifted C-band EDFAs than in C-band EDFAs. This effect is due to the higher gain provided by the gain-shifted C-band EDFA over the C-band EDFA. The higher power transients deteriorate network performance if not within the network margin.

For estimating the power transient at the output of each EDFA in the link, the mean, standard deviation and power swing versus number of cascaded EDFAs have been plotted. The relation between the standard deviation or swing of the power transient and the number of amplifiers in the chain is linear after the second EDFA because the first EDFA as we mentioned earlier has different power transient compared to other EDFAs (second to fifth in our simulations) of the chain. Therefore, these plots were used in our approach (for the first time to the best of our knowledge) for estimating power transient in the longer EDFA chains (such as 50 or more EDFAs) than the one which is used in our simulations because the required time for simulation (mentioned in Chapter 5) is rather long.

The Pump control technique was examined for mitigating the power transient phenomena. Minimizing the power transient overshoot and transient time is a requirement of all transient controlling techniques. In the case of the pump power controller being used, it depends on the available state of art in the optic and electronic fields for optimizing the transient power and time. Thus, each EDFA in the physical layer requires an electronic or optical circuit of PID controller that clamps each EDFA gain and suppresses the power transient during cross-gain saturation. However, The PID techniques are designed for small signal variation conditions. If the channels dropped or added to the network potentially causes large signal variations and so we studied the PID controller under these conditions.

Moreover, we observed that the speed of dropping or adding of channels is another important factor which affects the magnitudes of the gain parameters (K_i, K_d and K_p) in the controller design. Accordingly the PID parameters will be different for the same percentage of channels dropped or added as mentioned in Chapter 7. In addition to the above operating conditions, the modulated frequency of the input signal is also another operating condition that affects the gain parameters. Therefore, the PID controllers will be required to be designed each for specific application or network requirements as mentioned in Chapter 7. We report the optimised controller parameters under different operating conditions. We show for the first time, to our knowledge, the effect of modulation frequency, speed of dropping or adding different numbers of channels and their affect on the value of the controller gain

parameters for a single EDFA. Therefore, the standard PID technique does not work well due to that the PID stabilization designed for small signal changes and can give unacceptable performance with large signal changes. This results shows that the investigation of large power transients in networks is an important factor in network design.

8.2 Future work

The behaviour of the dynamic evolutions of the optical power and OSNR transients for single EDFAs and chains of EDFAs have been examined, and it is now necessary to investigate the transmission impairments caused by signal power and OSNR variations at the input of the optically preamplified intensity-modulation direct-detector (IM/DD) receiver. The effect of mis-adjustment of the receiver threshold from its optimum position due to the power variations needs to be quantified in terms of the Q-factor deteriorations. The relation of the OSNR variations to the Q-factor penalty also needs to be studied. Analysis and understanding of the Q-factor penalty which depends on signal and receiver characteristics is important for optical network performance evaluation.

The transmission degradations caused by the optical power and OSNR transients can arise due to a number of reasons as discussed in Chapter 2. Large penalties can be caused by mis-adjustments of receiver decision threshold with respect to its optimum position. Power reduction of a channel is usually followed by OSNR reduction, which then impairs the receiver BER performance. In the case of large input power variations the surviving signal power may fall below the receiver sensitivity level or rise above the receiver saturation level.

Nonlinear effects which appear with increase of the optical power level can also cause severe degradations. The quantification of these effects is necessary in assessing the need for power transient protection in optical networks. Thus, the effects of nonlinearities, such as FWM, SPM, XPM and Inter-Modulation mixing (see Section 1.7.7) need to be added to the existing gain dynamic model, to give a more complete assessment of the effect of transients on transmission performance. It is possible to connect the existing simulator with a simulator that provides nonlinear transmission of light pulses in the optical fibre to add the effect of nonlinear terms to the computed power transients.

Channel protection is possible without adding any hardware to the physical layer, such as

the link control scheme mentioned in Section 1.9.2. It would be extremely useful to develop such a protection technique, compatible with both circuit-switched and packet-switched networks and capable of mitigating the effects of the power transients in all cases of the networks without being particular to a specific condition.

A C-band EDFA could be connected in parallel with a gain-shifted C-band EDFA to obtain a 2-stage EDFA dynamic model. This would be a good basis for developing an in-line amplifier because it would provide flat gain, wide C-band EDFA with minimum ASE noise because the gain-shifted C-band has the same EDF length as the C-band. It could provide low background loss.

Experimental verification of the results is required for determining the impact of the SHB on the accuracy of the model's predictions. The SHB can affect the accuracy of the model's predicted signal power transients. In optical networks which contain many tens of EDFAs, the effect of SHB is predicted to be significant when a large number of channels are dropped and the surviving channels occupy only a very small part of the gain spectrum of the EDFA, this prediction needs to be tested

When investigating the effect of ATM-IP traffic of truncated Pareto distribution on the power transients, the simulation was limited to three channels and a maximum of five EDFAs in a chain due to the long simulation run-time(i.e. simulation time takes around 80 days). To investigate power transients of 20 or more EDFAs in a chain could be achieved using parallel programming and multi-processor environments.

References

[1] R. Ramaswami and K. N. Sivarajan, *Optical Networks, A practical Perspective*. Second edition, Academic Press, ISBN: 1-55860-655-6, 2002.

[2] A. Tanenbaum, *Computer Networks*. Fourth edition, Prentice Hall PTR, ISBN:0-13-066102-3, 2002.

[3] F. Halsall, *Data Communications, Computer Networks and Open Systems*. Fourth edition, Addison-Wesley Publishing Company Inc., ISBN:0-201-42293-X, 1996.

[4] B. Mukherjee, *Optical Communication Networks*. McGraw-Hill Companies, Inc., ISBN: 0-07-044435-8, 1997.

[5] G. P. Agrawal, *Fiber-optic communication systems*. Third edition, John Wiley & Sons, ISBN:0-471-21571-6, 2002.

[6] P. C. Becker, N. A. Olsson, and J. R. Simpson, *Erbium-Doped Fiber Amplifiers, Fundamentals and Technology*. Lucent Technologies, ISBN:0-12-084590-3, 1999.

[7] D. R. Goff, *Reference Guide, A practical Guide to Communications Technology*. Third edition, ISBN:0-240-80486-4, 2002.

[8] E. Desurvire, *Erbium-Doped Fiber Amplifiers, Principles and Applications*. JOHN WILEY and SONS INC., ISBN: 0-471-58977-2, 1994.

[9] A. Bjarklev, *Optical Fiber Amplifiers:Design and System Applications*. Artech House Inc., ISBN: 0-89006-659-0, 1993.

[10] R. P. S. HiGHWAVE OPTICAL TECHNOLOGIES, “GILES Parameter for simulation of C-band and L-band EDFA Amplifier,” *22300 Lannion Cedex, France, Website:www.highwave-tech.com*, 2002.

[11] B. Pedersen, “Small-signal erbium doped fiber amplifiers pumped at 980 nm: a design study,” *Optic Quantum Electronic*, vol. S273, no. 26, 1994.

[12] W. Barnes, R. I. Laming, E. J. Tarbox, and P. Morkel, “Absorption and Emission Cross Section of Er^{3+} Doped Silica Fibers,” *IEEE Journal of Quantum Electronics*, vol. 27, pp. 1004–1010, April 1991.

[13] C. Incorporated, “Corning single-mode optical fiber SMF-28, Product information.” Corning Incorporated, www.corning.com/opticalfiber, 2002. http://www.photonics.byu.edu/FiberOpticConnectors.parts/images/smf28.pdf.

[14] D. I. 27042, “Cisco ONS 15400 Series: Calculating the Maximum Attenuation for Optical Fiber Links.” CISCO, 2005. http://www.cisco.com/en/US/products/hw/optical/ps2006/products-_tech_note09186a00800e6eeb.shtml.

[15] P. A. D. Sheet, “EDFA C-Band Pre-amplifiers, booster amplifiers, and in-line amplifiers Specifications.” RED-C Optical Networking. www.redcinc.com.

[16] P. A. white Paper, “Introduction to Optical Amplifiers.” Website of Red-C Optical Networks Ltd, 2010. www.red-c.net.

[17] P. A. white Paper, “Introduction to EDFA Technology .” Website of Red-C Optical Networks Ltd, 2009. www.red-c.net.

[18] P. M. Aljaff and B. O. Rasheed, “Design Optimization for Efficient Erbium-Doped Fiber Amplifiers,” *World Academy of Science, Engineering and Technology*, vol. 46, pp. 40–43, 2008.

[19] N. S. Bergano, *Undersea Communication System, chapter 4, Optical Fiber Telecommunication IVB Systems and Impairments*. Academic Press, ISBN: 0-12-395173-0, 2002.

[20] U. Black, *Optical Networks, Third generation Transport Systems*. Prentice-Hall PTR, ISBN:0-13-060726-6, 2002.

[21] S. S. Dixit, *IP Over WDM, Building the Next Generation Optical Internet*. John Wiley & Sons. Inc., ISBN: 0-471-21248-2, 2003.

[22] J. E. Berthold, *SONET and ATM*. chapter 2, Optical Fiber Telecommunication IIIA, Academic Press, ISBN: 0-12-395170-4, 1997.

[23] R. O. Onvural, *Asynchronous Transfer Mode Networks, Performance Issues*. Artech House, ISBN: 0-89006-804-6, 1995.

[24] D. K. (editor), *ATM Networks, Performance Modelling and Analysis*. Volume 3, Chapman & Hall, ISBN: 0421-80970-2, 1997.

[25] T. I. Association, "Category 5 - TIA's Glossary of Telecommunication Term."

[26] P. corp./White paper, "The Evolution of Copper Cabling Systems from Cat5 to Cat5e to Cat6," pp. 1–6, 2003.

[27] S. Kawanishi, H. Takara, K. Uchiyama, I. Shake, and K. Mori, "3 Tbit/s (160 Gbit/s19 channel) optical TDM and WDM transmission experiment," *Electronics Letters*, vol. 35, May 1999.

[28] I.-T. S. Groups, "Optical transport networks and access network infrastructures," 2010. http://www.int/net/ITU-T, (ITU-T G.652,.

[29] C. R. Giles and M. Spector, "The Wavelength Add/Drop Multiplexer for Lightwave Communication Networks," *Bell labs Technical Journal*, vol. 4, pp. 207–229, January-March 1999.

[30] M. M. G. W. Z. S. M. Y. S. Li, B. Memon, "Optical static random access memory cell using an integrated semiconductor ring laser," *Photonics in Switching. PS'09. International Conference on*, pp. 1 – 2, 15-19 September 2009.

[31] B. A.-R. M. J. K. Premadi, A. Ng, "Real Time Optical Network Monitoring and Surveillance System," *Computer Technology and Development. ICCTD'09. International Conference on*, pp. 311 – 314, 13-15 NOVEMBER 2009.

[32] M. Horowitz and C. R. Menyuk, “Modeling the Saturation Induced by Broad-Band Pulses Amplified in an Erbium-Doped Fiber Amplifier,” *IEEE Photonics Technology Letters*, vol. 11, pp. 1235–1237, October 1999.

[33] G. P. Agrawal, *Lightwave Technology: Telecommunication Systems*. John Wiley & Sons, Inc., 2005.

[34] A. Ghatak and K. Thyagarajan, *Introduction to Fiber Optics*. Cambridge University Press, ISBN: 0 521 57785 3, 1998.

[35] B. L. Kasper and Y. C. O. Mizuhara, *Optical Fiber Telecommunication IVA Components*, pp. 784–851. T. Li, Academic Press, ISBN: 0-12-395172-0, 2002. High Bit-Rate receivers, transmitters, and Electronics, chapter 16.

[36] O. F. Technology, “System performance, fiber dispersion,” 2010.

[37] O. F. Technology, “Components, laser-diodes,” 2010.

[38] J. M. Senior, *Optical Fiber Communications Principles and Practice*. Prentice Hall International Series in Opto-electronics, Second edition, ISBN: 0-13-635426-2, 1992.

[39] L. Thylen, U. Westergren, P. Holmstrom, R. Schatz, and P. Janes, *Recent Developments in High-speed Optical Modulators*, vol. ISBN: 978-0-12-374171-4. Elsevier Inc., 2008. ISBN: 978-0-12-374171-4.

[40] D. R. Paschotta, “Effective Refractive Index: Correcting a Common Belief encyclopedia articles on effective refractive index.” The Photonics Spotlight, RP Photonics Consulting GmbH, 2007. http://www.rp-photonics.com/effective_refractive_index.html and http://www.rp-photonics.com/spotlight_2007_10_07.html.

[41] G. Bosco and P. Poggiolini, “On the accuracy of the Q-parameter to assess BER in the numerical simulation of optical DPSK systems,” *Proceedings of ECOC, paper Th2.3.5*, pp. 970–971, 2003.

[42] N. S. Bergano, F. W. Kerfoot, and C. R. Davidsion, “Margin measurements in optical amplifier system,” *Photonics Technology Letters*, vol. 5, pp. 304–306, March 1993.

[43] L. Gillner, “Transmission limitations in the All-Optical Network,” *ECOC 1996 Conference Proceedings, Paper WeB.2.2, OSLO, Norway*, September 1996.

[44] V. TECHNOLOGIES, “Fiber Optic Cable Plant Link Loss Budget Analysis,” 2010.

[45] S. TAKAOKA, F. OHKUBO, K. UCHIYAMA, K. KUNITAKE, C. TEI, T. KATO, T. OKUNO, M. TANAKA, and H. TAKAYANAGI, “Next Generation Non-Zero Dispersion Shifted Optical Fiber PureMetro for DWDM and Full Spectrum CWDM Systems,” *SEI TECHNICAL REVIEW*, pp. 95–98, JUNE 2002.

[46] C. W. Thiel, “Four-wave mixing and its applications.”

[47] D. N. et al., “Efficient high-power generation of visible and mid-infrared light by degenerate four-wave-mixing in a large-mode-area photonic-crystal fiber,” *Opt. Letter*, vol. 34, no. 22, p. 3499, 2009.

[48] M. J. Connelly, *Semiconductor Optical Amplifiers*. Springer-Verlag, ISBN:0-792-37657-9, 2002.

[49] A. J. S. K. Rottwitt, *Raman Amplification in Lightwave Communication Systems, Optical Fiber Telecommunications IVA Components*, pp. 213–257. Academic Press, 2002.

[50] I. Kaminow and T. L. Koch, *Solitons in High Bit-Rate, Long-Distance Transmission, Optical Fiber Telecommunication IIIA.* Academic Press, ISBN: 0-12-395170-4, 1997.

[51] J. F. M. et al., “Efficient High Power, High Gain, Erbium Doped Silica Fiber Amplifier,” *Electronics Letters*, vol. 26, no. 14, pp. 1038–1039, 1990.

[52] A. K. Srivastava and Y. Sun, “Advances in Erbium-doped Amplifiers,” *Optical Fiber Telecommunication IVA, edited by I.P. Kaminow and T. Li, Academic Press*, pp. 174–212, chapter 4, 2002. ISBN: 0-12-395172-0.

[53] D. Bayart, “Erbium-doped and Raman fiber amplifier,” *Optical Telecommunications, C.R. Physique 4*, pp. 65–74, 2003.

[54] W. J. Miniscalco, “Erbium-Doped Glasses for Fiber Amplifiers at 1500 nm,” *Journal of Lightwave Technology*, vol. 9, pp. 2234–2250, February 1991.

[55] M. E. S. Muhyaldin and K.J.Blow, “Modeling and Analysis of High Performance L-band Erbium-Doped Fiber Amplifier (EDFA),” *NLGW, Dresden, Germany*, 2005.

[56] C. R. Giles, E. Desurvire, and J. R. Simpson, “Transient Gain and Cross-talk in Erbium-doped Fiber Amplifier,” *Optics Letters*, vol. 14, no. 16, pp. 880–882, 1989.

[57] A. K. Srivastava and et al., “Fast Gain Control in Erbium-doped Fiber Amplifiers,” *Proceeding on Optical Amplifiers and their Applications, post deadline paper PDP4*, 1996.

[58] A. K. Srivastava and et al., “Fast-Link Control Protection of Surviving Channels in Multi-Wavelength Optical Networks,” *IEEE Photonics Technology Letters*, vol. 9, pp. 1667–1669, December 1997.

[59] A. K. Srivastava, J. L. Zykind, Y. Sun, and et al, “EDFA Transient Response to Channel Loss in WDM Transmission System,” *IEEE Photonics Technology Letters*, vol. 9, pp. 386–388, March 1997.

[60] V. Mehta, “EDFA ALL-Optical Gain Control Methodologies,” *ECE1654 Term Paper*, April 2003.

[61] M. Karasek and J. A. Valles, “Analysis of Channel Addition/Removal Response in All-Optical Gain-Controlled Cascade of Erbium-Doped Fiber Amplifiers,” *Journal of Lightwave Technology*, vol. 16, no. 10, pp. 1795–1803, 1998.

[62] M. Karasek and J. C. van der Plaats, “Analysis of Dynamic Pump-Loss Controlled Gain-Locking System for Erbium-Doped Fiber Amplifiers,” *IEEE Photonics Technology letters*, vol. 10, August 1998.

[63] E. D. Desurvire and e. a. M. Zirngibl, “Dynamic Gain Compensation in Saturated Erbium-Doped Fiber Amplifiers,” *IEEE Photonics Technology Letters*, vol. 3, pp. 453–455, May 1991.

[64] C. Dimopoulos and D. Simeonidou, “Dynamic performance evalution in WDM Trunk and Branch Networks incorporating 1:N wavelength protection,” *OFC ’2000 Technical Digest Baltimore, Maryland*, vol. paper ThD2, March 2000.

[65] J. Jackel and D. Richards, "All-Optical Stabilization of Cascaded Multi-Channel Erbium-doped Fiber Amplifiers with Changing Numbers of Channels," *OFC'97 Technical Digest, Dallas, TX*, pp. 84–85, 1997.

[66] M. Zirngibl, "Gain Control in Erbium-Doped Fiber Amplifier by an all-Optical Feedback Loop," *Electronic Letters*, vol. 27, pp. 560–561, 1991.

[67] G. . Luo and e. a. J. L. Zyskind, "relaxation Oscillations and Spectral Hole Burning in Laser Automatic Gain Control of EDFAs," *OFC97 Technical Digest, Dallas, TX*, pp. 130–131, February 1997.

[68] B. Landousies and e. a. T. Georges, "Low Power Transient in Multichannel Equalized and Stabilized Gain Amplifier Using Passive Gain Control," *Electronic Letter*, vol. 32, no. 20, 1996.

[69] L. Pavel, "Control Design for Transient power and Spectral Control in Optical Communication Networks," *in Proc. IEEE Conference on application*, pp. 1–8, 2003.

[70] R. Olivares and J. R. Souza, "A Comparative Study of Techniques to Control Power Transients in Optical WDM Networks," *10th European Conference on Networks and Optical Communications- NOC2005*, pp. 485–492, July 2005.

[71] C. Dimopoulos and D. Simeonidou, "Pilot tone interaction with transient suppression control scheme in chains of EDFAs," *Proceedings of Networks and Optical Communications Conference (NOC) 2000,Stuttgart, IOS Press, Germany*, vol. 1, (WDM and Photonic Networks), pp. 27–34, 2000.

[72] Y. Taing and L. Pavel, "EDFA H_∞ Controller for Suppression of Power Excursions Due to Pilot Tones and Network Traffic," *IEEE PHOTONICS TECHNOLOGY LETTERS*, vol. 18, no. 18, pp. 1916–1918, 2006.

[73] T. Jackson, M. Lee, T. Hahn, W. Lin, R. Wolff, B. Mumey, and K. Repasky, "EDFA Transient Reduction using Power Shaping," *Proceedings of the Eighth IASTED International Conference - actapress.com(USA)*, pp. 208–212, 2008.

[74] Y. Sun, G. Luo, J. Zyskind, A. A. M. Saleh, A. K. Srivastava, and J. W. Sulhoff, "Model for Gain Dynamics in Erbium-Doped Fiber Amplifiers," *Electronics Letters*, vol. 32, no. 16, pp. 1490–1491, August 1996.

[75] A. A. M. Saleh and et al, "Modeling of Gain in Erbium-doped Fibre Amplifier," *IEEE Photonics Technology Letter*, vol. 2, pp. 714–717, 1990.

[76] E. Desurvire and D. B. et al, *Erbium-Doped Fiber Amplifiers: Device and System Developments*. Johns Wiley and Sons, Inc, New York,, 2002.

[77] J. L. Zyskind and e. a. J.A. Nagel, *Erbium-Doped Fiber amplifiers for Optical Communications, Optical Fiber Telecommunication IIIB.*

[78] C. R. Giles and E. Desurvire, "Modelling Erbium-Doped Fiber Amplifiers," *Journal of Lightwave Technology*, vol. 9, pp. 271–283, February 1991.

[79] J. R. Simpson, L.F.Mollenauer, and e. a. N.A.Olsson, "Performance of a Distributed Erbium-Doped Dispersion-Shifted Fiber Amplifier," *Journal of Lightwave Technology*, vol. 9, pp. 228–233, February 1991.

[80] M. Bolshtyansky, "Theory, Simulation, and Measurements for New Model of Spectral Hole Burning in EDFA," *Conference on Optical Fiber Communication, Technical Digest Series*, vol. V86, pp. 604–605, 2003.

[81] V. Chernyak and L. Qian, "Modeling High-Concentration L-Band EDFA at High Optical Power Based on Inversion Function," *IEEE Journal of Selected Topics in Quantum Electronics*, vol. 8, pp. 569–574, May-June 2002.

[82] C. Giles and E. Desurvire, "Propagation of signal and noise in concatenated erbium-doped fiber optical amplifiers," *Journal of lightwave technology*, vol. 9, no. 2, pp. 147 – 154, 1991.

[83] S. Yamashita1 and T. Okoshi1, "Suppression of common-mode beat noise from optical amplifiers using a balanced receiver," *Electron. Letter*, vol. 28, p. 19701972, October 1992.

[84] A. Bahrampoura, M. Mahjoeib, and A. Rasoulib, "A theoretical analysis of the effects of erbium ion pair on the dynamics of an optical gain stabilized fiber amplifier ," *Optics Communications*, vol. 265, pp. 283–300, September 2006.

[85] E. A. Alireza Hassani and F. E. Seraji, "Intensity based erbium distribution for erbium doped fiber amplifiers," *Physics and Astronomy, Optical and Quantum Electronics*, vol. 39, pp. 35–50, 27 March 2007.

[86] R. M. Jopson and A. A. M. Saleh, "Modeling of Gain and Noise in Erbium-doped fiber Amplifier," *in Fiber Laser Sources and Amplifiers III, Proceeding SPIE*, vol. 1581, pp. 114–119, 1991.

[87] T. Goerges and E. Delevaque, "Analytic Modelling of High-Gain Erbium-Doped Fiber Amplifiers," *Optics letters*, vol. 14, pp. 1113–1115, August 1992.

[88] L. B. A. Bononi and L. A. Rusch, "Using SPICE to simulate gain dynamics in doped-fiber amplifier chains," *presented at OFC '98, workshop 204, Transmission modelling simulation tools, San Jose, CA*, 1998.

[89] A. Rieznik, "Analytical solution for the dynamic behavior of erbium-doped fiber amplifiers with constant population inversion along the fiber," *Optical Society of America*, vol. 21, October 2004.

[90] J. R. Simpson, "Fabrication of Rare-Earth Doped Glass Fiber. In Fiber Laser Sources and Amplifiers II," *2.SPIE Proceeding, Bellingham, WA:SPIE*, no. 1171, 1990.

[91] D. J. Digiovanni, "Fabrication of Rare-Earth Doped Optical Fiber. In Fiber Laser Sources and Amplifiers II," *2.SPIE Proceeding, Bellingham, WA:SPIE*, no. 1373, 1991.

[92] M. Shimizu and e. a. M. Yamada, "Erbium-doped amplifier s with an extremely high gain coefficient of 11.0 dB/mW," *Electronics Letters*, vol. 26, no. 20, pp. 1641–1643, 1990.

[93] T. Kashiwada and e. a. M. Shigematsu, "Erbium-doped fiber amplifier pumped at 1.48 μm with extremely high efficiency," *Electronics Letters*, vol. 3, no. 8, pp. 721–723, 1991.

[94] C. R. Giles, E. D. Desurvire, and e. a. J. R. Talman, "2-Gbit/s Signal Amplification at λ = 1.53 μm in an erbium-doped single-mode fiber amplifier," *IEEE Journal of Lightwave Technology*, vol. 7, pp. 651–656, April 1989.

[95] V. J. Mazurczyk and J. L. Zykind, "Polarization dependent gain in erbium-doped amplifiers," *Photonics Technical Letter*, vol. 6, no. 5, pp. 616–618, 1994.

[96] e. a. E. D. Desurvire, C. Randy Giles, "Gain Saturation Effects in high-speed multichannel erbium-doped fiber amplifiers at λ = 1.53 μm," *IEEE Journal of Lightwave Technology*, vol. 7, no. 12, pp. 2095–2104, 1989.

[97] Y. Sun, A. M. Saleh, J. L. Zyskind, D. L. Wilson, and A. Srivastava, "Time Dependent Perturbation Theory and Tones in Cascaded Erbium-doped Fiber Amplifier Systems," *Journal of Lightwave Technology*, vol. 15, pp. 1083–1087, July 1997.

[98] T. Chakma and D. Knipp, "Optical Signal to Noise Ratio (OSNR)." International University Bremen, 2005. International University Bremen, Course: Photonics and Optical Communication, http–www.faculty.iu-bremen.de-dknipp-c320352-Projects-PresentationsTC

[99] M. Abramowitz and M. W. Davidson, "Microscope Objectives: Numerical Aperture and Resolution." Wikipedia, April 22, 2004.

[100] E. D. Desurvire, "Analysis of Transient Gain Saturation and Recovery in Erbium-Doped Fibre Amplifiers," *IEEE Photonics Technology Letters*, vol. 1, pp. 196–199, August 1989.

[101] Y. Sun and A. Srivastava, "Dynamic Effects in Optically Amplified Networks," *Conference on Optical Amplifiers and their Applications, OAA 97, Victoria, Canada*, vol. 16, pp. 333–353, July 1997.

[102] C. R. Giles and E. Desurvire, "Propagation of Signal and Noise in Concatenated Erbium-doped Fiber Optical Amplifiers," *IEEE Journal of Lightwave Technology*, vol. 9, pp. 147–154, February 1991.

[103] Y. Maigron and et al, "Analysis of a Cascaded EDFA Link Time Behaviour," *Proceeding ECOC'92, Germany*, Paper WeP2, September 1992.

[104] C. Dimopoulos, D. Simeonidou, and et al., "Fast Optical Transient in Long-Haul WDM Fiber Networks: Is Optical Transient Suppression Always Necessary?," *Proceeding Networks and Optical Communication Conference (NOC 99) Netherlands*, pp. 125–132, IOS Press, 1999.

[105] Y. Sun, A. Srivastava, J. L. Zyskind, and et al, "Fast Power Transients in WDM Optical Networks with Cascaded EDFA's," *Electronics Letters*, vol. 33, pp. 313–314, February 1997.

[106] J. L. Zyskind, Y. Sun, and et al., "Fast Power Transients in Optically Amplified Multiwavelength Optical Networks," *OFC'96, Technical Digest, San Jose*, Paper PD31, 1996.

[107] A. Bononi and L. A. Rusch, "Doped-Fiber Amplifier Dynamics: A System Perspective," *Journal of Lightwave Technology*, vol. 16, pp. 945–956, May 1998.

[108] M. Menif, M. Karasek, K. Fouli, and L. A. Rusch, "Cross-gain Modulation Effect on the Behaviour of Packetized Cascaded EDFAs," *Journal of Optics: Pure and applied Optics*, vol. 3, pp. 210–217, 2001. www.iop.org/Journals/oa.

[109] A. Bononi, L. Tancevski, and L. Rusch, "Large Power Swings in Doped-Fiber Amplifiers with Highly Variable Data," *IEEE Photonics Technology Letters*, vol. 11, no. 1, pp. 131–133, 1999.

[110] B. I. L. M. Kopeetsky, Y.Ben-Ezra, "Influence of ATM/IP Traffic on Power Transients in the Optical Networks," *Journal of Optical Networks*, vol. 4, pp. 82–91, 2005.

[111] W. E. Leland and et al, "On the Self-similar Nature of Ethernet Traffic," *IEEE/ACM Trans. networking*, vol. 2, no. 1, pp. 1–15, 1994.

[112] J. Beran, M. S. T. R. Sherman, and W. Willinger, "Long-range Dependence in Variable-bit-rate Video traffic," *IEEE Trans. Communication*, vol. 43, pp. 1566–1579, 1995.

[113] L. Tancevski, A. Bononi, and L. A. Rusch, "Output Power and SNR Swings in Cascades of EDFA's for Circuit- and Packet-Switched Optical Networks," *Journal of Lightwave Technology*, vol. 17, pp. 733–742, May 1999.

[114] L. Tancevski, A. Bononi, and L. A. Rusch, "Large Power and SNR Swings in Cascaded EDFAs Carrying Highly Variable Traffic," *ECOC'98 Conference publication*, pp. 553–554, Spain, 1998.

[115] S. A. T. W. H. Press, *Numerical Recipes in C++, The Art of Scientific Computing*. Cambridge University Press, ISBN:052175033 4, 2002.

[116] D. Yang.

[117] H. M. Antia, *Numerical Methods for Scientists and Engineers*. Second edition, Birkhause Verlag, 2002. ISBN: 3-7643-6715-6.

[118] J. L. Zachary, *Introduction to Scientific Programming, Computational Problem Solving Using: Maple and C, Mathematica and C.* http://www.cs.utah.edu/ zachary/IntroSciProg.html-online, Springer-Verlag New York, Inc., 1996. ISBN 0-387-94630-6.

[119] L. J. e. a. Y. Sun, "Analytical Formula for the Transient Response of Erbium-doped fiber Amplifiers," *Applied Optics*, vol. 38, pp. 1682–1685, 20 March 1999.

[120]

[121] I. T. Mukai and etal, "Signal gain saturation in two channel common amplification using a 1.5 μm InGaAsP travelling-wave laser amplifier," *Electronics letters*, vol. 23, pp. 396–397, 1987.

[122] A. H. M. J. Pettitt and et a, "Crosstalk in Erbium doped fibre amplifiers," *Electronics letters*, vol. 25, no. 6, pp. 416–417, 1989.

[123] e. a. R. I. Laming, L. Reekie, "Multichannel crosstalk and pump noise characterisation of Er^{3+}-doped fiber amplifier pumped at 980 nm," *Electronics letters*, vol. 25, no. 7, pp. 455–456, 1989.

[124] B. J. J. Nilsson and et al, "Performance reduction and design modification of erbium-doped fibre amplifiers resulting from pair-induced quenching," *IEEE Photonics Technology Letters*, vol. 5, pp. 1427–1429, December 1993.

[125] M. Y. H. Ono and et al, "1.58 μm band gain flatted erbium-doped fiber amplifiers for WDM transmission systems," *Journal of lightwave Technology*, vol. 17, pp. 490–496, March 1999.

[126] N. E. H. Taga and et al, "Impact of polarization hole burning effect in transoceanic wavelength division multiplexed systems," *OFC 99 technical Digest, paper WE6, San Diego, California*, February 1999.

[127] F. A. Flood, "Impact of inhomogeneous broadening on L-band EDFAs," *ECOC'99 Conference Proceeding, Nice, France*, vol. 11, pp. 148–149, September 1999.

[128] F. A. Flood, "L-band erbium-doped fiber amplifiers," *OFC'2000 Technical Digest Baltimore, paper WG1, Maryland*, March 2000.

[129] A. S. Y. Sun, J. L. Zyskind, "Average Inversion Level, Modelling, and Physics of Erbium-doped Fiber Amplifiers," *IEEE Journal of selected Topics In Quantum Electronics*, vol. 3, pp. 991–1007, August 1997.

[130] A. J. L. A. T. Wu, "Efficient Multiwavelength Dynamic Model for Erbium-doped Fiber Amplifiers," *IEE Journals of Quantum Electronics*, vol. 34, pp. 1325–1331, August 1998.

[131] M. Nakamura, Y. Imai, Y. umeda, J.Endo, and Y. Akatsu, "A Burst-mode Optical Receiver with High Sensitivity Using a PIN-PD for a 1.25 Gbit/s PON System," *OSA*, vol. OFM6, no. 060.2340.060.4510, 2005.

[132] K. Schneider and H. Zimmermann, "Highly sensitive Wide-dynamic Range Optical Burst-mode Receivers for Ultra Fast Gain switching," *Analog Intergr Circ Sig Process*, vol. 49, pp. 141–149, 2006.

[133] M. I. Products, "Accurately Estimating Optical Receiver Sensitivity," *Application Note: HFAN-3.0.0, Re.1*, pp. 1–6, April 2008.

[134] M. S. Taqqu, W. Willinger, and R. Sherman, "Proof of a Fundamental Result in Self-similar Traffic Modelling," *Computer communication Review*, vol. 27, pp. 5–23, April 1997.

[135] O. N. A. Erramili and W. Willinger, "Experimental Queuing Analysis with Long-range Dependent Packet Traffic," *IEEE/ACM trans. networking*, vol. 4, pp. 209–223, April 1996.

[136] V. N. I. C. S. C. E. (SCEs), "Cisco Visual Networking Index: Usage Study." CISCO, 2010. http://www.cisco.com/en/US/solutions/collateral/ns341/ns525/ns537/ns705/Cisco_VNI_Usage_WP.html.

[137] L. K. Tee, "Packet Error Rate and Latency Requirements for a Mobile Wireless Access System in an IP Network," *Vehicular Technology Conference, VTC-2007*, pp. 249–253, Oct. 2007.

[138] J. E. Flood, *Telecommunications Switching, Traffic and Networks*. Prentice Hall, ISBN: 0-13-033309-3, 1999.

[139] L. T. A. Bononi and L. A. Rusch, "Fast dynamics and power swings in doped-fiber amplifiers fed by highly variable multimedia traffic," *Optical Fiber Communication conference*, vol. 2, no. WM31, pp. 213–217, 1998.

[140] M. D. Prycker, *Asynchronous Transfer Mode, Solution for Broadband ISDN*. Prentice Hall, ISBN:0-13-342171-6, 1995.

[141] M. M. Ali and S. Nadarajah, "A Truncated Pareto Distribution," *Computer Communications*, vol. 30, pp. 1–4, December 2006.

[142] V. Paxson and S. Floyd, "Wide-area Traffic: The Failure of Poisson Modelling," *IEEE/ACM Transaction on Networking*, vol. 3, pp. 226–244, June 1995.

[143] W. willinger V. Paxson and M. S. Taqqu, *Self-similarity and Heavy Tails: Structural Modeling of Network Traffic. In Practical Guide to Heavy Tails: Statistical Techniques and Applications*. 1998.

[144] A. B. M. Crovella, "Self-Similarity in World WideWeb Traffic: Evidence and Possible Causes," *IEEE/ACM Transactions on Networkin*, vol. 5, pp. 835–846, December 1997.

[145] M. Becchi, “From Poisson Process to self-Similarity: a Survey of Network Traffic Models.” http://www.cse.wustl.edu/ jain/cse567-06/traffic-modelsl.htm.

[146] L. Zaninetti and M. Ferraro, “On the Truncated Pareto Distribution with Applications,” *Central European Journal of Physics*, vol. 6, no. 1, pp. 1–6, 2008.

[147] M. W. Garrett and W. Willinger, “Analysis Modelling and Generation of Self-similar VBR Video Traffic,” *in Proceeding SIGCOMM’94*, pp. 269–280, 1994.

[148] K. Y. KO, M. S. Demokan, and H. Y. Tam, “Transient Analysis of Erbium-Doped Fiber Amplifiers,” *IEEE Photonics Technology Letters*, vol. 6, pp. 1436–1438, December 1994.

[149] J. A. Rice, *Mathematical Statistics and Data Analysis*. Duxbury Press, 2006.

[150] D. Yevick, “The Accuracy of Multicanonical System Models,” *IEEE Photonics Technology Letters*, vol. 15, pp. 224–226, February 2003.

[151] B. A. Berg, “Algorithmic Aspects of Multicanonical Simulations,” *Nuclear Physics B (Proc suppl.) 63A-C*, pp. 982–984, 1998.

[152] R. Hozlohner and C. R. Menyuk, “Use of Multicanonical Monte Carlo Simulations to Obtain Accurate Bit Error Rates in Optical Communications Systems,” *Optics Letters*, vol. 28, October 15 2003.

[153] e. a. C. Dimopoulos, D. Simeonidou, “Evolution of SNR during power transients in chains of saturated and gain equalized EDFAs,” *Electronics Letters*, vol. 35, pp. 1756–1758, 30th September 1999.

[154] e. a. F. Forghieri, R. Tkach, “Simple model of optical amplifier chains to evaluate penalties in WDM systems,” *Journal of Lightwave Technology*, vol. 16, pp. 1570–1576, 1998.

[155] D. Marcuse, “Derivation of analytical expression for the bit-error probability in lightwave systems with optical amplifiers,” *Journal of Lightwave Technology*, vol. 8, pp. 1816–1823, 1990.

[156] S. V. Kartalopoulos, “Optical Bit Error Rate, an estimation Methodology,” pp. chapter 7–9, 2004.

[157] J. P. B. e. a. Y. Maigron, J. F. Marcerou, “Analysis of a cascaded EDFA link time behaviour,” *Proceedings ECOC’92*, vol. WeP2, paper , Berlin Germany, September 1992.

[158] R. S. W. W. Lin and B. Mumeya, “Decreasing EDFA transients by power shaping,” *Optical Switching and Networking*, vol. 5, pp. 188–195, October 2008.

[159] M. G. J. Gurfinkel, D. Sadot, “Dynamic control analysis for semiconductor optical amplifier dynamics in optical network applications,” *Fiber Optics and Optical Communication, Opt. Eng.*, vol. 46, no. 3, 2007.

[160] M. Karasek and J. van der Plaats, “Analysis of Dynamic Pump-Loss Controlled Gain-Locking System for Erbium-Doped Fiber Amplifiers,” *IEEE photonic technology letters*, vol. 10, pp. 1171–1173, August 1998.

[161] M. Karasek and J. C. van der Plaats, “Modelling of a Pump-power-loss-controlled gain-locking system for EDFA application in WDM transmission systems,” *IEE Proceeding Optoelectron*, vol. 145, pp. 205–210, Augest 1998.

[162] A. Bononi, M. Papararo, and M. Fuochi, “Transient Gain Dynamics in saturated Raman Amplifiers,” *Optical Fiber Technology*, vol. 10, no. 1, pp. 91–123, 2004.

[163] M. Karasek, J. Kanka, D. Krcmarik, J. Radil, and J. Vojtech, “Surviving-Channel-Power Transients in Second-Order Pumped Lumped Raman Fiber Amplifier: Experimentation and Modeling,” *Journal of Light Technology*, vol. 25, no. 3, pp. 664–672, 2007.

[164] H. Krimmel, T. Pfeiffer, B. Deppisch, and L. Jentsch, “Hybrid Electro-Optical Feedback Gain-Stabilized EDFAs for Long-Reach Wavelength-Multiplexed Passive optical Networks,” *ECOC2009, Vienna, Austria*, September 2009.

[165] J. Shen, S. Wei, and C. Lin, “High Efficiency Automatic-Power Controlled and Gain-Clamped EDFA for Broadband Passive Optical Networking Systems,” *Journal of Infrared Milli Terahz Waves*, vol. 31, pp. 490–499, January 2010.

[166] N. Vijayakumar and R. Sreeja, "A Feed Forward Method for Stabilizing the gain and output power of an Erbium-Doped Fiber Amplifier," *Microwave and Optical technology letters*, vol. 51, pp. 2156–2160, September 2009.

[167] Y. Oikawa, Y. Horiuchi, Y. Tanaka, M. Shiga, and H. Nagaeda, "Super-Fast AGC-EDFA for the Burst-Mode Systems without Gain Excursion in 20-ns and 21-dB Ramped Input," *OFC/NFOEC*, vol. ThA15.pdf, 2008.

[168] T. Huang, L. Sheu, and S. Chi, "All-Optical Gain Clamped Erbium-Doped Fiber amplifier Using a DWDM Demultiplexer," *OFC/NFOEC2009*, vol. ThLP16, 2009.

[169] H. Li, Y. Zhang, Y. C. Soh, and C. Wen, "Design and Analysis of Dynamic Erbium-Doped Fiber Amplifier Gain-Clamping Systems with Feedback Control," *Optical Society of America*, vol. 24, pp. 1739–1748, August 2007.

[170] L.Rapp, "Transient Behaviour of EDFA Stages using Pump Power Splitting," *Journal of Lightwave technology*, vol. 25, pp. 726–732, March 2007.

[171] M. A. Mahdi and F. M. Adikan, "Characterization of Lasing-oscillation Direction in Optical Gain-Clamped Erbium-Doped Fiber Amplifiers," *Optics and laser Technology*, vol. 39, pp. 1020–1024, 2007.

[172] M. Ding and L. Pavel, "Gain Scheduling Control Design of an Erbium-Doped Fiber Amplifier by Pump Compensation," *Preceding of the 2005 IEEE conference on Control Applications*, vol. MC4.6, pp. 510–516, 2005.

[173] "Matlab PID Controller," *Carnegie-Mellon-University*, p. http://www.engin.umich.edu/group/ctm/PID/PID.html, 25th May 2010.

[174] J. G. Ziegler, N. B. Nichols, and N. Y. Rochester, "Optimum setting for Automatic Controller," *Transactions of the A.S.M.E, G. J. Dynamic. System Measurement Control*, vol. 4, pp. 759–763, November 1942.

[175] M. Fukushima and J. Miura, "Recent Progress of Erbium-Doped Amplifiers and their Components," *Proceeding of SPIE, Active and Passive Components for Communications VII*, vol. 6775, no. 677502, pp. 1–12, 2007.

[176] Motorola, “OA500 Series DWDM Erbium-Doped Fibre Amplifier,” *www.motorola.com/broadband*, 2002.

[177] S. Pachnicke, P. M. Krummrich, E. Voges, and E. Gottwald, “Transient gain dynamics in long-haul transmission systems with electronic EDFA gain control,” *Journal of Optical Networking*, vol. 6, no. 9, pp. 1129–1137, 2007.

[178] S. Pachnicke, M. Obholz, E. Voges, P. M. Krummrich, and E. Gottwald, “Electronic EDFA gain Control for the suppression of transient gain dynamics in long-haul transmission systems,” *Optical society America*, no. 1-55752-830-6, 2006.

[179] C.R.Yang, H. Y. H. Wang, and H. Hong, “A gain-Clamped Erbium-Doped Fibre Amplifier (CG-EDFA) for WDM Optical Packet-Switching System,” *Microwave and Optical Technology Letters*, vol. 32, pp. 316–319, February 2002.

[180] B. Shia, M. Williams, and A. G. al, “Investigation of fast power transient control in constant power-mode terminal EDFAs for 40Gb/s systems,” *Optical Fiber Communication and Optoelectronic Exposition and Conference (AOE, Shanghai, Asia)*, pp. 1–3, 2008.

[181] M. Yucel, “Fuzzy logic-based automatic gain controller for EDFA,” *Microwave and Optical Technology Letters*, vol. 53, pp. 2703–2705, November 2011.

[182] J. Zyskind and A. Srivastava, *Optically Amplified WDM Networks, Chapter 6 and 7*. Elsevier Inc., ISBN: 978-0-12-374965-9, 2010.

[183] H. Feng, E. Patzak, and J. Saniter, “Methods for Stabilizing the Gain of EDFAs in Burst Switching Optical Networks,” *Photonic Network Communication*, vol. 4, no. 2, pp. 151–166, 2002.

Appendix A

List of publications

1. S. Muhyaldin and Marc Eberhard, “Quality Criterion Modelling of Erbium-Doped Fibre Amplifiers”, New Concepts in Photonics and Optical Communications, University of Bourgogne, Dijon, France, June, 2004.

2. S. Muhyaldin and Marc Eberhard, Robin Ibbotson, et al “Investigation $LiNbO_3$ Modulator performance for New Transmission Applications”, New Concepts in Photonics and Optical Communications, University of Bourgogne, Dijon, France, June, 2004.

3. S. Muhyaldin and M. Eberhard, “High Precision Modeling of Erbium-Doped Fibre Amplifier”, Nonlinear Optics in Communications, Institute of Physics, London, 30 June, 2004.

4. S. Muhyaldin and Marc Eberhard, “Investigation of an L-band Erbium-Doped Amplifier (EDFA) Performance”, PREP2005, Postgraduate Conference in Electronics, Photonics, Communications and Networks and Computing Science, University of Lancaster, 2005.

5. S. Muhyaldin, Marc Eberhard, and K. J. Blow, “Modeling and Analysis of High Performance L-band Erbium-Doped Fibre Amplifier (EDFA)”, Dresden, Germany, NLGW, 2005.

6. S. Muhyaldin, M. Eberhard, and K. J. Blow, “System Analysis of Fast Power Transients in WDM Optical Networks for Added and Dropped Signals”, 10th European

Conference on Networks and Optical Communications (NOC 2005), University College London, U.K, July, 2005.

Appendix B

B.1 Basic model parameters

The main parameters in the design of an EDFA consist of the fibre glass material, the waveguide characteristics of the fibre, the length of fibre used, core diameter, cutoff wavelength, the pump source, the erbium concentration, and any active or passive components. Passive components composed of wavelength division multiplexers (WDM couplers) and isolators, while active components may consist of electronic device for automatic gain control. EDFA is applied in the wavelength routed optical networks in different applications. The intended application is the main point in the design of the EDFA, and the parameters are chosen and required to be considered as a whole. High gain, high output power, low noise figure, flatness of gain spectrum, reliability, etc. are main design objectives [5,6,8,34]. The power amplifier has different design parameter values than an in-line amplifier or a preamplifier as defined in chapters 1 and 2. The fibre parameters such as fibre length, core diameter, Er^{+3} ion, etc. can be achieved by numerically modeling the erbium-doped fibre amplifier performance for the intended application [55], then the obtained parameters are used in the manufacturing of doped fibre used in EDFA. The pump configurations are also one of the important EDFA design parameter. There may be different pump configurations for different application as explained in section 2.6 in chapter 2. We briefly demonstrate some of parameters definition, related to a fibre and used in the implementation of erbium-doped fibre for amplification.

B.1.1 Absorption and emission cross sections

The absorption and emission cross sections will depend on the particular host glass in which the Er^{3+} ion is embedded. The spectral shape of the cross sections in the 1.5 μm region, as well as the absolute magnitudes of the cross sections vary with the host environment. A standard technique involves either calculating the emission cross sections from the absorption cross sections or directly measuring the small signal gain in a short piece of uniformly inverted Er^{3+}-doped fibre. The emission cross section can be obtained accurately from the absorption cross sections through the McCumber relationship as shown below [8, 12]:

$$\sigma^{(e)}(\upsilon) = \sigma^{(a)}(\upsilon)\ \exp[(\varepsilon - h\upsilon)/kT] \tag{B.1}$$

Where $\sigma^{(e)}(\upsilon)$ is emission cross sections, $\sigma^{(a)}(\upsilon)$ is absorption cross sections, ε represents the mean transition energy between the two manifolds, h is 6.626 $\times 10^{-34}$ Js, Plank's constant, υ is frequency of the transition, K is 1.38 $\times 10^{-23} J/K$, the Boltzmann constant, T is the absolute temperature.

B.1.2 Amplified spontaneous emission(ASE)

An important factor present in all optical amplifiers is the amplified spontaneous emission. All the excited ions can spontaneously relax from the upper state to the ground state by emitting a photon that is uncorrelated with the signal photons. This spontaneously emitted photon can be amplified as it travels down the fibre and stimulates the emission of more photons from excited ions, photons that belong to the same mode of the electromagnetic field as the original spontaneous photon. This parasitic process, which can occur at any frequency within the fluorescence spectrum of the amplifier transitions, obviously reduces the gain from the amplifier. It absorbs photons that would otherwise participate in stimulated emission with the signal photons. It is known as ASE. To calculate the ASE at the output of the fibre, first it is required to calculate the spontaneous emission power at a given point in the fibre. This power is sometimes referred to as an equivalent noise power. For a single transverse mode fibre with two independent polarisations for a given mode at frequency υ, the noise power in a bandwidth $\Delta\upsilon$, corresponding to spontaneous emission, is equal to :

$$P^0_{ASE} = 2h\upsilon\Delta\upsilon \tag{B.2}$$

The total ASE power at a point z along the fibre is the sum of the ASE power from the previous sections of the fibre, added to local noise power P^0_{ASE}. This local noise power will stimulate the emission of photons from excited erbium ions, proportionally to the product $\sigma^{(e)}(\upsilon)N_2$, where $\sigma^{(e)}(\upsilon)$ is the stimulated emission cross section at frequency υ. The propagation equation for the ASE power propagating in a given direction is thus

$$\frac{dP_{ASE}(\upsilon)}{dz} = \left(N_2\sigma^{(e)}(\upsilon) - N_1\sigma^{(a)}(\upsilon)\right)P_{ASE}(\upsilon) + P^0_{ASE}(\upsilon)N_2\sigma^{(e)}(\upsilon) \tag{B.3}$$

ASE consists of two components, one in the direction of signal propagation (forward ASE) and the other in the direction opposite to the signal propagation (backward ASE) [5, 6, 8].

B.1.3 Overlap factor

The portion of the optical mode that overlaps with the erbium ion distribution will stimulate absorption or emission from the Er^{3+} ion transitions. In general, the erbium ion density can vary significantly in core and cladding regions. The amount of population inversion at some point in fibre depends on the pump and signal intensities at that point. This transverse variation of gain and absorption can be simplified by using a factor Γ. Thus, an effective average intensity can be expressed throughout the erbium doped region as [6, 8, 78]:

$$I_z = \frac{P_{(z)}\Gamma}{\pi R^2} = \frac{P_{(z)}\Gamma}{A} \tag{B.4}$$

Where $I_{(z)}$ is the intensity of the field at point z, $P_{(z)}$ is the power of the field at point z, Γ is the overlap factor between the field considered and the erbium ion distribution, A = πR^2 is the transverse area occupied by the erbium ions.

B.1.4 Lifetimes

The lifetime is another important parameter in the modeling of EDFA. The population of an excited level decays exponentially with a time constant equal to the lifetime. When there are

several pathways for the population to decay, the total probability is the sum of individual probabilities for each pathway. The two main paths for decay are, radiative and non-radiative as shown in Figure 2.10 (d), the total lifetime τ is:

$$\frac{1}{\tau} = \frac{1}{\tau_r} + \frac{1}{\tau_{nr}} \tag{B.5}$$

Where τ is the total lifetime, τ_r is the radiative lifetime, τ_{nr} is the non-radiative lifetime.

The radiative life time arises from the excited fluorescence level to all the levels below it. Non-radiative lifetimes depend largely upon the glass composition and the coupling between the vibrations of the mesh ions and the states of the rare earth ions. At high concentrations of erbium ions, an effect known as concentration quenching can take place which reduces the lifetimes of excited state [6, 8]. The variation of ion concentration and fibre length are performed during the development of the wide band (C+L) Amplifier at the initial stage of the research of this thesis [55].

B.1.5 Line-width and broadening

The line-width represents a finite spectrum of the gain in frequency domain. This happens due to broadening of the energy states, in other words, each of the energy states is actually a collection of many closely spaced energy levels . Normally this broadening is considered homogeneous to simplify the model equations but in more accurate models inhomogeneous broadening is taken into account. An inhomogeneous line is thus a superposition of a set of homogeneous lines [6, 8].

The inhomogeneous portion of the line-width broadening of the dopant ions produce in the gain spectrum an inhomogeneous component then the gain saturation occurs in an inhomogeneous manner. This effect is known as Spectral hole burning due to a high power signal at one wavelength which can 'burn' a hole in the gain for wavelengths near to that signal by saturation of the inhomogeneously broadened ions. Spectral holes vary in width depending on the characteristics of the optical fibre and the power of the burning signal, but are typically less than 1 nm at the small wavelength end of the C-band spectrum, and a few nm at the large wavelength end of the C-band spectrum. The depth of the holes are very small, though making it difficult to recognise in practice.

B.2 Gain model of EDFA

Reducing the three-level system to two-level system, the rate equation can be written in the terms concerning the total population densities of level 1 and 2 as explained in [6] and shown,

$$\frac{dN_2}{dt} = -\Gamma_{21}N_2 + (N_1\sigma_s^a - N_2\sigma_s^e)\,\phi_s - (N_2\sigma_p^e - N_1\sigma_p^a)\,\phi_p \tag{B.6}$$

$$\frac{dN_1}{dt} = \Gamma_{21}N_2 - (N_2\sigma_s^e - N_1\sigma_s^a)\,\phi_s - (N_1\sigma_p^a - N_2\sigma_p^e)\,\phi_p \tag{B.7}$$

Where σ_s^a , σ_s^e , σ_p^a , σ_p^e are the signal and pump absorption and emission cross sections, respectively, and the total ion population N is given by

$$N = N_1 + N_2 \tag{B.8}$$

N_2 can be calculated from Equations B.6 in terms of the signal and pump power, then N_1 can simply given by $(N - N_2)$. The ion population in the upper level (N_2) can be written as a function of position z along the fibre and total ion density N for the case of one pump field power and one signal field power,

$$N_2 = \frac{\frac{\tau\sigma_s^{(a)}}{Ah\upsilon_s}\Gamma_s P_s + \sum_j \frac{\tau\sigma_{\upsilon_j}^{(a)}}{Ah\upsilon_j}\Gamma_{\upsilon_j} P_A(\upsilon_j) + \frac{\tau\sigma_p^{(a)}}{Ah\upsilon_p}\Gamma_p P_p}{\frac{\tau(\sigma_s^{(a)}+\sigma_s^{(e)})}{Ah\upsilon_s}\Gamma_s P_s + \sum_j \frac{\tau(\sigma_{\upsilon_j}^{(a)}+\sigma_{\upsilon_j}^{(e)})}{Ah\upsilon_j}\Gamma_{\upsilon_j} P_A(\upsilon_j) + \frac{\tau(\sigma_p^{(a)}+\sigma_p^{(e)})}{Ah\upsilon_p}\Gamma_p P_p + 1} N \tag{B.9}$$

Where $\Gamma_{s,p}$ is the overlap factors between the light-field modes and the erbium distribution, and A is πR^2 the effective area of the erbium distribution. $P_A(\upsilon_j)$ is ASE power and composed of ASE forward-traveling power ($P_A^+(\upsilon_j)$), and ASE backward-traveling power ($P_A^-(\upsilon_j)$) as explained in appendix B.1.

The field propagation equations can also be written in terms of the field powers. The overlap factors, which is explained in more detail in appendix B.1, included to the propagation equations because the optical mode that overlaps with erbium ion dopant will experience gain or attenuation. The intrinsic loss in the fibre are also included into the field propagation equations and denoted by $\alpha_p^{(a0)}$, $\alpha_s^{(a0)}$, $\alpha_{\upsilon_j}^{(a0)}$,

These four equations B.10, B.11, B.12, B.13 are used as a model for the numerical simulation of EDFA gain verses distances (length of erbium-doped fibre) in early stage of this thesis research.

$$\frac{dP_p}{dz} = \left(N_2\sigma_p^{(e)} - N_1\sigma_p^{(a)}\right)\Gamma_p P_p - \alpha_p^{(a0)} P_p \tag{B.10}$$

$$\frac{dP_s}{dz} = \left(N_2\sigma_s^{(e)} - N_1\sigma_s^{(a)}\right)\Gamma_s P_s - \alpha_s^{(a0)} P_s \tag{B.11}$$

$$\frac{P_A^+(\upsilon_j)}{dz} = \left(N_2\sigma_{\upsilon_j}^{(e)} - N_1\sigma_{\upsilon_j}^{(a)}\right)\Gamma_s P_A^+(\upsilon_j) + N_2\sigma_{\upsilon_j}^{(e)}\Gamma_s h\upsilon_j\Delta\upsilon_j - \alpha_{\upsilon_j}^{(a0)} P_A^+(\upsilon_j) \tag{B.12}$$

$$\frac{P_A^-(\upsilon_j)}{dz} = -\left(N_2\sigma_{\upsilon_j}^{(e)} - N_1\sigma_{\upsilon_j}^{(a)}\right)\Gamma_s P_A^-(\upsilon_j) - N_2\sigma_{\upsilon_j}^{(e)}\Gamma_s h\upsilon_j\Delta\upsilon_j + \alpha_{\upsilon_j}^{(a0)} P_A^-(\upsilon_j) \tag{B.13}$$

B.3 Gain dynamic model of EDFA

In this section, the derivation of gain dynamic model presented in [74] is followed. The idea is to write the excited-state population equation as a derivatives of the field powers. The propagation equations for the pump and signal field powers are:

$$\frac{\partial P_p(z,t)}{\partial z} = \rho u\Gamma_p\left[(\sigma_p^e + \sigma_p^a)N_2(z,t) - \sigma_p^a\right]P_p(z,t) \tag{B.14}$$

$$\frac{\partial P_s(z,t)}{\partial z} = \rho\Gamma_s\left[(\sigma_s^e + \sigma_s^a)N_2(z,t) - \sigma_s^a\right]P_s(z,t) \tag{B.15}$$

$P_p(z,t)$ and $P_s(z,t)$ are the pump and signal powers in units of photons per unit time. Light beams traveling along the z direction from 0 to L, which is the length of erbium-doped fibre, are indicated by unit vector u_k = +1, and light beams moving the opposite direction by

u_k = -1. The fractional populations of the upper state $N_2(z,t)$ and of the lower state $N_1(z,t)$ satisfy the relationship, $N_2(z,t) + N_1(z,t) = 1$. Where σ_s^a , σ_s^e , σ_p^a , σ_p^e are the signal and pump absorption and emission cross sections, respectively, ρ is number of ions per unit volume, Γ_s and Γ_p are the signal and pump overlap factors with erbium ion distribution. The propagation of signal is assumed to be from z = 0 to z = L. The rate equation for the population which is apart of the model derivation equations is

$$\frac{\partial N_2(z,t)}{\partial t} = -\frac{N_2(z,t)}{\tau} - \frac{1}{\rho A}\left(\frac{\partial P_s(z,t)}{\partial z} + u\frac{\partial P_p(z,t)}{\partial z}\right) \tag{B.16}$$

The first term on the right-hand side of rate equation B.16 is the decay in the upper-state population originating from spontaneous emission. The absorption and emission due to the fields are combined in the second term of the right-hand side of the equation B.16. The latter term can be clarified as follow: The variation in the field power $\partial P_p(z,t)$ is the number of photons deposited in the fibre length *dz* per unit time at time *t*, then dividing this field power by both the cross-sectional area *A* traversed by the beam generates the photons deposited per unit volume, in the volume *Adz*, and by ion population ρ in unit ions/volume. The latter division produces the number of photons absorbed or emitted, then the fraction population of the excited-state will change accordingly. The rate equation for the fractional population of the upper state $N_2(z,t)$ is

$$\frac{\partial N_2(z,t)}{\partial t} = -\frac{N_2(z,t)}{\tau} - \frac{1}{\rho A}\sum_{k=1}^{M} u_k \frac{\partial P_k(z,t)}{\partial z} \tag{B.17}$$

The change of power in the kth beam is shown by

$$\frac{\partial P_k(z,t)}{\partial z} = \rho u_k \Gamma_k \left[(\sigma_k^e + \sigma_k^a)N_2(z,t) - \sigma_k^a\right] P_k(z,t) \tag{B.18}$$

During steady-state conditions, the population densities and optical powers are independent of time. Then, $N_2(z,t)$ is obtained by setting $\partial N_2(z,t)\partial t$ = 0 in equation B.17, then the equation can be written as

$$\frac{u_k}{P_k(z)} dP_k = -\left[\alpha_k + \frac{1}{P_k^{IS}}\sum_{j=1}^{M} u_j \frac{dP_j(z,t)}{dz}\right] dz \tag{B.19}$$

The upper-state population can be found from equation B.18, then used in equation B.17, then the equation below obtained

$$\tau\, u_k \frac{\partial}{\partial t}\left(\frac{1}{P_k(z)}\frac{\partial P_k(z,t)}{\partial z}\right) =$$

$$-u_k\left(\frac{1}{P_k(z)}\frac{\partial P_k(z,t)}{\partial z}\right) - \frac{1}{P_k^{IS}}\sum_{j=1}^{M} u_j \frac{dP_j(z,t)}{dz} - \alpha_k \tag{B.20}$$

Where P_k^{IS} is the intrinsic saturation power of the kth channel. $P_k^{in}(t)$ and $P_k^{out}(t)$ are the input and output powers of the *kth* channel at time *t*, $G_k(t)$ is overall gain parameter.

$$P_k^{IS} = \frac{A}{\Gamma_k\left(\sigma_k^e + \sigma_k^a\right)\tau} \tag{B.21}$$

$$G_k(t) = ln\left[\frac{P_k^{out}(t)}{P_k^{in}(t)}\right] \tag{B.22}$$

$$\alpha_k = \rho\Gamma_k\sigma_k^a \tag{B.23}$$

Integration of equation B.20 over z from 0 to L, the equation below obtained

$$\tau\frac{d}{dt}\left[ln\frac{P_k^{out}(t)}{P_k^{in}(t)}\right] =$$

$$-ln\frac{P_k^{out}(t)}{P_k^{in}(t)} - \frac{1}{P_k^{IS}}\sum_{j=1}^{M}\left[P_j^{out}(t) - P_j^{in}(t)\right] - \alpha_k L \tag{B.24}$$

Where A_k = $\rho\Gamma_k\sigma_k^a$L is the total absorption constant or absorption coefficient

$$A_k = \alpha_k L \tag{B.25}$$

Substituting $G_k(t)$ and A_k in the equation B.24, the equation below is obtained

$$P_k^{IS}\left[\tau\frac{dG_k(t)}{dt} + G_k(t) + A_k\right] =$$

$$-\sum_{j=1}^{M}P_j^{in}(t)\left[exp(G_j(t)) - 1\right] \tag{B.26}$$

Equation B.26 can be numerically solved with input power $P_k^{in}(t)$ and initial gain value $G_k(0) = G_k^0$ for all channels k = 1,2,3,...,M. Equation B.26 consists of a set of coupled ordinary differential equations derived from the coupled partial differential equations of equations B.17 and B.18. The coupled ordinary differential equations B.26 can be further simplified to a single equation. The right side of the equation B.26 is the same for all channels, so the combination of any two channels k and j to form equation below,

$$\tau\frac{dG_{kj}(t)}{dt} + G_{kj}(t) + A_{kj} = 0 \tag{B.27}$$

$$G_{kj}(t) = P_k^{IS}G_k(t) - P_j^{IS}G_j(t) \tag{B.28}$$

$$A_{kj} = P_k^{IS}A_k - P_j^{IS}A_j \tag{B.29}$$

$$G_{kj}(t) = \left[G_{kj}^0 + A_{kj}\right]\exp\left(\frac{-t}{\tau}\right) - A_{kj} \tag{B.30}$$

The gain in the *jth* channel can be written in terms of the gain in the *kth* channel, then equation 2.12 is obtained and shown below,

$$P_j^{IS}G_j(t) = P_k^{IS}G_k(t) - \left[G_{kj}^0 + A_{kj}\right]\exp\left(\frac{-t}{\tau}\right) + A_{kj} \tag{B.31}$$

Then the above equation can be written as below , the same equation (2.11),

$$\tau\frac{d}{dt}P_k^{IS}G_k(t) + P_k^{IS}G_k(t) + P_k^{IS}A_k =$$

$$-\sum_{j=1}^{M} P_j^{in}(t)\left\{\exp\left[\frac{P_k^{IS}G_k(t) - \left[G_{kj}^0 + A_{kj}\right]\exp\left(\frac{-t}{\tau}\right) + A_{kj}}{P_j^{IS}}\right] - 1\right\} \tag{B.32}$$

B.4 1 dB increase-time/decrease-time of OSNR

As we mentioned that the transients along thechain caused by variation of the input power. At time t=0, the network is at steady state and, in our case all eight signal channels are present. The steady state is computed by sequentially setting dG/dt = 0 in equation (3.5) for each EDFA and solving the resulting transcendental equation. For ASE computations, the integral in equation (3.7) computed over 200 frequency bands between 1490 nm to 1573 nm with 0.4 nm separation, with input power of -2 dBm the chain is balanced, in the sense that each EDFA can provide roughly 11.5 dB gain to the eight active channels, to compensate the span losses between EDFAs. At time one instant after time zero, t = 0+, the last four signal channels are dropped an the transients are determined by sequential solving the model (3.5) for each EDFA using numerical technique explained in appendix—B.6, in time resolution of 2 μs, The related 1 dB increase-time and decrease-time for power transients and OSNR transients versus amplifier number in the chain are shown in Figure 6.7 for the channel wavelength of 1549.2 nm, the OSNR computed as ratio of the signal power to the ASE statistical average power shown in equation (3.7).The theoretical values calculated for power and OSNR transients their detail is given in appendix B.4.1. Note that the transients become faster along the chain [105]. It is also noted that the transients of the output power are faster than the transients of the OSNR. Figures 6.2 and 6.4 shows the power and OSNR dB transient for probe channel at the output of 2nd to 24th EDFA. Note that at the beginning of the chain the OSNR transient is smaller than the power transient, but along the chain the power and OSNR transients become almost the same. As a good prove for that the OSNR is smaller than power transient at the beginning of the chain, it is noted that the value of OSNR transient does not reach the 1 dB value at the first EDFA as shown in Figure 6.7. This result will indicate that the OSNR transients in packet-switched network is also smaller than the power transients, which is shown by the PDF of power transients. The broadening of PDF indicates the amount of output power swings. The smaller broadening of the PDF the smaller the power transient and this indicate less problem at the receiver range limitations. if The OSNR transient high, this can represent a serious problem, indicating at receiver dynamic range limitations, deteriorates the bit error rate if the power exceeds certain thresholds for optical

nonlinearities or inadequate eye opening. It should be expressed that this study determines this effect qualitatively in the case of highly variable input power and as he number of EDFAs increase in the chain.

B.4.1 Theoretical calculation of 1 dB increase-time/decrease-time of the power and OSNR

The dynamic model of self-saturated EDFA (3.5) represents the EDFA gain as a continuous function of time. However, the variation in the input power results in a step transition in the output power, and such transient propagates along the chain of EDFAs. The EDFA gains evolve in time as (3.5), and the system converges toward a new steady-state solution. The speed of power transients can be characterised by the 1 dB time [105].

Let the input and output fluxes denoted by $Q^{in}_{j,k}$ and $Q^{out}_{j,k}$ respectively, of channel k at EDFA j. Let us define the dB-power transient of channel k at the output of EDFA j as $\Delta Q^{dB}_{j,k}(t) \approx 10log10[Q^{out}_{j,k}(t)/Q^{out}_{j,k}(0^+)]$ where $t = 0^+$ indicates one instant after transition at t = 0. Approximating $\Delta Q^{dB}_{j,k}(t)$ as a straight line in t and defining the normalised slope

$$\Delta_{j,k} \approx \frac{d}{dt}(lnQ^{out}_{j,k}(t)|_{t=0^+} \tag{B.33}$$

A simple approximation of the 1 dB time as the inverse of the slope can be obtained

$$t_{1-dB} = 1/(10log10\, e\Delta_{j,k} \tag{B.34}$$

The span losses are time invariant, the time derivative of the input power of one EDFA is equal to the time derivative of the output power of the previous EDFA, guiding to the following recurrence

$$\Delta_{j,k} = \frac{d}{dt}(lnQ^{in}_{j,k}(t)|_{t=0^+} + \frac{d}{dt}(lnG_{j,k}(t)|_{t=0^+} \tag{B.35}$$

$$= \frac{d}{dt}(lnQ^{out}_{j,k}(t)|_{t=0^+} + \frac{d}{dt}(lnG_{j,k}(t)|_{t=0^+} \tag{B.36}$$

$$= \Delta_{j-1,k} + \frac{d}{dt}(lnG_{j,k}(t)|_{t=0^+} \tag{B.37}$$

Where $\Delta_{0,k}$ = 0. This is a difference equation describing the slope evolution along the chain with initial condition that the slope of the input power at the first EDFA is zero. Finally, assuming the system is at steady state before the transition, the derivative of the gain can be found by calculating (3.5)

$$\frac{dG_{j,k}(t)}{dt} = \sum_{i=0}^{N} \frac{\Delta Q_{j,i}}{\tau Q^{IS}_k}\left(e^{G_{j,i}(0)} - 1\right) \tag{B.38}$$

Where $\Delta\, Q_{j,i} \approx Q^{in}_{j,i}(0^+)$ - $Q^{in}_{j,i}(0)$, and we have $\Delta\, Q_{j,i} = \Delta\, Q_{j-1,i}\, e^{G_{j-1,i}}/L_{j-1,i}$ and $\Delta\, Q_{0,i}$ is the step transition of the input power to the first EDFA. $L_{j-1,i}$ is the loss between EDFA $j-1$ and i

The information of the slope evolution along the chain and the related 1 dB time could be put into practical implementation in approaching a gain control technique by switching the pump. In this case-study, the pump is switched after a certain amount of pump power change should be such that it gives a useful gain control technique of the slope could be used to build a pump compensation scheme that exactly counter-measures the slope by inducing an additional slope with the opposite sign. Hence, from B.38, the pump change $\Delta Q_{j,0}$ (photons/s) required to compensate the slope at the jth EDFA is provided by

$$\Delta Q_{j,0} \approx \frac{1}{1-e^{G_{j,0}(0)}} \sum_{i=0}^{N} \Delta Q_{j,i}(e^{G_{j,i}(0)}-1) \tag{B.39}$$

This is a photon flux conservation, valid also for equilibrium compensation: The pump should vary its flux so as the number of excited ions in the EDFA by the amount corresponding to the ions used/saved by the total channel flux variation.

B.5 Euler technique

Euler numerical technique is used for implementation of the gain dynamic model as initial stage of this work,

```
Simulation time-step denoted by 'n' which is = 10000;
tini represents simulation initial-time = 0.0;
tend represents simulation final-time = 100 ms in circuit switching
and 600 ms or more in packet switching in order to get stable-results
double euler(int n)     //explicit Euler
{
   double ht = (tend-tini)/n;   //grid size
     for(int k = 0 ; k <n-1; k++)
      {
double time_slot = (tini+ht*k);
      if ( time_slot > 50*pow(10,-3))
        {
     survivech_pump = 5; //4 signal channels dropped at 50 ms
}
        if ( time_slot> 80*pow(10,-3))
       {
       survivech_pump = 9;//4 signal channels retained to system at 80 ms
       }

      G[k+1] = G[k] + ht*Gfn(G[k], lambedak, tini+ht*k, k);
Gfnj1(G[k+1],lambedak, tini+ht*k, k);
     }
     return G[k];
 }
```

B.6 Fourth-order Runge-Kutta

Fourth-order Runge-Kutta is a numerical technique which is used for the implementation of the gain dynamic model

```
double RK4(int n)      //explicit Rung-Kutta
{
  double f1 = 0.0;
  double f2 = 0.0;
  double f3 = 0.0;
  double f4 = 0.0;

   double ht = (tend-tini)/n;   //grid size
    for(int k = 0 ; k <n-1; k++)
      {
double time_slot = (tini+ht*k);
    if ( time_slot > 50*pow(10,-3))
        {
     survivech_pump = 5; //4 signal channels dropped at 50 ms
}
        if ( time_slot> 80*pow(10,-3))
       {
       survivech_pump = 9;//4 signal channels retained to system at 80 ms
       }
       f1 =  ht*Gfn(G[k], lambedak, time_slot, k);
       f2 =  ht*Gfn((G[k] + (f1*0.5)), lambedak, (time_slot+ (ht*0.5)), k);
       f3 =  ht*Gfn((G[k] + (f2*0.5)), lambedak, (time_slot+ (ht*0.5)), k);
       f4 =  ht*Gfn((G[k] + (f3)), lambedak, (time_slot+ ht), k);

       G[k+1] = G[k] + ((f1 + 2*f2 + 2*f3 + f4)/6);
 Gfnj(G[k+1],lambedak, tini+ht*k, k);
     }
     return G[k];
 }
```

B.7 Bisection technique for transcendental non-linear equations

This logarithm can be depicted in the following example:

Find the square root of 2. let f(x) = 2-x^2. f(1) = 1, f(2) = -2. let x_1 = 1 and x_2 = 2. Then x_p = 1.5 and f(x_p) = -0.25. So x_1 = 1, and x_2 = 1.5 Then next x_p = 1.25 and f(1.25) = 0.4375, So x_1 = 1.25 and x_2 = 1.5

The above numerical technique, defined by Bisection, is implemented in C-language for self-saturated gain dynamic model 2.21 at steady-state condition (when dG(t)/dt = 0). Note that the initial conditions obtained with the Sun [74] routine do not incorporate the ASE noise and are used in this case just as a starting point for the Bisection algorithm.